



UNIVERSITY OF
BIRMINGHAM

**EXPERIMENTAL AND NUMERICAL
INVESTIGATION OF A NEW MOF BASED
ADSORPTION WATER DESALINATION
SYSTEM**

By

Peter George Asaad Youssef

*A thesis submitted to the
University of Birmingham
For the degree of*

Doctor of Philosophy

Department of Mechanical Engineering
School of Engineering
College of Engineering and Physical Sciences
The University of Birmingham
December - 2017

UNIVERSITY OF
BIRMINGHAM

University of Birmingham Research Archive

e-theses repository

This unpublished thesis/dissertation is copyright of the author and/or third parties. The intellectual property rights of the author or third parties in respect of this work are as defined by The Copyright Designs and Patents Act 1988 or as modified by any successor legislation.

Any use made of information contained in this thesis/dissertation must be in accordance with that legislation and must be properly acknowledged. Further distribution or reproduction in any format is prohibited without the permission of the copyright holder.

ABSTRACT

Drinking water shortage is a wide spread problem in many countries which adversely affects the quality of life for millions of people. Although desalination technologies can provide a solution to water shortage problem, they suffer from high energy demand and CO₂ emissions. In the last decade, adsorption desalination technology has attracted interest since it can be driven by waste heat sources resulting in reduced energy requirements and CO₂ emissions. Adsorption desalination requires 1.38kWh.m⁻³ of produced water compared to 8.2 kWh.m⁻³ consumed by Reverse Osmosis and produces CO₂ emissions of 0.64 kg.m⁻³ compared to 3.78 kg.m⁻³ for reverse osmosis. This research work was conducted to enhance the performance of adsorption desalination systems through number of techniques including the use of advanced adsorbent materials known as metal organic frameworks (MOFs), various cycle configurations and operating conditions.

A Simulink model was developed to simulate the heat and mass transfer processes associated with the adsorption/desorption processes, evaporation of seawater and condensation of potable water. For the first time, this model has been used to investigate a number of new adsorbents; "AQSOA-Z02" (the commercial name for silica-aluminophosphates, SAPO-34), "Aluminium Fumarate", "CPO-27Ni" (The commercial name for Co-ordination Polymer of Oslo) and "MIL-101Cr" (The commercial name for Materials Institute Lavoisier) for the purposes of water desalination using adsorption technology as well as cooling as a secondary output. A number of operating parameters have been investigated including; effect of condenser, evaporator and bed's heating secondary fluid temperatures as well as half cycle time.

From these investigations, it was concluded that lowering condenser temperature, enhances cycle performance, therefore, a new system configuration was developed that enables decreasing the condenser temperature by exploiting all or part of the cooling generated by the evaporator. The system comprises of two cycles linked with combined evaporator-condenser while each cycle has two adsorber beds. The system configuration allows for three operating scenarios that can be selected according to desalinated water and cooling requirements. A thermal model was developed using Simulink software to simulate this system and its performance was compared to the conventional double bed adsorption system. It was found that this new system configuration can produce daily up to 15.4 m³ per tonne of adsorbent material which is three folds that of the conventional one.

Two experimental testing facilities, single-bed and double-bed, were developed to investigate two different metal organic framework MOF materials at various operating conditions. As the metal organic framework MOF porous materials are known for their high surface area and exceptional high water adsorption capability, CPO-27Ni was tested in the single bed adsorption system while the double bed adsorption system was initially tested using CPO-27Ni to compare its performance with the single bed then Aluminium Fumarate was packed and tested. It was found that CPO-27Ni is very sensitive to the desorption pressure ratio ($P_{\text{condenser}}/P_{\text{desorber bed}}$) therefore a decrease in the pressure ratio from 0.05 to 0.01 can lead to an increase in specific daily water production (SDWP) and specific cooling power (SCP) by 49% and 35.4% respectively. On the other hand, it was found that Aluminium Fumarate is insensitive to changes in condenser or desorption temperatures where it can work at 65°C desorption temperature and produce SDWP of 16.9 m³ of water per tonne of adsorbent material per day. From these experimental

investigations, it was proved that these two MOF materials, CPO-27Ni and Aluminium Fumarate can result in maximum SDWP of 22.8 and 25.3 $\text{m}^3\cdot\text{tonne}^{-1}\cdot\text{day}^{-1}$ respectively, while the maximum SDWP reported experimentally for Silica-gel is 13.46 $\text{m}^3\cdot\text{tonne}^{-1}\cdot\text{day}^{-1}$. Finally, an experimental study was carried out to assess the effect of fed seawater salinity on the adsorption desalination system performance and it was found that the adsorption desalination system can desalinate seawater with high salinity of 64000 ppm and produce fresh water with salinity as low as 0 ppm.

Dedicated To

My parents for all their love, support and putting me through the best education possible. I appreciate their sacrifices and I wouldn't have been able to get to this stage without them.

ACKNOWLEDGEMENT

Firstly, I would like to thank my supervisor Dr. Raya K. Al-dadah for giving me the opportunity to complete my Ph.D thesis under her supervision, it is truly an honour. I am greatly indebted to her for her help in applying for this project and getting a scholarship. Thank you for all the advice, ideas, moral support and patience in guiding me through this long journey project, and for giving me the opportunity to grow in this field of research.

My sincere gratitude is reserved for Dr. Saad M. Mahmoud for his supervision, continuous support, for his deep insights that helped me at various stages of my research. Special thanks for you for keeping me motivated throughout the writing and editing of the articles bounded in this thesis.

I am extremely grateful to Mr. John Whitehouse (director of Weatherite Holding limited) for sponsoring me for three years in collaboration with the University of Birmingham.

I would like to thank Mr. Simon Rowan for the guidance and support he gave to me, for believing in me during the development and construction of the two adsorption testing facilities. Thank you, Hassan Dakkama, for all your tremendous help in constructing our testing facilities as they have never been built up without you. Thanks also to Mr. Carl Hingley and Mr. Peter Thornton for their advice and help.

Words cannot express the feelings I have for the most important person in my life- my wife Mary. I can honestly say that it was only her determination and constant encouragement that ultimately made it possible for me to see this project through to the end. Finally, I would like to thank my son Thomas and my daughter Carole for their patience and forbearance of saints over the years this thesis has taken.

TABLE OF CONTENTS

Abstract	I
Acknowledgement	V
Table of contents	VI
List of Figures	XII
List of tables	XXII
Nomenclature	XXIV
List of publications	XXVII
CHAPTER 1: Introduction	1
1.1 Introduction	1
1.2 Aims and objectives	2
1.3 Thesis outline	3
CHAPTER 2: Literature review	6
2.1 Introduction	6
2.2 Description of desalination processes	7
2.2.1 Thermally activated processes (heat addition)	7
2.2.2 Thermal heat extraction processes	13
2.2.3 Membrane based water desalination processes.....	15
2.2.4 Chemical water desalination processes	19
2.2.5 Adsorption desalination processes.....	23
2.3 Performance of Desalination processes	25
2.3.1 Brackish or seawater salinity	25
2.3.2 Produced water salinity	25
2.3.3 Type and amount of energy required	27
2.3.4 Environmental impact.....	28

2.3.5	Cost.....	29
2.4	Overview of adsorption desalination Cycles	30
2.4.1	Conventional water desalination system.....	30
2.4.2	Evaporator-Condenser heat recovery water desalination system	33
2.4.3	Water desalination system with integrated evaporator-condenser device	34
2.5	Adsorbent-water working pairs.....	35
2.6	Summary	39
CHAPTER 3: Modelling of Adsorption Desalination cycle		40
3.1	Introduction	40
3.2	Specifications of modelled adsorption desalination system.....	40
3.3	Adsorbent material physical characteristics.....	44
3.4	Adsorption desalination system modelling	45
3.4.1	Adsorbent material modelling	45
3.4.2	Energy balance equations	50
3.4.3	Heat transfer	54
3.4.4	Mass balance equations.....	59
3.4.5	Cycle performance indicator equations	60
3.5	Simulink modelling of the adsorption water desalination system	61
3.5.1	Simulink model validation	64
3.6	Summary	66
CHAPTER 4: Investigation of Operating conditions in Adsorption Desalination Cycle		67
4.1	Introduction	67
4.2	Operating conditions under investigation	67
4.2.1	Effects of bed heating and evaporator water temperature.....	68
4.2.2	Effect of half cycle time	76
4.2.3	Effect of condenser cooling water temperature	83

4.3	Summary	87
CHAPTER 5: Performance investigation of Integrated Adsorption Cycle for Desalination and Cooling..... 90		
5.1	Introduction	90
5.2	System description.....	90
5.3	System modelling.....	94
5.3.1	Evaporator equations (Lower cycle):.....	94
5.3.2	Combined evaporator - condenser equations:.....	95
5.3.3	Condenser equations (Upper cycle):	96
5.3.4	Adsorber bed equations (Upper and Lower cycles):	96
5.3.5	System performance indicators:.....	96
5.4	Results and discussion	98
5.4.1	Proposed cycle results at operating scenarios '1, 2 and 3':.....	98
5.5	Economic Analysis.....	105
5.6	Summary	107
CHAPTER 6: Experimental Investigation of CPO-27Ni performance in single bed adsorption system 109		
6.1	Introduction	109
6.2	Test facility description	109
6.2.1	Adsorber bed	112
6.2.2	Evaporator.....	114
6.2.3	Condenser	116
6.2.4	Chilled water reservoir.....	118
6.2.5	Water chiller.....	119
6.2.6	Water pumps	121
6.2.7	Flow control valves.....	122

6.2.8	Hot and cold water tanks.....	124
6.2.9	Vacuum pumps	126
6.3	Measuring devices	127
6.3.1	Pressure measurements.....	127
6.3.2	Temperature measurements.....	129
6.3.3	Flowrate measurements	132
6.4	Test rig commissioning	133
6.5	Testing procedure	135
6.5.1	Initialization.....	135
6.5.2	Cycling.....	136
6.5.3	Finalizing.....	137
6.6	Repeatability test.....	137
6.7	Validation of the Simulink model.....	139
6.8	Experimental test results.....	141
6.8.1	Effect of switching time.....	141
6.8.2	Effect of half cycle time	142
6.8.3	Effects of evaporator and condenser inlet water temperature	144
6.9	Summary	148

CHAPTER 7: Experimental Investigation of double bed adsorption system using MOF materials 149

7.1	Introduction	149
7.2	Test facility description	149
7.2.1	Adsorber bed	150
7.2.2	Evaporator.....	154
7.2.3	Condenser	157
7.2.4	Freshwater/brine accumulator	158

7.2.5	Water pumps	159
7.2.6	Flow control valves.....	159
7.2.7	Vacuum pump.....	163
7.3	Measuring devices	164
7.4	Test rig commissioning	165
7.5	Testing procedure	165
7.5.1	Initialization.....	166
7.5.2	Cycling.....	167
7.5.3	Finalizing.....	168
7.6	Double bed system compared to single bed system	169
7.7	Experimental test results.....	171
7.7.1	Effect of half cycle time	172
7.7.2	Effect of mass recovery time.....	173
7.7.3	Effects of desorption and evaporator water inlet temperature	175
7.7.4	Effect of inlet seawater salinity	177
7.8	Validation of double-bed Simulink model using Aluminium Fumarate.....	180
7.9	Summary	183
CHAPTER 8: Conclusions and future work.....		184
8.1	Introduction.....	184
8.2	Conclusions.....	185
8.2.1	Comparison between desalination technologies	185
8.2.2	Simulink model development.....	186
8.2.3	Integrated adsorption desalination cycle.....	187
8.2.4	Experimental investigation of single-bed adsorption desalination system.....	188
8.2.5	Experimental investigation of double-bed adsorption desalination system ...	189
8.3	Future work	190

References.....	192
Appendix I.....	205
Appendix II.....	214
Appendix III.....	227

LIST OF FIGURES

Figure 2-1, Classification of desalination technologies [18, 19]	7
Figure 2-2, Schematic diagram for MSF system [18, 34].....	8
Figure 2-3, Schematic diagram for MED system [18, 38].....	10
Figure 2-4, Schematic diagram for MVC system [18, 41]	11
Figure 2-5, Schematic diagram for closed-air open-water heated, HDH system [18, 49].....	12
Figure 2-6, Schematic diagram for direct solar desalination system [18, 55].....	13
Figure 2-7, Schematic diagram for direct freezing desalination system [18, 64].....	14
Figure 2-8, Schematic diagram for indirect freezing desalination system [18, 68]	15
Figure 2-9, Schematic diagram for RO desalination process [18, 70].....	16
Figure 2-10, Schematic diagram for FO desalination system [18, 73].....	17
Figure 2-11, Schematic diagram for NF desalination system [18, 78].....	18
Figure 2-12, Schematic diagram for ED desalination system [18, 80].....	19
Figure 2-13, Schematic diagram for I.Ex desalination system [18, 83]	20
Figure 2-14, Schematic diagram for G.HYD desalination system [18, 87]	22
Figure 2-15, Schematic diagram for LLE desalination system [18, 90].....	23
Figure 2-16, Schematic of a double-bed Adsorption desalination system [93]	24
Figure 2-17, Desalination capabilities of different desalination technologies according to feed water salinity, [18, 31, 32, 37, 42, 99-105].....	26
Figure 2-18, Desalination capabilities of different desalination technologies according to produced water salinity, [5, 18, 28, 31, 100, 106-114]	26
Figure 2-19, Energy needs for various desalination technologies, [18, 99, 107, 118-126].....	28
Figure 2-20, CO ₂ emissions (kg.m ⁻³) for various desalination technologies [18].....	29

Figure 2-21, Potable water production cost (US\$.m ⁻³), for various desalination technologies [18, 31, 99, 119-121, 127-133]	30
Figure 2-22, Schematic of a conventional double-bed adsorption desalination system [134].	32
Figure 2-23, Schematic of a 4-bed adsorption desalination system with master-slave arrangement [7]	32
Figure 2-24, Schematic of a 4-bed adsorption desalination system with heat recovery circuit between evaporator and condenser [95].....	34
Figure 2-25, Schematic of an advanced desalination cycle with integrated evaporator-condenser device [33]	35
Figure 3-1, Pictorial view for the modelled adsorption machine [139]	41
Figure 3-2, Schematic diagram for the modelled adsorption system [11]	41
Figure 3-3, Rectangular finned tube adsorber bed [139], (a) Schematic, (b) Pictorial view	43
Figure 3-4, Forming process of finned tube heat exchanger [152]	43
Figure 3-5, Isotherms of adsorbent materials under investigation at 25°C.....	46
Figure 3-6, Schematic diagram of the adsorber bed.....	50
Figure 3-7, Schematic diagram of the evaporator.....	51
Figure 3-8, Schematic diagram of the condenser.....	53
Figure 3-9, Schematic of the heat transfer resistances in the adsorber bed.....	55
Figure 3-10, Schematic of heat transfer resistances in the evaporator.....	56
Figure 3-11, Schematic of heat transfer resistances in the condenser	58
Figure 3-12, Simulink model of the adsorption desalination cycle.....	62
Figure 3-13, Flow diagram for the Simulink model of the 2-bed adsorption desalination cycle	63

Figure 3-14, Validation of the double bed adsorption desalination Simulink model, temperature profiles of adsorber beds, evaporator and condenser [94]	65
Figure 3-15, Comparison between experimental and numerical results of SDWP for Silica-gel	65
Figure 4-1, Effect of desorption and evaporator water temperatures on SDWP (a), SCP (b) and OCR (c) of double-bed adsorption desalination system (Silica-gel)	69
Figure 4-2, Effect of desorption and evaporator water temperatures on SDWP (a), SCP (b) and OCR (c) of double-bed adsorption desalination system (AQSOA-Z02).....	71
Figure 4-3, Effect of desorption and evaporator water temperatures on SDWP (a), SCP (b) and OCR (c) of double-bed adsorption desalination system (Al-Fumarate).....	72
Figure 4-4, Effect of desorption and evaporator water temperatures on SDWP (a), SCP (b) and OCR (c) of double-bed adsorption desalination system (CPO-27Ni).....	74
Figure 4-5, Effect of desorption and evaporator water temperatures on SDWP (a), SCP (b) and OCR (c) of double-bed adsorption desalination system (MIL-101Cr).....	75
Figure 4-6, Effect of half cycle time and desorption water temperature on SDWP (a), SCP (b) and OCR (c) of double-bed adsorption desalination system (Silica-gel)	77
Figure 4-7, Effect of half cycle time and desorption water temperature on SDWP (a), SCP (b) and OCR (c) of double-bed adsorption desalination system (AQSOA-Z02).....	78
Figure 4-8, Effect of half cycle time and desorption water temperature on SDWP (a), SCP (b) and OCR (c) of double-bed adsorption desalination system (AL-Fumarate)	79
Figure 4-9, Effect of half cycle time and desorption water temperature on SDWP (a), SCP (b) and OCR (c) of double-bed adsorption desalination system (CPO-27Ni).....	81
Figure 4-10, Effect of half cycle time and desorption water temperature on SDWP (a), SCP (b) and OCR (c) of double-bed adsorption desalination system (MIL-101Cr).....	82

Figure 4-11, Effect of condenser and evaporator water temperatures on SDWP for Silica-gel (a), AQSOA-Z02 (b), AL-Fumarate (c), CPO-27Ni (d) and MIL-101Cr (e)	85
Figure 4-12, Effect of condenser and evaporator water temperatures on SCP for Silica-gel (a), AQSOA-Z02 (b), AL-Fumarate (c), CPO-27Ni (d) and MIL-101Cr (e)	86
Figure 4-13, Effect of condenser and evaporator water temperatures on OCR for Silica-gel (a), AQSOA-Z02 (b), AL-Fumarate (c), CPO-27Ni (d) and MIL-101Cr (e)	88
Figure 4-14, Recommended adsorbent materials according to operating conditions and application.....	89
Figure 5-1, Schematic of a conventional double-bed adsorption desalination system [11].....	91
Figure 5-2, A schematic of the integrated adsorption desalination and cooling cycle [11]	92
Figure 5-3, Schematic diagram for the operating modes of the new integrated adsorption cycle with desalinated water produced from both condensers at all scenarios [11]	93
Figure 5-4 Specific daily water production (a) and Specific cooling power (b) for scenario '1' at various lower evaporator inlet water temperatures [11]	99
Figure 5-5 Specific daily water production (a) and Specific cooling power (b) for scenario '2' at various upper cycle evaporator inlet water temperatures [11]	101
Figure 5-6 Specific daily water production in case of scenario '3' [11].....	102
Figure 5-7 Overall conversion ratio at various lower and upper evaporator inlet water temperatures for scenarios '1' (a) and '2' (b) [11]	103
Figure 5-8 Comparison of uptake between conventional and proposed systems at operating scenarios, '1, 2, and 3' respectively [11]	104
Figure 6-1, Schematic diagram for the single bed test facility	111
Figure 6-2, Pictorial view of the single bed test facility [186]	112

Figure 6-3, Finned tube heat exchangers, Pictorial view(a &b), Schematic diagram (c) [186]	113
Figure 6-4, Pictorial view for the evaporator with different inlet and outlet ports and connections.....	115
Figure 6-5, Pictorial view for the evaporator chilled water spiral copper coil [12]	115
Figure 6-6, Pictorial view for the condenser with different inlet and outlet ports and connections.....	117
Figure 6-7, Pictorial view for the condenser cooling water helical copper coil.....	117
Figure 6-8, Pictorial view of the fresh water collection system	118
Figure 6-9, Pictorial view for the chilled water reservoir	119
Figure 6-10, Pictorial view of the CU-700 water heater/chiller.....	120
Figure 6-11, Adsorber bed circulating water pump, "SS-9R-MD"	121
Figure 6-12, Evaporator chilled water circuit water pump, "MSP-3"	121
Figure 6-13, Manual ball valve, "FIG.966S WRAS"	122
Figure 6-14, Solenoid valve, "SMV2530"	123
Figure 6-15, National Instruments control board, "NI 6008"	123
Figure 6-16, User interface of the "Labview" software to control the solenoid valves.....	124
Figure 6-17, Electric circuit of the control of solenoid valves	124
Figure 6-18, Pictorial view of the hot water tank.....	125
Figure 6-19, Pictorial view of the cold water tank.....	126
Figure 6-20, Vacuum pumps used in the single bed testing facility	127
Figure 6-21, Pressure transducer "PXM319-0.35AI"	128
Figure 6-22, Pressure-current relationship of the pressure transducer "PXM319-0.35AI" ...	128
Figure 6-23, Wiring diagram of the pressure transducer connection to the data logger	128

Figure 6-24, Assembly of thermocouple compression fitting	129
Figure 6-25, Assembly of thermocouple KF-flanged feedthrough	130
Figure 6-26, Assembly of RTD, PT100, thermocouple compression fitting	131
Figure 6-27, Data logger used for logging temperature and pressure readings, “dataTaker DT85”	132
Figure 6-28, Flow meter of adsorber bed water circuit.....	132
Figure 6-29, Vacuum inspection in pipe fittings; (a) no leakage, (b) leakage is detected	133
Figure 6-30, Vacuum inspection using the diaphragm technique	134
Figure 6-31, Adsorber bed, evaporator and condenser temperatures of repeatability test...	138
Figure 6-32, Adsorber bed, evaporator and condenser pressures of repeatability test	139
Figure 6-33, Validation of the single bed adsorption desalination Simulink model using CPO-27Ni, temperature profiles of adsorber bed, evaporator and condenser [186].....	140
Figure 6-34, Comparison between experimental and simulation results of SDWP and SCP for CPO-27Ni [186].....	140
Figure 6-35, Temperature profile of adsorber bed through 5 consecutive cycles at various switching times [186].....	142
Figure 6-36, Specific daily water production and amount of water collected per cycle for various half cycle times [186]	143
Figure 6-37, Specific cooling power for various half cycle times [186].....	144
Figure 6-38, Specific daily water production at various evaporator and condenser water inlet temperatures [186]	145
Figure 6-39, Specific cooling power for various evaporator and condenser water inlet temperatures [186]	146

Figure 6-40, Overall conversion ratio of Single-bed system at various evaporator and condenser water inlet temperatures.....	146
Figure 6-41, Temperature profiles of Adsorber bed (a), Evaporator (b) and Condenser (c) at condenser water inlet temperatures of 5°C (L) and 30°C (H) with an accuracy of $\pm 0.3^\circ\text{C}$ [186]	147
Figure 7-1, Schematic of the double-bed adsorption system.....	151
Figure 7-2, Testing facility of the double-bed adsorption system.....	152
Figure 7-3, Adsorber bed; (a) Cylinder, (b) Top plate.....	153
Figure 7-4, Finned tube heat exchangers of the adsorber bed	153
Figure 7-5, Pictorial view for the evaporator of the double bed system with different connecting ports.....	155
Figure 7-6, Pictorial view of the evaporator chilled water helical copper coil.....	156
Figure 7-7, Seawater feed system.....	156
Figure 7-8, Seawater spraying nozzle in the evaporator	156
Figure 7-9, Pictorial view for the condenser of the double bed system with different connecting ports.....	157
Figure 7-10, Pictorial view of the condenser spiral conical copper coil	157
Figure 7-11, Freshwater/brine accumulator	158
Figure 7-12, Adsorber and desorber bed water pumps.....	159
Figure 7-13, Manual ball valves connected to the manifold	160
Figure 7-14, Electrically-actuated ball valve for bed heating/cooling water circuit	160
Figure 7-15, Electrically-actuated manual ball valve for water vapor circuit	161
Figure 7-16, National Instruments chassis and relay control board	162

Figure 7-17, User interface of the “Labview” software to control the actuated ball valves ..	163
Figure 7-18, “DVP” Vacuum pump.....	164
Figure 7-19, Salinity sensor, “CDH-45”	165
Figure 7-20, Comparison of specific daily water production for Single and Double bed adsorption systems using (CPO-27Ni).....	170
Figure 7-21, Comparison of specific cooling power for Single and Double bed adsorption systems using (CPO-27Ni).....	170
Figure 7-22, Specific daily water production and amount of produced fresh water per cycle at various half cycle times using (Al-Fumarate).....	172
Figure 7-23, Specific cooling power at different half cycle times using (Al-Fumarate)	173
Figure 7-24, Specific daily water production and amount of produced fresh water per cycle at various mass recovery times using (Al-Fumarate)	174
Figure 7-25, Specific cooling power at different mass recovery times using (Al-Fumarate)	175
Figure 7-26, Specific daily water production at various desorption and evaporator water inlet temperatures using (Al-Fumarate)	176
Figure 7-27, Specific cooling power at various desorption and evaporator water inlet temperatures using (Al-Fumarate).....	177
Figure 7-28, Overall conversion ratio of double-bed system at various desorption and evaporator water inlet temperatures using (Al-Fumarate).....	177
Figure 7-29, Salinity of feed seawater and discharged brine at different test runs using (Al-Fumarate)	179
Figure 7-30, Specific daily water production and specific cooling power at different fed seawater salinity using (Al-Fumarate).....	180

Figure 7-31, Validation of the double bed adsorption desalination Simulink model using Aluminium Fumarate, temperature profiles of adsorber beds, evaporator and condenser .	181
Figure 7-32, Comparison between experimental and simulation results of SDWP and SCP for Aluminium Fumarate.....	182
Figure A.I- 1, Main block diagram of the double bed system.....	205
Figure A.I- 2, Simulink sub blocks of the Adsorption bed block (Double bed Cycle)	206
Figure A.I- 3, Simulink sub blocks of the Evaporator block (Double bed Cycle)	207
Figure A.I- 4, Simulink sub blocks of the Condenser block (Double bed Cycle).....	208
Figure A.I- 5, Main block diagram of the integrated adsorption desalination/cooling cycle	209
Figure A.I- 6, Simulink sub blocks of the Adsorber bed block (Integrated Cycle)	210
Figure A.I- 7, Simulink sub blocks of the Lower Evaporator block (Integrated Cycle)	211
Figure A.I- 8, Simulink sub blocks of the Combined Evaporator-Condenser block (Integrated Cycle)	212
Figure A.I- 9, Simulink sub blocks of the Upper Condenser block (Integrated Cycle).....	213
Figure A.II- 1, Thermocouples calibration kit.....	215
Figure A.II- 2, Pressure transducer calibration kit	215
Figure A.II- 3, Calibration chart for different types of thermocouples, Single-bed system ..	217
Figure A.II- 4, Calibration chart for adsorber bed pressure transducer, Single-bed system.	217
Figure A.II- 5, Calibration chart for different types of thermocouples, Double-bed system	220
Figure A.II- 6, Calibration chart for adsorber beds' pressure transducers, Double-bed system	221
Figure A.III- 1, Front panel of the Labview code.....	228
Figure A.III- 2, Main block diagram of the Labview control code.....	229
Figure A.III- 3, Case no. 1, "Drying"	230

Figure A.III- 4, Case no. 2, “Adsorber bed temperature preparation before cycle starting”	230
Figure A.III- 5, Case no. 3, “Switching 1”	231
Figure A.III- 6, Case no. 4, “Adsorption-Desorption”	231
Figure A.III- 7, Case no. 5, “Mass recovery 1”	232
Figure A.III- 8, Case no. 6, “Switching 2”	232
Figure A.III- 9, Case no. 7, “Desorption-Adsorption”	233
Figure A.III- 10, Case no. 8, “Mass recovery 2”	233

LIST OF TABLES

Table 2-1, Adsorbent/Water working pairs as in Literature	37
Table 2-2, Published research work on adsorption for desalination and cooling purposes [11]	38
Table 3-1, Specifications of the modelled adsorption system [139]	42
Table 3-2, Physical properties of adsorbent materials [154-163]	45
Table 3-3, Dubinin-Astakhov equation constants for Silica-gel and CPO-27Ni [5, 172].....	47
Table 3-4, LDF equation constants for the adsorbent materials [5, 8, 12, 159].....	49
Table 3-5, Operating conditions of the double bed validation test using Silica-gel [99].....	64
Table 3-6, Error in the validation of the double bed adsorption desalination cycle using Silica-gel	66
Table 5-1, System outputs at different operating modes [11]	91
Table 5-2, Cost estimation of cycle outputs [11]*	107
Table 5-3, Proposed cycle outputs compared to double-bed conventional cycle [11]	108
Table 6-1 Heat exchanger characteristics and dimensions (single bed system) [12]	114
Table 6-2, Specifications of water chiller, "CU-700" [12, 188].....	120
Table 6-3, Operating parameters of repeatability test.....	138
Table 6-4, Water and cooling production of repeatability test	138
Table 6-5, Error in the validation of the single bed adsorption desalination cycle using CPO-27Ni [186].....	141
Table 7-1, Heat exchanger characteristics and dimensions (double-bed system).....	154
Table 7-2, Automated valves On/Off schedule during system operation	162
Table 7-3, Operating conditions of the CPO-27Ni test on double bed system	169

Table 7-4, Operating conditions of the double bed system parametric study.....	171
Table 7-5, Sea salt chemical characterization	179
Table 7-6, Operating conditions of the validation test using Aluminium Fumarate	181
Table 7-7, Error in the validation of the double bed adsorption desalination Simulink model using Aluminium Fumarate	182
Table A.II- 1, Uncertainties of all thermocouples of the single bed adsorption system.....	218
Table A.II- 2, Uncertainties of pressure transducers' measurements of the single-bed adsorption testing facility	219
Table A.II- 3, Uncertainties of all thermocouples of the double bed adsorption system.....	222
Table A.II- 4, Uncertainties of pressure transducers' measurements of the double-bed adsorption testing facility	223

NOMENCLATURE

A	Area	(m ²)
c	Uptake	(kg.kg ⁻¹)
c*	Equilibrium uptake	(kg. kg ⁻¹)
c _o	Maximum uptake	(kg. kg ⁻¹)
c _p	Specific heat at constant pressure	(kg. kg ⁻¹ .K ⁻¹)
COP	Coefficient of performance	(-)
d	Diameter	(m)
E	Characteristic energy	(kJ.mol ⁻¹)
g	Gravitational acceleration	(m.s ⁻²)
h	Convective heat transfer coefficient	(kJ.m ² .K ⁻¹)
h _{fg}	Latent heat	(kJ.kg ⁻¹)
k	Thermal conductivity	(W.m ⁻¹ .K ⁻¹)
k _o	Pre-exponential constant	(s ⁻¹)
L	Tube length	(m)
LMTD	Logarithmic mean temperature difference	(K)
M	Mass	(kg)
<i>m</i>	Mass flow rate	(kg.s ⁻¹)
Nu	Nusselt number	(-)
OCR	Overall conversion ratio	(-)
P	Pressure	(kPa)
PP	Electric pumping power	(kJ.s ⁻¹)
Pr	Prandtl number	(-)
PR	Performance ratio	(-)
Q	Rate of heat transfer	(kJ.s ⁻¹)
Q _{st}	Isosteric heat of adsorption	(kJ.kg ⁻¹)
R	Universal gas constant	(kJ.kmol ⁻¹ .K ⁻¹)
Re	Reynolds number	(-)
SCP	Specific cooling power	(W.kg ⁻¹)

SDWP	Specific daily water production	$(\text{m}^3 \cdot \text{tonne}^{-1} \cdot \text{day}^{-1})$
t	Time	(s)
T	Temperature	(K)
TDS	Total dissolved solids	(ppm)
U	Overall heat transfer coefficient	$(\text{kJ} \cdot \text{m}^2 \cdot \text{K}^{-1})$
v	Water velocity in pipe	$(\text{m} \cdot \text{s}^{-1})$
X	Salt concentration	$(\text{kg}_{\text{salt}} \cdot \text{kg}_{\text{seawater}}^{-1})$
z	Flag for adsorption/desorption processes	(-)

Greek symbols

θ	Flag for seawater charging	(-)
γ	Flag for brine discharge	(-)
μ	Dynamic viscosity	(Pa.s)
η	Efficiency	(-)
ρ	Density	$(\text{kg} \cdot \text{m}^{-3})$
σ	Surface tension	$(\text{N} \cdot \text{m}^{-1})$
τ	No of cycles per day	(-)

Subscripts

<i>a</i>	Adsorbent material
<i>abe</i>	Adsorbed water vapor
<i>ads</i>	Adsorption
<i>brine</i>	Highly concentrated seawater
<i>chilled</i>	Water flowing in the evaporator coil
<i>Cond.</i>	Condenser

<i>cw</i>	Cooling Water
<i>d</i>	Distillate water
<i>Des.</i>	Desorption
<i>Evap.</i>	Evaporator
<i>f</i>	Liquid
<i>g</i>	Vapor
<i>hw</i>	Heating Water
<i>HX</i>	Heat exchanger
<i>in</i>	inlet
<i>ads</i>	adsorber bed
<i>des</i>	desorber bed
<i>out</i>	outlet
<i>s</i>	Seawater

LIST OF PUBLICATIONS

Parts of this research work have been published in peer reviewed journals and international conferences. Papers numbered 1, 4, 8, 9, 11 and 12 are part of chapters 3 and 4. Papers numbered 2 and 7 are part of chapter 2. Paper number 3 is part of chapter 5 while papers numbered 5, 6 and 10 are part of chapter 6.

Journal Publications

- 1) P. Youssef, S. Mahmoud, R. AL-Dadah, "Performance analysis of four bed adsorption water desalination/refrigeration system, comparison of AQSOA-Z02 to silica-gel". *Desalination*, 2015, Vol. 375, pp 100- 107. (Impact Factor: 5.527)
- 2) P. Youssef, S. Mahmoud, R. AL-Dadah, "Seawater desalination technologies". *International Journal of Innovation Sciences and Research*, 2015, Vol. 4, No.8, pp 402-422. (Impact Factor: 1.255)
- 3) P. Youssef, S. Mahmoud, R. AL-Dadah, "Numerical simulation of combined adsorption desalination and cooling cycles with integrated evaporator/condenser". *Desalination*, 2016, Vol. 392, pp 14- 24. (Impact Factor: 5.527)
- 4) E. Elsayed, R. Al-Dadah, S. Mahmoud, P. Anderson, A. Elsayed, P. Youssef, "CPO-27(Ni), aluminium fumarate and MIL-101(Cr) MOF material for adsorption water desalination". *Desalination*, 2017, Vol. 406, pp 25- 36. (Impact Factor: 5.527)
- 5) P. Youssef, H. Dakkama, S. Mahmoud, R. AL-Dadah, "Experimental investigation of adsorption water desalination/cooling system using CPO-27Ni MOF". *Desalination*, 2017, Vol. 404, pp 192- 199. (Impact Factor: 5.527)

- 6) H. Dakkama, P. Youssef, R. AL-Dadah, S. Mahmoud, "Adsorption ice making and water desalination system using metal organic frameworks/water pair". Energy Conversion and Management, 2017, Vol. 142, pp 53- 61. (Impact Factor: 5.589)

Conference Publications

- 7) P. Youssef, R. AL-Dadah, S. Mahmoud, "Comparative Analysis of Desalination Technologies", The 6th Int. conference on applied energy, ICAE 2014, Taipei Taiwan.
- 8) P. Youssef, R. AL-Dadah, S. Mahmoud, "Effect of Evaporator and Condenser Temperatures on the Performance of Adsorption Desalination Cooling Cycle". The 7th Int. conference on applied energy, ICAE 2015, Abu Dhabi, UAE.
- 9) P. Youssef, S. Mahmoud, R. AL-Dadah, "Effect of Evaporator Temperature on the Performance of Water Desalination / Refrigeration Adsorption System Using AQSOA-Z02". The 17th Int. Conference on Desalination and Renewable Energy, ICDRE 2015, Copenhagen, Denmark.
- 10) H. Dakkama, P. Youssef, R. AL-Dadah, S. Mahmoud, W. Al-Shohani "Adsorption ice making and freeze water desalination using Metal Organic Framework materials". Int. Conference for Students on Applied Engineering, ICSAE 2016, New Castle, UK.
- 11) P. Youssef, S. Mahmoud, R. AL-Dadah, E. Elsayed, O. El-Samni, "Numerical Investigation of Aluminum Fumarate MOF adsorbent material for adsorption desalination/cooling application". The 9th Int. conference on applied energy, ICAE 2017, Cardiff, UK.
- 12) E. Elsayed, R. AL-Dadah, S. Mahmoud, P. Anderson, A. Hassan, P. Youssef, "Numerical Investigation of MIL-101(Cr)/Gro composite performance in adsorption cooling systems". The 9th Int. conference on applied energy, ICAE 2017, Cardiff, UK.

CHAPTER 1: INTRODUCTION

1.1 Introduction

Despite the fact that 70% of planet earth is covered with water, 97.5% of the world water resources are salty and 2.5% are fresh water. Oceans, seas and some lakes are the reservoirs of salty water while 30% of the fresh water is stored underground and 70% is capped in mountainous regions, Antarctic and Arctic in the form of ice and snow and only 0.3% is usable by humans [1, 2]. The World Health Organization (WHO) has reported that around the world, there are 2.4 billion people suffering from limited access to fresh water while 884 million have no access [3]. With this world population and limited fresh water resources, desalination can fill in the increasing gap between the limited fresh water sources and the increasing needs to ensure sustainable life for all world population.

Various desalination technologies are used including thermal, membrane and chemical systems [4]. However, factors like increased energy demand associated with high production cost and emissions, resulted in limiting the use of desalination technologies. Recently, investigations have been conducted on adsorption technology for purpose of water desalination where low temperature waste heat (50–85°C) or solar energy can be utilized while using environmentally friendly refrigerants to produce potable water thus reducing energy consumption, cost and CO₂ emissions [5, 6].

Adsorption desalination system is an open system thermodynamic cycle formed of four thermodynamic processes namely; evaporation, adsorption, desorption and condensation [7]. Seawater is fed into the evaporator where it boils generating vapor which is then adsorbed by the adsorbent material [8]. Evaporation of the seawater results from the

adsorbing action of the adsorbent material in addition to the supplied heat load at temperature of 10°C to 30°C provided by the chilled water flowing in the evaporator coil which stabilizes evaporation temperature. Adsorbing process is an exothermic process therefore cooling water flows inside the adsorber bed to absorb the generated heat of adsorption. To release the adsorbed water vapor, the adsorbent material is heated and the generated water vapor is directed to the condenser. Another cooling circuit exists in the condenser where water vapor is condensed and the freshwater is collected then pumped out of the condenser [9]. Another considerable by-product of the cycle is the cooling obtained from the evaporator where flowing chilled water temperature drops down as a result of the evaporation process [10, 11].

All published work shows that “Silica-gel” was the only adsorbent used in adsorption desalination systems [11]. However, there has been advancement in other adsorbent materials like Zeolites and metal organic framework materials. Metal Organic Framework (MOF) materials are a new class of porous materials that have high surface area with exceptionally high water adsorption capabilities [12]. Although many MOF materials have been developed in the literature [13-17], only few MOFs are commercially available and in large quantities. CPO-27Ni and Aluminium Fumarate are two MOF materials with higher water uptake values than silica gel in the range of partial pressure ratios suitable for water desalination and cooling production applications.

1.2 Aims and objectives

The main aim of this PhD work is to develop an efficient two-bed adsorption desalination system using advanced metal organic framework adsorbent materials (MOF). To achieve this aim, the following objectives have been identified:

1. Review of experimental and numerical research work on adsorption desalination cycles and identifying the available adsorbents/water working pairs.
2. Investigating different adsorption desalination cycle configurations working with different adsorbents at various operating conditions.
3. Developing a new adsorption cycle that can produce higher quantities of potable water through better utilization of cooling effects produced during cycle operation.
4. Understanding the operating process of adsorption desalination systems by modifying an existing single bed adsorption system to work for desalination purpose.
5. Developing a complete fully-automated double-bed system that is capable of accommodating different types of adsorbent materials and investigating their performance at various operating conditions.

1.3 Thesis outline

This thesis consists of eight chapters; the first chapter is an introduction presenting the aim and objectives of the research work and a brief outline of the thesis.

The second chapter is the literature review where fourteen desalination technologies are studied and their working principles are presented. Then, a comparison between all these techniques is conducted in terms of their capabilities to produce potable water with minimum salinity from the maximum feed water salinity in addition to water production cost, energy usage and CO₂ emissions. Finally, a review on available adsorbent/water pairs has been conducted in addition to the adsorption desalination cycles available in the literature.

The third chapter describes the developed Simulink model that is used to simulate a full sized double-bed adsorption desalination machine. To model the behaviour of the adsorbent material, the adsorption characteristics equations have been presented for five different adsorbent materials namely; Silica-gel, AQSOA-Z02, Al-Fumarate, CPO-27Ni and MIL-101Cr. In addition, the governing energy and mass transfer equations have been presented to predict the behaviour of the adsorber/desorber bed, evaporator and condenser which form the adsorption desalination systems. Finally, the developed Simulink model was validated against the published experimental results of Silica-gel.

Chapter four present the results of the Simulink model where the above mentioned five adsorbents are investigated using double-bed adsorption system at different operating conditions. The operating conditions under investigation includes effect of condenser, evaporator and bed's heating secondary fluid temperatures on adsorption cycle outputs for the purpose of seawater desalination mainly and for cooling as a by-product.

Chapter five describes the modelling of a new integrated adsorption cycle developed to produce larger amount of water than the conventional double-bed system. The theoretical principle of this cycle is decreasing the condenser temperature by partially or fully utilization of the cooling effect obtained from the evaporator, which leads to enhancing the system performance. AQSOA-Z02 is the adsorbent under investigation in this system, which is studied at different evaporator temperatures ranging from 5 to 20°C.

Chapter six describes the first test rig which is a single-bed adsorption system in terms of construction, commissioning and operation. This test rig is used to investigate the performance of a MOF material, CPO-27Ni, at different evaporating and condensing

temperatures. In addition, validation of a developed single-bed Simulink model is presented using the obtained data from CPO-27Ni investigations.

Chapter seven presents the development of a fully-automated double-bed adsorption desalination system in terms of construction, commissioning and operation. Initially, CPO-27Ni is tested in this system and a comparison between the single and double bed systems performances is performed. Then another MOF adsorbent material called Aluminium Fumarate is tested in this system at different heating and evaporating temperatures in addition to investigating the effect of feed water salinity on system performance. Furthermore, validation of the developed double-bed Simulink model is presented using the obtained data from Aluminium Fumarate investigations.

Finally, chapter eight concludes the conclusions from this extensive study and summarizes the main findings then few points are suggested for future work for further improving the performance of adsorption desalination systems.

CHAPTER 2: LITERATURE REVIEW

2.1 Introduction

Many areas around the world are suffering from high weather temperature and inadequate fresh water resources. Therefore, seawater desalination and air conditioning are becoming increasingly needed. Many technologies can be used to fulfil these needs, but with high energy consumption, adverse environmental effects and high cost [18, 19].

Desalination technologies can be categorized into three main types; thermal, membrane and chemical [19]. In thermally activated techniques, salt is separated from seawater either by heating seawater to boil (phase change; liquid to vapor) or by cooling it to freeze (phase change; liquid to solid). For membrane-based systems, salt is separated from seawater by applying either pressure or an electric field to the salty water forcing only pure water to pass through the membrane and salts remain behind. Chemical based techniques depend on chemical concentration differences rather than pressure differences or phase change as in other technologies [18-22].

Under thermally-based desalination systems number of processes exist such as multi-stage flash (MSF), multi-effect distillation (MED), mechanical vapor compression (MVC), humidification - dehumidification (HDH), solar distillation (SD) and freezing desalination (Frz) [18, 19, 23, 24]. About 40% of the distilled water around the world is produced using one of these thermal methods [25]. Membrane based systems use permeable membranes made of polymers that allow only fresh water molecules to penetrate while salts remain as a waste [18, 19, 26-28]. These membrane-based systems include reverse osmosis (RO), forward

osmosis (FO), nanofiltration (NF) and electro-dialysis (ED) [18, 19, 29]. Techniques such as ion-exchange (I.Ex), gas hydrate (G.Hyd) and liquid–liquid extraction (LLE) are examples of chemically-based desalination systems [18, 19, 30-32].

Recently, investigations have been conducted on adsorption technology for the purpose of water desalination application where an adsorbent porous material is used to adsorb the water vapor then it releases it again where fresh water is collected in a condenser [18, 19, 33].

Figure 2-1 shows a diagram for the aforementioned desalination technologies [18, 19]. The next sections (2.2 and 2.3) will include description to each one of these desalination techniques then an assessment to these techniques will be carried out in terms of cost, energy and CO₂ emissions.

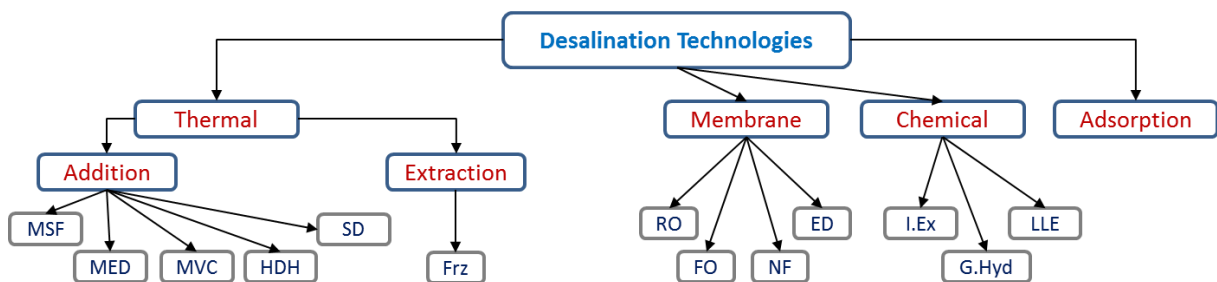


Figure 2-1, Classification of desalination technologies [18, 19]

(MSF) Multi stage flash	(MED) Multi-effect distillation	(MVC) Mechanical vapor compression
(SD) Solar distillation	(Frz) Freezing desalination	(HDH) Humidification - dehumidification
(RO) Reverse osmosis	(FO) Forward osmosis	(NF) Nanofiltration
(ED) Electro-dialysis	(I.Ex) Ion-exchange	(G.Hyd) Gas hydrate
(LLE) Liquid–liquid extraction		

2.2 Description of desalination processes

2.2.1 Thermally activated processes (heat addition)

Multi stage flash, (MSF) has been extensively utilized for many years until it became one of the widest used technologies around the world [4, 18]. Such systems comprise of two main

sections as shown in Figure 2-2 [18, 34], heat addition devices and heat recovery devices. Firstly, seawater is preheated in the condenser utilizing the latent heat released from the condensation of the distilled water. Secondly, seawater is heated further in the brine heater heat exchanger where steam is provided from a steam power plant [18, 35] to heat the seawater flowing inside tubes and then seawater is directed to the flashing chamber. As flashing chambers operate at vacuum pressure levels, seawater flash when fed into them and the resulting vapor rises to the condenser where freshwater is obtained then collected and stored in a tank. In such systems, a number of consecutive flashing chambers exist (15 to 40) and their pressure decreases from one to another allowing decrease in evaporation temperature of the seawater as well as ensuring higher recovery rates of seawater [18, 35, 36]. Finally, highly concentrated brine is extracted from the last flashing chamber. MSF systems can desalinate seawater with high salinity of 60 – 70 ppt while the resulting freshwater has a salinity of 0.01 ppt [18, 34].

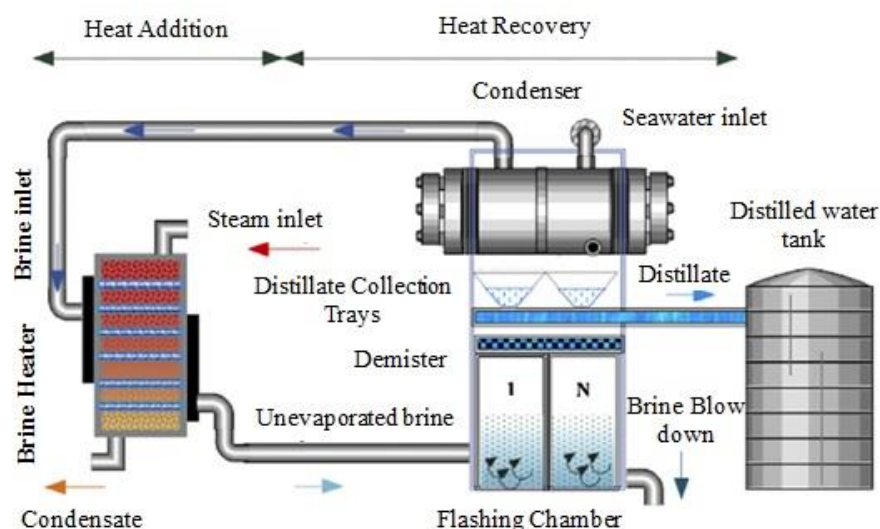


Figure 2-2, Schematic diagram for MSF system [18, 34]

Multi effect desalination, (MED) is similar to MSF where it depends on seawater evaporation at different zones and the remaining concentrated brine is collected and extracted from the system. However, differences lie in the evaporation technique and heat transfer processes [18, 37]. As shown in Figure 2-3 [18, 38], MED plant consists basically of flashing boxes, number of effects (stages) and condenser. Seawater is firstly preheated in the condenser where the water vapor produced from the last stage condenses and its heat of condensation is utilized to heat the incoming seawater. Exiting from condenser, seawater is sprayed at all effects forming a mist that fall over tubes positioned horizontally with a heating fluid flowing inside. The resulting water vapor rises up then it is directed to the next effect to work as a heat source. The tubes at each effect are heated by external source of steam in the first stage but in the remaining stages, the evaporated seawater from the preceding stage is the source of heating [18].

Heating steam is provided from turbines of steam power plants, special boiler or from waste heat [18, 39]. As water vapor passes inside tubes, it loses heat while heating up the sprayed mist leading to water vapor condensation in tubes which is then flashed in flashing boxes. Flowing through these consecutive desalination effects, evaporation pressure and temperature decrease until the final effect is reached where exiting vapor in addition to vapor from flashing boxes are forwarded to the condenser so fresh water can be collected [18, 40].

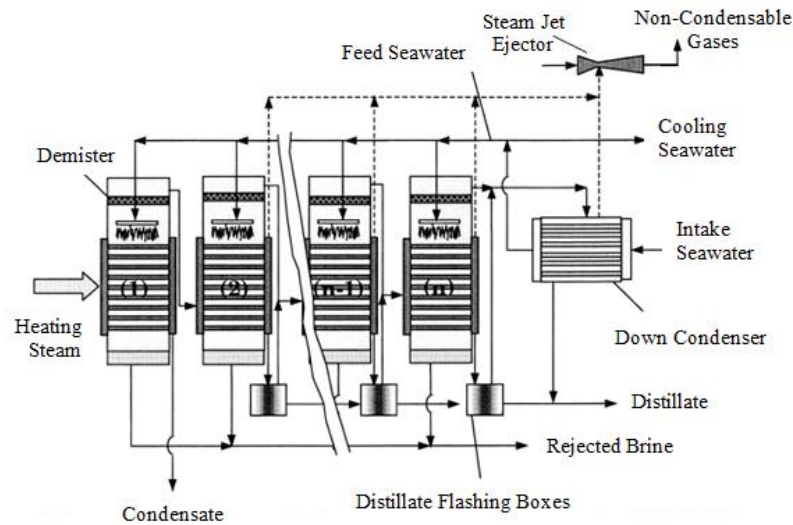


Figure 2-3, Schematic diagram for MED system [18, 38]

Mechanical vapour compression, (MVC) is one of the thermal desalination processes that rely on evaporation-condensation processes. As shown in Figure 2-4 [18, 41], the primary elements of such systems are the mechanical compressor, the evaporator/condenser unit and heat exchanging devices that act as preheaters for seawater. Firstly, the seawater stream is split to feed two heat exchangers to recover the thermal energy of rejected brine and condensed distilled water. Then, seawater is pumped and sprayed in the evaporator/condenser device forming mist that falls on heating tubes which results in steam that rises up then it is forwarded to the compressor. The compressed steam is forced to pass through the tubes of the evaporator/condenser device to heat the sprayed seawater and accordingly, distilled water starts to form as condensate inside tubes. In these systems, a vacuum pump is needed to extract any no-condensable gases from the system [18, 41-47].

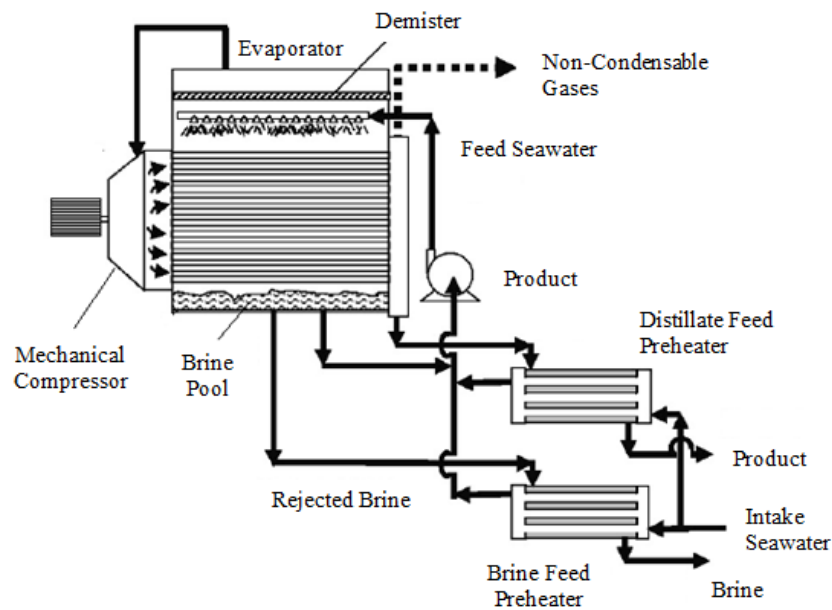


Figure 2-4, Schematic diagram for MVC system [18, 41]

The humidification-dehumidification (HDH) process is similar to the rain cycle that occurs in nature. Saline water is evaporated then air carries this pure water vapor (humidification process) which is condensed later to obtain distillate water (dehumidification process), Figure 2-5 [18, 48, 49]. The principle idea of these systems depends on the increasing ability of dry air to carry water vapor and heat energy with the elevation of its temperature. For example, 1 kg of dry air is able to carry an amount of 0.5 kg of water vapor and thermal energy of 2.8 MJ when its temperature rises from 30°C to 80°C [18, 50]. The main components of typical HDH system are humidifier, dehumidifier, heat source, water pumps and air blowers. There are different cycle configurations either water heated like; closed-air open-water, multi-effect closed-air open-water and closed-water open-air, or air heated configuration as closed air-open water systems [18, 48, 49].

In all systems, seawater is sprayed in the humidifier device where heat and mass are exchanged with air. The humidified air is directed to the dehumidifier to condense the water vapour so distilled water is produced. With that procedure, many cycle configurations could be applied as either water or air loops are closed and heating is either applied on air or water [18].

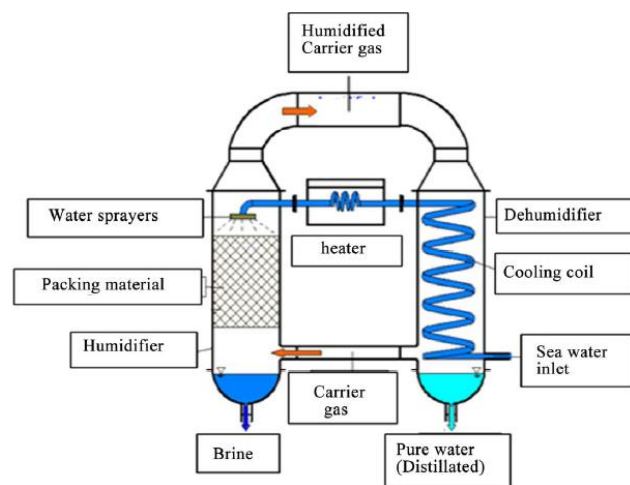


Figure 2-5, Schematic diagram for closed-air open-water heated, HDH system [18, 49]

Solar desalination, (SD) systems utilize the energy of the sun to distil water and are classified in two categories, separated (indirect) or integrated (direct). Indirect systems are those which use solar energy only for heating seawater or for generating steam for conventional water desalination plants like MSF, MED or RO. Direct systems use solar collectors and condensers in integration for evaporation and condensation of water [18, 51-54]. This section will deal only with direct systems as indirect ones were covered earlier. Direct systems are suitable only for low production requirements typically up to 200m³/day as the operating temperature and pressure are low [18]. The basic solar still, Figure 2-6 [18, 55], consists of a basin covered with tilted glass allowing air to be in between. The basin is filled with

seawater which evaporates when receiving solar rays. As the water vapor is produced it mixes with air and goes up until it touches the cooler glass cover then it condenses. The condensed distilled water moves along the tilted surface by gravitational force to be collected from the sides of the basin and the unevaporated brine is drained from the bottom of the basin [18, 55]. As this system design suffers from low efficiency, 30-40% [18, 56], development techniques could be made as single slope or double slope basin still [57], still with cover cooling [58], still with additional condenser or still with black die [55]. Other modifications are wick still [59], solar still greenhouse combination [60] or multiple-effect basin stills [61]. However due to the low cost of the conventional solar stills, they are suitable for remote areas.

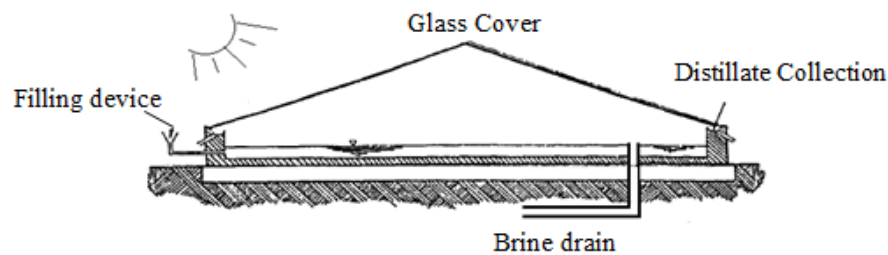


Figure 2-6, Schematic diagram for direct solar desalination system [18, 55]

2.2.2 Thermal heat extraction processes

The main reason of using freezing desalination processes, (Frz) is its reduced cost compared to other heat addition desalination processes where latent heat of water evaporation is seven times that of fusion of ice [18, 62]. Also the heat addition in freezing cycles is not considered as energy input to the system as compressor work is the only input energy. Freezing systems have two major categories, direct and indirect contact depending on the type of the cooling

system [18]. Direct contact systems uses the flow of refrigerant in contact with seawater to freeze and separate the salt but for indirect contact systems, a heat exchange surface is used to separate the refrigerant from seawater while allowing heat transfer between them [18, 63]. In the direct freeze system, Figure 2-7 [18, 64] shows that the refrigerant could be the seawater itself or another cold fluid. If seawater is used as refrigerant, the system operates under very low pressure so it flashes absorbing heat from seawater making ice. If another fluid is used as refrigerant, it should be more volatile and less soluble in water such as N-Butane, HFE-7100 and R410A [64-67]. Firstly, refrigerant is compressed then cooled to a temperature lower than seawater freezing point. Afterwards, refrigerant is injected through nozzles in the water so ice crystals are formed while the refrigerant evaporates. For melting the ice, the refrigerant is compressed and is used to melt the collected ice for the production of distilled water [18, 64].

The second type of freezing systems is indirect contact systems. As shown in Figure 2-8 [18, 68], incoming seawater enters a heat exchanger to cool down then is pumped to the freezer where it cools till ice crystals are formed.

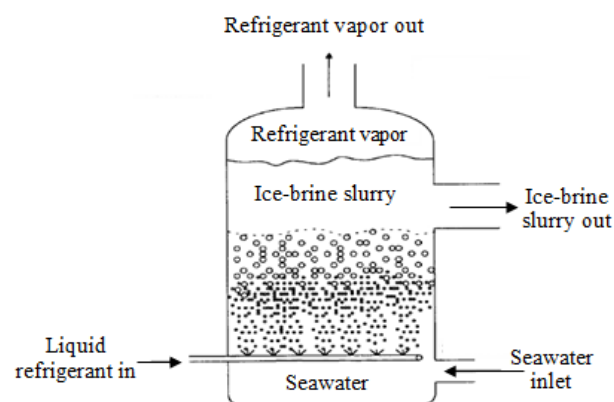


Figure 2-7, Schematic diagram for direct freezing desalination system [18, 64]

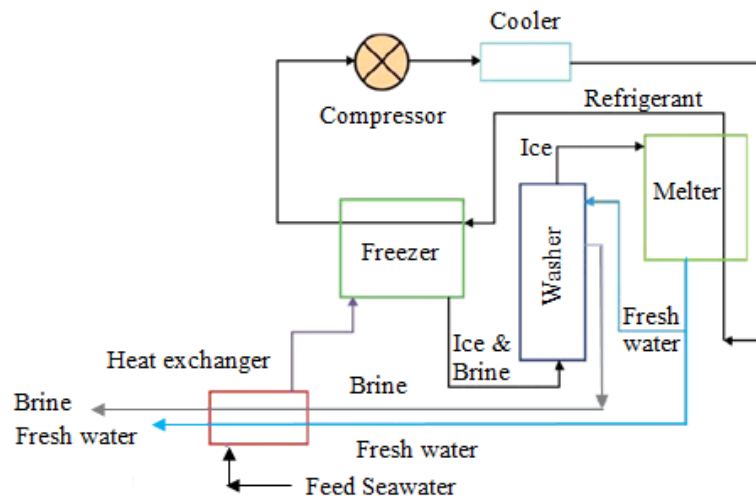


Figure 2-8, Schematic diagram for indirect freezing desalination system [18, 68]

A washer column is then used to separate the ice crystals and the brine. The ice is moved to the melter where it is converted to fresh distilled water by utilizing the heat of condensation of the compressed refrigerant. The fresh water is firstly used as a cooling fluid for the incoming seawater then it is collected outside the system. Also the separated brine in the washer is directed to the heat exchanger to cool down the seawater. Small part of the fresh water after formation in the melter is used in the washer for the separation of ice and brine process [18, 68].

2.2.3 Membrane based water desalination processes

Unlike thermal based desalination systems, membrane based desalination techniques rely on differences in pressure or electric charges between two membranes positioned next to each other [18, 69]. Systems depending on pressure difference are reverse osmosis, forward osmosis and nano-filtration while electro-dialysis depends on electric charge difference.

Osmosis process is a natural phenomenon happens when there is a salt concentration difference across a membrane where water tends to leave the low concentration zone and pass to the more concentrated one through a membrane. This process continues until a pressure difference equivalent to the osmotic pressure is reached which occurs when chemical equilibrium is achieved as in Figure 2-9 (a) [18, 70].

Reverse osmosis system, (RO), employs the opposite of this natural phenomenon (osmosis process) where water is forced to pass through a semi permeable membrane travelling from the more concentrated region to the lower one while leaving salts to remain as a waste. To perform such process, seawater is pumped to a pressure above the osmotic pressure to force only fresh water to travel to the other side of the membrane, Figure 2-9 (b) [18, 27, 70, 71].

The reverse osmosis plant originally consisted of four main components; pre-treatment device, high pressure pumping system, membrane separation system and pre-treatment for produced water. High pressure is needed, about 55-70 bars, depending on the membrane type and seawater salinity. As this technique is energy intensive, pressurized rejected brine is utilized to recover some of its energy through rotating a turbine coupled to an electric generator to provide electric power for the water pumps [18, 72].

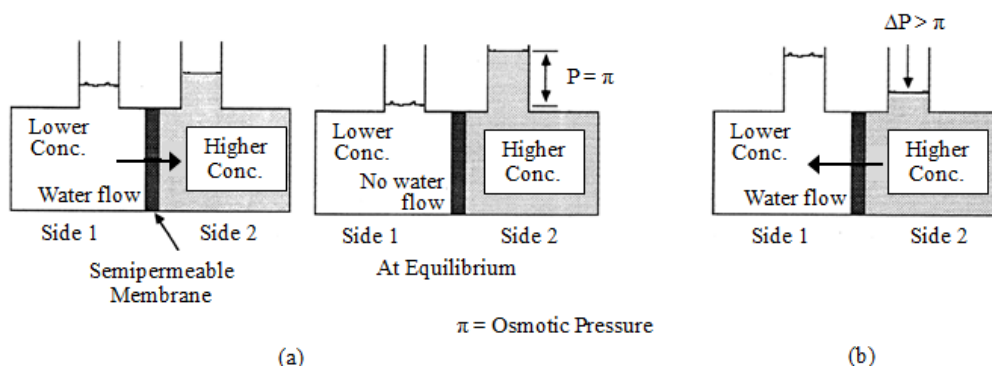


Figure 2-9, Schematic diagram for RO desalination process [18, 70]

Because of the intensive electric energy needed in the reverse osmosis desalination technique, forward osmosis (FO) was found to be an alternative. The forward osmosis technique depends also on the osmotic phenomenon. However; the pressure difference equivalent to osmotic pressure is reached through increasing the concentration on the opposite side where seawater exists. As shown in Figure 2-10 [18, 73], draw solution such as “ammonia-carbon dioxide” with zero or trace water is added to the other side of the membrane opposite to the seawater side. By doing that, it allows the draw solution side to have lower water content than the seawater side which attracts pure water towards the solution because of the osmotic phenomenon. To recover the pure water from the draw solution, heat is added so that fresh water can be separated and the draw solution is returned back to the membrane separation chamber [18, 73-76].

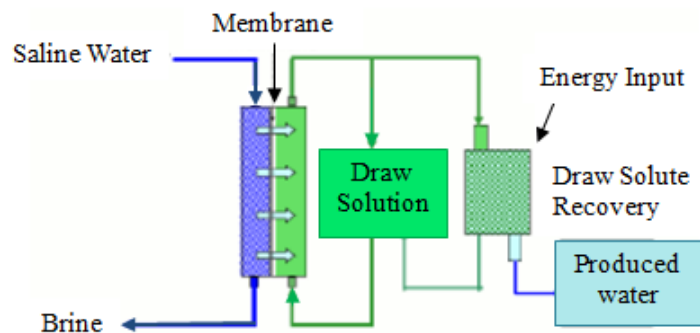


Figure 2-10, Schematic diagram for FO desalination system [18, 73]

In nano-filtration (NF) technique, semi-permeable membranes do not permit salts from flowing through them. This technique differs from reverse osmosis in the ability to prevent certain dissolved salts from passing through the membrane [18]. NF membranes are capable of preventing calcium and sulphate ions from passing through, while they have less degree

of rejection for sodium and chloride ions (mono-valent ions). NF membranes can be used to separate salts with a particle sizes ranging from 0.01 to 0.001 micrometer [18, 77].

Due to this selectivity nature which limits the ability to prevent some salts from passing through the membranes, nano-filtration techniques are basically used for brackish water with low salt concentrations. However, other improvements have been applied to this technology to allow for usage in seawater desalination applications as using dual-stage NF techniques [18]. As shown in Figure 2-11 [18, 78], in dual-stage nano-filtration systems seawater is fed into the system where high pressure pump forces salty water to pass through a first stage equipped with certain efficient NF membranes that can deal with seawater salinity levels and produce brackish water with low salinity. The produced brackish water is then pumped and forwarded to a second stage of nano-filtrations where fresh water is produced and the rejected concentrated brine is returned back and mixed with the seawater feed line [18, 78, 79].

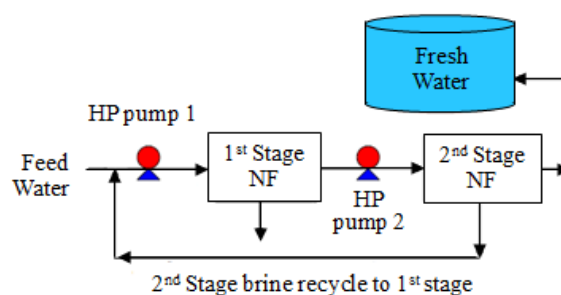


Figure 2-11, Schematic diagram for NF desalination system [18, 78]

In electro-dialysis systems, (ED), electric field is applied on two electrodes acting as anode (positive charged) and cathode (negative charged) while membranes and seawater exists in between. Membranes are either anion exchange membranes “AEM” or cation exchange membranes “CEM” based on their electric charge which separate salts from seawater

according to electric charge differences [18]. As shown in Figure 2-12 [18, 80], positive and negative ions in the salty water are attracted to the negative and positive electrodes respectively while passing through AEM and CEM membranes. As a result of ions migration process, each membrane will have concentrated brine on one side while the other will have fresh water. In order to avoid scale formation on the membranes, polarity of electrodes is changed at intervals of 20 minutes in a procedure known as electro-dialysis reversal (EDR) [18, 80-82].

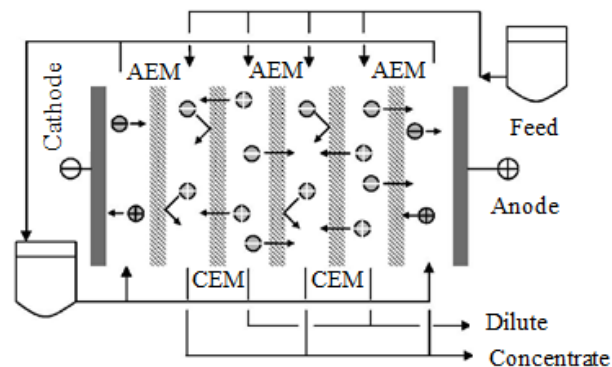


Figure 2-12, Schematic diagram for ED desalination system [18, 80]

2.2.4 Chemical water desalination processes

Unlike other desalination techniques, chemical desalination systems depend on chemical differences rather than pressure differences or phase change. Ion exchange, (I.Ex), is an analytical chemical separation technique where different ionic materials are allowed to be selectively retained on an ion exchange resin [18]. These resins consist of large amounts of firmly attached bonds on their surfaces. They can absorb one type of ions reversibly. Resins are like small spheres with diameters in the range of 0.4 to 0.8 micro meters. Positive charged ions are captured by cation exchange resin, while anion exchange resin capture negatively charged ions [18, 83].

In an ion-exchange unit as shown in Figure 2-13 [18, 83], water enters a tank containing high capacity exchange beads (cation exchange resin). These beads are saturated with either sodium or potassium which are known as replacement ions. While water passes through this tank, an exchange occurs between contaminant ions and replacement ions which are released to the water. A regeneration process is needed to recover replacement ions which were released into the water [18].

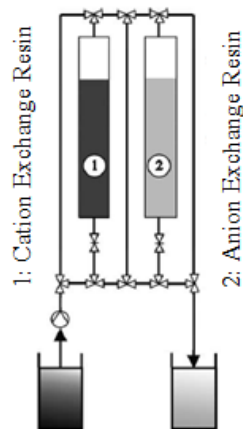


Figure 2-13, Schematic diagram for I.Ex desalination system [18, 83]

A salt brine solution is used to flush the ion exchange resin for the regeneration process. For removal of negative ions such as nitrate, arsenic and bicarbonate, anion exchange resin is used. In this resin, beads are saturated with negatively charged ions such as chloride and hydroxide. This type of desalination was found to be suitable for water treatment and for brackish water desalination [18, 84-86].

Gas hydrates, (G.HYD), are crystalline solid structures that consist of water and other molecules like N_2 , CO_2 , CH_4 , H_2 and others which are employed for water desalination purposes and they are formed under low temperature and high pressures [18]. In other

words, if small hydrocarbon molecules or non-hydrocarbon compounds are in gas or liquid phase and at high pressure was cooled to temperature near 0°C, then solid crystals like snow may form. These solid water crystals act as host molecules that form cage structure which contains guest compounds entrapped inside. This is called gas hydrate [18].

Desalination processes depend on phase change from liquid to solid then physical processes are required to separate solids from the existing liquid. As shown in Figure 2-14 [18, 87], seawater is pumped then cooled in the first heat exchanger by the counter current flow of brine and potable water streams. Then, a reactor is used to form slurry containing hydrate crystals which are filtered and washed in the separator that results in two streams; brine and washed hydrate crystals. This brine exchanges heat with seawater and the excess hydrate former (i.e. refrigerant) in first and second heat exchangers, respectively then discharged. Washed hydrate crystals are pumped to a decomposer which produces potable water and hydrate former. Potable water exchanges heat in the first and second heat exchangers then is collected out of the system. The hydrate former goes to a throttling valve then to the reactor [18]. In the reactor, hydrate crystals are formed as heat is removed from it by vaporization of liquid hydrate former which then takes part in hydrate structure. A compressor compresses the excess hydrate former which is then directed to the decomposer for destroying hydrate crystals and cooling. Finally, this hydrate former is further cooled in the third and second heat exchangers and then throttled in the throttling valve [18, 32, 87-89].

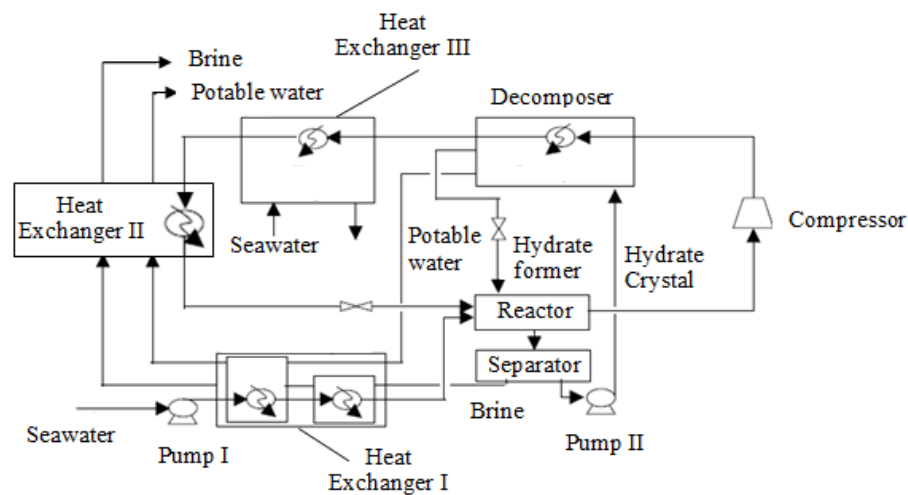


Figure 2-14, Schematic diagram for G.HYD desalination system [18, 87]

In the Liquid-liquid extraction system, (LLE), a specially tailored polymer solvent is used to extract fresh water in a desalination process at temperatures not more than 60°C. When seawater is contacted with these polymer solvents, two phases are produced; a polymer phase with dissolved water and another aqueous phase with insoluble polymer [18]. As shown in Figure 2-15 [18, 90], seawater is mixed with a polymer solvent thereby forming aqueous two phase systems the first is polymer rich extract phase and the other is polymer lean phase. Change in temperatures is applied to recover the polymer without water evaporation. This is done as the polymer solvent is miscible in water at lower temperatures and with slight increase in temperature; it becomes immiscible in water so water can be extracted. The main solvents applicable are amines and polymers but there are no such commercial plants available [18, 31, 90, 91].

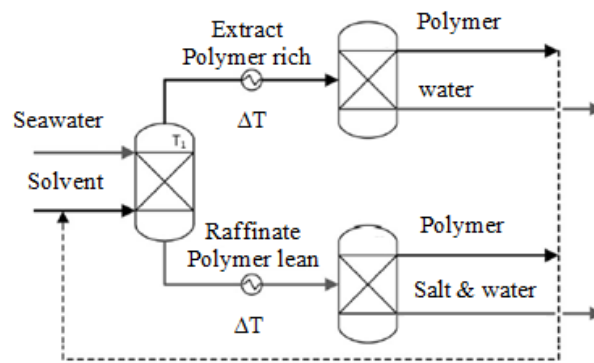


Figure 2-15, Schematic diagram for LLE desalination system [18, 90]

2.2.5 Adsorption desalination processes

The adsorption process relies on the ability of a porous adsorbent material to adsorb water on its surface. High affinity of unsaturated adsorbent materials allows adsorption of water vapor on its surface within a half cycle. Regeneration of the adsorbed water vapor is applied by heating it in the next half cycle using low temperatures heat sources in the range of 50 to 85°C depending on the type of adsorbent [18]. The adsorbents used are hydrophilic and highly porous materials with high surface areas in the range of 500 to 5900 m²g⁻¹ [18, 92]. Silica-gel adsorbent is the most commonly used in the adsorption desalination processes [11]. The basic components in an adsorption desalination plant as shown in Figure 2-16 [18, 93] are adsorber bed, evaporator and condenser. Firstly, seawater is charged in the evaporator where it evaporates at low temperature and pressure. As valve 1 is opened, water vapor is adsorbed by the adsorbent packed in “Bed I” [94]. This adsorption process is exothermic, so cooling water is required to remove this heat. After bed 1 becomes saturated, valve 1 is closed and valve 2 is opened. To regenerate the adsorbed water, hot fluid is supplied in the heating coil inside the bed for completion of desorption process.

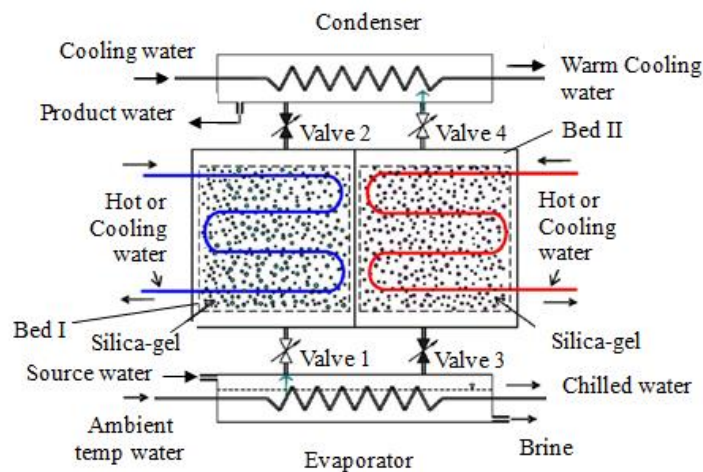


Figure 2-16, Schematic of a double-bed Adsorption desalination system [93]

The produced water vapor exiting from the bed is condensed in the condenser using a cooling coil where it is condensed and collected as potable water. When all of the water vapor is regenerated, valve 2 is closed and the cycle is repeated. For “Bed II”, the same processes occur but alternating with bed 1 [5, 9, 18].

For getting higher cycle efficiencies, many modifications to this basic cycle have been investigated. Improvements are performed by using four adsorber beds instead of two or evaporator- condenser heat recovery circuit either internally (integrated evap.-cond. device) or externally (heat recovery water loop) [6, 18, 33, 95]. Adsorption desalination systems have the advantages of no moving parts except for pumps and valves. Also they are capable of desalinating both brackish and seawater even if organic compounds exist. Moreover, they can be driven by low grade waste heat which reduces global warming and CO₂ emissions. Working at low temperatures reduces fouling and corrosion inside the evaporator. Furthermore, these systems can also produce cooling effect in addition to desalination which is important in the regions with limited supply of fresh water and they have long life cycle time of 30 years [18, 96-98].

2.3 Performance of Desalination processes

There are number of parameters that influence the performance of desalination technologies, these are: salinity levels of feed and produced water, capital and running costs for the selected technology, type of available input energy, environmental impact of the technology and available site properties. In this section, comparative assessments of these parameters for the various technologies described above are presented [18, 19].

2.3.1 Brackish or seawater salinity

According to salinity level, water is normally classified as either seawater or brackish water. Seawater has average salinity of 35,000 ppm while brackish water salinity levels lie between 1,000 and 25,000 ppm [22, 24]. Figure 2-17 [18], compares the maximum feed water salinity level that can be processed by each technology. It is clear that most of the technologies can handle water with a salinity of less than 45,000ppm while the MSF and Ads technologies can handle higher values of salinity close to 70,000ppm [18, 19].

2.3.2 Produced water salinity

Figure 2-18 [18], shows the salinity level of the produced water for each desalination technology. It is clear that FO, MED, MVC, MSF, RO, Ads and I.Ex produce water with salinity level less than 13ppm, while the remaining technologies produce water salinity level of 100 to 250ppm [18, 19].

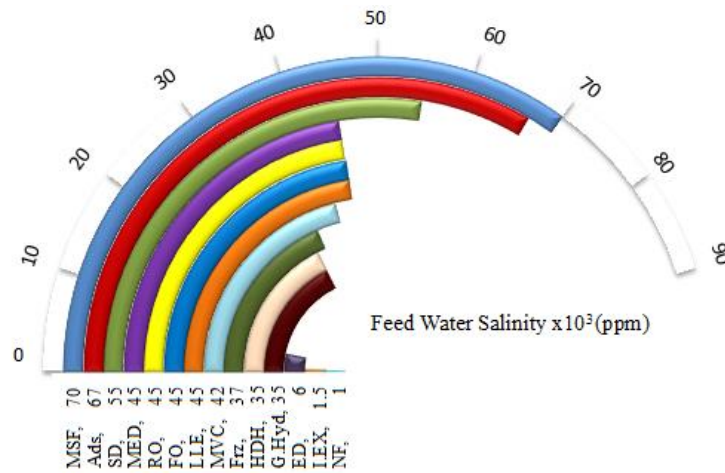


Figure 2-17, Desalination capabilities of different desalination technologies according to feed water salinity, [18, 31, 32, 37, 42, 99-105]

- | | | |
|--------------------------------|---------------------------------|---|
| (MSF) Multi stage flash | (MED) Multi-effect distillation | (MVC) Mechanical vapor compression |
| (SD) Solar distillation | (Frz) Freezing desalination | (HDH) Humidification - dehumidification |
| (RO) Reverse osmosis | (FO) Forward osmosis | (NF) Nanofiltration |
| (ED) Electro-dyalysis | (I.Ex) Ion-exchange | (G.Hyd) Gas hydrate |
| (LLE) Liquid-liquid extraction | | |

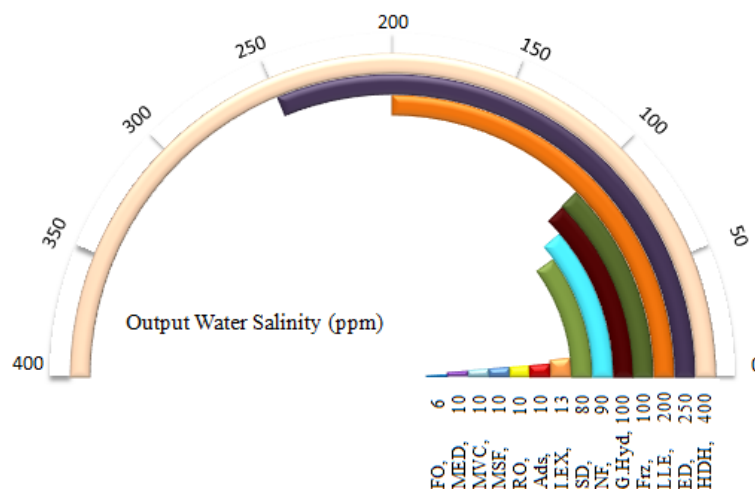


Figure 2-18, Desalination capabilities of different desalination technologies according to produced water salinity, [5, 18, 28, 31, 100, 106-114]

- | | | |
|--------------------------------|---------------------------------|---|
| (MSF) Multi stage flash | (MED) Multi-effect distillation | (MVC) Mechanical vapor compression |
| (SD) Solar distillation | (Frz) Freezing desalination | (HDH) Humidification - dehumidification |
| (RO) Reverse osmosis | (FO) Forward osmosis | (NF) Nanofiltration |
| (ED) Electro-dyalysis | (I.Ex) Ion-exchange | (G.Hyd) Gas hydrate |
| (LLE) Liquid-liquid extraction | | |

2.3.3 Type and amount of energy required

The type of energy source required to drive the desalination systems is important in determining its overall cost and the environmental impact. MSF and MED systems can use steam coming from either an external boiler, steam power plant or flashed steam from a waste energy source with steam temperature ranging from 75 to 115°C [18, 36, 39]. MVC requires mechanical energy to rotate the compressor; this energy is usually obtained from an electric motor or from coupling to a wind turbine [18, 115]. HDH systems use heaters for either heating air or water at temperatures from 70 to 95°C. These heaters may be electric heaters, solar water heaters, steam ejectors or geothermal spring [18, 50]. SD use solar energy for the desalination processes at temperatures of 100 to 400°C depending on the type of solar system [18, 116]. Freezing systems need electrical energy to drive the compressor of the refrigerating system [18, 64]. RO, FO and NF systems utilize pumps driven by electric motors [18, 117]. Electric energy is applied in ED systems to produce the required electric field between the anode and cathode. For gas hydrate desalination systems, in addition to the use of a hydrate former, mechanical energy is required to drive the compressor. The operating pressure of the gas hydrate former ranges from 1 to 44 bars depending on the type of hydrate former used [18, 107]. Finally, adsorption desalination can utilize low temperature waste heat at temperatures of 55 to 85°C or solar energy by which it can produce fresh water without any fossil fuel input or energy from carbon based fuels [18, 22]. Figure 2-19 [18], compares the amount and type of purchased energy used in each desalination technology. As shown in this figure, apart from the SD technology, the Ads, G. Hyd and I.Ex consumes the lowest amount of electrical input energy of 1.58kWh/m³, while Frz and MVC consume the highest electrical input of around 12kWh/m³ [18, 19].

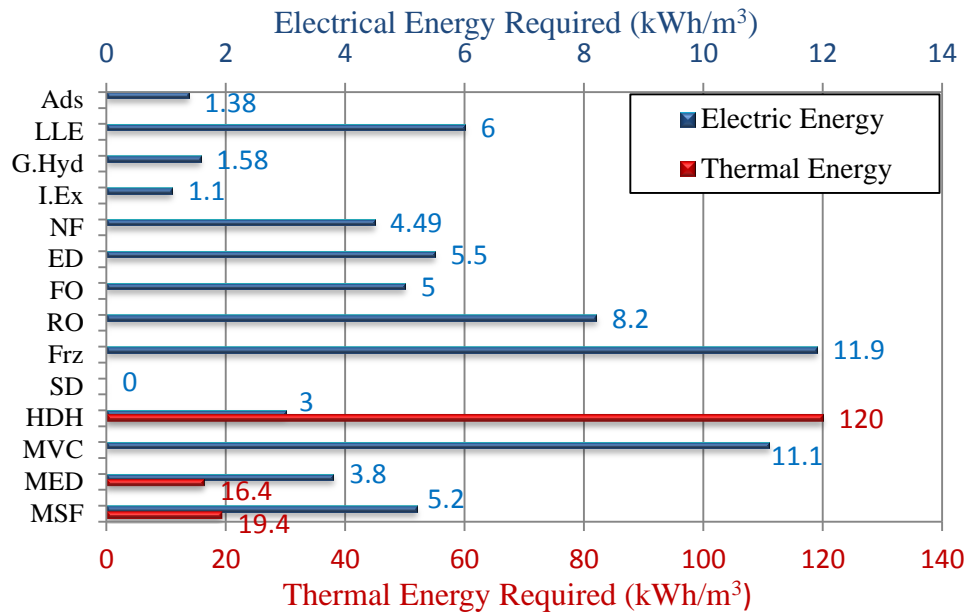


Figure 2-19, Energy needs for various desalination technologies, [18, 99, 107, 118-126]

(MSF) Multi stage flash

(SD) Solar distillation

(RO) Reverse osmosis

(ED) Electro-dialysis

(LLE) Liquid-liquid extraction

(MED) Multi-effect distillation

(Frz) Freezing desalination

(FO) Forward osmosis

(I.Ex) Ion-exchange

(MVC) Mechanical vapor compression

(HDH) Humidification - dehumidification

(NF) Nanofiltration

(G.Hyd) Gas hydrate

2.3.4 Environmental impact

In the previous section, the amount of energy required to operate each individual technology was presented. Using this data, the amount of CO₂ emitted can be calculated. Figure 2-20 [18], shows a breakdown of the calculated CO₂ emissions for each technology. CO₂ emissions were calculated using emission factor for natural gas burning of $6.42 \times 10^{-5} \text{ tCO}_2 \cdot \text{MJ}^{-1}$ (thermal energy sources) and $0.4612 \text{ tCO}_2 \cdot \text{MWh}^{-1}$ of generated electricity [19, 120]. It can be seen that HDH produces the largest CO₂ emissions of 29.12 kg/m^3 while Ads, I.Ex and SD produce the least CO₂ emissions of less than 0.64 kg/m^3 [18, 19].

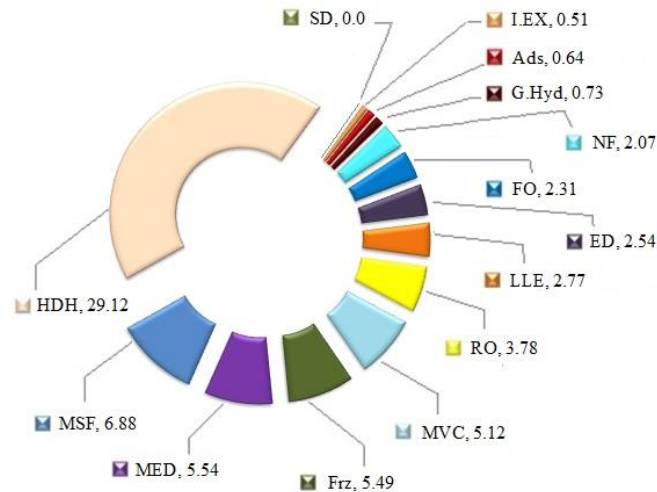


Figure 2-20, CO₂ emissions (kg.m⁻³) for various desalination technologies [18]

(MSF) Multi stage flash	(MED) Multi-effect distillation	(MVC) Mechanical vapor compression
(SD) Solar distillation	(Frz) Freezing desalination	(HDH) Humidification - dehumidification
(RO) Reverse osmosis	(FO) Forward osmosis	(NF) Nanofiltration
(ED) Electro-dialysis	(I.Ex) Ion-exchange	(G.Hyd) Gas hydrate
(LLE) Liquid-liquid extraction		

2.3.5 Cost

One of the important parameters in selecting desalination technology is the cost. These costs are divided into capital cost and running cost. Many factors affect these costs like plant location, availability of required energy, methods of storing produced potable water, associated labor cost and disposal of produced brine [18]. Because not all of these desalination technologies have been commercialized and some of them are still under development, their capital costs are not yet estimated, cost analysis will be only based on running cost. A rough cost estimation for potable water production has been performed by Mezher et al [127]. As presented in Figure 2-21 [18], Ads can produce potable water with the lowest cost of 0.2US\$.m⁻³ while the HDH produces potable water at the highest cost of 3.93US\$.m⁻³ [18, 19].

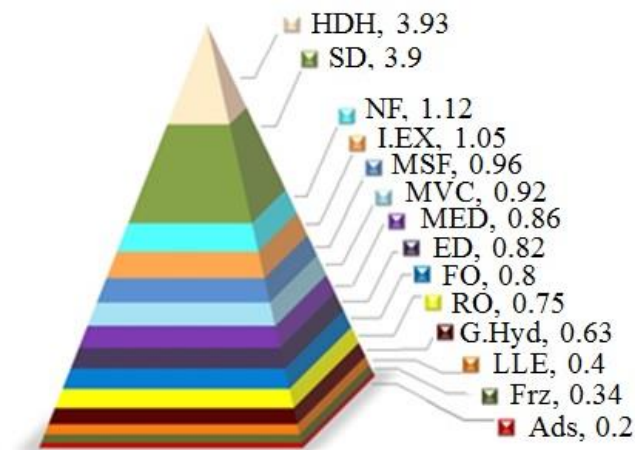


Figure 2-21, Potable water production cost (US\$.m⁻³), for various desalination technologies

[18, 31, 99, 119-121, 127-133]

(MSF) Multi stage flash	(MED) Multi-effect distillation	(MVC) Mechanical vapor compression
(SD) Solar distillation	(Frz) Freezing desalination	(HDH) Humidification - dehumidification
(RO) Reverse osmosis	(FO) Forward osmosis	(NF) Nanofiltration
(ED) Electro-dyalysis	(I.Ex) Ion-exchange	(G.Hyd) Gas hydrate
(LLE) Liquid-liquid extraction		

2.4 Overview of adsorption desalination Cycles

Many adsorption desalination cycles have been introduced by different researchers that can produce either desalinated water only or water and cooling. All cycles have the basic components of any adsorption system which are adsorption/desorption beds, evaporator and condenser but they differ according to the number of beds used, configuration and the heat recovery processes that could be used in the system.

2.4.1 Conventional water desalination system

As mentioned before, all adsorption systems have adsorption/desorption bed, evaporator and condenser. As explained in section 2.2.5, in this system the evaporator is connected to the adsorbing bed with cooling water flowing into the bed while the condenser is connected

to the heated desorbing bed for regeneration of the water vapor. In this cycle evaporator chilled water and condenser cooling water are independent from each other which make it possible to produce cooling from the evaporator as seawater evaporates and extracts heat from the chilled water [9]. This system could have two adsorbing/desorbing beds, Figure 2-22 [134], or four adsorbing/desorbing beds working in a master-slave arrangement as heating or cooling water passes through master beds and the outlet from these beds goes to the slave beds, Figure 2-23 [7]. This master-slave technique in the four bed arrangement ensures better exploitation of the available heat source in addition to more stable water production rate as one of the beds is connected to the evaporator and one to the condenser at all times [96]. In case of silica-gel system with 36 kg adsorbent material packed in each bed, a two bed system achieved water production in the range of 6.1-8.7 m³.tonne⁻¹.day⁻¹ while with 4-beds it was 6.2-10 m³.tonne⁻¹.day⁻¹ with bed heating water temperature of 65-85°C [96]. From literature, it was reported that when cooling is produced, two and four bed systems can produce 25 and 35 Rton.tonne⁻¹ respectively at evaporator temperature of 10°C along with 3-5 m³.tonne⁻¹.day⁻¹ of desalinated water [135]. At lower evaporator temperature of 5.4°C, the cooling and water produced from a 4-bed cycle were 18 Rton and 2.4m³.day⁻¹ per tonne of Silica-gel respectively [136].

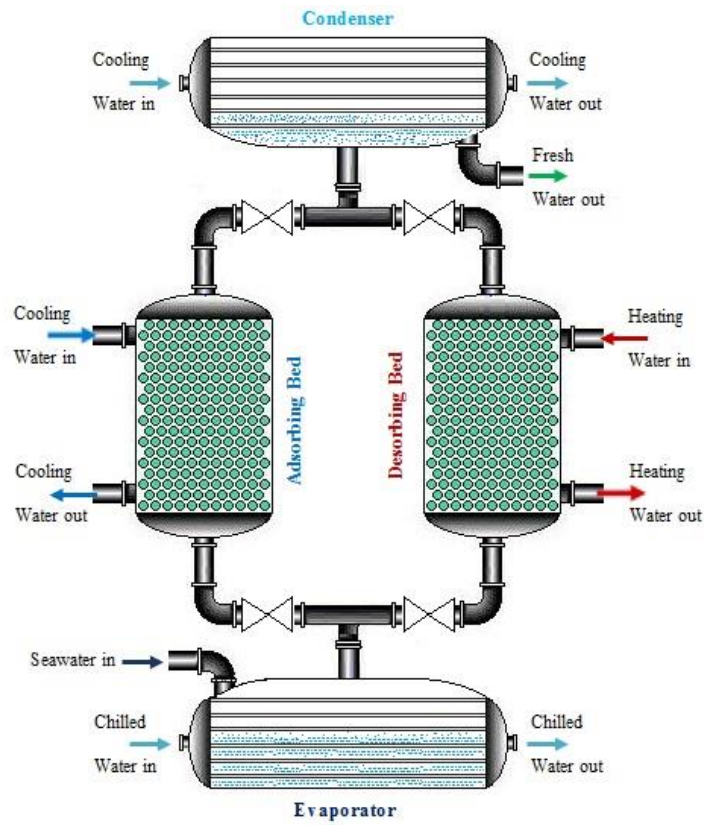


Figure 2-22, Schematic of a conventional double-bed adsorption desalination system [134]

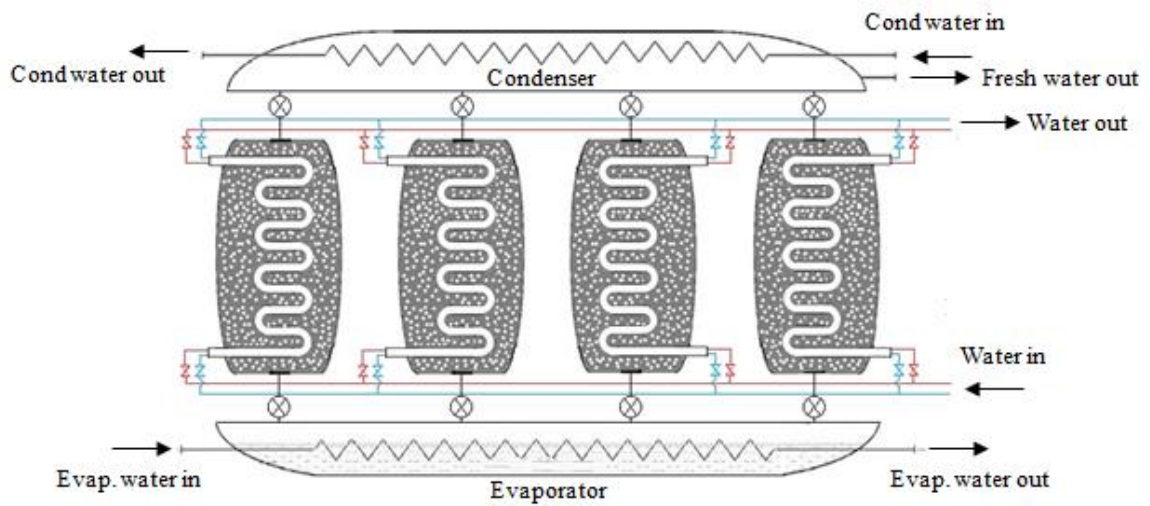


Figure 2-23, Schematic of a 4-bed adsorption desalination system with master-slave arrangement [7]

2.4.2 Evaporator-Condenser heat recovery water desalination system

This system is like the conventional system described in the previous section but with a heat recovery between evaporator chilled water and condenser cooling water as shown in Figure 2-24 [95]. In this heat recovery technique, the output cold water from the evaporator is fed to the condenser and vice versa so the produced cooling effect in the evaporator is utilized in the condenser [120]. By this method, lower condenser and higher evaporator temperatures are achieved which enhances the cycle water production but its drawback is that no cooling can be produced from this cycle. Experiments showed that with silica-gel used at 70°C, the specific daily water production (SDWP) achieved was 9.24 m³.tonne⁻¹.day⁻¹ with a performance ratio¹ (PR) of 0.75. Moreover, it was found that the cycle is operational at low heating temperature of 50°C which produced 4.3 m³.tonne⁻¹.day⁻¹. Simulations revealed that maximum SDWP produced by this system was found to be 13.2 m³.tonne⁻¹.day⁻¹ at PR of 0.74 [95].

¹ Performance ratio (PR) is the ratio between heat of condensation to heat of desorption [96].

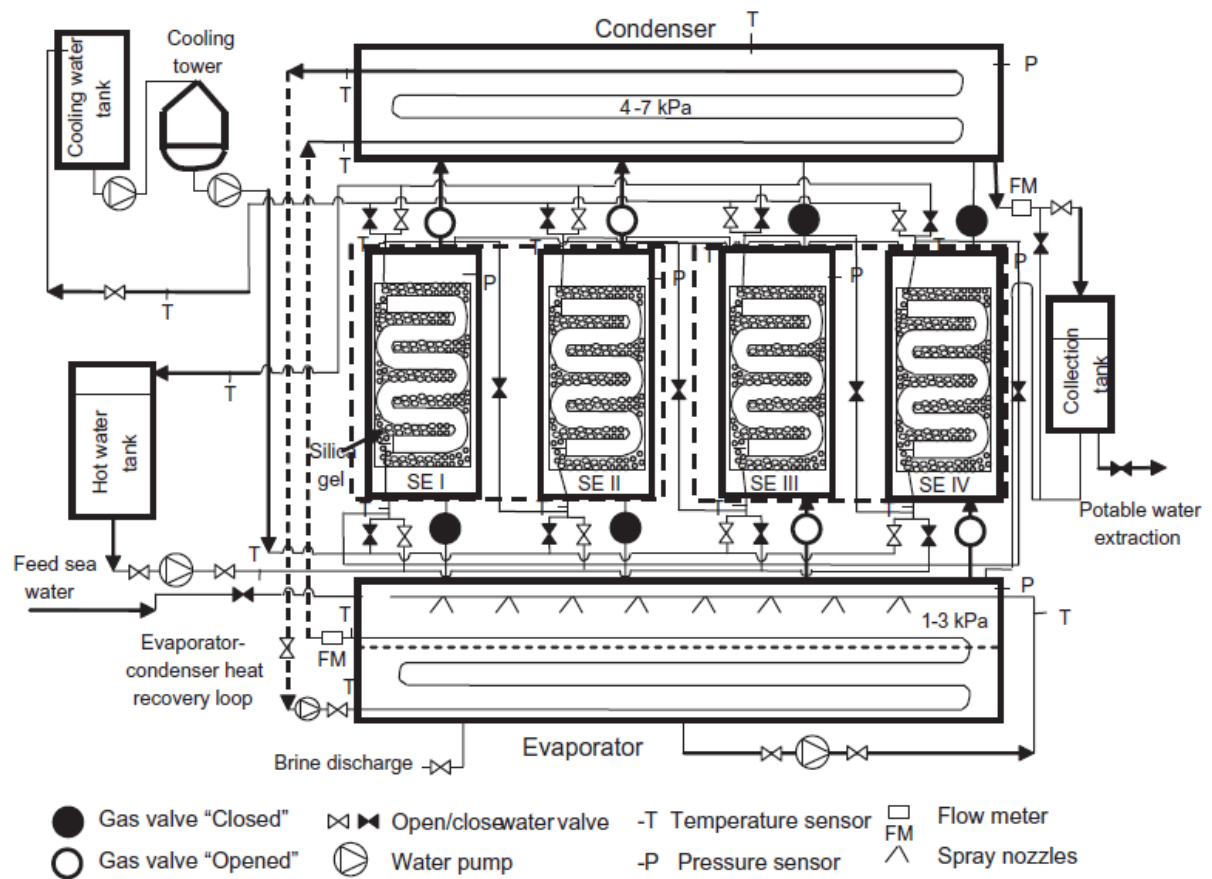


Figure 2-24, Schematic of a 4-bed adsorption desalination system with heat recovery circuit between evaporator and condenser [95]

2.4.3 Water desalination system with integrated evaporator-condenser device

This advanced desalination cycle consists of 2-beds and a heat exchanger device which comprises internally of an evaporator and a condenser, Figure 2-25 [33]. As condenser is encapsulated by the evaporator, all heat of condensation is utilized by the evaporator which allows higher evaporation rates and better heat transfer. Moreover as seawater evaporates in the evaporator, heat is extracted from condenser and no cooling system is required for the condenser which reduces pumping power. Using advanced silica-gel A⁺⁺ and at hot water

mesoporous ($50\text{nm} > \text{pore diameter} > 2\text{nm}$) or macro-porous (pore diameter $> 50\text{nm}$) [138, 139]. Many adsorbent-adsorbate working pairs have been used in different adsorption based applications as water desalination, cooling, energy storage and drying. However, this section will only consider adsorbent-water working pairs since the main concern is water desalination applications where the adsorbate has to be the water vapor resulting from seawater evaporation in the evaporator. Table 2-1 lists adsorbent/ water working pairs that were investigated in different adsorption applications along with their maximum water uptake capacities. It can be seen that these adsorbents cover wide range of uptakes starting from $0.12 \text{ g}\cdot\text{g}^{-1}$ "Natural Zeolite" up to $1.43 \text{ g}\cdot\text{g}^{-1}$ "MIL-101(Cr)" metal organic framework material. However, only silica-gel is used as an adsorbent in adsorption water desalination applications as shown in Table 2-2 [11] with majority of contribution in the field of adsorption desalination has been reported by the research groups of "National University of Singapore, Singapore" and "King Abdullah University of Science and Technology, Saudi Arabia".

Based on this literature review, a number of adsorbent materials will be investigated for adsorption desalination applications namely; AQSOA-Z02, Aluminium Fumarate, CPO-27Ni and MIL-101Cr. Selection of these materials is based on availability in the market as well as high uptake capabilities compared to Silica-gel.

Table 2-1, Adsorbent/Water working pairs as in Literature

Adsorbent group	Working pair	Equilibrium uptake ($\text{g}_{\text{water}} \cdot \text{g}_{\text{ads}}^{-1}$)	Ref.
Silica-Gel	Silica-gel, type 3A / H ₂ O	0.33	[140]
	Silica-gel, type A / H ₂ O	0.4	[141]
	Silica-gel, type RD / H ₂ O	0.45	[141]
	Silica-gel, type A ⁺ / H ₂ O	0.52	[142]
Activated Carbon	Activated Carbon Fibers, ACF KF-1000 / H ₂ O	0.32	[143]
Zeolites	Natural Zeolite / H ₂ O	0.12	[144]
	Zeolite 4A / H ₂ O	0.2	[145]
	AQSOA-Z01 / H ₂ O	0.21	[146]
	AQSOA-Z05 / H ₂ O	0.23	[147]
	Zeolite-13x / H ₂ O	0.3	[148]
	AQSOA-Z02 / H ₂ O	0.31	[147]
Metal Organic Frameworks	MOF-841 / H ₂ O	0.48	[13]
	Aluminium Fumarate / H ₂ O	0.49	[14]
	CPO-27NI / H ₂ O	0.576	[15]
	MIL-100 (Al) / H ₂ O	0.5	[16]
	MIL-100 (Fe) / H ₂ O	0.7	[16]
	MIL-101 (Cr) / H ₂ O	1.43	[17]

Table 2-2, Published research work on adsorption for desalination and cooling purposes [11]

Author	Used system configuration	Experimental/ Numerical	Adsorbent material	T _{hot}	SDWP (m ³ .tonne ⁻¹ .day ⁻¹)	SCP (Rton.tonne ⁻¹) @ Evap. temp. (°C)
Thu et al. [96]	2 & 4 Bed	Experimental	Silica-gel, type RD	85°C	8.79 - 10	0 @ 30°C
Ng et al. [5]	4-Bed mode	Numerical	Silica-gel, type RD	85°C	8	51.6 @ 30°C
Ng et al. [135]	2 & 4 Bed	Exp. & Sim.	Silica-gel, type RD	85°C	3-5	25-35 @ 10°C
Thu et al. [95]	2-Bed (heat recovery)	Experimental	Silica-gel, type RD	70°C	9.2	0 @ 30°C
Thu et al. [22]	2-Bed, Evap.-Cond. heat recovery	Experimental	Silica-gel, type A ⁺⁺	85°C	13.46	0 @ 32°C
Mitra et al. [136]	4-Bed mode	Experimental	Silica-gel, type RD	85°C	2.4	18 @ 5.4°C
Mitra et al. [149]	2-Stage	Experimental	Silica-gel, type RD	85°C	1	7.5 @ 15°C
Akahira et al. [150]	4-Bed cascading	Numerical	Silica-gel, type A	85°C	-	85.7 @ 7°C
Alam et al. [151]	2-Stage	Numerical	Silica-gel	65°C	-	14.3 @ 10°C
Thu et al. [33]	2-Bed, Integrated Evap./Cond.	Numerical	Silica-gel, type A ⁺⁺	85°C	26	0 @ 42°C

2.6 Summary

In this chapter, methods of seawater desalination have been reviewed and their working principles have been presented. A comparison between all presented techniques has been carried out in terms of feed and produced water salinity, energy usage, cost and environmental impact. It was concluded that adsorption desalination technology have the advantage of desalinating water with high salinity of 67 ppt with low energy consumption and minimal environmental impact at lowest cost of 0.2US\$.m⁻³ [19].

In addition, adsorption seawater desalination cycles and their maximum outputs have been discussed. A summary of these cycles outputs are furnished in Table 2-2 [11].

CHAPTER 3: MODELLING OF ADSORPTION DESALINATION CYCLE

3.1 Introduction

One of the primary and effective tools to develop and assess any thermal system is through modelling. This chapter presents the modelling of a basic twin bed adsorption desalination cycle which can be used to investigate the performance of five adsorbents from different families like zeolites and metal organic framework “MOFs” materials namely; Silica-gel, AQSOA-Z02, AL-Fumarate, CPO-27Ni and MIL-101Cr. A Simulink model is developed to simulate a commercial two-bed adsorption machine manufactured by the industrial partner, “Weatherite Manufacturing LTD” with 895 kg of Silica-gel RD per bed.

3.2 Specifications of modelled adsorption desalination system

In chapter 2, principle of operation of adsorption desalination systems has been presented for various cycle configurations with all systems consisting of the same basic components; adsorber bed, evaporator and condenser. In this chapter, the modelling of these components is introduced with the model being applied for a commercial adsorption machine originally manufactured to work as a chiller. The adsorption chiller is a two bed system manufactured by “Weatherite Manufacturing LTD” and is shown in Figure 3-1 while a schematic diagram for the system is shown in Figure 3-2, [11], and its complete specifications are listed in Table 3-1 [139]. The adsorber bed consists of a number of modules; each one is made of rectangular aluminium finned copper tubes while the adsorbent material is packed between the fins as shown in Figure 3-3 [139].



Figure 3-1, Pictorial view for the modelled adsorption machine [139]

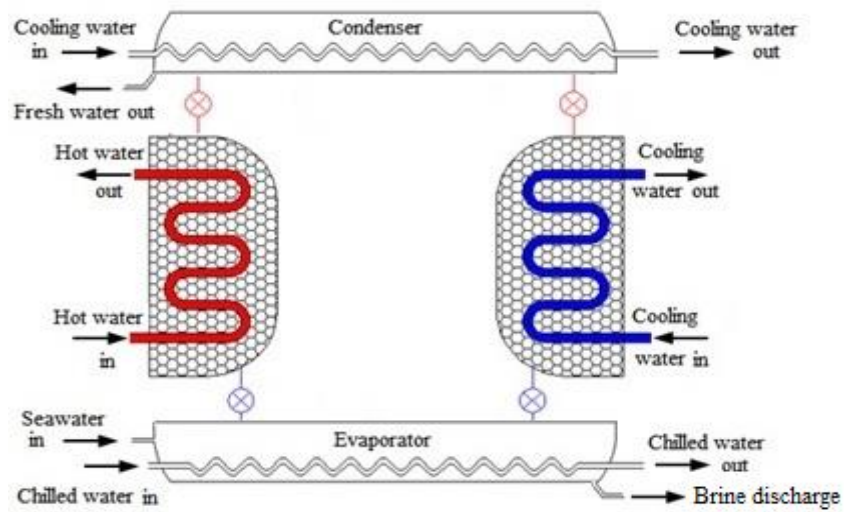


Figure 3-2, Schematic diagram for the modelled adsorption system [11]

Table 3-1, Specifications of the modelled adsorption system [139]

Adsorber bed reactor	
Adsorbent mass	895 kg per bed (based on Silica-gel)
Tube type	Bare copper tube
Tube outside diameter	5/8''
Tube wall thickness	0.8 mm
Tube length	3400 mm
Tube number	672 tube per bed (divided into 56 module,12 tubes/module)
Fins type	Rectangular aluminium fins
Fin length	340 mm
Fins height	28 mm
Fins thickness	0.95 mm
Fin pitch	1.5 mm
Fins number in one module	2266
Total fins number in one bed	126896
Condenser	
Tube type	Bare copper tube
Outside diameter	3/4''
Tube wall thickness	0.8 mm
Tube number	457
Tube length	2654 mm
Evaporator	
Tube type	Externally enhanced copper tube
Nominal tube diameter	3/4''
Root diameter	17.75mm
Fin diameter	18.85mm
Fin thickness	0.2mm
Fin pitch	0.45mm
Fin height	0.55mm
Inside diameter	16.33mm
Total tube number	224
Tube length	3894 mm

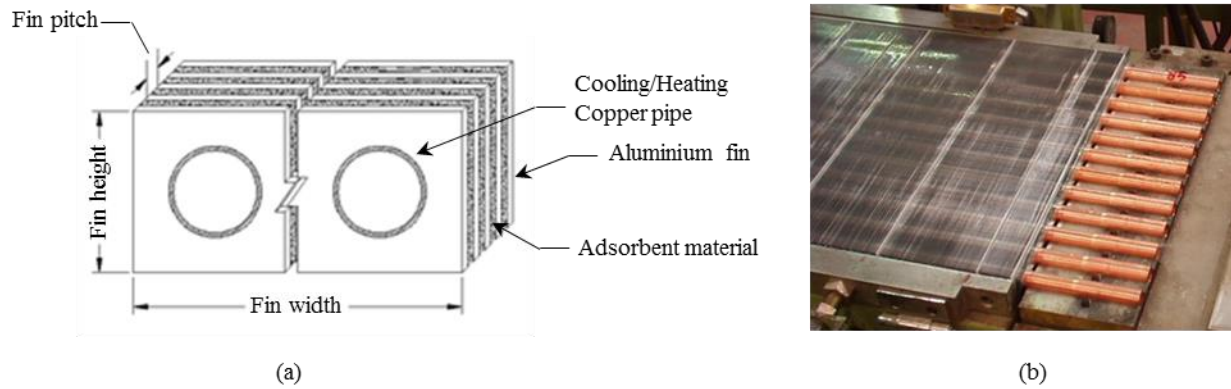


Figure 3-3, Rectangular finned tube adsorber bed [139], (a) Schematic, (b) Pictorial view

As adsorbent material is packed between fins, heat transfer from tubes to the fins should be maximised through minimizing thermal contact resistance between fins and tubes so that the system can operate more efficiently. To do so, their manufacturing process is done as follows; fins are positioned in their place then tubes are inserted inside the circular openings of the fins. After inserting all tubes as shown in Figure 3-4 [152], an expanding die/bullet is passed through each tube which expands it enlarging its outer diameter and ensures best fitting of the tube with minimal contact resistance. Both evaporator and condenser are in the form of a shell and tube heat exchanger with the tubes made of copper for the water circuits to pass through while the shell side contain the evaporating seawater and condensed fresh water respectively.

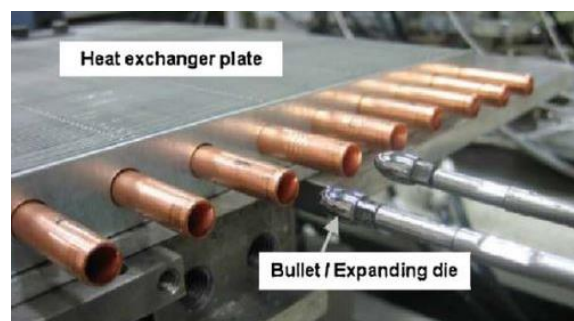


Figure 3-4, Forming process of finned tube heat exchanger [152]

3.3 Adsorbent material physical characteristics

As mentioned earlier, five adsorbent materials are modelled in the conventional double-bed adsorption desalination system described in section 3.2. This section will describe their physical properties and the modelling techniques used to determine their adsorption characteristics.

The five adsorbent materials under consideration are; Silica-gel, AQSOA-Z02, AL-Fumarate, CPO-27Ni and MIL-101Cr. Silica-gel is from mesoporous silicates family and it is the only adsorbent that has been used for adsorption desalination applications therefore it is important to be investigated so that other adsorbents can be compared to it. AQSOA-Z02 is from Zeolites category and it has different isotherm shape than silica-gel where adsorption uptake rises very steeply at low pressure ratios less than 0.1 which makes it important to be studied as it will behave differently than silica-gel. AL-Fumarate, CPO-27Ni and MIL-101Cr are all metal organic framework adsorbent materials which are characterized by their high surface area and uptake in addition to having different isotherm shapes than silica-gel which give them again good chance to perform differently than silica-gel [153]. Also, all these materials are available in the market except MIL-101Cr but it is investigated due to its high uptake value of $1.4 \text{ kg}_{\text{water}}/\text{kg}_{\text{ads}}$. The physical properties of all the selected adsorbent materials are listed in Table 3-2 [154-163]

Table 3-2, Physical properties of adsorbent materials [154-163]

Property	Silica-gel	AQSOA-Z02	AL-Fumarate	CPO-27Ni	MIL-101Cr
Granules size (mm)	0.18-1	0.25-0.4	0.13	0.24	70-500E-4
BET surface area (m ² /g)	840	650-770	1015-1082	1113	3460
Bulk Density (g/cm ³)	1	0.5-0.7	0.769	0.407	0.157-0.28

3.4 Adsorption desalination system modelling

To model any adsorption system, various equations are needed for the determination of adsorbent material behaviour, energy balance for adsorber beds, evaporator, condenser and secondary heating/cooling water circuits as well as mass and salt balances for the evaporator and finally cycle performance indicators [96, 164].

3.4.1 Adsorbent material modelling

Adsorption phenomenon starts when adsorbent material is subjected to a vapor and continues for long time until equilibrium is reached. In this state, the amount of vapor adsorbed per kg of the adsorbent material is called equilibrium uptake, c (kg_w/kg_{ads}) which depends on equilibrium pressure, adsorbent material temperature and properties of adsorbent/adsorbate working pair [165]. As equilibrium state takes long time to be reached and in reality adsorption cycle time is defined, therefore adsorbent uptake variation with time needs to be determined which is called adsorption kinetics [166]. As a result, characterization of any adsorbent material involves two important parameters; adsorbent equilibrium isotherms and adsorbent kinetics [141, 167, 168].

3.4.1.1 Adsorbent material Isotherms:

As described in the literature review, section 2.5, there are many adsorbent materials that were used with water as refrigerant and hence can be used for water desalination. Five adsorbent materials were selected to investigate their performance for water desalination, Figure 3-5 shows their water adsorption isotherms. As shown in Figure 3-5, isotherms of the five adsorbents [141, 159, 169, 170] are different in shape; therefore more than one mathematical adsorbent isotherm model is needed to predict each adsorbent material performance. Examples of isotherm models include; “Langmuir, Freundlich, Modified Freundlich, Dubinin-Astakhov, Toth and Sips” in addition to empirical approaches that correlate the experimental uptake measurements [171].

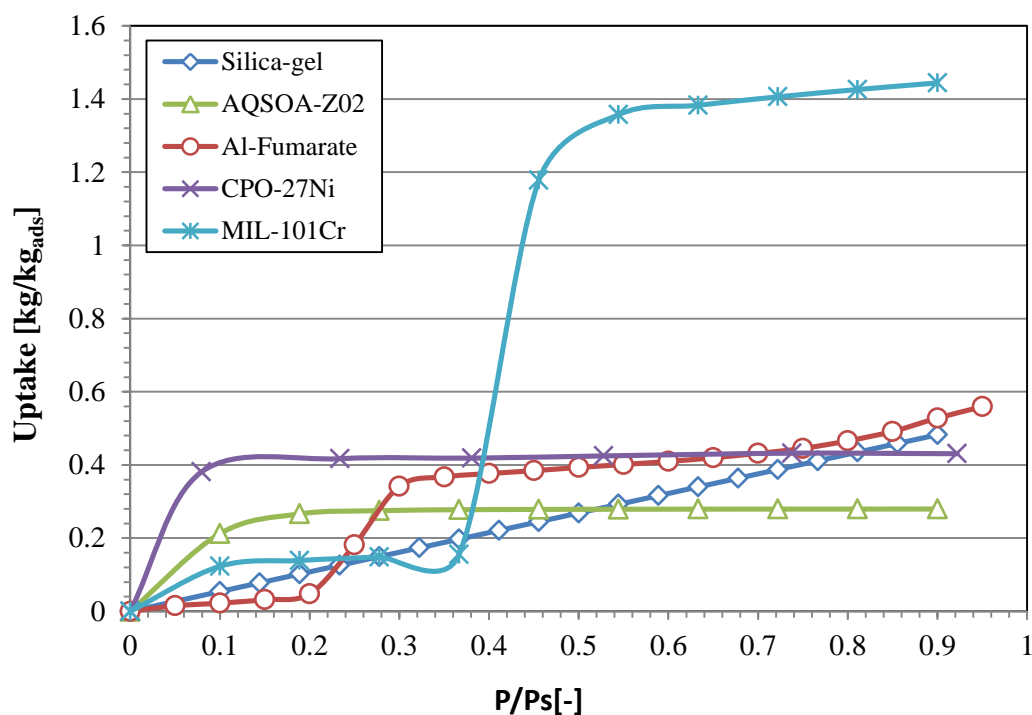


Figure 3-5, Isotherms of adsorbent materials under investigation at 25°C

Silica-gel and CPO-27Ni isotherms are modelled by the Dubinin-Astakhov (D-A) model, equation (3-1), with the constants given in Table 3-3 [5, 172]. However, other isotherm models can be used as in case of Silica-gel where Toth model was employed to correlate its uptake experimental measurements [141].

$$c^* = c_0 \exp \left[- \left(\frac{RT}{E} \ln \left(\frac{P}{P_0} \right) \right)^n \right] \quad (3-1)$$

Where, c^* is the equilibrium uptake (kg.kg^{-1}), c_0 is the maximum adsorbed amount, R is the universal gas constant ($\text{kJ.mol}^{-1}.\text{K}^{-1}$), T is the temperature of the adsorbent (K), E is the characteristic energy (kJ.mol^{-1}), n is the D-A constant, P and P_0 are the saturation pressures at refrigerant and adsorbent temperatures respectively [173].

Table 3-3, Dubinin-Astakhov equation constants for Silica-gel and CPO-27Ni [5, 172]

Symbol	Value		Unit
	Silica-gel	CPO-27Ni	
c_0	0.592	0.46826	Kg.kg^{-1}
E	3.105	10.0887	kJ.mol^{-1}
n	1.1	5.6476	(-)
R	8.314		$\text{kJ.mol}^{-1}.\text{K}^{-1}$

AQSOA-Z02 adsorption isotherm is modelled via the modified Toth isotherm model developed by Sun et al. [169] as in equations (3-2) and (3-3).

$$\frac{c^*}{c_0} = \frac{K(P/P_0)^m}{1 + (K - 1)(P/P_0)^m} \quad (3-2)$$

$$K = \alpha \exp[m(Q_{st} - h_{fg})/RT] \quad (3-3)$$

Where, m is a constant called heterogeneity factor and equals to 3.18, α is a constant equals to 9×10^{-7} , Q_{st} is the isosteric heat of desorption (3600 kJ.kg^{-1}) and h_{fg} is the latent heat (kJ.kg^{-1}) [169].

AL-Fumarate isotherm is modelled using polynomial and exponential expressions developed by Elsayed et al. [159] as in equations (3-4) to (3-7).

$$c^* = 0.111993 \exp[-0.000258797 A] \quad (A > 3987) \quad (3-4)$$

$$c^* = 2.36129 - 9.93768 \times 10^{-4} A + 1.05709 \times 10^{-7} A^2 \quad (2900 \leq A \leq 3987) \quad (3-5)$$

$$c^* = 0.5948 - 3.12 \times 10^{-4} A + 1.68302 \times 10^{-7} A^2 - 3.124455 \times 10^{-11} A^3 \quad (A < 2900) \quad (3-6)$$

Where “ A ” is the adsorption potential given by equation (3-7),

$$A = -RT \ln \left(\frac{P}{P_0} \right) \quad (3-7)$$

Similar to AL-Fumarate, the isotherm of MIL-101Cr is S-shaped; therefore a polynomial and exponential expressions, equations (3-8) to (3-11), are used to describe the equilibrium uptake accurately with maximum error (between experimental measurement and numerical model) of 9.3% at pressure ratio of 0.51 [160, 174].

$$c^* = 0.42434 \exp[-0.0002825 A] \quad (\text{Pr} \leq 0.15) \quad (3-8)$$

$$c^* = 0.4636 - 2.4 \times 10^{-4} A + 5.4 \times 10^{-8} A^2 - 4.06 \times 10^{-12} A^3 \quad (0.15 \leq \text{Pr} \leq 0.4) \quad (3-9)$$

$$c^* = 1.51 - \left(\frac{A}{1.35 \times T} \right) \quad (0.4 \leq \text{Pr} \leq 0.5) \quad (3-10)$$

$$c^* = 1.51 - 2.66 \times 10^{-4} A + 3.63 \times 10^{-5} A^2 - 1.77 \times 10^{-8} A^3 \quad (\text{Pr} > 0.5) \quad (3-11)$$

3.4.1.2 Adsorbent material kinetics:

As mentioned earlier, equilibrium uptake alone can not predict the cycle dynamic adsorption capacity and hence, adsorption kinetics models are needed. Many models exist to model adsorption kinetics like Fickian Diffusion (FD), Linear Driving Force (LDF) and Quadratic Driving Force (QDF) [175]. However, the most simple, widely used and yet accurate (error range is 1.5-3.5% [148]) kinetics model is the LDF one developed by Glueckauf [176] as in equations (3-12) and (3-13) [177].

$$\frac{dc}{dt} = k(c^* - c) \quad (3-12)$$

$$k = k_0 e^{\left(\frac{-E_a}{RT}\right)} \quad (3-13)$$

Where, “c” is the instantaneous uptake level at a certain time “t”, k_0 is a pre-exponential constant and E_a is the activation energy constant [177].

The constants of equation (3-13), for silica-gel, AQSOA-Z02, Al-Fumarate, CPO-27Ni and MIL-101Cr are listed in Table 3-4 [5, 8, 12, 159].

Table 3-4, LDF equation constants for the adsorbent materials [5, 8, 12, 159]

Adsorbent material	Silica-gel	AQSOA-Z02		AL-Fumarate	CPO-27Ni		MIL-101Cr		
		Pr range	Constant		Pr range	Constant	Pr range	Constant	Pr range
	0 to 1	≤0.1	>0.1	0 to 1	≤0.2	>0.2	≤0.15 Or >0.5	> 0.15 and ≤0.4	> 0.4 and ≤0.5
k_0^a	15.7E-4	1846	3.2344	1.29	81.561	0.7779	6.36E3	0.72	0.033
$E_a \times 10^4^b$	4.2	1.770	4.4423	1.8	3.2006	1.4806	3.6	1.3	1.3

Units are; ^a = 1/s, ^b = J/mol

3.4.2 Energy balance equations

3.4.2.1 Adsorber /desorber bed energy balance equation:

As shown in Figure 3-6, water vapor is either entering the adsorber bed during adsorption process or exiting during desorption process to be adsorbed/desorbed by the adsorber granules. At the same time, there is a coil where cooling or heating fluid is passing through the adsorber bed during adsorption or desorption processes respectively. To simplify modelling of the adsorber bed, it is assumed that it has the same temperature at all points which is not the case in reality as adsorbent material granules have different temperatures depending on the position of the cooling/heating coil and the exposure to the water vapor. The energy balance equation is applied on the adsorber bed components as in equation (3-14) which [9].

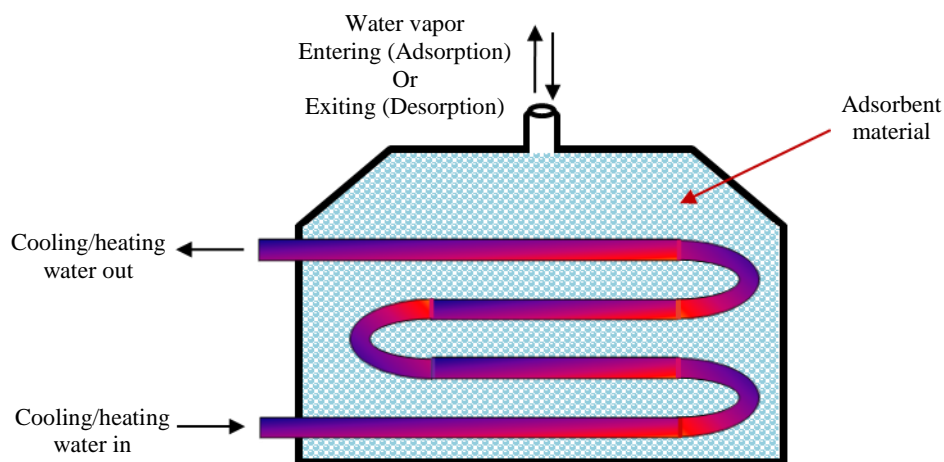


Figure 3-6, Schematic diagram of the adsorber bed

$$\begin{aligned}
 & [M_a c_{p,a} + M_{HX} c_{p,HX} + M_{abe} c_{p,abe}] \frac{dT_{ads/des}}{dt} \\
 & = z \cdot Q_{st} M_a \frac{dc_{ads/des}}{dt} + m_{cw/hw} c_p (T_{cw/hw,in} - T_{cw/hw,out})
 \end{aligned}
 \tag{3-14}$$

Where, z is a flag equals 1 at all times except at heat recovery phase where its value is 0.

The terms on the left hand side of equation (3-14), are the rate of heat required to be either extracted or added to the adsorbent granules, heat exchanger metal parts and the adsorbed water vapour inside adsorbent pores during adsorption/desorption processes respectively.

The terms on the right hand side of equation (3-14), are the rate of heat generated or extracted during adsorption or desorption processes respectively, and the heat transferred to or from the secondary fluid in adsorption or desorption processes respectively.

3.4.2.2 Evaporator energy balance equation:

As shown in Figure 3-7, different streams of fluids are entering and exiting from the evaporator. Entering fluids are seawater and chilled water acting as the heat load, while exiting fluids are the vaporized water vapor going to the adsorber bed, concentrated brine and the chilled water after being cooled. According to the inlet and outlet fluid streams, the energy balance is applied as in equation (3-15) [9].

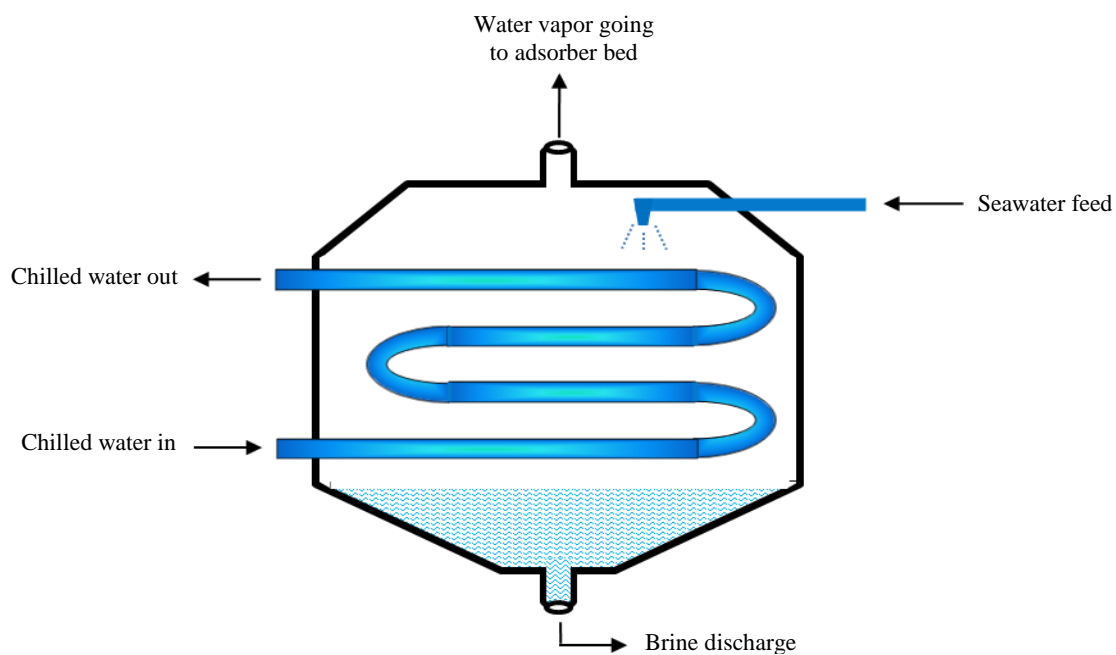


Figure 3-7, Schematic diagram of the evaporator

$$\begin{aligned}
& [M_{s,evap}c_{p,s}(T_{evap}, X_{s,evap}) + M_{HX,Evap}c_{p,HX}] \frac{dT_{evap}}{dt} \\
& = \theta \cdot h_f(T_{evap}, X_{s,evap}) m_{s,in} - z \cdot h_{fg}(T_{evap}) \frac{dc_{ads}}{dt} M_a \\
& - \gamma h_f(T_{evap}, X_{s,evap}) m_{brine} \\
& + m_{chilled}c_p(T_{evap})(T_{chilled,in} - T_{chilled,out})
\end{aligned} \tag{3-15}$$

Where, θ is a flag equal to 1 during seawater feed into evaporator and 0 in all other cases and γ is a flag equal to 1 during concentrated brine discharge from evaporator and 0 in all other cases.

The terms on the left hand side of equation (3-15), are the rate of heat extracted from seawater in evaporator and rate of heat removed from evaporator fins and tubes. The right hand side terms represent rate of heat added by the fed seawater, rate of heat extracted from seawater due to the evaporation effect, rate of heat removed by discharged brine out of the evaporator and rate of heat extracted from chilled water passing through evaporator coil respectively.

3.4.2.3 Condenser energy balance equation:

As shown in Figure 3-8, the condenser receives the water vapor discharged from the adsorber bed during the desorption process which in turn losses its latent heat and condenses by the cooling provided via the cooling fluid in the coil and finally the condensed fresh water is collected from the bottom. For these three streams of fluids, the energy balance equation is applied as in equation (3-16) [9].

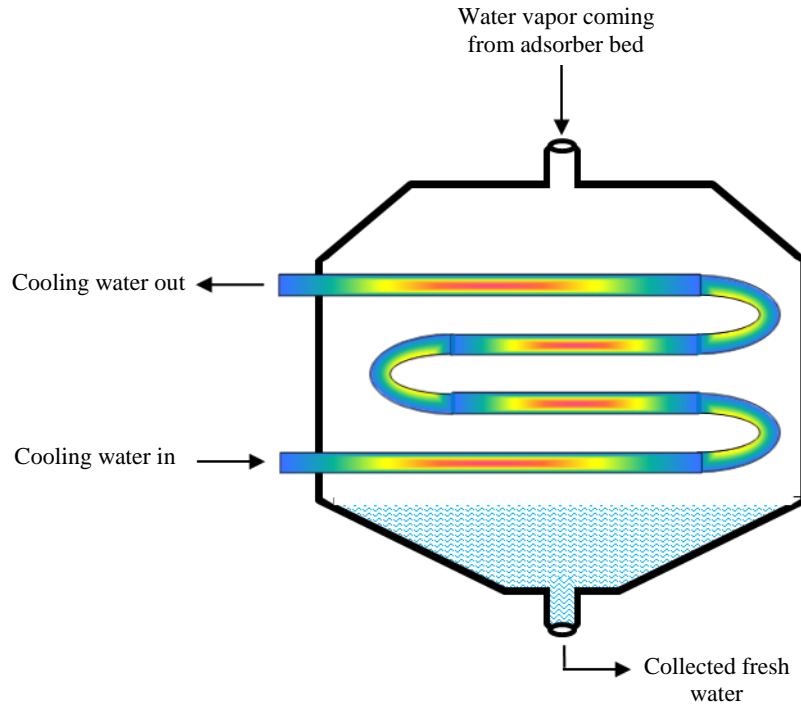


Figure 3-8, Schematic diagram of the condenser

$$\begin{aligned}
 & [M_{\text{cond}}c_p(T_{\text{cond}}) + M_{\text{HX,Cond}}c_{p,\text{HX}}] \frac{dT_{\text{cond}}}{dt} \\
 & = z \cdot h_{\text{fg}}(T_{\text{cond}}) M_a \cdot \frac{dc_{\text{des}}}{dt} - h_f(T_{\text{cond}}) \frac{dM_d}{dt} \\
 & + m_{\text{cond}}c_p(T_{\text{cond}})(T_{\text{cond,in}} - T_{\text{cond,out}})
 \end{aligned} \tag{3-16}$$

The terms on the left hand side of equation (3-16), are the rate of heat extracted from condenser fresh water in the condenser and heat extracted from condenser fins and tubes.

The right hand side terms represent rate of heat transfer due to condensation of water vapour coming from desorbing bed, rate of heat removed by fresh water leaving the condenser and rate of heat transfer to condenser cooling water respectively.

3.4.3 Heat transfer

This part of the modelling is essential to determine the outlet temperature of the secondary fluid from all devices in the adsorption desalination cycle namely; adsorber bed, evaporator and condenser. The heat transfer coefficient, " U ", is related to the secondary fluid inlet, " T_i ", and exit, " T_o ", temperatures as in equation (3-17) [178].

$$U \times A \times \text{LMTD} = \dot{m} c_p (T_o - T_i) \quad (3-17)$$

Where, \dot{m} and c_p are mass flow rate and specific heat of the secondary fluid respectively. " A " is the heat transfer area, LMTD is the logarithmic mean temperature difference between inlet, outlet secondary fluid temperatures and heat exchanger temperature [178].

3.4.3.1 Adsorber /desorber bed heat transfer equations:

To determine the heat transfer coefficient, " U_{bed} ", the heat resistances need to be identified first as shown in Figure 3-9. Inside the tube, convective heat transfer resistance, " $R_{w,bed}$ " exist where the secondary fluid flows inside the tubes then a conductive heat transfer resistance " $R_{t,bed}$ " is found through adsorber/desorber bed tubes wall and finally the outside tube heat transfer resistance " $R_{o,bed}$ " arises through fins and adsorbent granules. Heat transfer coefficient, " U_{bed} ", is calculated using equation (3-18) after all heat resistances are calculated using equations (3-19) to (3-24) [179, 180].

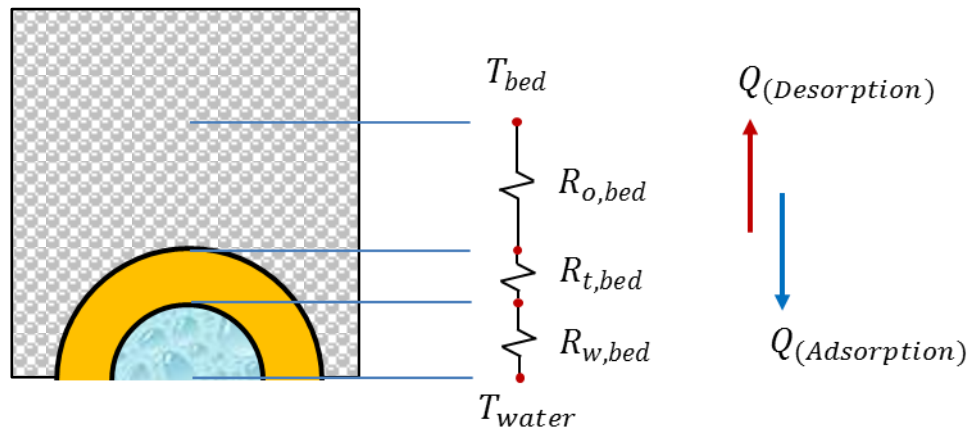


Figure 3-9, Schematic of the heat transfer resistances in the adsorber bed

$$U_{bed} x A_{bed} = \frac{1}{(R_{w,bed} + R_{t,bed} + R_{o,bed})} \quad (3-18)$$

$$R_{w,bed} = \frac{1}{h_i A_{tube}} \quad (3-19)$$

$$h_i = \frac{Nu k}{D_{tube}} \quad (3-20)$$

$$Nu = \begin{cases} 4.36 & , \quad \text{(Laminar flow, } Re < 3000) \\ \frac{(f/8)(Re - 1000)Pr}{1 + 12.7\sqrt{f/8}(Pr^{2/3} - 1)} & , \quad \text{(Turbulent flow, } 3000 < Re < 5 \times 10^6) \end{cases} \quad (3-21)$$

$$Nu = \begin{cases} 4.36 & , \quad \text{(Laminar flow, } Re < 3000) \\ \frac{(f/8)(Re - 1000)Pr}{1 + 12.7\sqrt{f/8}(Pr^{2/3} - 1)} & , \quad \text{(Turbulent flow, } 3000 < Re < 5 \times 10^6) \end{cases} \quad (3-22)$$

$$f = \frac{1}{\left\{ 1.8 \log_{10} \left[\frac{6.9}{Re} + \left(\frac{\epsilon/d}{3.7} \right)^{1.11} \right] \right\}^2} \quad (3-23)$$

Where, Nu is the Nusselt number, k is the thermal conductivity of the secondary fluid, f is the friction factor, Pr is the Prandtl number and ϵ is the wall roughness [179, 180].

$$R_{t,bed} = \frac{\ln(d_o/d_i)}{2\pi k_{tube} L_{tube}} \quad (3-24)$$

Finally, $R_{o,bed}$ is estimated using the equations developed by Rizk et al. [139].

3.4.3.2 Evaporator heat transfer equations:

Like the case in the adsorber bed, the evaporator has three heat resistances, " $R_{w,evap}$, $R_{t,evap}$ and $R_{boiling,evap}$ " as shown in Figure 3-10 which are used to determine the heat transfer coefficient " U_{evap} " as in equation (3-25). " $R_{w,evap}$ " is the convective heat transfer resistance of the evaporator chilled water flowing inside the tubes while " $R_{t,evap}$ " is the conductive heat transfer resistance through evaporator tubes. Both heat resistances are calculated as in the previous section from equation (3-19) and (3-24) respectively. $R_{boiling,evap}$ is the heat transfer resistance in the evaporator space where seawater boils. It is predicted using the modified Rohsenov correlation for saline solutions evaporating at sub-atmospheric pressures [181], equations (3-26) and (3-27).

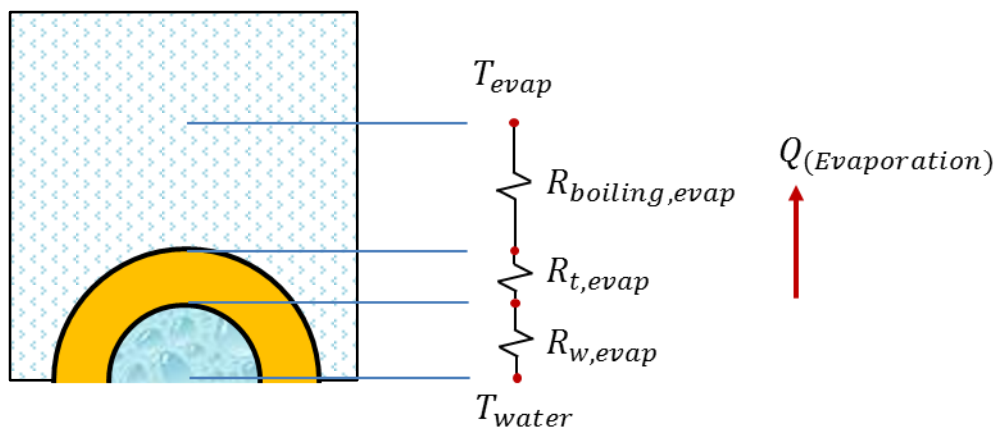


Figure 3-10, Schematic of heat transfer resistances in the evaporator

$$U_{evap} \times A_{evap} = \frac{1}{R_{w,evap} + R_{t,evap} + R_{boiling,evap}} \quad (3-25)$$

$$R_{boiling,evap} = \frac{1}{h_{boiling,evap} A_{tube,evap}} \quad (3-26)$$

$$h_{\text{boiling, evap}} = (\mu_f h_{fg} \Delta T_{\text{surf-vapor}})^2 \left[\frac{g(\rho_f - \rho_g)}{\sigma} \right]^{1/2} \quad (3-27)$$

$$\left[\frac{c_{p,f}}{h_{fg} C_{sf} Pr_f^s} \right]^3 \left[\left(\frac{P_{\text{atm}}}{P_{\text{sat, evap}}} \right)^{0.293} \right]^3 \left[\left(\frac{A_{\text{base}}}{A_{\text{wetted}}} \right)^{-0.0984} \right]^3$$

Where, μ is the dynamic viscosity of boiling seawater, h_{fg} is the latent heat of vaporization, g is the gravitational acceleration, ρ is density of boiling seawater, σ is the surface tension, C_{sf} and s are correlation constants and they equal to 0.0068 and 1 respectively. Also, the two subscripts, f and g denote the fluid and gas phases, respectively of any mentioned property.

3.4.3.3 Condenser heat transfer equations:

Figure 3-11 shows the heat transfer resistances in the condenser, " $R_{w, \text{cond}}$ ", " $R_{t, \text{cond}}$ " and " $R_{\text{condensing, cond}}$ " which determine the overall heat transfer coefficient " U_{cond} " as in equation (3-28). " $R_{w, \text{cond}}$ " is the convective heat transfer resistance of the condenser cooling water flowing inside pipes and " $R_{t, \text{cond}}$ " is the conductive heat transfer resistance through condenser tubes. These two heat transfer resistances are estimated via equations (3-19) and (3-24) respectively. " $R_{\text{condensing, cond}}$ " is the heat transfer resistance in the condensing process of the desorbed water vapor in the condenser during the formation of the liquid fresh water. It is predicted using the correlation of average laminar film condensation over tube bank as in equations (3-29) and (3-30) [182].

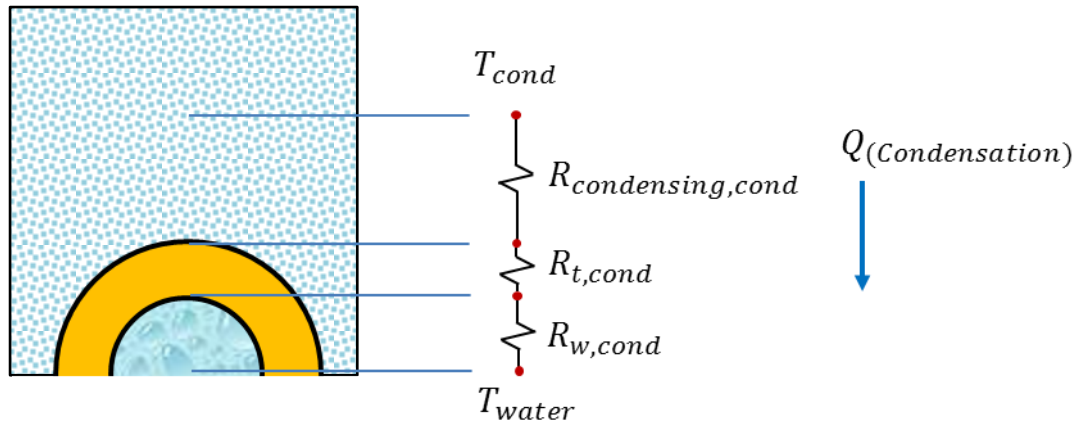


Figure 3-11, Schematic of heat transfer resistances in the condenser

$$U_{\text{cond}} \times A_{\text{cond}} = \frac{1}{R_{w,\text{cond}} + R_{t,\text{cond}} + R_{\text{condensing,cond}}} \quad (3-28)$$

Where, $R_{w,\text{cond}}$ is the convective heat transfer resistance of the condenser cooling water flowing inside pipes and it is calculated from equation (3-19). $R_{t,\text{cond}}$ is the conductive heat transfer resistance through condenser tubes and it is estimated via equation (3-24). $R_{\text{condensing,cond}}$ is the condensation heat transfer resistance of the water vapor condensing in the condenser during the formation of the liquid fresh water. It is predicted using the Nusselt correlation of average laminar film condensation over tube bank as in equations (3-29) and (3-30) [182].

$$R_{\text{condensing,cond}} = \frac{1}{h_{\text{condensing,cond}} A_{\text{tube,cond}}} \quad (3-29)$$

$$h_{\text{condensing,cond}} = 0.728 \left[\frac{\rho_f (\rho_f - \rho_g) g h_{fg} k_f^3}{D_{\text{tube,out}} \mu_f \Delta T_{\text{vapor-surf}}} \right]^{1/4} \quad (3-30)$$

3.4.4 Mass balance equations

3.4.4.1 Evaporator mass balance equation:

As shown in Figure 3-7, seawater is fed into the evaporator then the evaporated water vapor exits and goes to the adsorber bed while the remaining concentrated seawater (brine) is discharged. A mass balance is applied using equation (3-31) [9], to determine the instantaneous amount of seawater inside the evaporator.

$$\frac{dM_{s, \text{evap}}}{dt} = \theta \dot{m}_{s, \text{in}} - \gamma \dot{m}_{\text{brine}} - M_a \frac{dc_{\text{ads}}}{dt} \quad (3-31)$$

The left hand side of equation (3-31) is the rate of seawater mass change in the evaporator while the right hand side terms represent rate of seawater feed, rate of brine discharge and rate of evaporated seawater respectively.

3.4.4.2 Evaporator salt balance equation:

Salt concentration in the evaporator is essential in the operation and modelling of the adsorption desalination systems as it determines when brine is to be discharged and when seawater needs to be fed. Therefore a salt balance in the evaporator is applied using equation (3-32) where X is the mass fraction of salts in the entire seawater with a unit of $\text{kg}_{\text{salt}}/\text{kg}_{\text{seawater}}$ [9].

$$M_{s, \text{evap}} \frac{dX_{s, \text{evap}}}{dt} = \theta X_{s, \text{in}} \dot{m}_{s, \text{in}} - \gamma X_{s, \text{evap}} \dot{m}_{\text{brine}} - X_g \frac{dc_{\text{ads}}}{dt} M_a \quad (3-32)$$

The left hand side of equation (3-32) is the rate of change of evaporator seawater salt concentration while the right hand side terms represent increased salt concentration because

of seawater feed, decreased salt concentration due to brine discharge and evaporated seawater leaving the evaporator respectively.

3.4.5 Cycle performance indicator equations

To assess performance of adsorption desalination cycle, two indicators are used; specific daily water production (SDWP) and performance ratio (PR) [7]. Specific daily water production is the amount of water produced daily in cubic meters per tonne of packed adsorbent while performance ratio is a measure of cycle efficiency as it is the ratio between heat of condensation to heat of desorption [11]. These two parameters are calculated using equations (3-33) and (3-34) [9].

$$SDWP = \int_0^{t_{\text{cycle}}} \frac{Q_{\text{cond}}}{h_{\text{fg}} M_a} dt \quad (3-33)$$

$$PR = \int_0^{t_{\text{cycle}}} \frac{Q_{\text{cond}}}{Q_{\text{des}}} dt \quad (3-34)$$

Where,

$$Q_{\text{cond}} = \dot{m}_{\text{cond}} c_p (T_{\text{cond,out}} - T_{\text{cond,in}}) \quad (3-35)$$

$$Q_{\text{des}} = \dot{m}_{\text{hw}} c_p (T_{\text{hw,in}} - T_{\text{hw,out}}) \quad (3-36)$$

In applications where the cooling effect associated with boiling of the seawater is used, another two indicators are calculated which are the specific cooling power (SCP) and coefficient of performance (COP) [11]. SCP is the amount of cooling produced per unit mass of adsorbent material (equation (3-37)) and its unit is either W.kg^{-1} or Rton.tonne^{-1} where “Rton” is the Ton of refrigeration defined as the amount of heat needed to melt 1000 kg of ice in 24 hours. COP is a measure of the efficiency of the cycle it is calculated using equation

(3-38). To assess the overall cycle performance, another parameter called overall conversion ratio is evaluated using equation (3-39) which takes into account the cycle water and cooling production [5].

$$SCP = \int_0^{t_{\text{cycle}}} \frac{Q_{\text{evap}}}{M_a} dt \quad (3-37)$$

$$COP = \int_0^{t_{\text{cycle}}} \frac{Q_{\text{evap}}}{Q_{\text{des}}} dt \quad (3-38)$$

$$OCR = \int_0^{t_{\text{cycle}}} \frac{Q_{\text{evap}} + Q_{\text{cond}}}{Q_{\text{des}}} dt \quad (3-39)$$

Where,

$$Q_{\text{evap}} = \dot{m}_{\text{evap}} c_p (T_{\text{evap,in}} - T_{\text{evap,out}}) \quad (3-40)$$

3.5 Simulink modelling of the adsorption water desalination system

Simulink is an interactive visual tool for performing computational simulations through the use of blocks and Matlab embedded functions. It offers rapid construction of models as well as flexibility in modifying the blocks which facilitates investigating various designs. Four main blocks are created in the Simulink model to simulate the adsorption desalination cycle as shown in Figure 3-12 while a flow diagram for the model is shown in Figure 3-13. These blocks are the main heat exchanging devices in the cycle which are two adsorber/desorber beds, evaporator and condenser. Also, there is number of auxiliary blocks to direct the inputs to the main blocks according to the operating phase and other blocks to produce the main cycle results. Under each main block, there are other subsystem blocks and Matlab functions to model the energy balance and heat transfer equations while in case of adsorber/desorber bed blocks, additional blocks exist to model adsorbent material

performance. Moreover, under evaporator main block, there are supplementary blocks to model mass and salinity balance equations in addition to controlling seawater feeding and brine discharging flags.

This Simulink model performs numerical integration using an ordinary equation solver (ODE45) based on an explicit Runge-Kutta (4, 5) formula developed by Dormand and Prince with a variable time step and relative tolerance of 10^{-3} [11, 183].

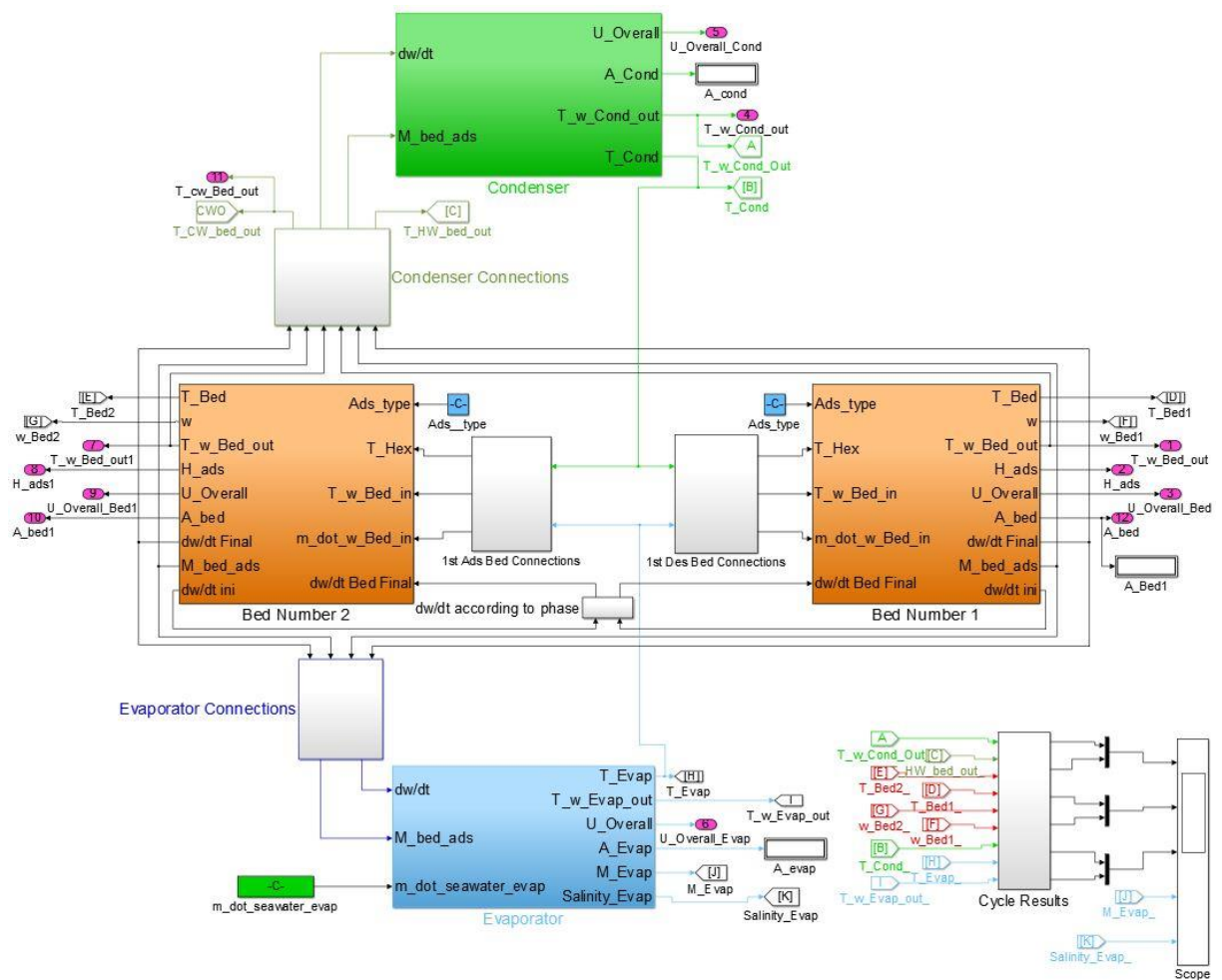


Figure 3-12, Simulink model of the adsorption desalination cycle

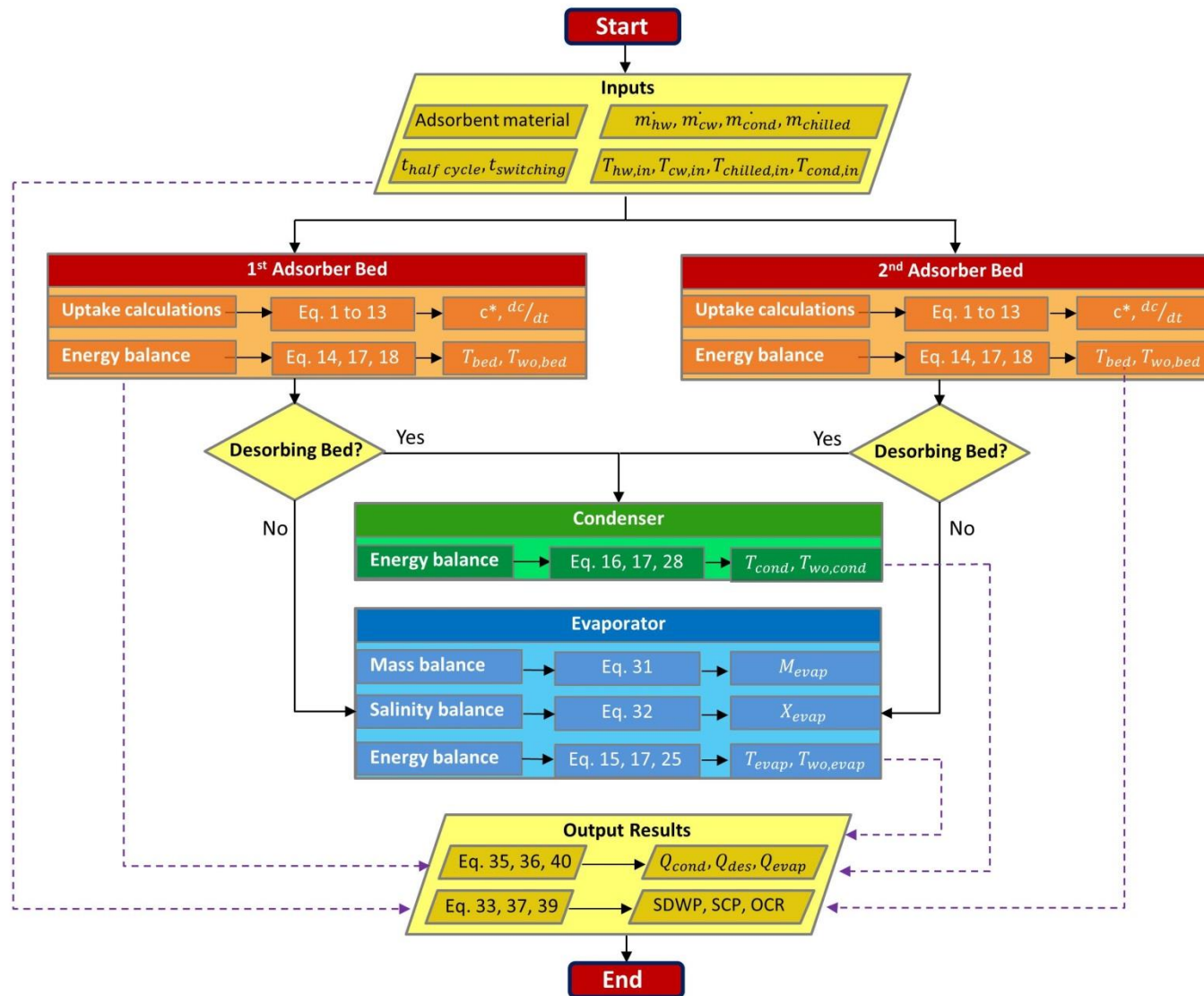


Figure 3-13, Flow diagram for the Simulink model of the 2-bed adsorption desalination cycle

3.5.1 Simulink model validation

The developed double bed adsorption desalination Simulink model is validated against the published measured experimental results of two-bed Silica-gel adsorption desalination system at the operating conditions listed in Table 3-5 [99].

Table 3-5, Operating conditions of the double bed validation test using Silica-gel [99]

Parameter	Average deviation
Heating water temperature	85°C
Cooling water temperature	30°C
Condenser cooling water inlet temperature	30°C
Evaporator chilled water inlet temperature	30°C
Half cycle time	600 seconds

Figure 3-14, [94], shows comparison between numerical results against experimentally measured results for the main components of the basic adsorption system namely; adsorber/desorber beds, evaporator and the condenser while SDWP results are shown in Figure 3-15. To ensure that validation is performed at cyclic steady state results, numerical model results are taken after 5 complete cycles while experimental temperature measurements are taken after running the system for two complete cycles [99]. Based on equation (3-41), the instantaneous error between steady state experimental and numerical results is calculated and the maximum error was found to be 9.7% (1st adsorber bed at time of 65 seconds, Figure 3-14) while error range for all components is shown in Table 3-6 which reflects the accuracy of the Simulink model.

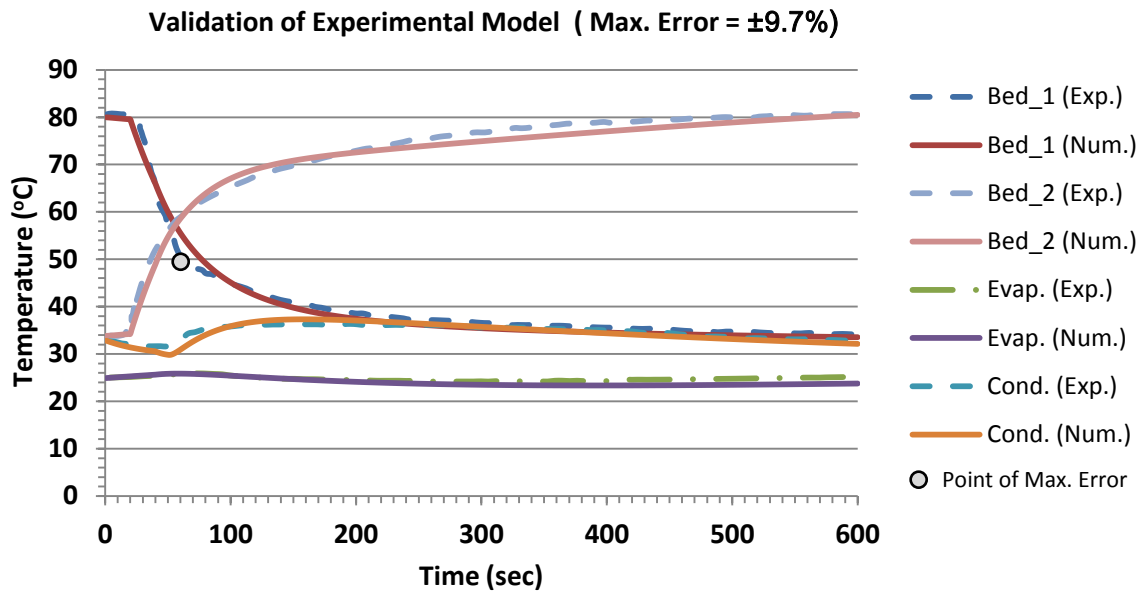


Figure 3-14, Validation of the double bed adsorption desalination Simulink model, temperature profiles of adsorber beds, evaporator and condenser [94]

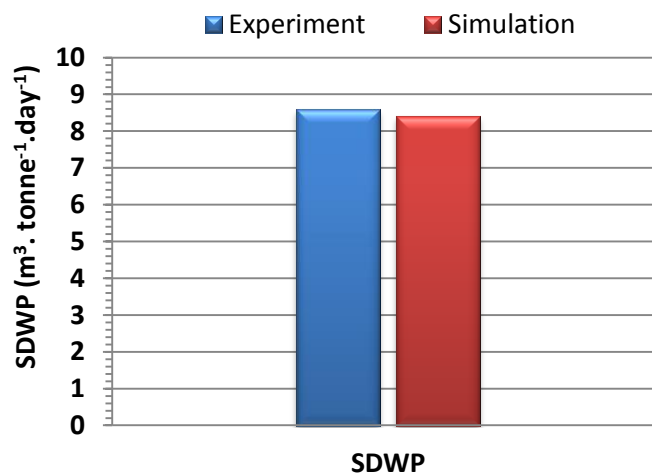


Figure 3-15, Comparison between experimental and numerical results of SDWP for Silica-gel

Error calculation equation:

$$\text{Error} = \frac{T_{num.}(\text{°C}) - T_{exp.}(\text{°C})}{T_{exp.}(\text{°C})} \times 100 \quad (3-41)$$

Where, $T_{num.}$ and $T_{exp.}$ are the temperatures obtained numerically and experimentally, respectively.

Table 3-6, Error in the validation of the double bed adsorption desalination cycle using Silica-gel

Parameter	Error
1 st Adsorber bed	-7.1 to 9.7 %
2 nd Adsorber bed	-7.8 to 2.7%
Condenser	-6.6 to 2.8%
Evaporator	-5.7 to 0.84%
Specific daily water production (SDWP)	2.2%

3.6 Summary

In this chapter modelling of an adsorption desalination system was introduced for five different adsorbents; Silica-gel, AQSOA-Z02, Al-Fumarate, CPO-27Ni and MIL-101Cr. The specifications of a real adsorption machine produced by “Weatherite Manufacturing LTD” used in modelling the performance of these materials in such system were presented. The modelling process included modelling the behaviour of adsorbent materials in addition to modelling of the adsorber/desorber bed, evaporator and condenser which form any adsorption desalination cycle. Moreover, brief details of the Simulink model and its components were given while more details are given in Appendix I. Finally, the developed Simulink model has been validated against the published experimental measurements of double bed adsorption desalination system based on Silica-gel with maximum deviation of $\pm 9.7\%$ [94].

CHAPTER 4: INVESTIGATION OF OPERATING CONDITIONS IN ADSORPTION DESALINATION CYCLE

4.1 Introduction

As presented in chapter 2, Silica-gel was the only adsorbent material investigated for water desalination applications using adsorption technology. In this chapter, a number of advanced zeolite and metal organic framework materials namely; AQSOA-Z02, Al-Fumarate, CPO-27Ni and MIL-101Cr will be investigated using double-bed adsorption system at different operating conditions and their performance is compared to Silica-gel [8, 94, 134, 184]. The operating conditions under investigation includes effect of condenser, evaporator and bed's cooling and heating secondary fluids temperatures on adsorption cycle outputs for the purpose of seawater desalination mainly and for cooling as a by-product. In addition, silica-gel will be studied at other operating conditions that have not been investigated before like condenser cooling water temperature [94].

4.2 Operating conditions under investigation

Adsorption desalination system performance depends on a number of factors like desorption, adsorption, evaporator and condenser water circuits' temperatures in addition to cycle time. Some of these parameters are uncontrolled as they depend on weather conditions like adsorption and condenser cooling water temperature which are further cooled via cooling tower or a heat exchanger using the available sources of water as rivers or the sea. The other operating conditions can be controlled or selected by the designer of the

system according to the available heat source temperature and evaporator load temperature for desorption and evaporator temperatures respectively.

In this section, water inlet temperature of condenser and adsorber bed cooling circuits is kept constant at 30°C but evaporator and desorption inlet water temperatures are varied in the range of (10-30°C) and (65-140°C) respectively with half cycle time of 450 seconds. Then, half cycle time is investigated in the range of 50-900 seconds at an evaporator inlet temperature of 30°C while desorption water inlet temperature varies in the range of 65 to 140°C. The system under consideration here is a full scale double-bed adsorption system, produced by "Weatherite Manufacturing Ltd." with a size corresponds to each adsorber bed packed with 890 kg of silica-gel which was modelled in chapter 3.

4.2.1 Effects of bed heating and evaporator water temperature

4.2.1.1 Silica-gel:

Figure 4-1 shows the specific daily water production (SDWP), specific cooling power (SCP) and overall conversion ratio (OCR) for Silica-gel at different evaporator water inlet temperatures (10 to 30°C) and different adsorber bed water heating temperatures (65-140°C). As shown in Figure 4-1, as desorption and evaporator water inlet temperatures increase, water and cooling production increase. However, at all evaporating temperatures for desorption temperatures above 95°C, changes in SDWP are less than 8.7%. At evaporator temperature of 30°C, SDWP increased from 9.28 to 9.71 m³.ton⁻¹.day⁻¹ when desorption temperature changes from 95 to 140°C with a percentage of change of 4.4%. Similarly, SCP is less sensitive to desorption temperature changes above 95°C as it increases by only 9% when desorption temperature increases from 95°C to 140°C compared to 49% increase when desorption temperature increased from 65°C to 95°C. On the other hand, at all evaporator

inlet water temperatures, OCR is at its highest values at temperatures equal to 85°C as it reaches 0.98 at evaporator temperature of 30°C and desorption temperature of 85°C.

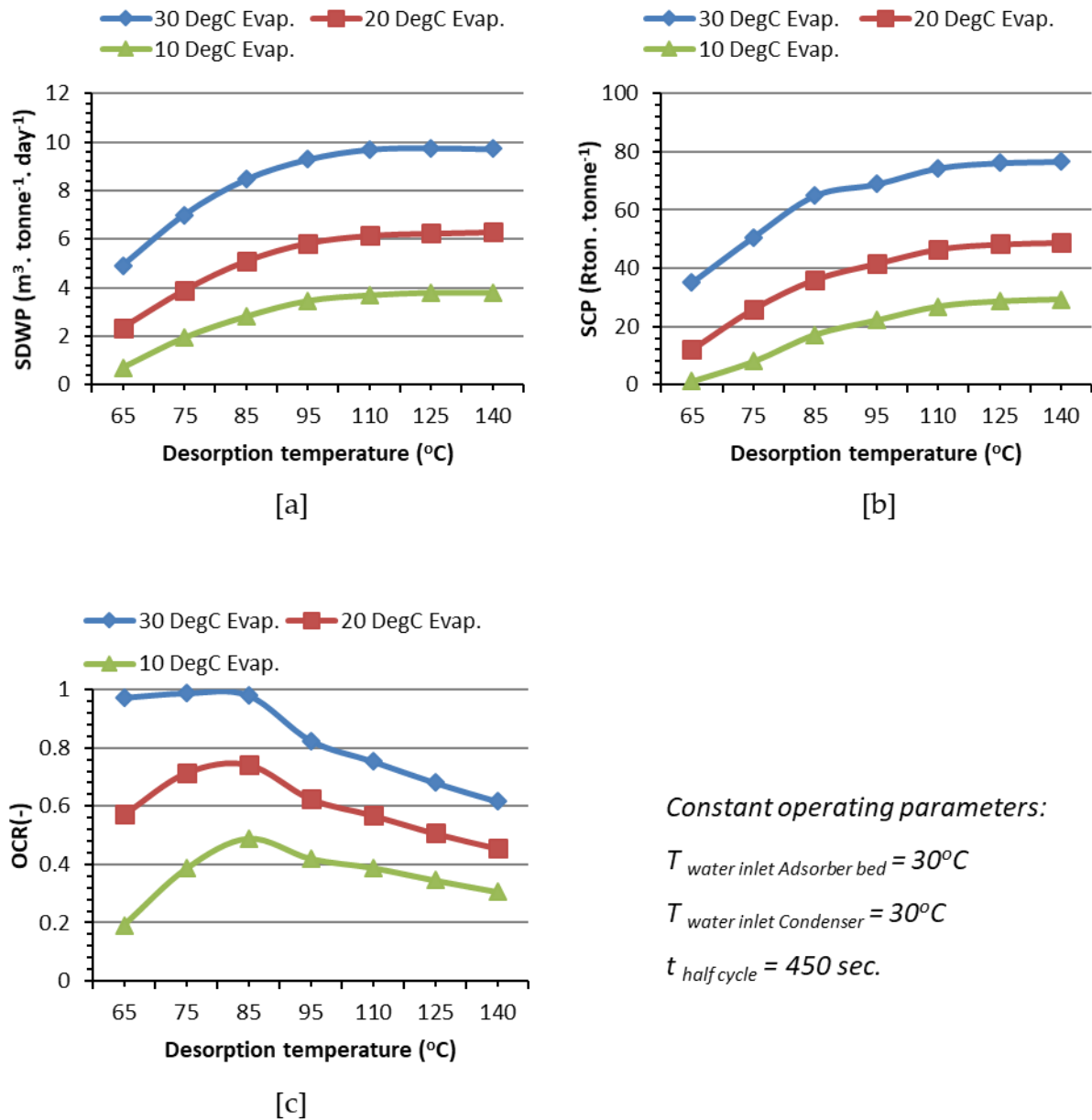


Figure 4-1, Effect of desorption and evaporator water temperatures on SDWP (a), SCP² (b) and OCR (c) of double-bed adsorption desalination system (Silica-gel)

² SCP unit is (Rton.tonne⁻¹) where "Rton" is the Ton of refrigeration defined as the amount of heat needed to melt 1000 kg of ice in 24 hours.

4.2.1.2 AQSOA-Z02:

Using AQSOA-Z02 as the adsorbent, effects of changing evaporator and desorber bed water inlet temperatures on SDWP, SCP and OCR are presented in Figure 4-2. It is noticed that changing desorption inlet water temperature is more dominant than evaporator water temperature due to isotherm shape of AQSOA-Z02 which is very steep at low partial pressure ratios [11]. It is also noticeable that above 95°C desorption temperature, evaporator temperature affects system outputs. The reason is that at low desorption temperatures, desorption rates are low therefore at any evaporator temperature (i.e. any adsorption rate) the adsorbent material can only desorb a certain amount of water vapor which in turn results in almost the same cycle outputs at different evaporator temperatures. In contrast, at higher desorption temperatures and therefore desorption rates, the material can desorb the whole amount of water vapor that has been adsorbed and hence the effect of evaporator temperature appears where higher evaporator temperatures reflects higher adsorption capabilities for the adsorbent material. At evaporator water inlet temperature of 30°C and desorption temperatures equal to and above 125°C, AQSOA-Z02 reaches its maximum water and cooling production of 20.6 m³.ton⁻¹.day⁻¹ and 169.1 Rton.ton⁻¹ respectively with an OCR of 0.87. However, OCR reaches its maximum of 0.91 at a lower desorption temperature of 110°C.

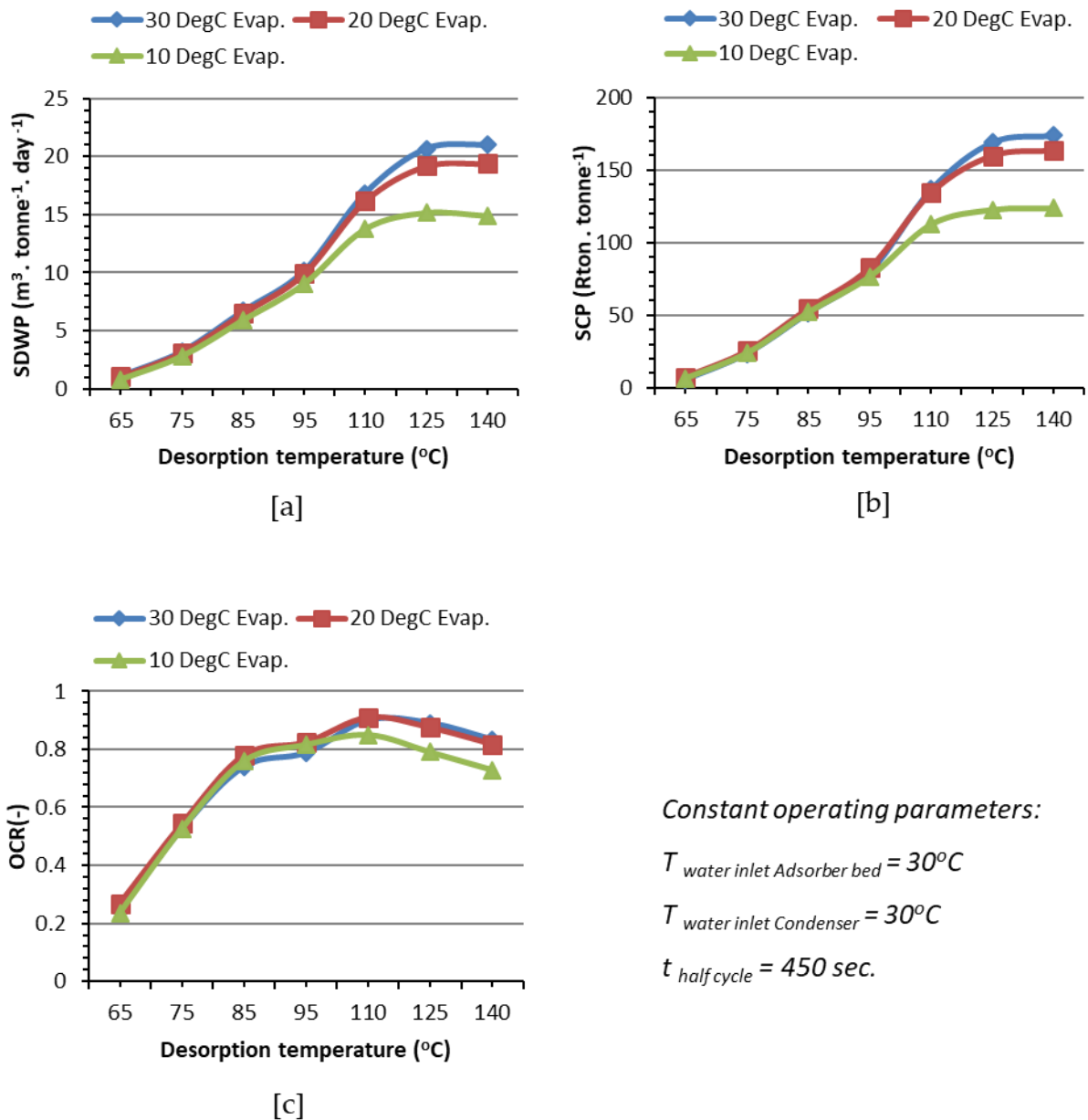


Figure 4-2, Effect of desorption and evaporator water temperatures on SDWP (a), SCP (b) and OCR (c) of double-bed adsorption desalination system (AQSOA-Z02)

4.2.1.3 Al-Fumarate:

As shown in Figure 4-3, performance of Al-Fumarate is greatly affected by the range of evaporator water inlet temperature where it becomes more effective at temperatures above 20°C. Similar to the other adsorbents, increasing desorption water temperature, increases productivity as at evaporator and desorption water temperatures of 30°C and 140°C, SDWP

and SCP reached $13.27 \text{ m}^3 \cdot \text{tonne}^{-1} \cdot \text{day}^{-1}$ and $101.44 \text{ Rton} \cdot \text{tonne}^{-1}$ respectively. However, OCR increased by decreasing desorption temperature as it reached its maximum of 1.2 at low desorption temperature of 65°C . However, at desorption temperature of 95°C , OCR still has high value of 0.9 with only 7.5% and 11.5% reduction in SDWP and SCP respectively compared to their highest values at 140°C desorption temperature.

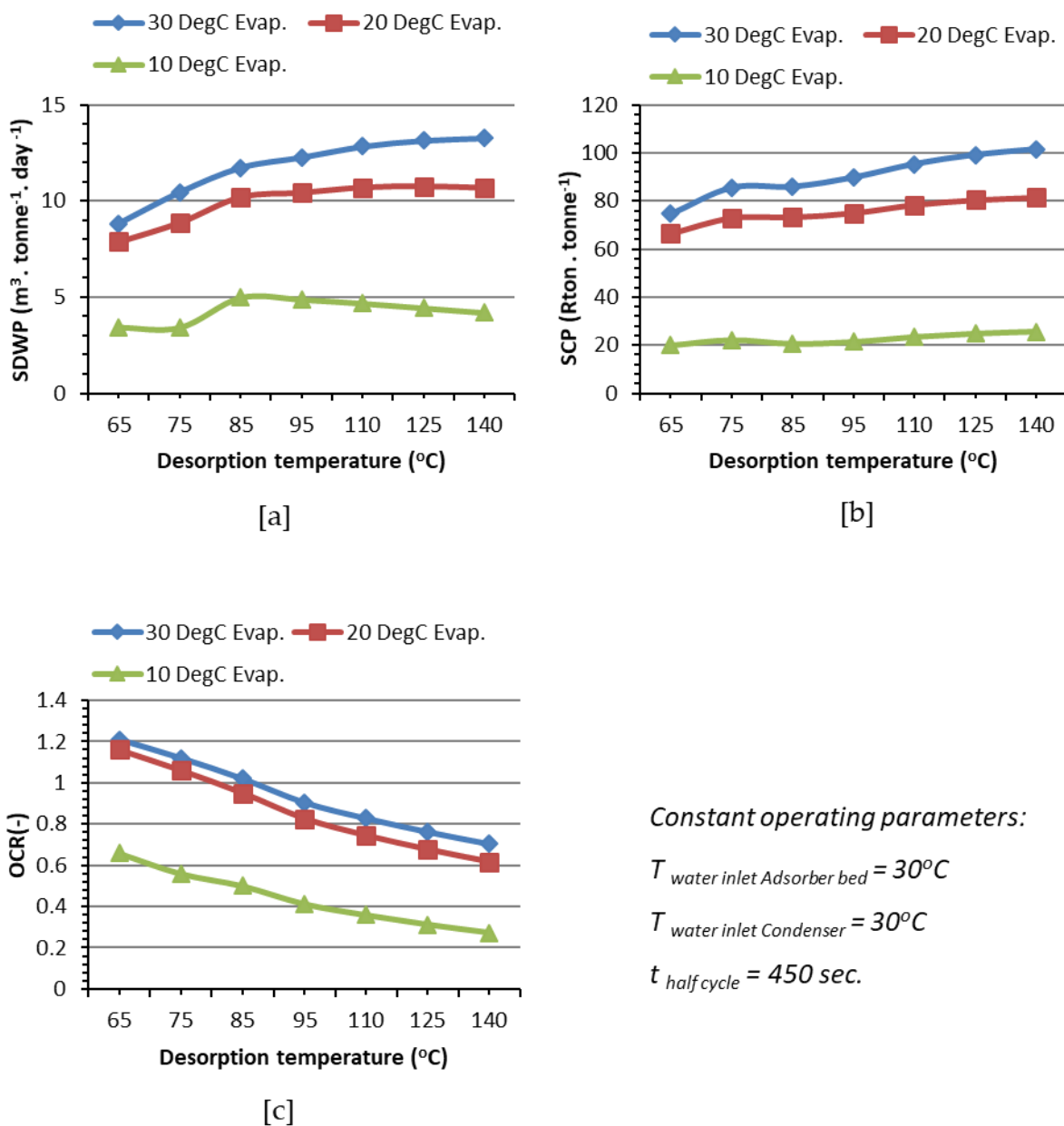
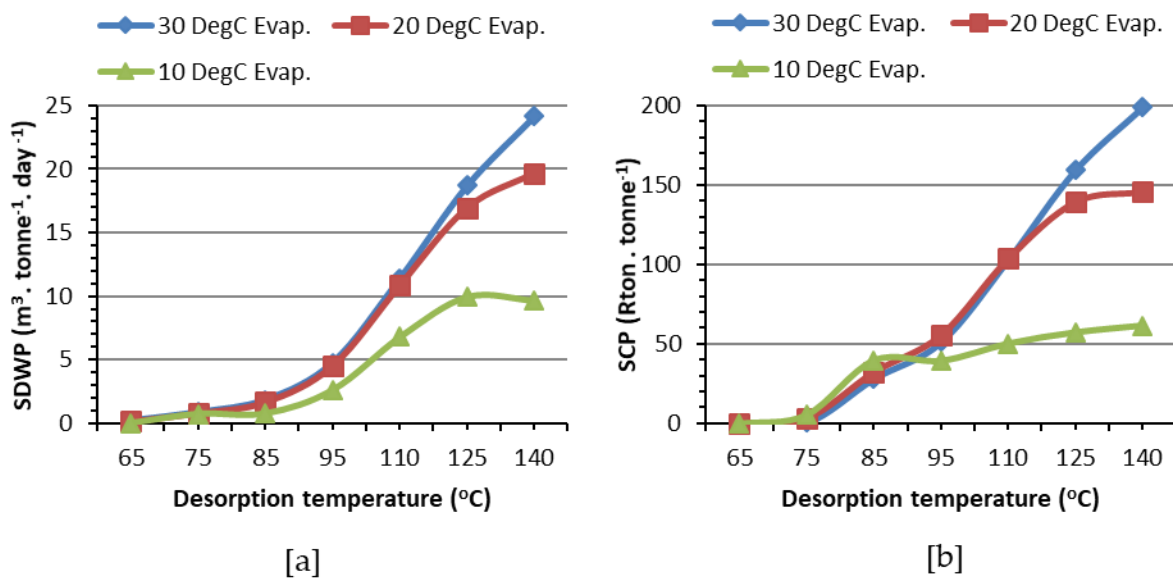


Figure 4-3, Effect of desorption and evaporator water temperatures on SDWP (a), SCP (b) and OCR (c) of double-bed adsorption desalination system (Al-Fumarate)

4.2.1.4 CPO-27Ni:

Similar to AQSOA-Z02 and because of the similarity in their isotherm shape, desorption temperature significantly affects the performance of CPO-27Ni as shown in Figure 4-4 while evaporator temperature has less effect specially at low desorption temperatures below 95°C. At desorption temperature below 95°C and at all evaporator water temperatures, water production of CPO-27Ni is very low (less than 5 m³.ton⁻¹.day⁻¹) compared to the previously discussed adsorbents at the same operating conditions. However, as desorption water temperature increases, cycle water production increases steeply to reach SDWP of 24.14 m³.ton⁻¹.day⁻¹ at 140°C desorption water temperature and 30°C evaporator water temperature. Again with desorption temperature increase, SCP can reach 199 Rton.ton⁻¹ at desorption temperature of 140°C and evaporator temperature of 30°C. Unsurprisingly maximum OCR is achieved at high desorption temperatures with values higher than 1 at desorption temperature of 125°C and evaporator temperature of 30°C as shown in Figure 4-4(c).



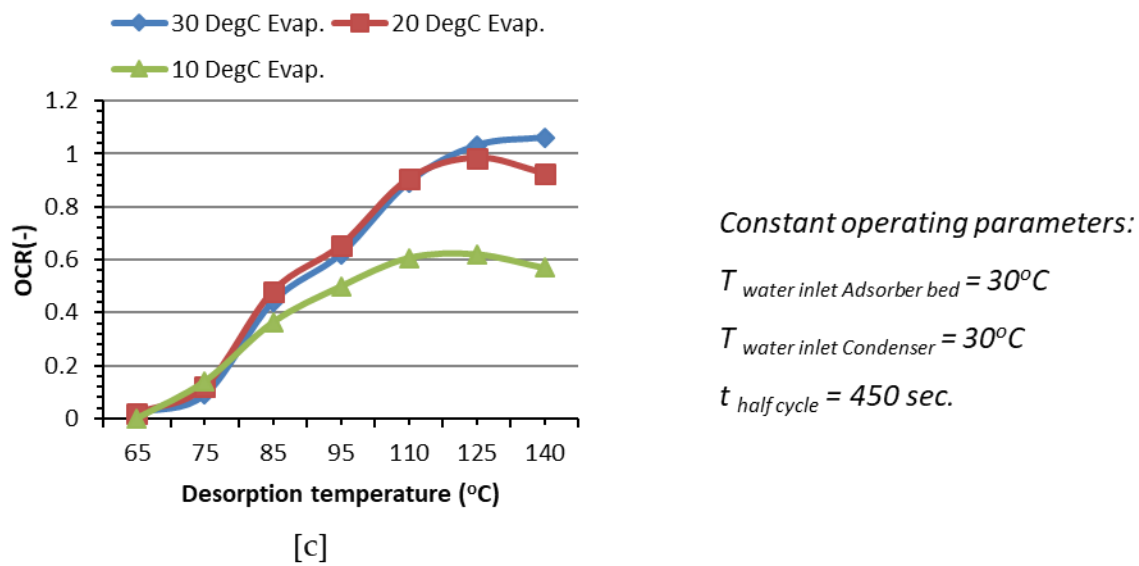


Figure 4-4, Effect of desorption and evaporator water temperatures on SDWP (a), SCP (b) and OCR (c) of double-bed adsorption desalination system (CPO-27Ni)

4.2.1.5 MIL-101Cr:

Figure 4-5 shows the effect of desorption and evaporator temperatures on SDWP, SCP and OCR of the adsorption desalination system with MIL-101Cr used as adsorbent. It is clear that desorption water temperature has little effect on cycle outputs as the difference between minimum and maximum SDWP at 65°C and 125°C desorption temperatures is only 9.1% which means that MIL-101Cr is capable of working effectively when relatively low temperature heating sources are available. In contrast, the evaporator water temperature had significant effect on the produced water and cooling where SDWP and SCP increased with the increase in evaporator temperature. For example, at 95°C desorption water temperature SDWP increased from 9.03 to 23.4 $m^3 \cdot ton^{-1} \cdot day^{-1}$ when evaporator water temperature increased from 10 to 30°C respectively. Also for the same operating conditions, SCP increased from 36.8 to 135.3 $Rton \cdot ton^{-1}$ and OCR increased from 0.54 to 0.89. It can also be seen that OCR increases by lowering desorption temperature where it reaches 1.15 at 65 and 30°C desorption and evaporator water temperatures respectively.

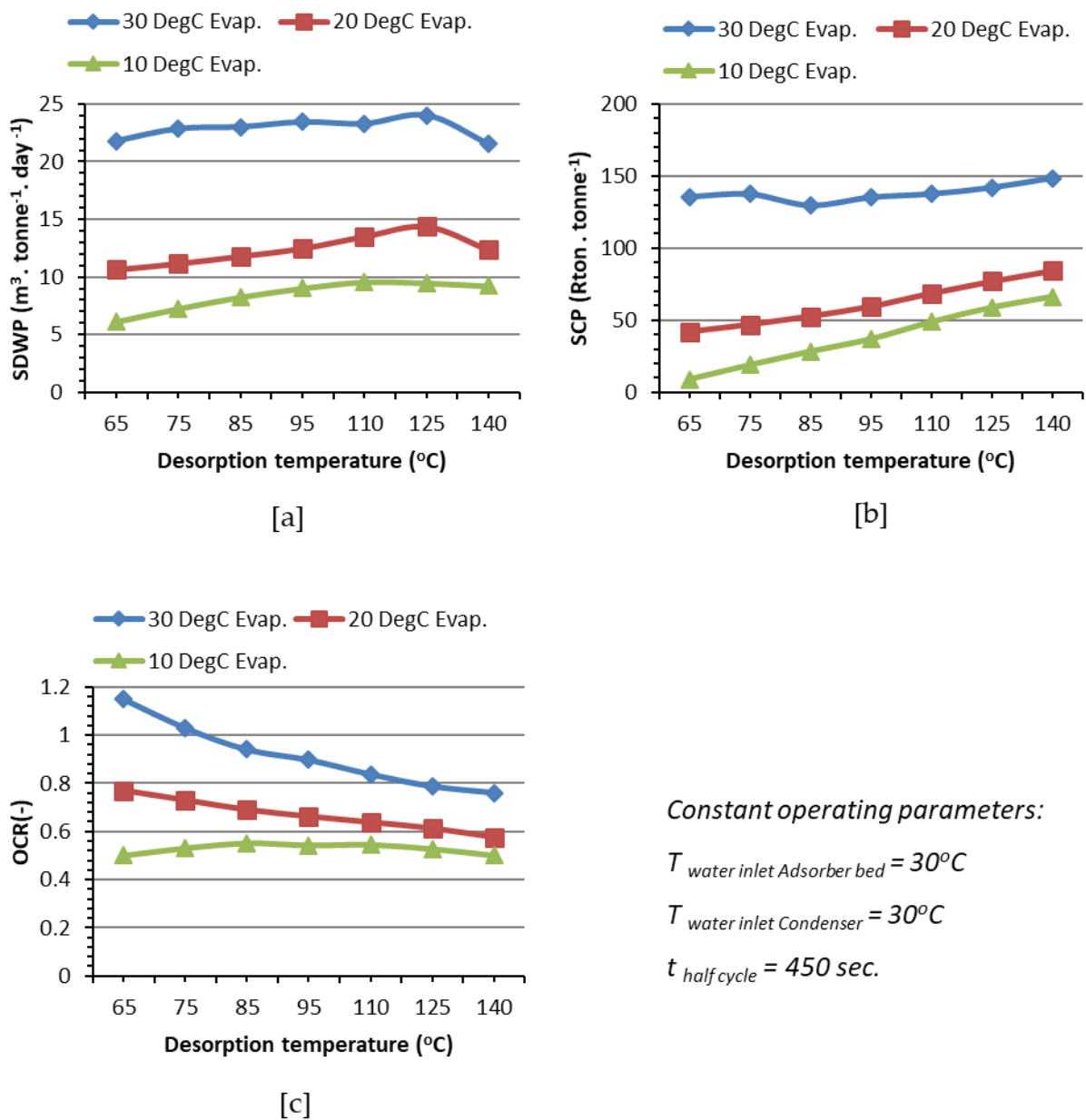
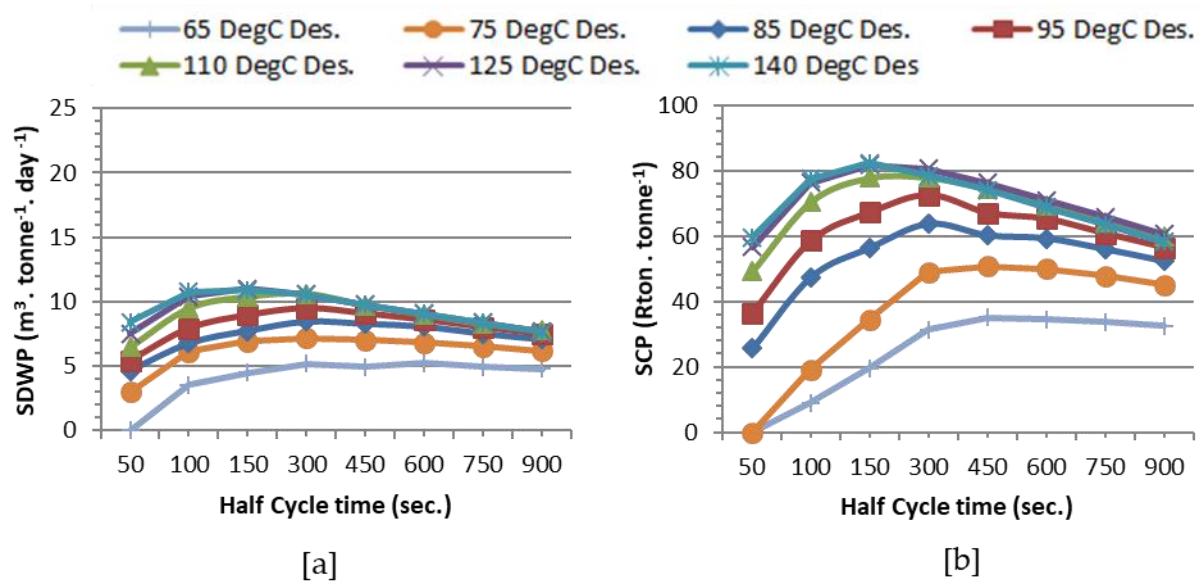


Figure 4-5, Effect of desorption and evaporator water temperatures on SDWP (a), SCP (b) and OCR (c) of double-bed adsorption desalination system (MIL-101Cr)

4.2.2 Effect of half cycle time

4.2.2.1 Silica-gel:

In this section, half cycle time effect is studied at evaporator, condenser and adsorber bed inlet water temperatures of 30°C while desorber bed inlet water temperature is varied in the range of 65 to 140°C. Figure 4-6 shows SDWP, SCP and OCR for silica-gel showing that optimum cycle time depends on the desorption temperature where longer cycle times are needed at low desorption temperature. At 85°C desorption water temperature, maximum SDWP of 8.6 m³.ton⁻¹.day⁻¹ is achieved at half cycle time of 450 seconds while at 140°C, maximum SDWP of 10.89 m³.ton⁻¹.day⁻¹ is achieved at 150 seconds. The same trend happens for the cooling production but at slightly different cycle times, therefore cycle time should be selected according to application demands. It is also noticed that increasing desorption temperature, increases cycle outputs but in contrast decreases OCR resulting in the highest OCR of 1.13 at 65°C and longest half cycle time of 900 seconds.



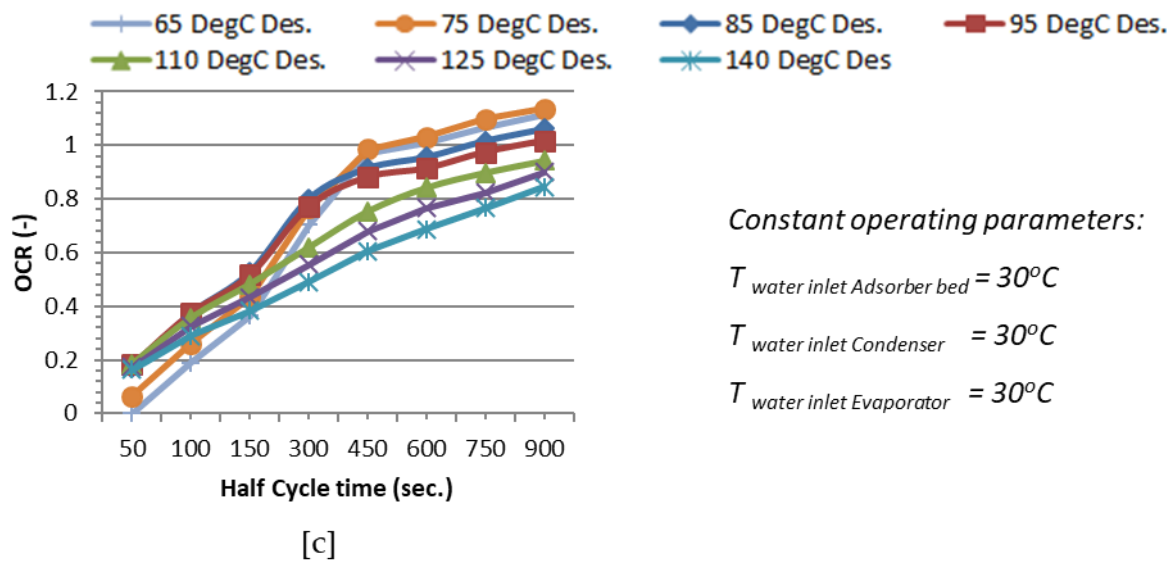


Figure 4-6, Effect of half cycle time and desorption water temperature on SDWP (a), SCP (b) and OCR (c) of double-bed adsorption desalination system (Silica-gel)

4.2.2.2 AQSOA-Z02:

As seen in Figure 4-7 (a and b), best cycle time depends on the desorption temperature where SDWP and SCP reach their maximum values at half cycle time of 300 seconds for desorption temperatures less than 125°C while 150 seconds results in highest SDWP and SCP at higher desorption temperatures. It is noticed that AQSOA-Z02 can result in maximum SDWP of $27.6 \text{ m}^3 \cdot \text{ton}^{-1} \cdot \text{day}^{-1}$ and maximum SCP of $230.8 \text{ Rton} \cdot \text{ton}^{-1}$ at half cycle time of 150 seconds while operating at the maximum desorption temperature of 140°C. Also, OCR is affected by desorption temperature and cycle time as it mainly increases by the increase of both desorption temperature and cycle time. However, at longer cycle times than 300 seconds and for desorption temperatures above, 125°C, OCR becomes lower than that of desorption temperature of 110°C.

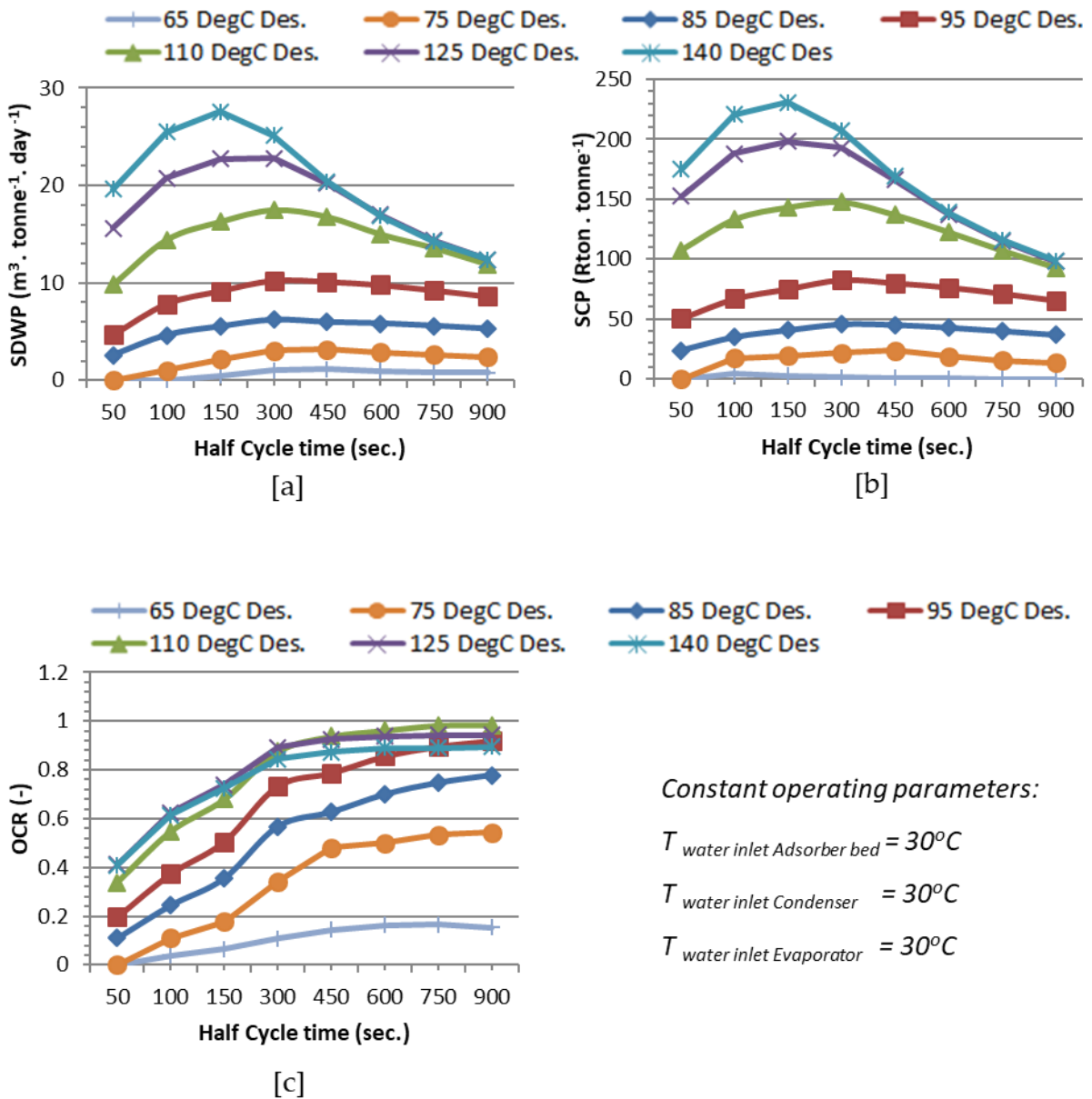


Figure 4-7, Effect of half cycle time and desorption water temperature on SDWP (a), SCP (b) and OCR (c) of double-bed adsorption desalination system (AQSOA-Z02)

4.2.2.3 Al-Fumarate:

As shown in Figure 4-8, effect of changing desorption temperature is limited compared to the effect of half cycle time on SDWP, SCP and OCR. It is noticed that 300 seconds is the optimum cycle time for both SDWP and SCP for all desorption temperatures where $13.2 \text{ m}^3 \cdot \text{ton}^{-1} \cdot \text{day}^{-1}$ and $104.3 \text{ Rton} \cdot \text{ton}^{-1}$ respectively are produced at 140°C desorption

temperature at this half cycle time. However, OCR increases in direct proportion with half cycle time and inversely with desorption temperature. At 85°C desorption temperature, OCR increases from 0.26 to 1.22 when half cycle time changes from 50 to 900 seconds. In addition, at 900 seconds the OCR increases from 0.98 to 1.39 when decreasing desorption temperature from 140 to 65°C.

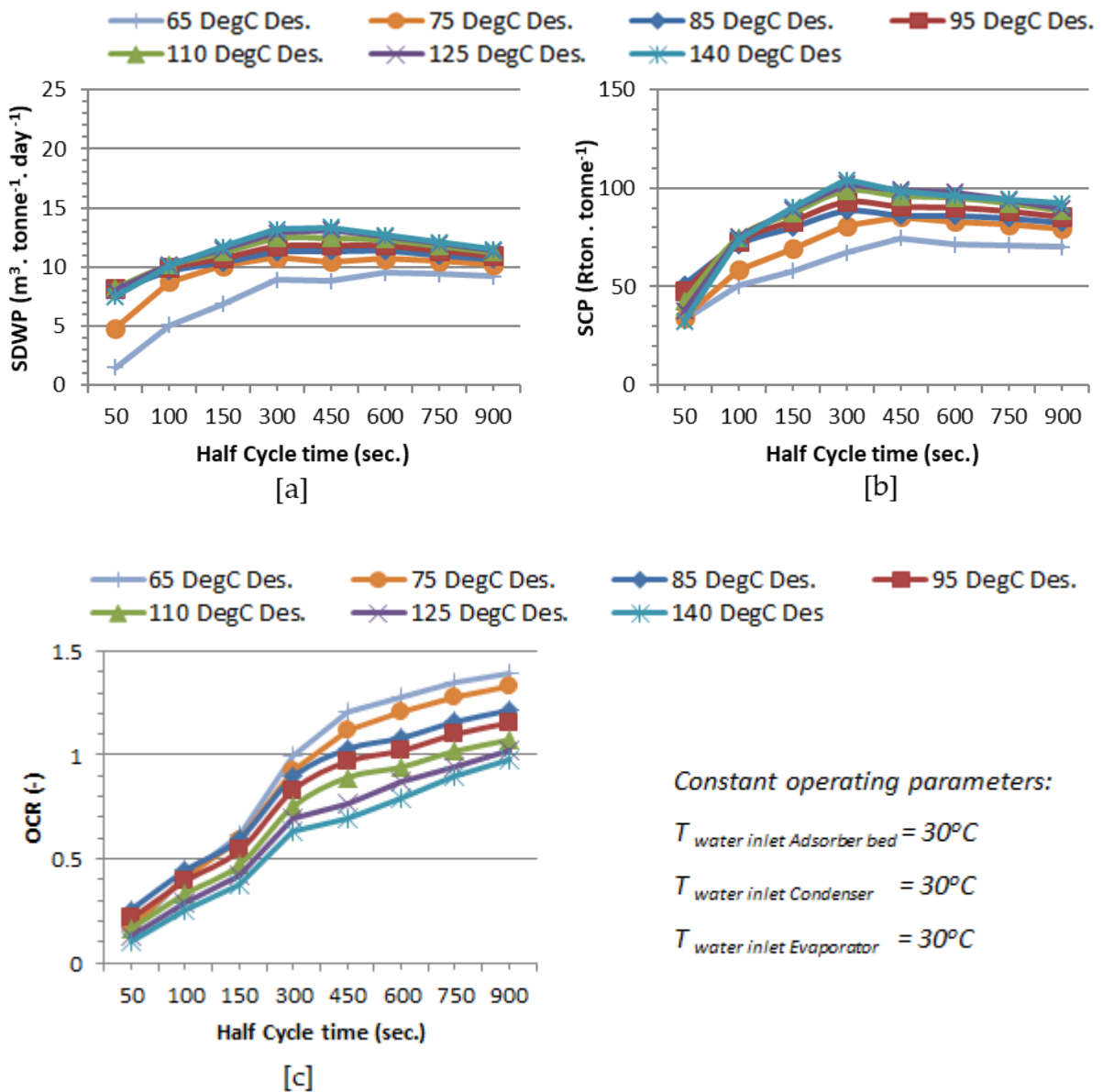
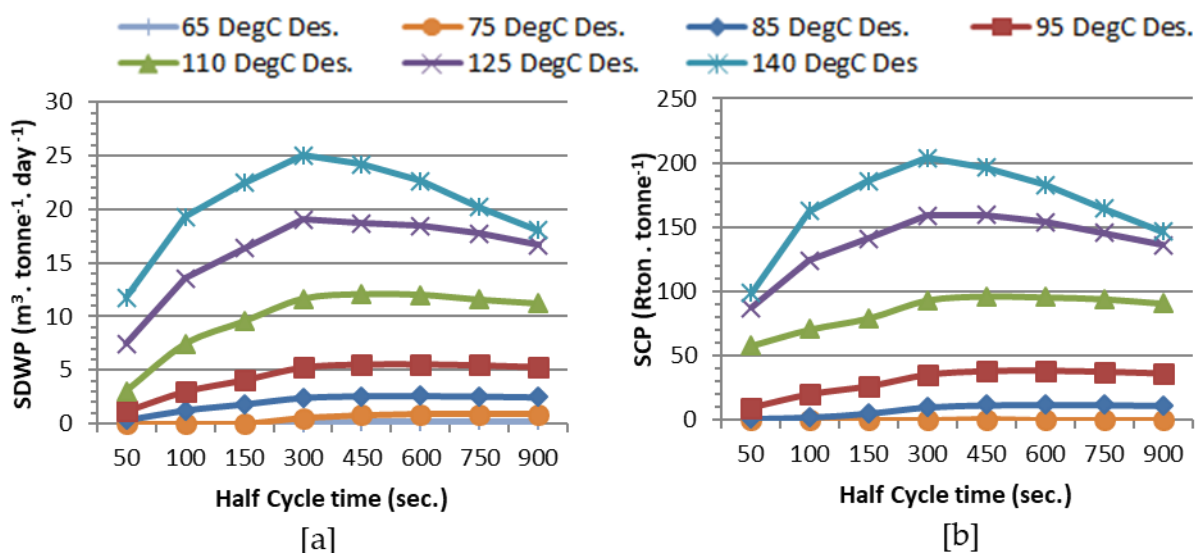


Figure 4-8, Effect of half cycle time and desorption water temperature on SDWP (a), SCP (b) and OCR (c) of double-bed adsorption desalination system (AL-Fumarate)

4.2.2.4 CPO-27Ni:

As shown in Figure 4-9, SDWP, SCP and OCR depend on both desorption temperature and cycle time. For desorption temperatures above 110°C, maximum SDWP of 25 m³.ton⁻¹.day⁻¹ and SCP of 203.78 Rton.ton⁻¹ are produced at 300 seconds and at 140°C desorption temperature. At 110°C desorption temperature, 450 seconds is found to be the optimum half cycle time while at lower temperatures, 600 seconds results in the highest water and cooling production as SDWP and SCP reach 2.58 m³.ton⁻¹.day⁻¹ and 12.04 Rton.ton⁻¹ respectively at 85°C. Similar to previous adsorbents, OCR increases with increase in cycle time and with increase in desorption temperature like "AQSOA-Z02". At 900 seconds, it is found that OCR reaches 0.49 and 1.26 at 85 and 140°C desorption temperatures respectively. Although maximum OCR is not obtained at the best half cycle time, its value is still considerable at 300 seconds for example at desorption temperatures above 110°C where it ranges from 0.93 to 0.98.



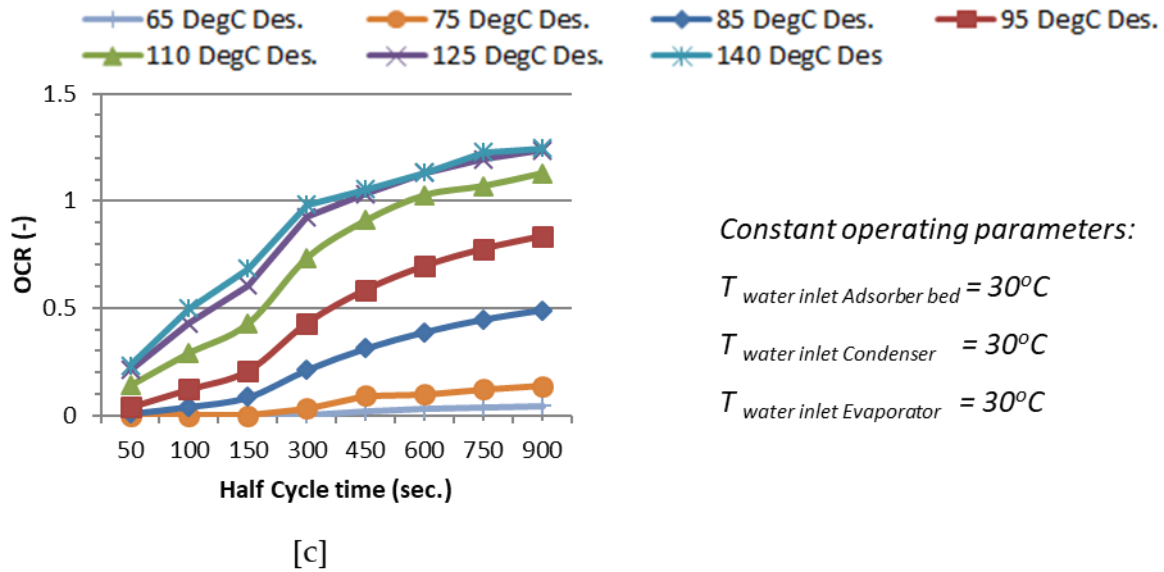


Figure 4-9, Effect of half cycle time and desorption water temperature on SDWP (a), SCP (b) and OCR (c) of double-bed adsorption desalination system (CPO-27Ni)

4.2.2.5 MIL-101Cr:

Figure 4-10, shows that desorption temperature has minimal effect on SDWP and SCP but the OCR, decreases by a percentage ranging from 21 to 66% when increasing desorption temperature from 65 to 140°C. For water production, it is noticed that half cycle times longer than 150 seconds result in nearly the same SDWP at different desorption temperatures, at each half cycle time as in Figure 4-10(a). At shorter half cycle times of 150 seconds and below, it is found that increasing desorption temperature more than 110°C affects cycle performance as SDWP reaches $15 \text{ m}^3 \cdot \text{ton}^{-1} \cdot \text{day}^{-1}$ compared to $26.8 \text{ m}^3 \cdot \text{ton}^{-1} \cdot \text{day}^{-1}$ at 95°C and at the same time of 50 seconds. The reason is that at short cycle times after heating the adsorber bed to high temperature, some more time is needed for the bed to cool down during the following adsorption phase which affects the adsorption process and hence the cycle performance. For cooling, SCP has low values at short cycle durations but it increases to maximum values and then stays almost constant at longer half cycle times more than 300

seconds where it ranges from 136.9 to 150.3 Rton.ton⁻¹ for desorption temperatures of 65 to 140°C respectively. The cycle OCR, shown in Figure 4-10(c), increases with longer cycle time and decreases with rising desorption temperature while its value lies in a wide range of 0.21 to 1.2. According to the SDWP, SCP and OCR results, it is recommended that MIL-101Cr to be used at desorption temperatures below 95°C and at relatively shorter half cycle times (150 to 300 seconds) to get the optimum water and cooling productions in addition to being efficient where OCR is around 0.88.

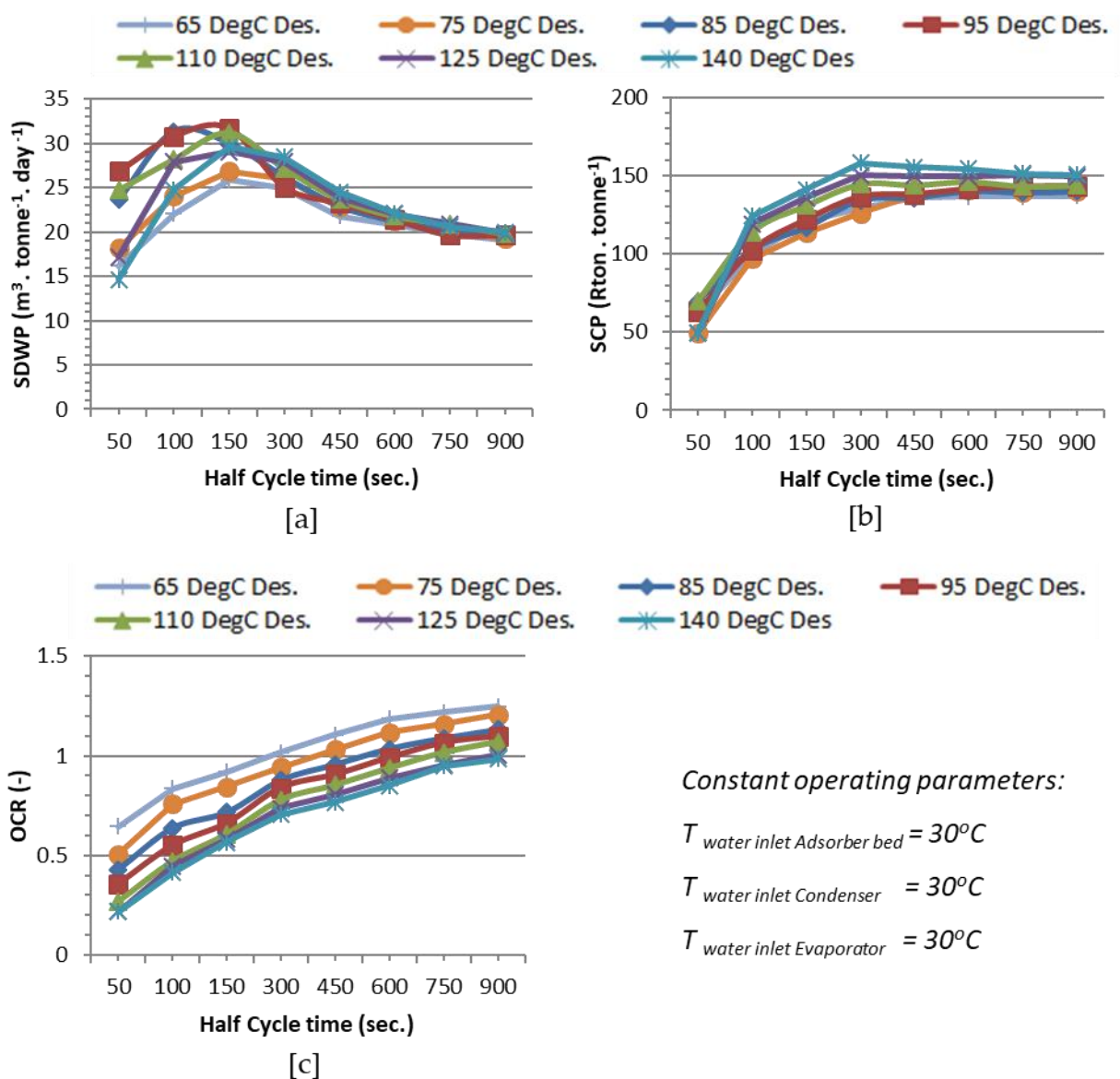


Figure 4-10, Effect of half cycle time and desorption water temperature on SDWP (a), SCP (b) and OCR (c) of double-bed adsorption desalination system (MIL-101Cr)

4.2.3 Effect of condenser cooling water temperature

As discussed earlier, two categories of operating parameters exist; controllable (which has been discussed in the previous section) and uncontrollable which will be discussed in this section. From the previous parametric study, it was concluded that adsorbent materials performance depends on desorption water temperature and cycle time where longer cycle times are needed at lower desorption temperatures. Therefore, in this section two sets of operating conditions will be discussed at various condenser cooling water inlet temperature (10 to 30°C) and evaporator inlet water temperature (10 to 30°C). These sets of operating conditions are high desorption temperature of 125°C at short half cycle time of 300 seconds and the other set is at low desorption temperature of 85°C and at longer half cycle time of 600 seconds while adsorber bed cooling water temperature is kept constant at 30°C.

The following sections will present the performance of the same five adsorbent materials with the lines on the figures appearing as either continuous or dotted lines for high and low desorption temperatures respectively.

4.2.3.1 *Specific daily water production (SDWP):*

The five materials under investigation in this section have three different Isotherm shapes which affect the water production as shown in Figure 4-11. For all materials increasing evaporator water temperature increases SDWP but increasing condenser water temperature only affects AQSOA-Z02 and CPO-27 Ni. As shown in Figure 4-11(a), at high desorption temperature, effect of changing condenser temperature on SDWP for Silica-gel is minimal compared to the case of low desorption temperature. At 30°C evaporator inlet water temperature, SDWP decreases by 2% when condenser water temperature increases from 10 to 30°C. At the same operating conditions, but at low desorption temperature, SDWP

decreases by 14%. AQSOA-Z02 and CPO-27Ni, Figure 4-11(b & d), have similar behaviours as at low desorption temperature almost all evaporator water inlet temperatures result in the same SDWP but with significant reduction in water production when condenser temperature increase. SDWP of AQSOA-Z02 and CPO-27Ni decreases by 60% and 73%, respectively when condenser inlet water temperature increases from 10 to 30°C. For higher desorption temperature, effect of changing condenser temperature is minimal which could be attributed to the low value of the partial pressure ratio at higher desorption temperature and hence further decrease in condenser temperature does not reduce the pressure ratio further thus the uptake value remains almost the same. Finally Al-Fumarate and MIL-101Cr, Figure 4-11(c & e), are not greatly affected by changes in condenser temperature whether at high or low desorption temperature which could be due to the flat isotherm curve at low partial pressure ratios where uptake is nearly constant.

4.2.3.2 *Specific cooling power (SCP):*

Similar to SDWP behaviour, SCP has the same trend in terms of evaporator and condenser water temperatures effect for all adsorbent materials. As seen in Figure 4-12, higher evaporator and desorption temperatures result in more cooling production. Also, condenser temperature does not affect considerably cooling production at high desorption temperature for all materials except for CPO-27Ni where the SCP decreases by 21% when increasing condenser water inlet temperature from 10 to 30°C.

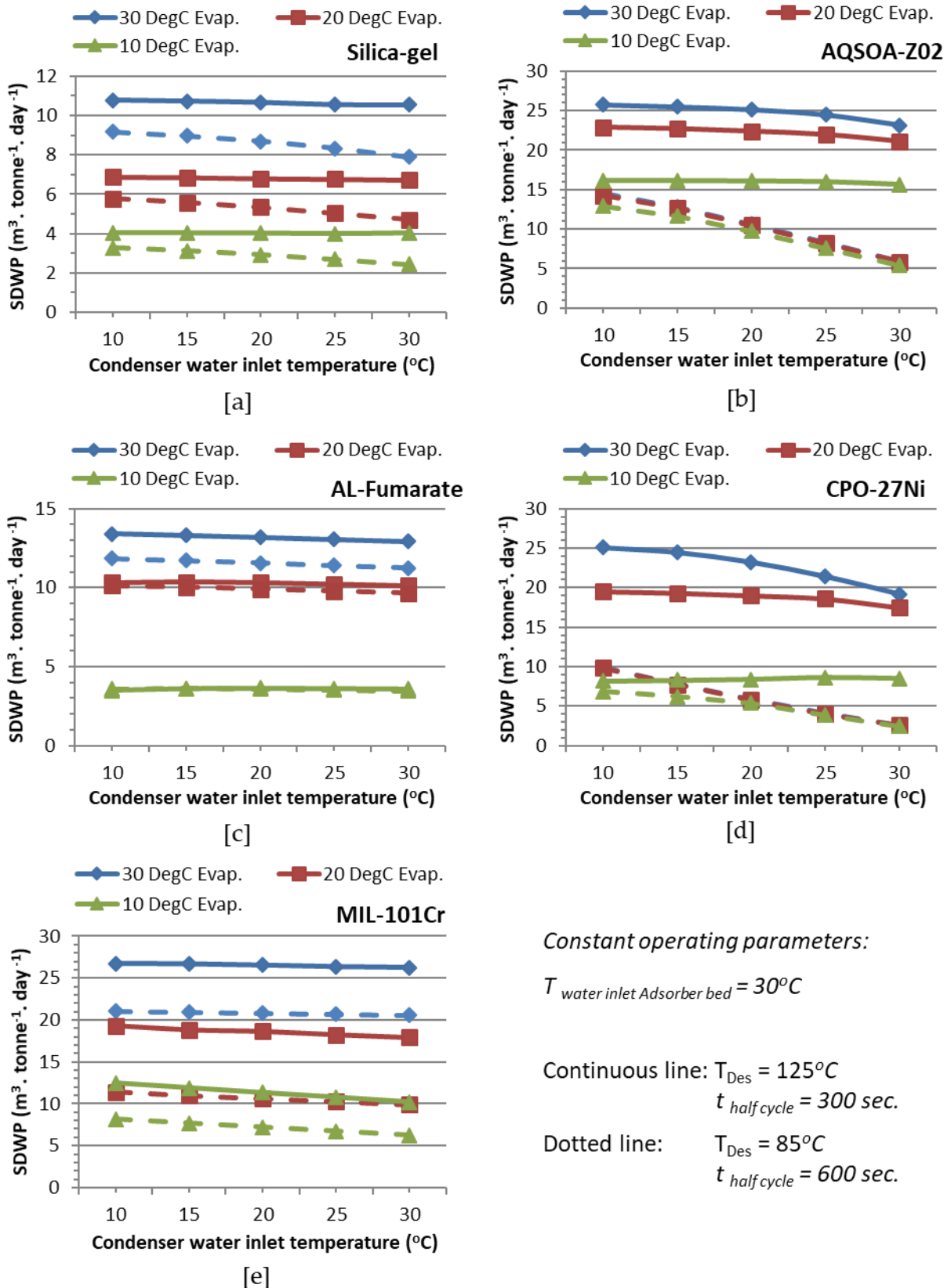


Figure 4-11, Effect of condenser and evaporator water temperatures on SDWP for Silica-gel (a), AQSOA-Z02 (b), AL-Fumarate (c), CPO-27Ni (d) and MIL-101Cr (e)

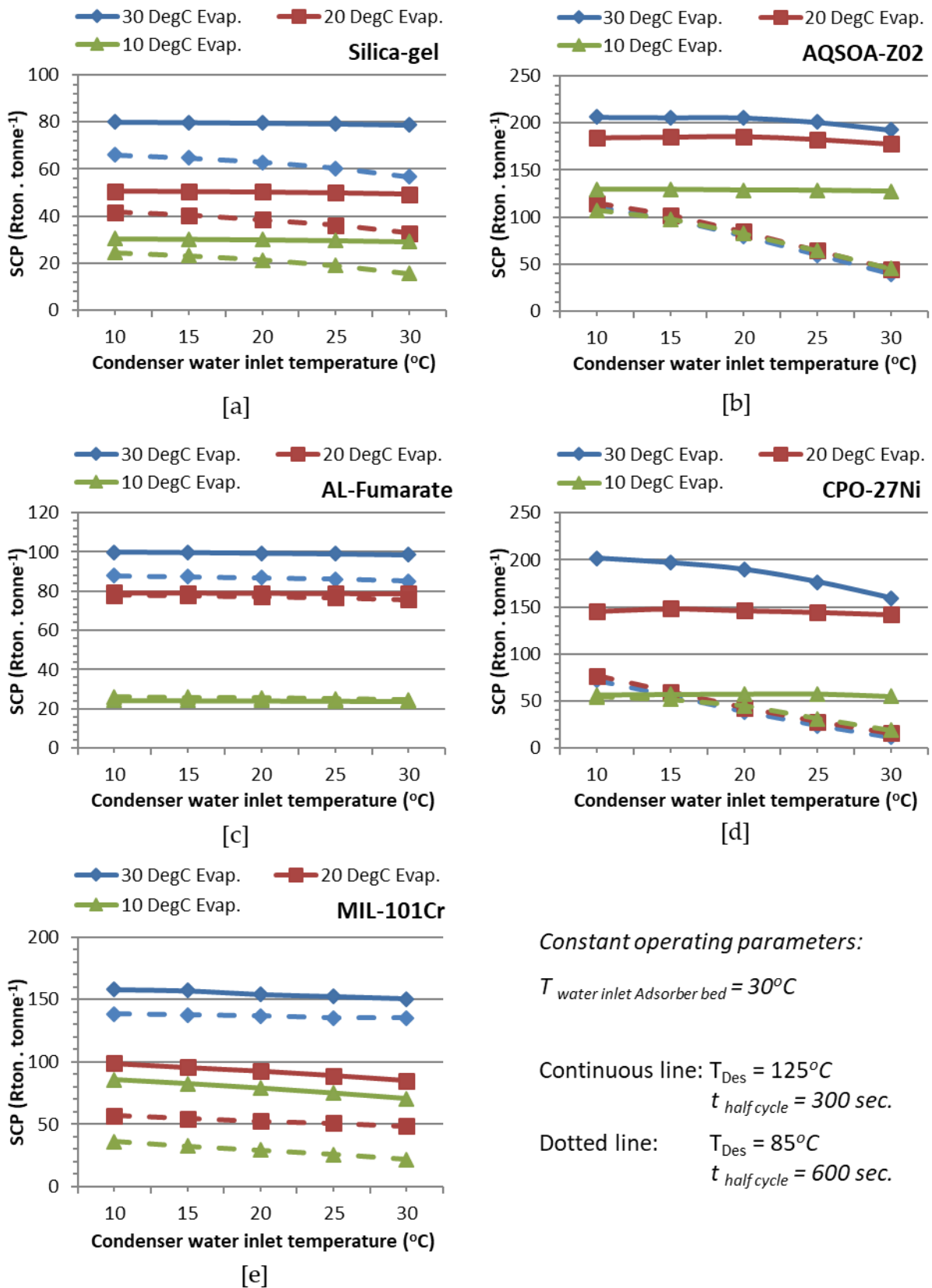


Figure 4-12, Effect of condenser and evaporator water temperatures on SCP for Silica-gel (a), AQSOA-Z02 (b), AL-Fumarate (c), CPO-27Ni (d) and MIL-101Cr (e)

4.2.3.3 Overall conversion ratio (OCR):

As seen in Figure 4-13, all adsorbent materials have higher OCR at lower desorption temperature except CPO-27Ni which needs higher desorption temperatures to work at OCR above 0.8. It can also be seen that all materials work better at higher evaporator temperatures which result in increased values for OCR. For the condenser inlet water temperature effect on OCR, it is the same as that on SDWP and SCP where OCR for Silica-gel, Al-Fumarate and MIL-101Cr are less sensitive to condenser temperature changes specially at high desorption temperatures.

4.3 Summary

In this chapter effect of changing operating conditions on cycle specific daily water production (SDWP), specific cooling power (SCP) and overall conversion ratio (OCR) have been investigated. Two categories of operating conditions were discussed; controlled and uncontrolled. Desorption water temperature, evaporator water inlet temperature and cycle time are the controlled parameters while condenser inlet cooling water temperature lies under the uncontrolled category. Five different adsorbents have been investigated namely; Silica-gel, AQSOA-Z02, AL-Fumarate, CPO-27Ni and MIL-101Cr. Figure 4-14 shows the recommended adsorbent material according to the application (desalination only or desalination and cooling) and according to the available desorption temperature. It was found that longer cycle times are needed at lower desorption temperatures and higher evaporator inlet water temperatures result in higher cycle outputs. Finally, it was found that condenser cooling water temperature does not greatly affect performance of Silica-gel, AL-Fumarate and MIL-101Cr at higher desorption temperatures only while AQSOA-Z02 and CPO-27Ni are affected by condenser temperature at high and low desorption temperatures.

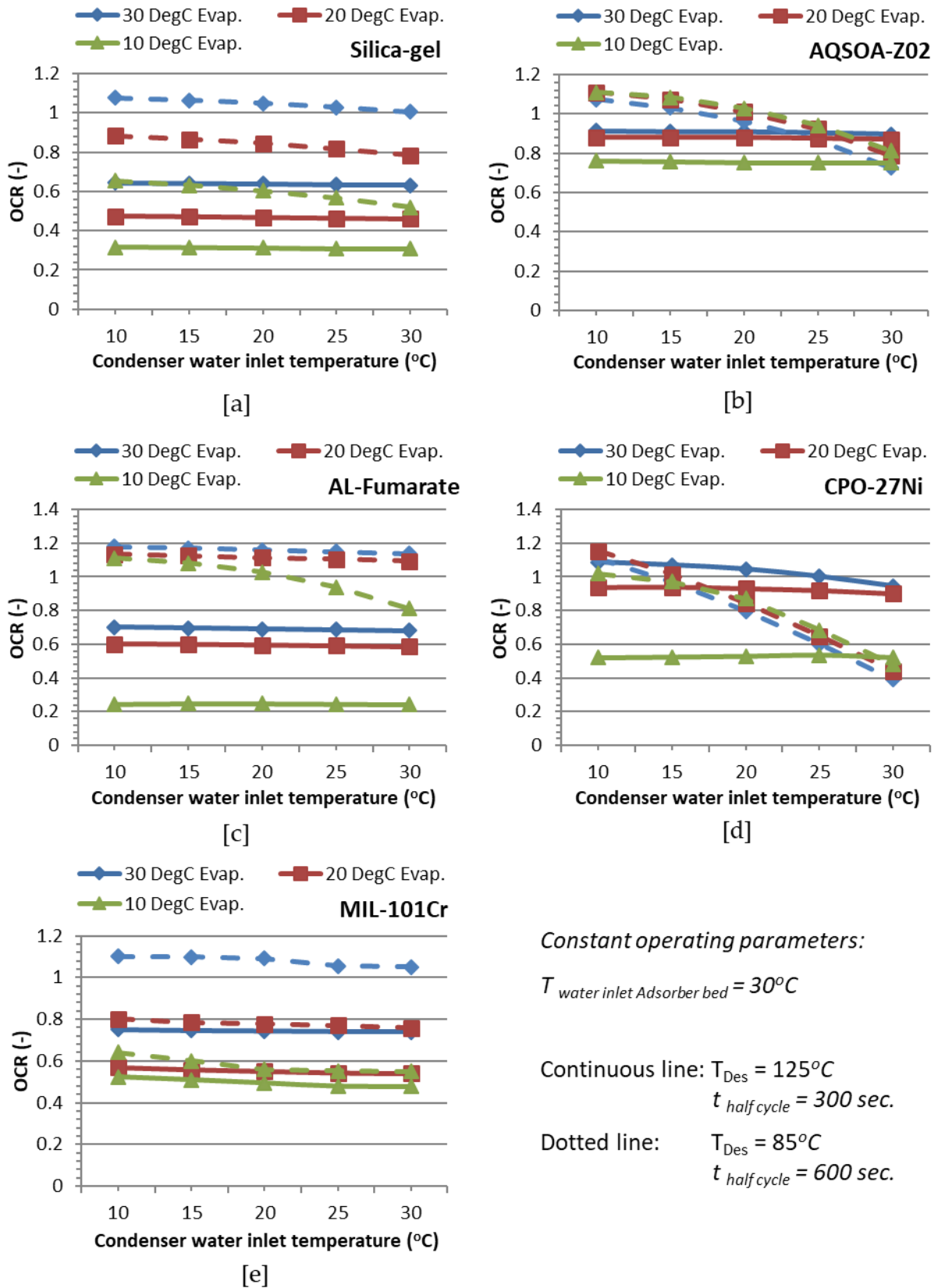


Figure 4-13, Effect of condenser and evaporator water temperatures on OCR for Silica-gel (a), AQSOA-Z02 (b), AL-Fumarate (c), CPO-27Ni (d) and MIL-101Cr (e)

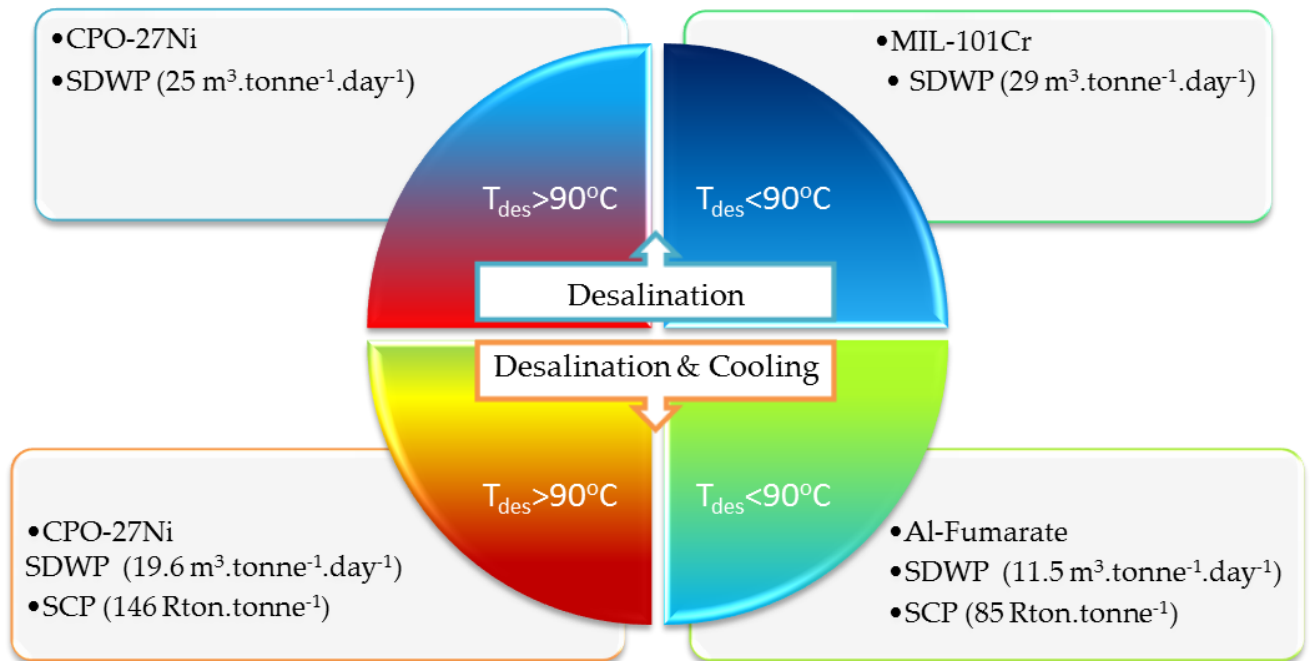


Figure 4-14, Recommended adsorbent materials according to operating conditions and application

CHAPTER 5: PERFORMANCE INVESTIGATION OF INTEGRATED ADSORPTION CYCLE FOR DESALINATION AND COOLING

5.1 Introduction

As discussed in Chapter 4, many adsorbents have been investigated for water desalination and cooling purposes. It was found that one of the techniques to increase cycle output of adsorbents like AQSOA-Z02 and CPO-27Ni is decreasing the condenser temperature. In this chapter, a new integrated adsorption desalination cycle is introduced, which has the ability to decrease the condenser temperature by partially or fully utilization of the cooling effect obtained from the evaporators [11]. Therefore, cooling could be obtained as a by-product at some operating conditions as well as an improvement in the cycle performance is achieved. AQSOA-Z02 is used in this investigation to illustrate the capability of the new cycle configuration at different evaporator temperatures ranging from 5 to 20°C [11].

5.2 System description

Conventional double-bed system, as shown in Figure 5-1, [11], consists of two adsorber beds, evaporator and condenser. Figure 5-2, [11], shows the proposed system configuration, which is basically two double-bed cycles (upper and lower) linked together via combined evaporator-condenser heat exchanger. In this system, the upper cycle has 2-beds, condenser and its evaporator is combined with the condenser of the lower cycle, which has another 2 beds and evaporator. The combined evaporator-condenser unit has three water flowing circuits, two of them are rejecting heat (chilled and condensing water passes) and the other

fluid is absorbing this heat, which is the seawater. During system operation, each cycle is working independently from the other one as no water vapor is flowing from any cycle to the other. However, to further enhance the cycle energy efficiency, heat is recovered by the heating fluid exiting from the upper desorbing bed being fed into the desorbing bed of the lower cycle, Figure 5-3 [11].

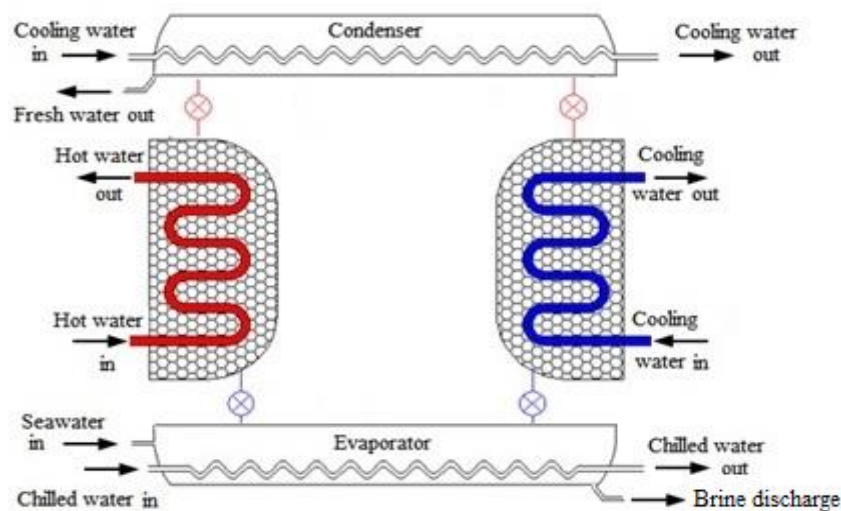


Figure 5-1, Schematic of a conventional double-bed adsorption desalination system [11]

Three operating scenarios are available for this cycle which differ from each other by the way of connecting the heat exchanging devices and amount of water and cooling produced. At all operating modes, desalinated water is produced from the two available condensers, while cooling is produced from the lower evaporator at scenario '1' and from the upper evaporator at scenario '2', Table 5-1 [11].

Table 5-1, System outputs at different operating modes [11]

Output Source Operating Scenario	Upper Cycle	Combined		Lower Cycle
	Condenser	Evaporator-Condenser		Evaporator
'1'	Fresh water	No Cooling	Fresh water	Cooling
'2'	Fresh water	Cooling	Fresh water	No Cooling
'3'	Fresh water	No Cooling	Fresh water	No Cooling

In scenario '1', as shown in Figure 5-3 (a), cooling is only produced by the lower evaporator where chilled water is circulating. In scenario '2', as shown in Figure 5-3 (b), cooling output of this mode is obtained from the upper evaporator where chilled water is passing through. In addition, chilled water is circulated between lower evaporator and upper condenser to utilize the cooling produced from that evaporator. In scenario '3', desalinated water is the only output from the system where the system operates like scenario '2' but without feeding chilled water to the upper evaporator, Figure 5-3 (c) [11].

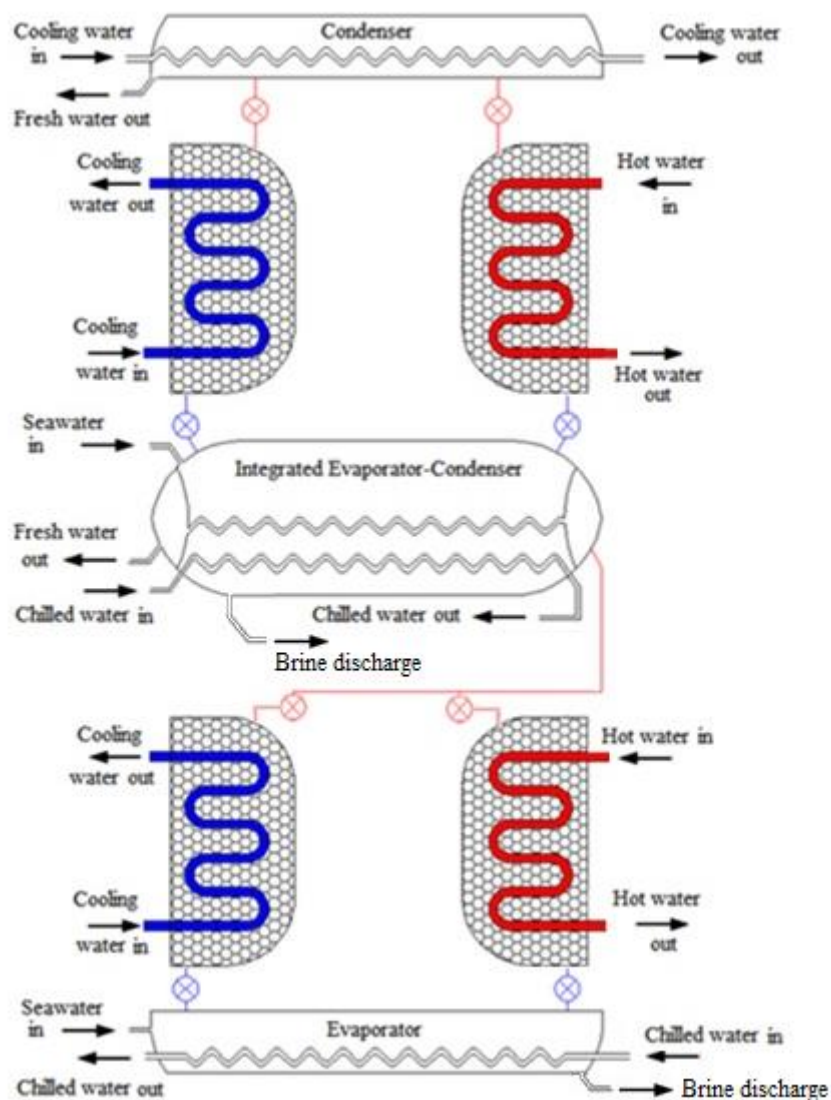
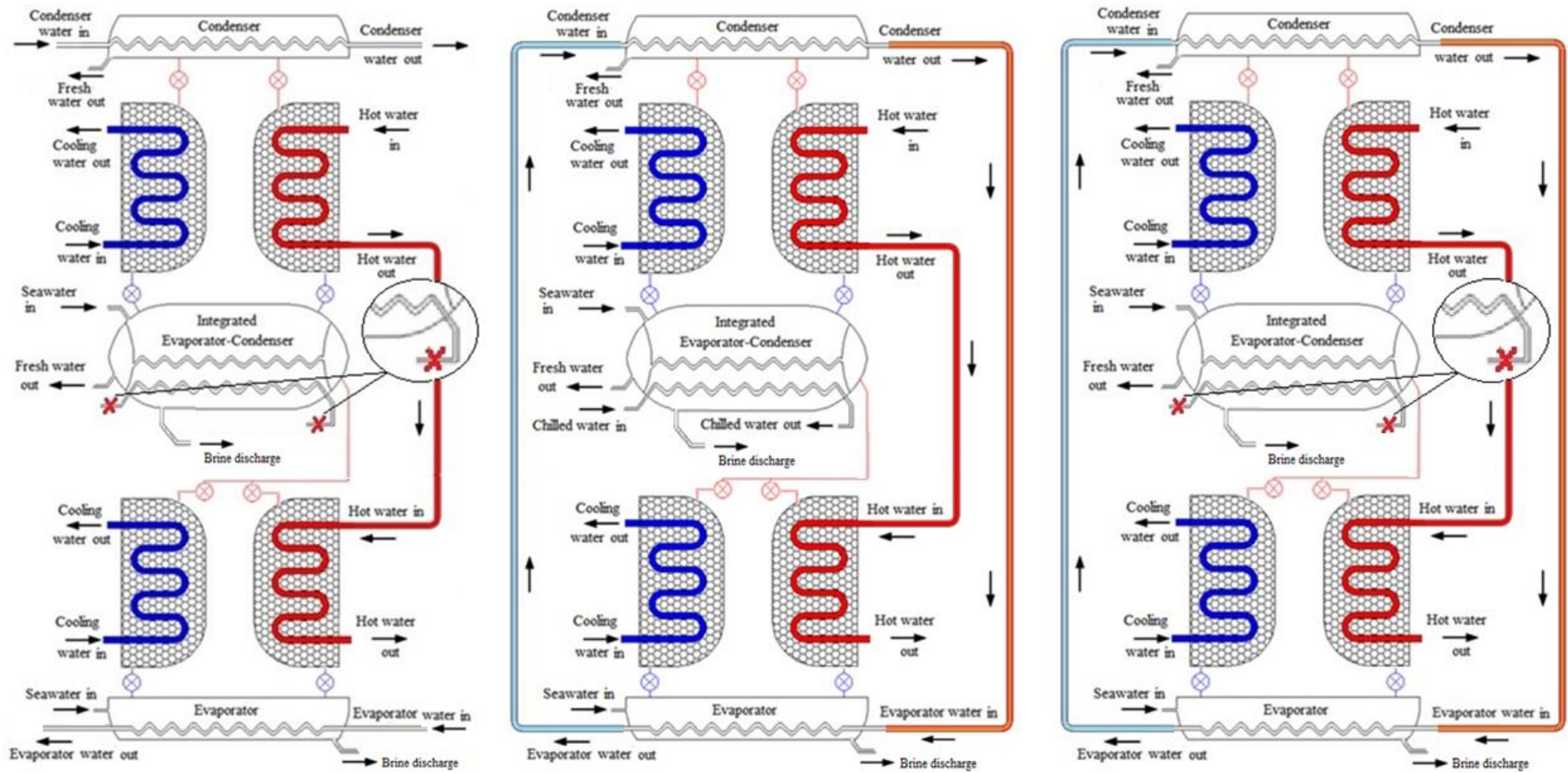


Figure 5-2, A schematic of the integrated adsorption desalination and cooling cycle [11]



Scenario '1'

Scenario '2'

Scenario '3'

Cooling: lower cycle evaporator

Cooling: upper cycle evaporator

No cooling is produced

Figure 5-3, Schematic diagram for the operating modes of the new integrated adsorption cycle with desalinated water produced from both condensers at all scenarios [11]

5.3 System modelling

Simulink is used to model an adsorption system similar to that manufactured by Weatherite but using AQSOA-Z02 as the adsorbent material with each bed packed with 845 kg. The balancing equations [9, 11, 33], Eq. (5-1) to (5-12), are solved for the system components; adsorbing/desorbing beds, evaporator, condenser and the combined evaporator-condenser unit using the built-in ODE45 solver. The system components are assumed to be perfectly insulated (no heat losses) and lumped, which means that each component in the system is momentarily at the same temperature. As this system is basically two adsorption cycles comprising of 2 beds each, the validation of this model is considered to be that of the double-bed conventional system, which was presented in chapter 3 [11].

5.3.1 Evaporator equations (Lower cycle):

Mass balance equation:

$$\frac{dM_{s,evap}}{dt} = \theta \dot{m}_{s,in} - \gamma \dot{m}_{brine} - \frac{dc_{ads}}{dt} z \cdot M_a \quad (5-1)$$

Salt balance equation:

$$M_{s,evap} \frac{dX_{s,evap}}{dt} = \theta X_{s,in} \dot{m}_{s,in} - \gamma X_{s,evap} \dot{m}_{brine} - X_D \frac{dc_{ads}}{dt} z \cdot M_a \quad (5-2)$$

Energy balance equation:

$$\begin{aligned} & [M_{s,evap} c_{p,s}(T_{evap}, X_{s,evap}) + M_{HX,Evap} c_{p,HX}] \frac{dT_{evap}}{dt} \\ & = \theta \cdot h_f(T_{evap}, X_{s,evap}) \dot{m}_{s,in} - z \cdot h_{fg}(T_{evap}) \frac{dc_{ads}}{dt} M_a \\ & + \dot{m}_{chilled} c_p(T_{evap})(T_{chilled,in} - T_{chilled,out}) \\ & - \gamma h_f(T_{evap}, X_{s,evap}) \dot{m}_{brine} \end{aligned} \quad (5-3)$$

5.3.2 Combined evaporator - condenser equations:

Mass balance equation:

$$\frac{dM_{s,evap-cond}}{dt} = \theta \dot{m}_{s,in} - \gamma \dot{m}_{brine} - \frac{dc_{ads}}{dt} z \cdot M_a \quad (5-4)$$

Salt balance equation:

$$M_{s,evap-cond} \frac{dX_{s,evap-cond}}{dt} = \theta X_{s,in} \dot{m}_{s,in} - \gamma X_{s,evap-cond} \dot{m}_{brine} - X_D \frac{dc_{ads}}{dt} z \cdot M_a \quad (5-5)$$

Evaporator side energy balance and wall equations:

$$\begin{aligned} & [M_{s,evap} c_{p,s}(T_{evap}, X_{s,evap}) + M_{HX,evap-cond} c_{p,HX}] \frac{dT_{evap}}{dt} \\ & = \theta \cdot h_f(T_{evap}, X_{s,evap}) \dot{m}_{s,in} - z \cdot h_{fg}(T_{evap}) \frac{dc_{ads}}{dt} M_a \end{aligned} \quad (5-6)$$

$$+ \dot{m}_{chilled} c_p(T_{evap})(T_{chilled,in} - T_{chilled,out})$$

$$+ U_{evap-cond} \cdot A (T_{cond} - T_{evap}) - \gamma h_f(T_{evap}, X_{s,evap}) \dot{m}_{brine}$$

$$\begin{aligned} & [M_{HX,evap-cond} c_{p,HX}] \frac{dT_{w-evap}}{dt} \\ & = -h_{evap} \cdot A_{evap} (T_{w-evap} - T_{evap}) + \frac{2\pi kL}{\ln \frac{d_i}{d_o}} (T_{w-cond} - T_{w-evap}) \end{aligned} \quad (5-7)$$

Condenser side energy balance and wall equations:

$$\begin{aligned} & [M_{cond} c_p(T_{cond}) + M_{HX,cond} c_{p,HX}] \frac{dT_{cond}}{dt} \\ & = -h_f(T_{cond}) \frac{dM_a}{dt} + z \cdot h_{fg}(T_{cond}) \frac{dc_{des}}{dt} M_a \end{aligned} \quad (5-8)$$

$$- U_{evap-cond} \cdot A (T_{cond} - T_{evap})$$

$$\begin{aligned} & [M_{HX,evap-cond} c_{p,HX}] \frac{dT_{w-cond}}{dt} \\ & = h_{cond} \cdot A_{cond} (T_{cond} - T_{w-cond}) - \frac{2\pi kL}{\ln \frac{d_i}{d_o}} (T_{w-cond} - T_{w-evap}) \end{aligned} \quad (5-9)$$

5.3.3 Condenser equations (Upper cycle):

Energy balance equation:

$$\begin{aligned}
 & [M_{cond}c_p(T_{cond}) + M_{HX,Cond}c_{p,HX}] \frac{dT_{cond}}{dt} \\
 & = -h_f \frac{dM_a}{dt} + z \cdot h_{fg}(T_{cond}) M_a \left(\frac{dc_{des}}{dt} \right) \\
 & + \dot{m}_{cond} c_p(T_{cond})(T_{cond,in} - T_{cond,out})
 \end{aligned} \tag{5-10}$$

5.3.4 Adsorber bed equations (Upper and Lower cycles):

Energy balance equation (Adsorption phase):

$$\begin{aligned}
 & [M_a c_{p,a} + M_{HX} c_{p,HX} + M_{abe} c_{p,abe}] \frac{dT_{ads}}{dt} \\
 & = z \cdot Q_{st} M_a \frac{dc_{ads}}{dt} - \dot{m}_{cw} c_p(T_{cw,out} - T_{cw,in})
 \end{aligned} \tag{5-11}$$

Energy balance equation (Desorption phase):

$$\begin{aligned}
 & [M_a c_{p,a} + M_{HX} c_{p,HX} + M_{abe} c_{p,abe}] \frac{dT_{des}}{dt} \\
 & = z \cdot Q_{st} M_a \frac{dc_{des}}{dt} + \dot{m}_{hw} c_p(T_{hw,in} - T_{hw,out})
 \end{aligned} \tag{5-12}$$

Where, z is a flag equals 1 at all times except at heat recovery phase where its value is 0.

5.3.5 System performance indicators:

To evaluate cycle performance, different parameters are calculated to show cycle outputs and efficiency in producing both desalinated water and cooling. The amount of water produced daily in cubic meters per tonne of packed adsorbent is the specific daily water production (SDWP). Performance ratio (PR) is a measure of cycle efficiency as it is the ratio between heat of condensation to heat of desorption [11]. Specific cooling power (SCP) is the amount of cooling produced per kg of adsorbent material. Coefficient of performance (COP) is the ratio between amount of cooling produced in the evaporator to heat of desorption

while the overall conversion ratio (OCR) is the ratio between cycle useful outputs to heat of desorption. All these parameters are calculated using equations (5-13) to (5-17), where upper and lower subscripts refer to the values of variables at the corresponding upper or lower cycles, respectively [5, 11, 33].

$$SDWP = \int_0^{t_{cycle}} \left[\left(\frac{Q_{cond}}{h_{fg}(T_{cond})M_a} \right)_{Upper} + \left(\frac{Q_{cond}}{h_{fg}(T_{cond})M_a} \right)_{Lower} \right] dt \quad (5-13)$$

$$PR = \frac{1}{t_{cycle}} \int_0^{t_{cycle}} \frac{(m_d h_{fg})_{Upper} + (m_d h_{fg})_{Lower}}{Q_{DesUpper} + Q_{DesLower}} dt \quad (5-14)$$

$$SCP = \int_0^{t_{cycle}} \frac{Q_{evapUpper} + Q_{evapLower}}{M_{aUpper} + M_{aLower}} dt \quad (5-15)$$

$$COP = \int_0^{t_{cycle}} \frac{Q_{evapUpper} + Q_{evapLower}}{Q_{DesUpper} + Q_{DesLower}} dt \quad (5-16)$$

$$OCR = \int_0^{t_{cycle}} \frac{Q_{evapUpper} + Q_{evapLower} + Q_{condUpper} + Q_{condLower}}{Q_{DesUpper} + Q_{DesLower}} dt \quad (5-17)$$

Where,

$$Q_{condUpper} = \dot{m}_{cond} c_p(T_{cond})(T_{cond,out} - T_{cond,in}) \quad (5-18)$$

$$Q_{condLower} = h_{cond} \cdot A_{cond} (T_{cond} - T_{w-cond}) \quad (5-19)$$

$$Q_{evapUpper} = h_{Evap} \cdot A_{Evap} (T_{w-evap} - T_{evap}) \quad (5-20)$$

$$Q_{evapLower} = \dot{m}_{chilled} c_p(T_{evap})(T_{chilled,in} - T_{chilled,out}) \quad (5-21)$$

$$Q_{DesUpper/Lower} = \dot{m}_{hw} c_p(T_{hw,in} - T_{hw,out}) \quad (5-22)$$

5.4 Results and discussion

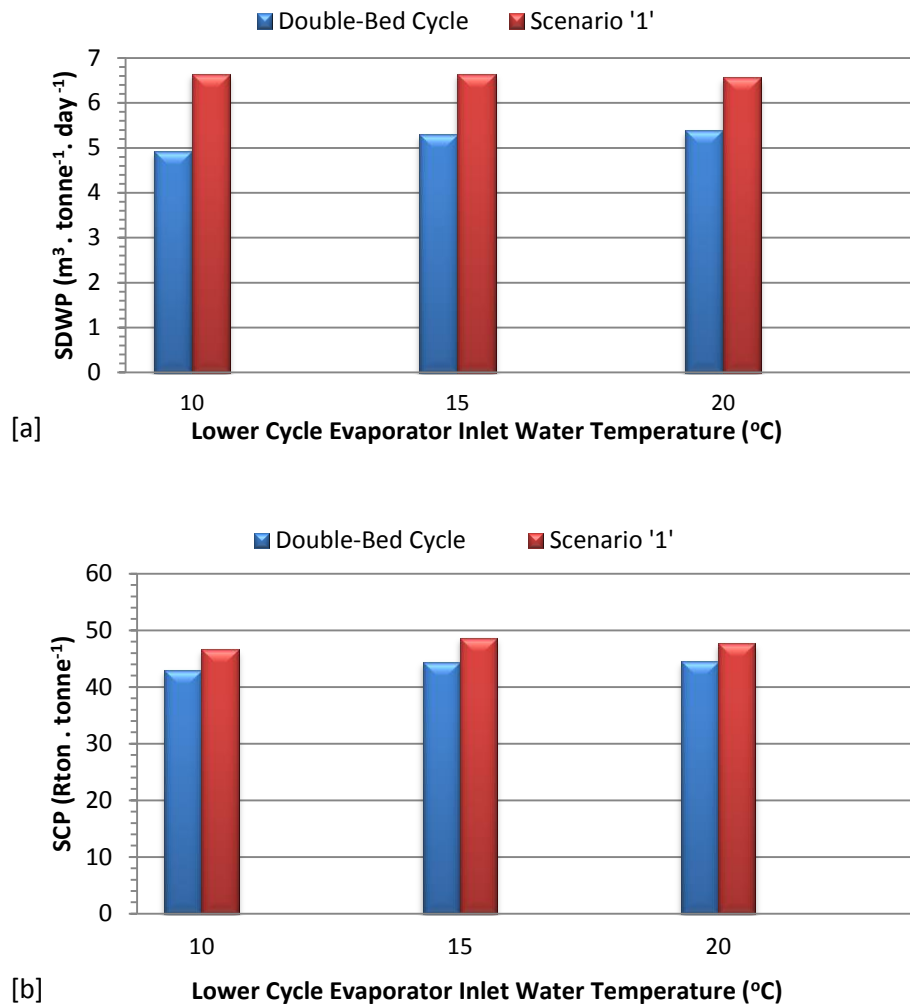
5.4.1 Proposed cycle results at operating scenarios '1, 2 and 3':

As found in section 4.2.3, the condenser temperature is an important parameter in determining cycle performance. Therefore, the three operating modes of the proposed cycle aim to decrease condenser temperature in different ways by utilizing the cooling obtained from the evaporators. Heating and cooling water temperatures used in the simulation are kept constant at 85 and 30°C at all conditions for upper cycle beds. However, lower cycle beds are heated by lower water temperature than 85°C as heating is applied using the exiting heating water from desorbing bed in the upper cycle but cooling of the beds is performed by water at temperature of 30°C. Both upper and lower cycle times are kept constant at 850 seconds: each half-cycle lasts for 400 seconds adsorbing or desorbing plus 25 seconds for switching.

5.4.1.1 Water and cooling outputs at operating scenario '1':

In scenario '1', three different evaporator water temperatures are investigated in the range of 10-20°C while condenser water temperature is kept constant at 30°C. Figure 5-4, [11], shows SDWP and SCP for scenario '1' and compares them to those of the conventional two bed system [184]. As can be seen from Figure 5-4 (a & b), at all evaporator water temperatures, scenario '1' produces more water and cooling compared to the conventional double-bed system. At 10°C evaporator water temperatures, 35% more water is produced from the system where 6.65 m³.tonne⁻¹.day⁻¹ is achieved while the conventional system produces 4.9m³.tonne⁻¹.day⁻¹. At the same temperature, 8.5% more cooling effect is achieved by scenario '1' (46.6 Rton.tonne⁻¹) compared to the double-bed cycle (43 Rton.tonne⁻¹). It can also be noticed that changing the lower cycle evaporator temperature in this mode slightly affects

cycle outputs. This is due to the fact that isotherm of AQSOA-Z02 yields nearly the same water uptake at all pressure ratios above 0.2 (evaporator water temperatures $> 10^{\circ}\text{C}$), at these operating conditions [169]. Also, in this mode, the lower and upper condensers' temperatures are not affected by evaporator temperatures.



Scenario "1": No chilled water is supplied to upper cycle evaporator.

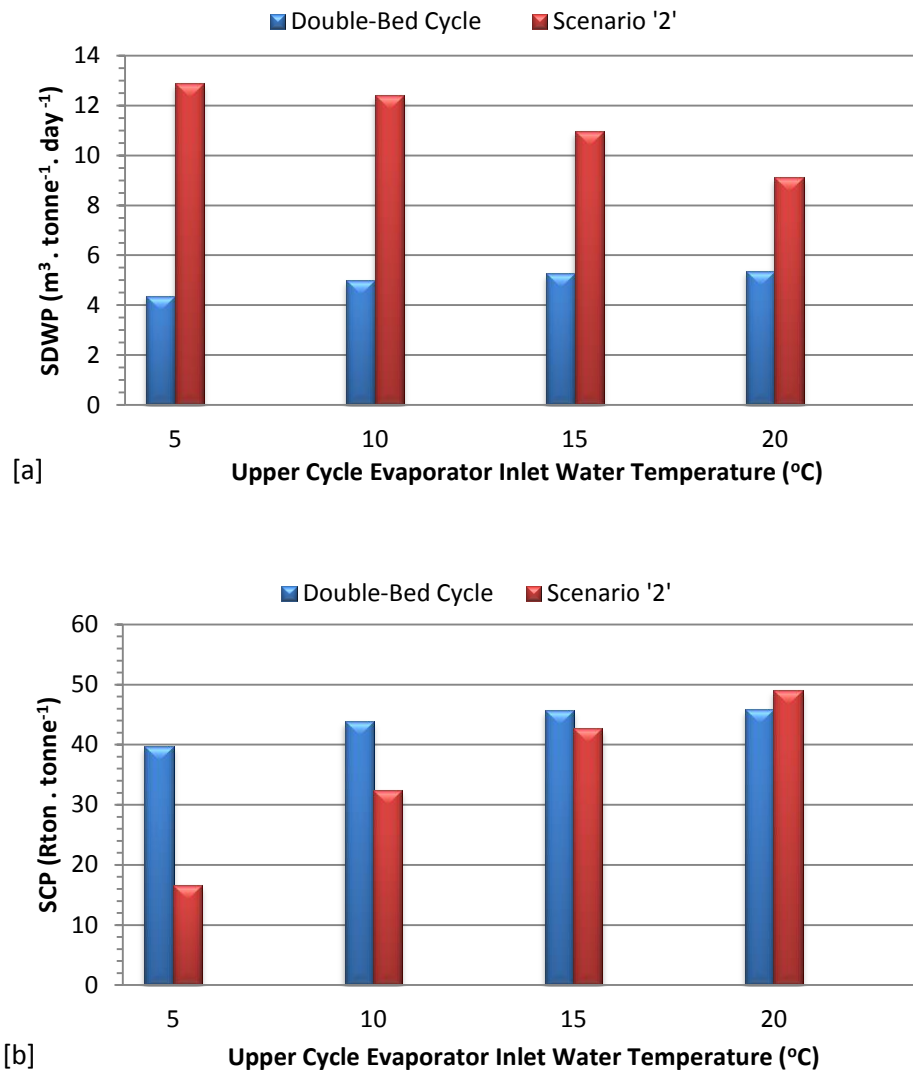
Cooling is produced from lower cycle evaporator.

Figure 5-4 Specific daily water production (a) and Specific cooling power³ (b) for scenario '1' at various lower evaporator inlet water temperatures [11]

³ SCP unit is $(\text{Rton} \cdot \text{tonne}^{-1})$ where "Rton" is the Ton of refrigeration defined as the amount of heat needed to melt 1000 kg of ice in 24 hours.

5.4.1.2 Water and cooling outputs at operating scenario '2':

When operating at scenario '2', a wider range of evaporating water temperatures is investigated (5-20°C) for the upper cycle evaporator, while no control on the lower cycle evaporator temperature because its chilled water loop is connected to the upper cycle condenser. In scenario '2', significant improvements are achieved in water production as it reaches three times that of the double-bed system at 5°C evaporator water temperature (12.9 m³.tonne⁻¹.day⁻¹ to 4.3 m³.tonne⁻¹.day⁻¹), as shown in Figure 5-5(a) [11]. By increasing evaporator water temperature, water outputs decrease due to the temperature increase of lower cycle condenser; but in all cases, scenario '2' continues to produce more water. As a result of this significant increase in the water production levels, the amount of cooling produced is less than that for the double-bed system as shown in Figure 5-5(b) [11]. The reason for this drop in cooling production is due to cooling the condenser of the upper cycle using all the cooling obtained from the evaporator of the lower cycle thus maximizing water outputs. Therefore, scenario '2' is only recommended to be used when desalinated water is the main required product while cooling is still needed, but has less importance. However, changing the evaporator water temperature can control the proportion of produced cooling to water, as shown in Figure 5-5 [11].



Scenario "2": Water circulates between lower cycle evaporator and upper cycle condenser.

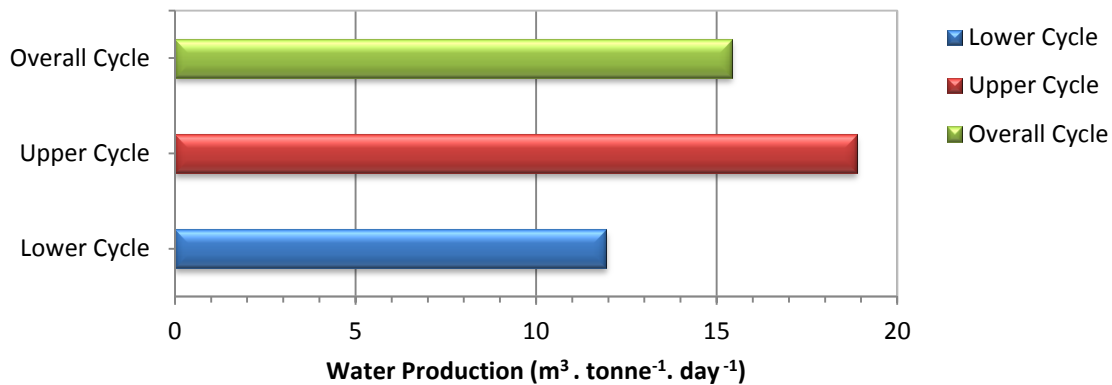
Cooling is produced from Upper cycle evaporator.

Figure 5-5 Specific daily water production (a) and Specific cooling power (b) for scenario '2' at various upper cycle evaporator inlet water temperatures [11]

5.4.1.3 Water and cooling outputs at operating scenario '3':

As shown in Figure 5-6 [11], maximum cycle water production is achieved when operating at scenario '3' with no cooling produced. In this mode, $18.87 \text{m}^3 \cdot \text{tonne}^{-1} \cdot \text{day}^{-1}$ in addition to $11.94 \text{m}^3 \cdot \text{tonne}^{-1} \cdot \text{day}^{-1}$ are produced from the upper and lower cycles respectively, which results in an overall system SDWP of $15.41 \text{m}^3 \cdot \text{tonne}^{-1} \cdot \text{day}^{-1}$. This increase in water

production compared to scenario '2' is due to limiting the heat interaction in the combined evaporator-condenser unit to be only between the evaporating seawater and the condensing freshwater with no sharing from the chilled water side.



Scenario "3": Water circulates between lower cycle evaporator and upper cycle condenser.

No chilled water is supplied to upper cycle evaporator.

No cooling is produced from the system.

Figure 5-6 Specific daily water production in case of scenario '3' [11]

5.4.1.4 Overall conversion ratio for operating scenarios '1, 2 & 3':

In this system, two outputs are produced: fresh water and cooling; therefore, system efficiency is assessed via the overall conversion ratio (OCR), which is the summation of PR and COP. Figure 5-7, [11], shows the OCR at different evaporator operating temperatures at scenarios '1' and '2' in the form of stacked columns representing PR and COP. In scenario '1', Figure 5-7(a), all evaporator temperatures result in nearly the same OCR of the double-bed system as both of them lie in the range of 0.665 to 0.7 but with higher PR for scenario '1'. As scenario '2' produces higher amounts of water than that of the double-bed system, PR is higher reaching 0.51 while it is 0.3 for the conventional cycle. However, COP of the double-bed system remains greater than COP of scenario '2' because of the extra cooling generated

by the conventional double-bed system. As scenario '3' is producing water only, so OCR in this case is the same as PR which reaches 0.64.

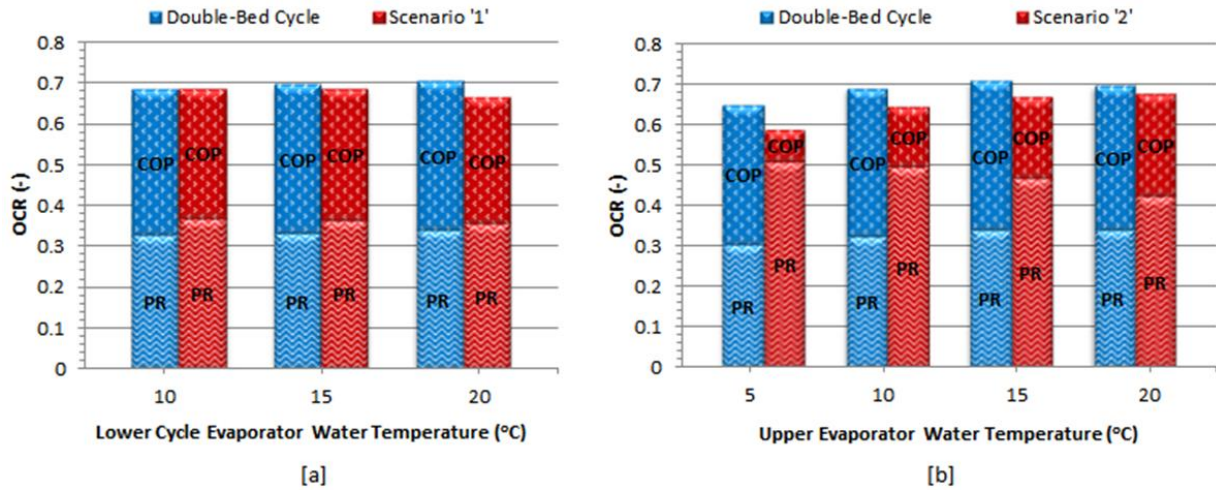


Figure 5-7 Overall conversion ratio at various lower and upper evaporator inlet water temperatures for scenarios '1' (a) and '2' (b) [11]

5.4.1.5 Condenser temperature effect on cycle uptake:

Figure 5-8, [11], illustrates how the condenser temperature affects cycle performance through uptake. Cycle output is maximized when the biggest difference between higher and lower uptakes is achieved, which is controlled through operating pressure ratios in adsorbing and desorbing beds. As shown in Figure 5-8, for all modes of operation, reduction in the pressure ratio of desorption is observed when condenser temperature is reduced which leads to decrease of equilibrium uptake and accordingly allowing increased desorbing rates and cycle outputs [11].

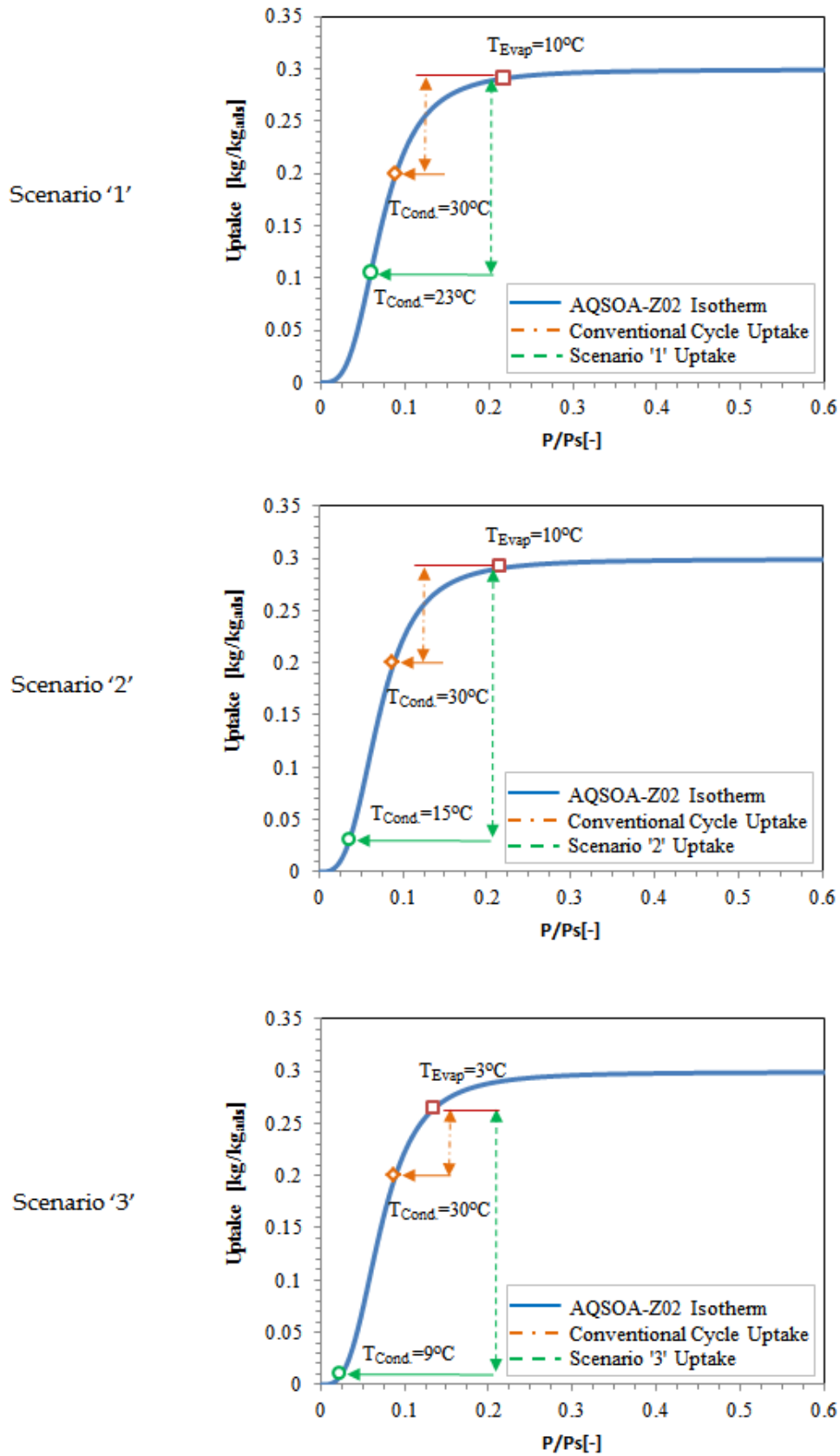


Figure 5-8 Comparison of uptake between conventional and proposed systems at operating scenarios, '1, 2, and 3' respectively [11]

5.5 Economic Analysis

Brief cost estimation for fresh water and cooling production is carried out in this section for the three operating scenarios '1, 2 and 3'. Two types of costs could be considered: capital and running. In this case, the running costs are only calculated as in the approach done by Thu et al. [98, 99], where the pumping power is the only factor of energy usage. As these systems run by solar or waste energy, thus heating energy is not considered in the cost estimation as it is deemed free of charge [99]. Equations (5-23) to (5-31) are used to calculate the costs of pumping water in adsorber beds, lower evaporator, the combined evaporator-condenser unit and upper condenser [11].

$$\Delta h_f = \frac{f L v^2}{2 g d} \quad (5-23)$$

where Δh_f is the pumping head loss, f is the coefficient of friction, L is pipe length, v is water velocity inside pipe and d is the pipe inner diameter [11].

$$PP_{elec.} = \frac{\Delta h_f \cdot g \cdot \dot{m}_{water}}{\eta_{pump}} \quad (5-24)$$

$$PP_{elec.-total} = PP_{Beds} + PP_{Lower\ Evap.} + \alpha \cdot PP_{Upper\ Evap.} + PP_{Upper\ Cond.} \quad (5-25)$$

where PP is the electric pumping power, η_{pump} is the pump efficiency (which is assumed to be 85%) and α is a flag equal to 1 at scenario '2' and equal to 0 at both scenarios '1' and '3'.

Specific energy consumption is calculated for water and cooling outputs as follows; firstly portion of power (POP) needed to produce each product is estimated by equations (5-26) and (5-27), then the cost per unit product could be calculated using equations (5-30) and (5-31).

$$POP_{water} = \frac{Q_{cond.}}{Q_{cond.} + Q_{evap}} \quad (5-26)$$

$$POP_{cooling} = \frac{Q_{evap.}}{Q_{cond.} + Q_{evap}} \quad (5-27)$$

$$Specific\ energy\ consumption_{water} = \frac{POP_{water} \cdot PP_{elec.-total} \cdot 24}{SDWP \cdot M_a} \quad (5-28)$$

$$Specific\ energy\ consumption_{cooling} = \frac{POP_{cooling} \cdot PP_{elec.-total}}{SCP \cdot M_a} \quad (5-29)$$

$$Cost_{water\ unit} = Energy\ rate_{elec.} \times Specific\ energy\ consumption_{water} \quad (5-30)$$

$$Cost_{daily\ cooling\ unit} = Energy\ rate_{elec.} \times Specific\ energy\ consumption_{cooling} \times 24 \quad (5-31)$$

Table 5-2, [11], presents the outcome of this cost estimation study for the three operating scenarios at evaporator chilled water inlet temperature of 10°C with an electric energy costs ($Energy\ rate_{elec.}$) of 0.144 US dollars.kWh⁻¹ [185]. It was found that water production costs ranged from 0.169-0.136 US\$.m⁻³ which is less than the value of 0.18 US\$.m⁻³ reported by Thu et al. [98]. In addition, a minimum cooling cost of 0.018 US\$.Rton⁻¹.day⁻¹ was achieved at scenario '2'.

Table 5-2, Cost estimation of cycle outputs [11]*

Product	Scenario '1'		Scenario '2'		Scenario '3'	
	Water	Cooling	Water	Cooling	Water	Cooling
Total pumping power (kW)	2.052		2.467		2.052	
Percentage of required power (%)	53.4	46.5	75.64	24.35	100	0
Specific energy consumption [kWh. m ⁻³] - [kW. Rton ⁻¹]	1.17	6.07E-3	1.06	5.5E-3	0.94	0
Cost per unit product [US\$.m ⁻³]- [US\$.Rton ⁻¹ .day ⁻¹]	0.169	0.021	0.154	0.018	0.136	0

* Estimated at 10°C evaporator inlet water temperature

5.6 Summary

A novel adsorption cycle for desalination and cooling applications has been developed in this chapter using AQSOA-Z02 as an adsorbent. The cycle comprises of two parts, upper and lower, with each one having two adsorber beds, and these parts are linked together via combined evaporator-condenser heat exchanger. The proposed system has three modes of operation where lower condenser temperature can be achieved to increase cycle outputs. A summary of the system outputs and percentage of improvement compared to the conventional double-bed system is presented on Table 5-3 for the three operating scenarios, '1, 2 and 3' [11].

Table 5-3, Proposed cycle outputs compared to double-bed conventional cycle [11]

Scenario	Specific daily water production		Specific cooling power	
	Value (m ³ .tonne ⁻¹ .day ⁻¹)	Improvement	Value (Rton.tonne ⁻¹)	Improvement
1 ^a	6.64	35%	46.6	8.5%
2 ^a	12.4	250%	32.4	-26%
3	15.4	314%	0	-

^aOutputs at 10°C evaporator inlet water temperature

CHAPTER 6: EXPERIMENTAL INVESTIGATION OF CPO-27NI PERFORMANCE IN SINGLE BED ADSORPTION SYSTEM

6.1 Introduction

This chapter presents the construction, commissioning and operation of a single bed adsorption desalination system at different operating conditions using MOF adsorbent material namely; CPO-27Ni. Based on the conclusions of chapter 4, it was recommended to use CPO-27Ni as an adsorbent for desalination and cooling applications. Furthermore, it was found that this advanced MOF material is commercially available through its manufacturer, “Johnson Matthey Ltd”. System outputs are assessed at various parameters including switching time, half cycle time, as well as water inlet temperatures of evaporator and condenser [186].

6.2 Test facility description

Figure 6-1 and Figure 6-2, show schematic diagram and pictorial view of the developed experimental test facility consisting of an adsorber bed, evaporator and condenser [12, 186, 187]. The adsorber bed is a steel cylinder containing two finned tube heat exchangers connected in series and the adsorbent material is packed between the fins [186]. Both evaporator and condenser are in cylindrical shape and made of heavy-duty powder coated steel. Copper helical coils are used in both evaporator and condenser for heat transfer between chilled water/ seawater in the evaporator and between condenser cooling water/fresh water vapour in the condenser. Hot and cold water tanks are connected to the

adsorber bed to supply hot and cold water during desorption and adsorption processes respectively with only one pump to deliver both water streams which are controlled by 4 solenoid valves. A stainless steel water tank fitted with an electric heater is used as a reservoir for the evaporator chilled water circuit to supply the evaporator cooling load at a controlled temperature. A separate chiller with a built in pump is used to adjust the temperature of the condenser cooling water inlet temperature. Two dry vacuum pumps are linked to the adsorber bed, evaporator and condenser during the initialization of the system to achieve the required vacuumed pressure level. In addition, an oil lubricated vacuum pump connected to an accumulator is used to collect the produced fresh water in the condenser at the end of the experimental testing. Measuring instruments like pressure transducers, thermocouples and flow meters are used at different positions in the system to measure pressure, temperature and flow rate respectively.

The next section describes in detail each component of the system including the adsorber-bed, evaporator, condenser, water circuits, measuring devices, flow control solenoid and manual valves and data acquisition systems.

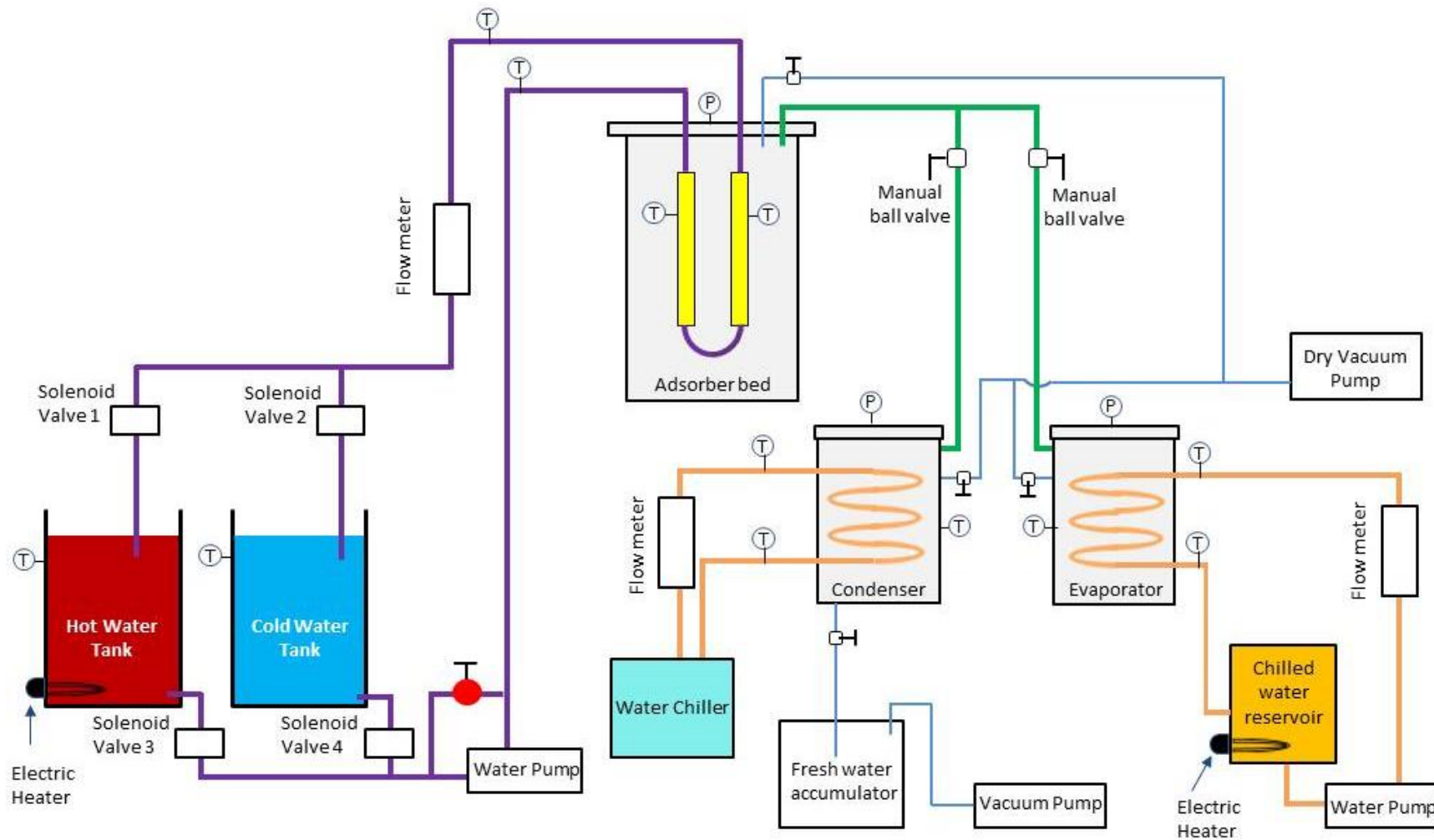


Figure 6-1, Schematic diagram for the single bed test facility

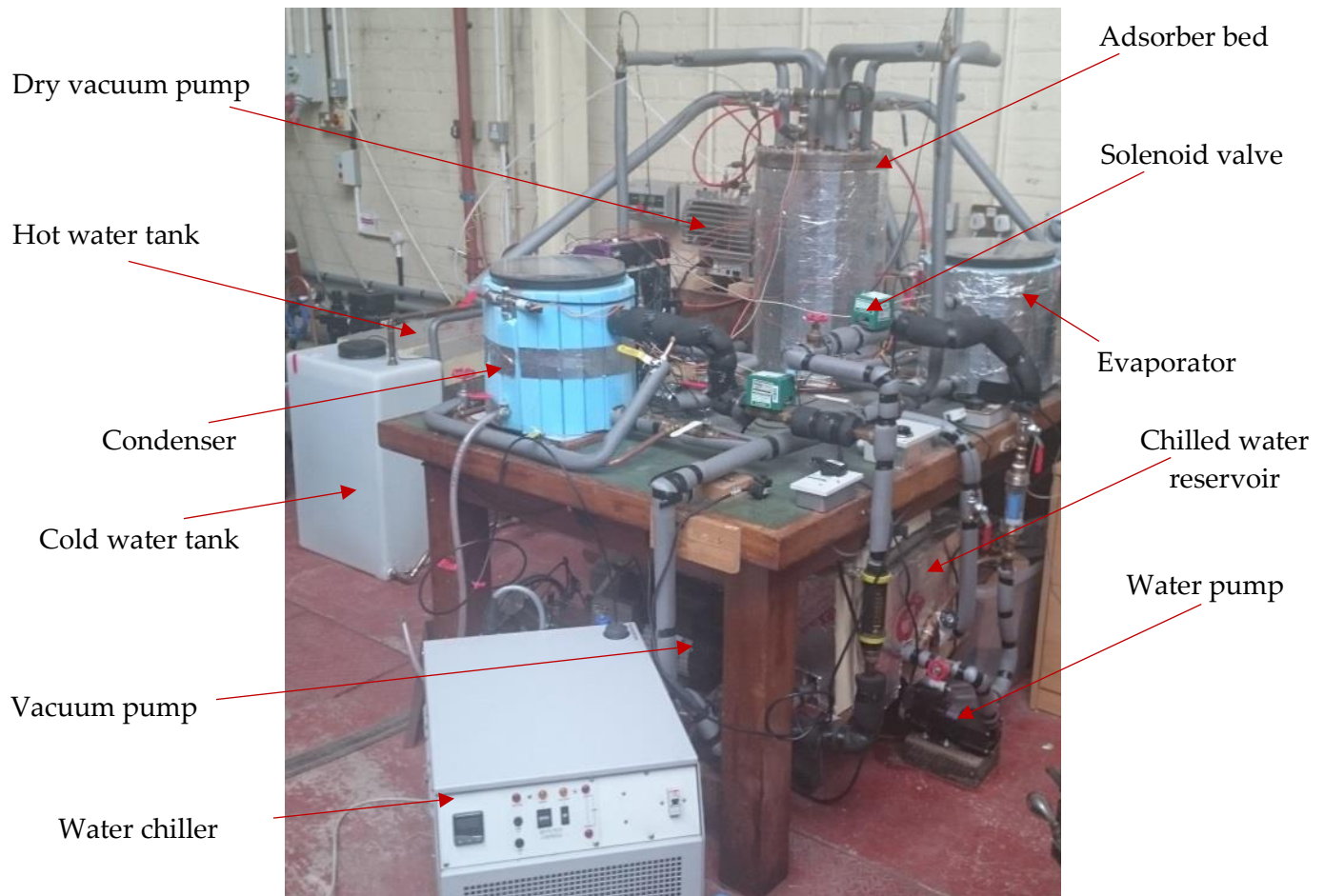


Figure 6-2, Pictorial view of the single bed test facility [186]

6.2.1 Adsorber bed

The adsorber bed is an important part of the adsorption system where the adsorbent material is packed to adsorb and desorb the water vapor which allows continuous operation of the system. In this system, two heat exchangers are connected in series acting as first and second passes (see Figure 6-3) [186]. Each heat exchanger consists of four copper tubes finned with Aluminium rectangular fins, where the adsorbent material is packed in between as shown in Figure 6-3 with all dimensions furnished in Table 6-1 [12]. A cylindrical steel shell contains the aforementioned heat exchangers which are connected to the cylinder lid by brass tube

fittings (made by Swagelok, part number B-1010-1-8) to maintain the required vacuum inside the bed. A detailed description for the adsorber bed cylinder is available at [12].

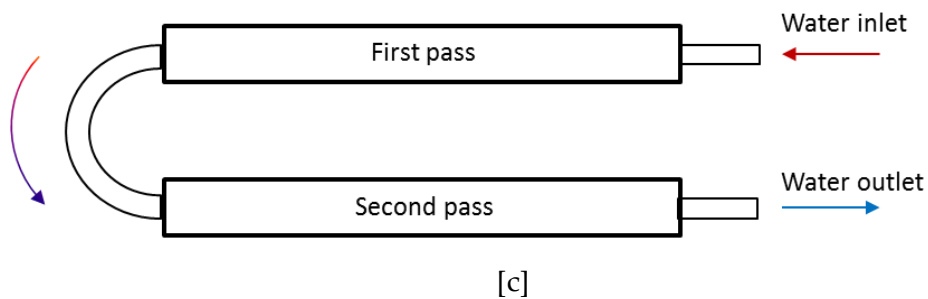
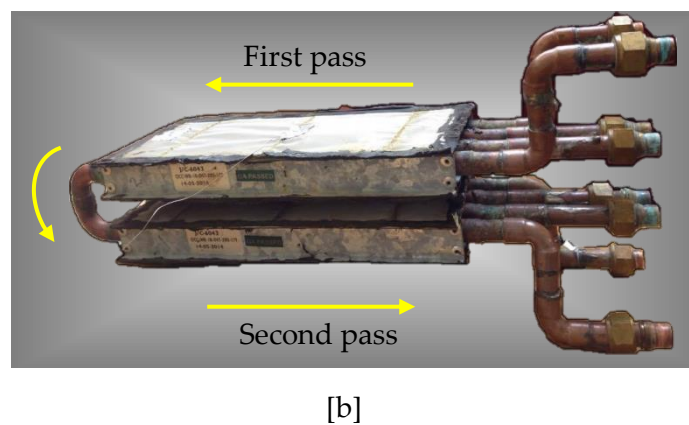
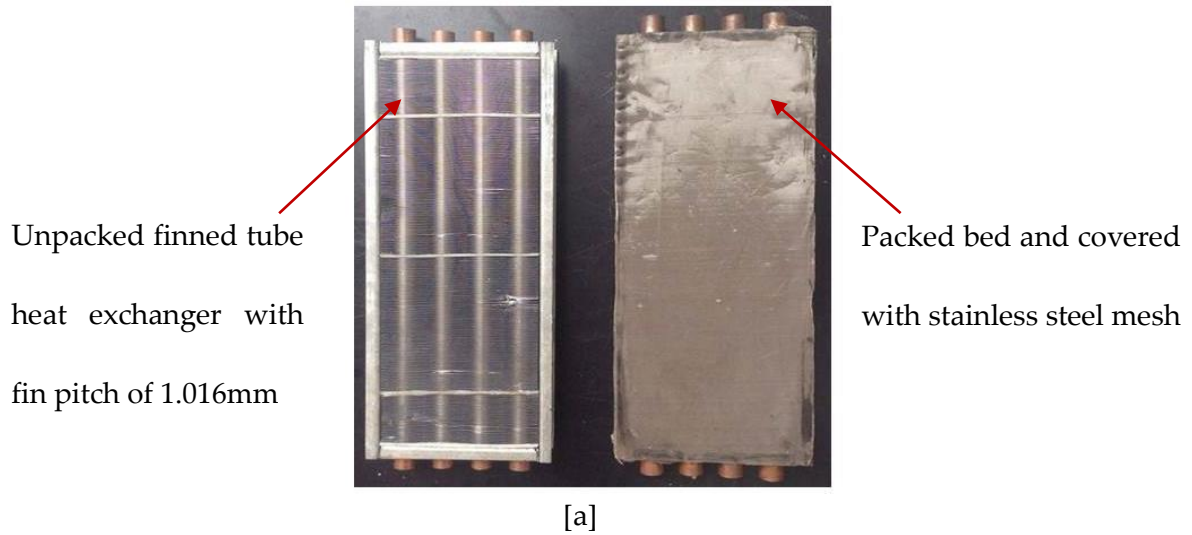


Figure 6-3, Finned tube heat exchangers, Pictorial view(a &b), Schematic diagram (c) [186]

Table 6-1 Heat exchanger characteristics and dimensions (single bed system) [12]

Parameter	Value
Heat exchanger length	275 mm
Fin width	115 mm
Fin height	30 mm
Fin pitch	1.016 mm
Fin thickness	0.105 mm
Tube outer diameter	15.875 mm
Tube thickness	0.8 mm
Number of fins in one heat exchanger	270
Amount of CPO-27Ni packed in one heat exchanger	0.335 kg

6.2.2 Evaporator

The evaporator is the device where salty water is fed into the system and where the cooling effect is generated due to the evaporation of the seawater. It consists of a shell and tube coil. The shell is a ready made 26 litre vacuum chamber made by “easy composites” from heavy-duty powder-coated steel with a transparent Perspex lid. Vacuum sealing is performed via rubber gasket located along the top edge of the cylindrical vessel where the lid sets on. Therefore when pressure inside the evaporator becomes lower than atmospheric pressure, the lid is pulled down providing vacuum sealing. Additional ports were fitted to the vacuum chamber for water vapor exit, chilled water coil inlet/outlet and connections of thermocouple, pressure transducer and vacuum pump as shown in Figure 6-4. Chilled water coil is made of 8 mm OD copper pipe in a spiral form (Figure 6-5 [12]) which acts as a heat source for the evaporation of seawater. Due to the heat extracted from the chilled water, the cooling effect is produced.

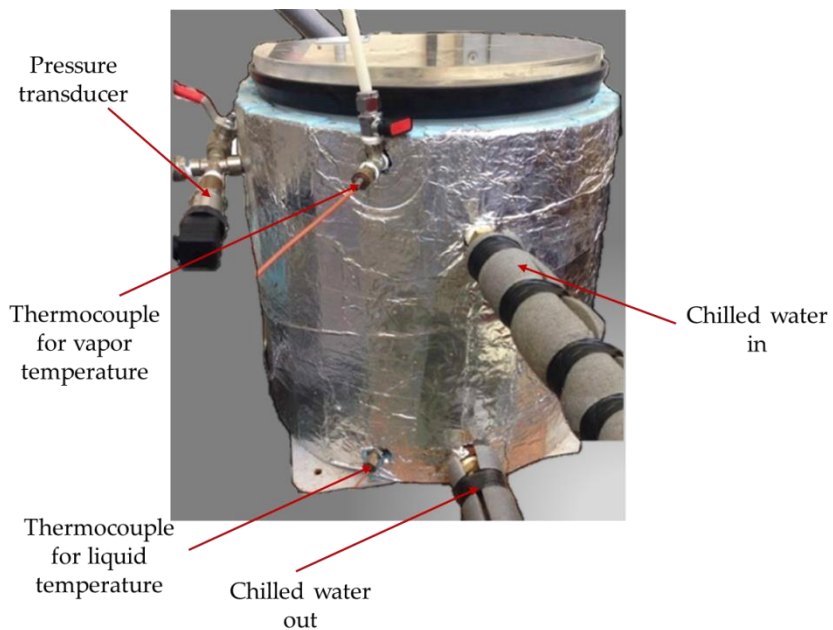


Figure 6-4, Pictorial view for the evaporator with different inlet and outlet ports and connections



Figure 6-5, Pictorial view for the evaporator chilled water spiral copper coil [12]

6.2.3 Condenser

The condenser is where water vapor condenses and fresh water is produced. Similar to the evaporator, the condenser is made of a shell and helical copper coil. The shell is made of heavy-duty powder-coated steel and covered with a transparent Perspex lid which sits on a rubber gasket made by “easy composites” as shown in Figure 6-6 and has a volume of 26 litres. A cooling water coil is fitted in the condenser to receive the latent heat of condensation of the desorbed water vapor which results in condensed fresh water that accumulates at the bottom of the condenser shell. The cooling coil is 6 m long, made of 8 mm OD copper tube in a helical form with a diameter of 250 mm and has 8 turns as shown in Figure 6-7. Other ports have been welded into the condenser shell to allow the flow of water vapor to be condensed, vacuum pump, pressure transducer, input/output of condenser cooling water coil and finally a special KF-flange fitting for vacuum applications for the connection of the thermocouples.

At the end of the test, after certain number of cycles, the fresh water is collected in an accumulator as shown in Figure 6-8. The water collection system consists of a vacuum pump, a glass flask and 6 mm OD flexible tubes. The vacuum pump is connected to the top of the glass flask through a tapered rubber plug. The flask is also fitted with another rubber plug through which a 6 mm OD flexible tubing is connected. To collect the fresh water, the vacuum pump is operated creating vacuum in the flask then when the free end of the flexible tube is inserted in the bottom of the condenser, the fresh water is drawn into the flask where it is then measured and collected.



Figure 6-6, Pictorial view for the condenser with different inlet and outlet ports and connections



Figure 6-7, Pictorial view for the condenser cooling water helical copper coil

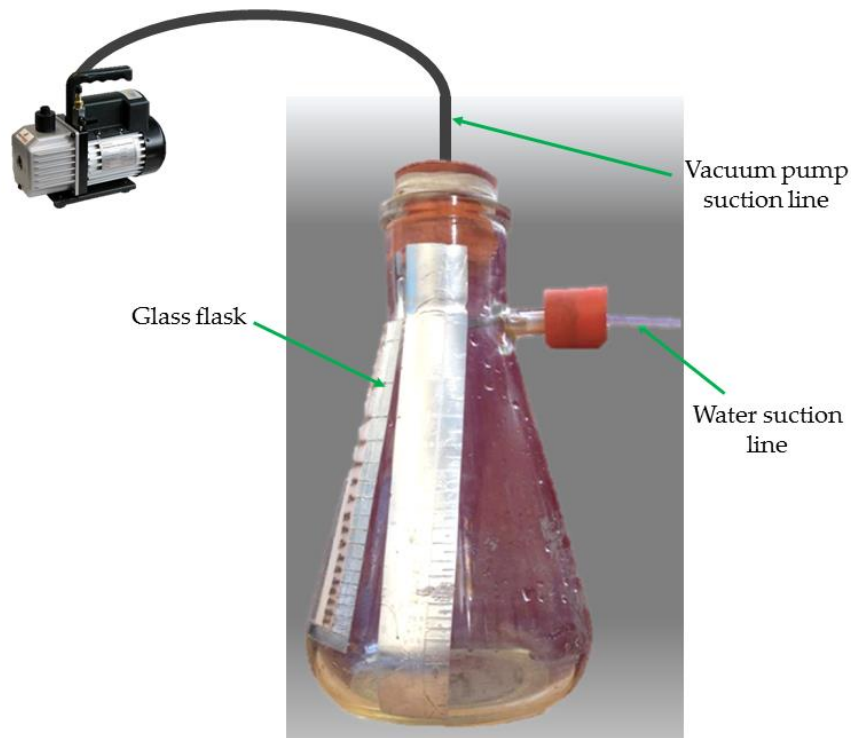


Figure 6-8, Pictorial view of the fresh water collection system

6.2.4 Chilled water reservoir

The chilled water reservoir is a stainless-steel tank equipped with a 3 kW electric heater and a copper helical coil with a total storage capacity of 60 litres as shown in Figure 6-9. This reservoir is located in the evaporator chilled-water circuit to allow for constant water temperature fed into the evaporator. As the evaporator cools the chilled water, an electric heater is used to act as the heating load which in turn adjusts the temperature of the chilled water before returning to the evaporator. The heater is controlled by a thermostat that works in the range of 0 to 40°C with a temperature differential of $3\pm 1^\circ\text{C}$. During initialization of the system, water temperature in the reservoir needs to be adjusted to the required evaporator working temperature so cooling or heating might be necessary. In case of heating, the electric

heater is used but if cooling is to be performed, the immersed copper helical coil is then connected to the chiller, which decreases the temperature of the water in the reservoir until it reaches the required operating temperature. This reservoir is insulated with a 100 mm PIR foam insulation sheet with a thermal conductivity of $0.023 \text{ W.m}^{-1}\text{K}^{-1}$.



Figure 6-9, Pictorial view for the chilled water reservoir

6.2.5 Water chiller

To ensure constant cooling water temperature supplied to the condenser, a water heater/chiller is used. This heater/chiller unit is made by “Betta-Tech” company with the model number of CU-700 and the specification listed on Table 6-2 [12, 188]. It is capable of controlling water temperature in the range of -15°C to 70°C through a PID controller with an accuracy of 0.1°C [12]. As shown in Figure 6-10, it has two ports for inlet and outlet which are connected directly to the condenser cooling water coil and with the built-in pump, constant flow of water is supplied.

Table 6-2, Specifications of water chiller, “CU-700” [12, 188]

Parameter	Value
Temperature range	-15 to 70°C
Cooling capacity at 15°C water supply	2.9 kW
Heating capacity	2.5 kW
Maximum pump flow at zero head	15 L/min
Tank Capacity	3 Litre
Electrical Supply	240 V
Dimensions	610 x 450 x 500 mm
Weight	82 kg



Figure 6-10, Pictorial view of the CU-700 water heater/chiller

6.2.6 Water pumps

Two water pumps are used in the system, one for circulating the cooling/heating water in the adsorber bed and the second one for circulating the chilled-water in the evaporator coil. The adsorber bed pump is used for both hot and cold water supply, therefore it is capable of withstanding maximum temperature of 120°C with maximum flowrate of 60 Litre.min⁻¹ and maximum pumping head of 8 mH₂O. It is a single-stage magnetically driven centrifugal pump with a model number of SS-9R-MD, made by “MarchMay” company as shown in Figure 6-11. The chilled water pump is a multistage magnetically driven centrifugal pump with a model number of MSP-3, made by “MarchMay” company as shown in Figure 6-12. As this pump is used for cold water, its maximum operating temperature is 88°C with maximum water flowrate of 20 Litre.min⁻¹ and maximum pumping head of 18 mH₂O.



Figure 6-11, Adsorber bed circulating water pump, “SS-9R-MD”



Figure 6-12, Evaporator chilled water circuit water pump, “MSP-3”

6.2.7 Flow control valves

Two types of flow control valves exist in this system, solenoid and manual ball valves. Four solenoid valves are fitted in the adsorber bed water supply and return lines for both hot and cold water streams while two manual ball valves are installed in the vacuum lines that transport the water vapor from evaporator to adsorber bed and from adsorber bed to condenser. As shown in Figure 6-13, the manual ball valve has two ports, made by “Boss” company with a model number of FIG.966S WRAS. It has PTFE seat and gland packing which insures high levels of vacuum sealing while on the same time it is capable of working at maximum temperature of 180°C and maximum pressure of 40 bar.



Figure 6-13, Manual ball valve, “FIG.966S WRAS”

As shown in Figure 6-14, the solenoid valve has two ports and one-direction flow, made by “Inta” company with a model number of SMV2530. It is capable of working at maximum temperature of 120°C which is safe for the hot water system as its maximum temperature can not exceed 100°C [12]. As per solenoid valves, numbering shown on Figure 6-1, during the desorption half cycle, solenoid valves 1 and 3 are opened while solenoid valves 2 and 4 are closed. In contrast, during adsorption half-cycle, solenoid valves 2 and 4 are opened while solenoid valves 1 and 3 are closed.

These four solenoid valves are controlled using “Labview” software through a control board made by “National instruments” company with the model number of NI 6008, (Figure 6-15) [187]. As shown in Figure 6-16, “Labview” software was programmed to alternate automatically between three different modes; drying the bed (for initialization), adsorption and desorption. To start operation, two fields are required to be filled; half cycle time and number of complete cycles needed before the software terminates the test. The output of the control board which is driven by the software is either 0 or 5 volts signal that triggers a relay to close or open the electric circuit of the solenoid valve as shown in Figure 6-17.



Figure 6-14, Solenoid valve, “SMV2530”



Figure 6-15, National Instruments control board, “NI 6008”

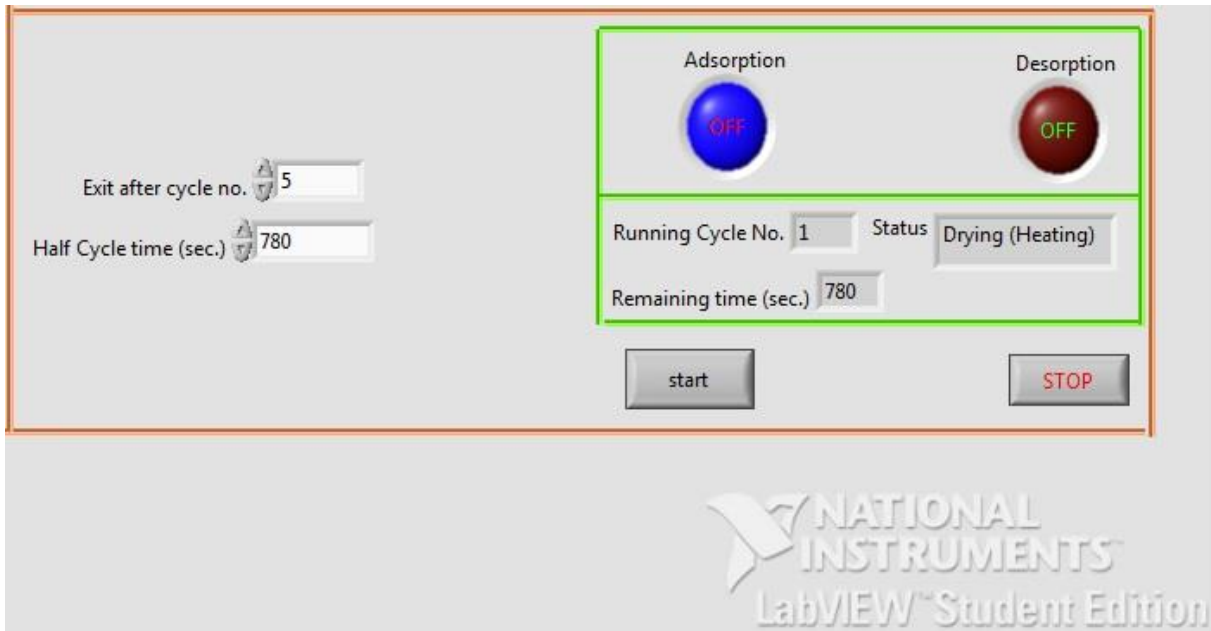


Figure 6-16, User interface of the “Labview” software to control the solenoid valves

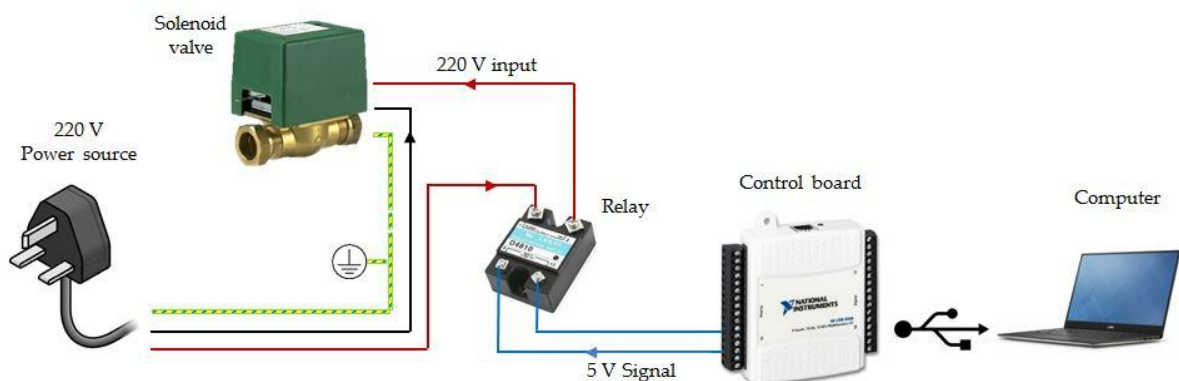


Figure 6-17, Electric circuit of the control of solenoid valves

6.2.8 Hot and cold water tanks

For the desorption and adsorption phases, hot and cold water streams are needed therefore hot and cold water tanks are necessary. As shown in Figure 6-18, the hot water tank is made of stainless steel with a capacity of 70 litre and fitted with two 9 kW, three phase electric

heaters controlled by a thermostat with operating range of 0 to 120°C and a temperature differential of 4 ± 1 °C to ensure constant hot water temperature supplied to the adsorber bed. In addition, a copper float valve is used to maintain the water level in the tank. The tank is insulated with a 100 mm PIR foam insulation sheet with a thermal conductivity of $0.023 \text{ W}\cdot\text{m}^{-1}\text{K}^{-1}$ to decrease heat losses to the surroundings.



Figure 6-18, Pictorial view of the hot water tank

The cold water tank, as shown in Figure 6-19, is made of natural translucent medium density polyethylene with a total capacity of 105 litres, manufactured by “Tanks Direct” company. To ensure constant water temperature supplied to the adsorber bed during cycle operation, the tank is supplied continuously with a fresh stream of mains water while the returning water exiting from the adsorber bed is drained.



Figure 6-19, Pictorial view of the cold water tank

6.2.9 Vacuum pumps

Two types of vacuum pumps exist in this system: dry and oil-lubricated vacuum pumps, as shown in Figure 6-20. The dry vacuum pump model is “nXDS15i” manufactured by “Edwards” company with maximum pumping speed of $15.1 \text{ m}^3.\text{hr}^{-1}$ and capable of achieving minimum pressure of 0.007 mbar. Two pumps of this model are used during initialization of the system to create the required vacuum and are connected to the adsorber bed, evaporator and condenser via 8 mm OD flexible tubes. One oil-lubricated vacuum pump, “ECVP425” manufactured by “Easy Composites” company, with maximum pumping speed of $2.5 \text{ m}^3.\text{hr}^{-1}$, is used to collect the condensed fresh water in the condenser as described in section 6.2.3.



Figure 6-20, Vacuum pumps used in the single bed testing facility

6.3 Measuring devices

Various measuring devices are installed in this test facility including pressure, temperature and flowrate sensors. Pressure and temperature are measured electronically and are logged into the computer using a data logger while flowrates are measured manually. The calibration and uncertainty assessments of these measuring instruments are presented in Appendix II.

6.3.1 Pressure measurements

Three pressure transducers are fitted in the system at the adsorber bed, evaporator and condenser. The pressure transducer is "PXM319-0.35AI" produced by "OMEGA" with the range of 0-350 mbar and accuracy of ± 0.8 mbar, as shown in Figure 6-21 [187]. The output signal of this pressure transducer is 4 to 20 mA with a linear relationship between the current and the measured pressure as shown in Figure 6-22. To measure the pressure, the output current signal is converted to a voltage signal using a 100 ohm resistance connected to one of the data logger analogue channel terminals. The wiring diagram of the pressure transducer, power supply and data logger is shown in Figure 6-23.



Figure 6-21, Pressure transducer “PXM319-0.35AI”

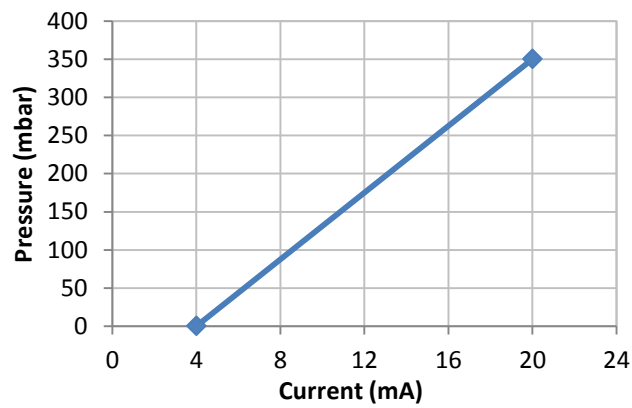


Figure 6-22, Pressure-current relationship of the pressure transducer “PXM319-0.35AI”

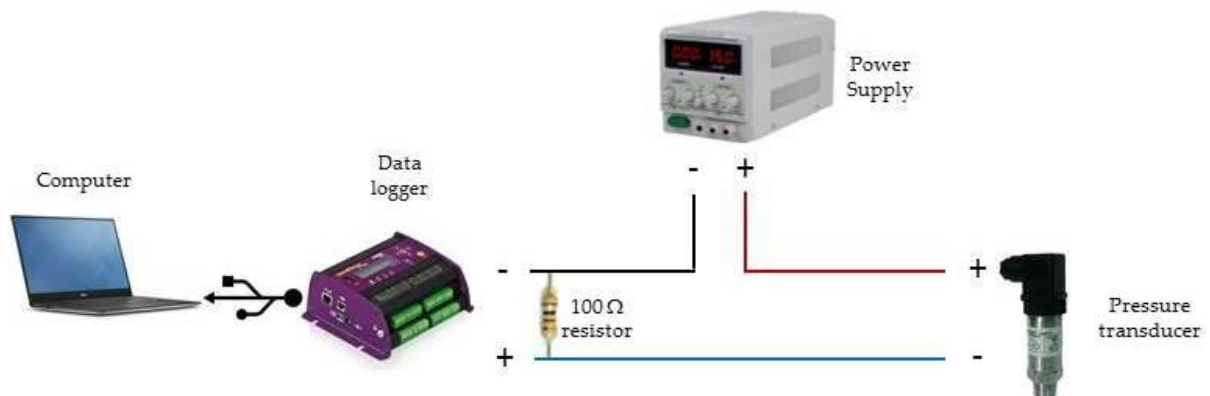


Figure 6-23, Wiring diagram of the pressure transducer connection to the data logger

6.3.2 Temperature measurements

Three types of thermocouples are used in the system, namely “T”, “K” and “RTD” thermocouples. In the adsorber bed, five thermocouples of the type “T” measure temperatures of vapor inside the shell as well as adsorbent material temperature at four different positions: first heat exchanger centre, first heat exchanger bottom, second heat exchanger centre and second heat exchanger bottom. In the evaporator, two “T” type thermocouples are used to measure the temperature of vapor and liquid, while in the condenser vapor and liquid temperatures are measured via two “K” type thermocouples [186, 187]. Six “RTD” thermocouples are used to measure the flowing water temperature at inlet and exit of adsorber bed, evaporator chilled water circuit and condenser cooling water circuit [12, 186, 187].

Type “T” thermocouples are produced by “OMEGA” with a model number of “TJC100-CPSS” and can measure temperature up to 260°C. They have stainless steel compact transition joint probes with diameter of 4.5 mm and length of 30 mm, while sheath diameter is 1.5 mm. To fix the thermocouples probes on the adsorber bed cover plate and evaporator shell, a compression seat, nut and ring are used as shown in Figure 6-24 which ensures sealing of these components.

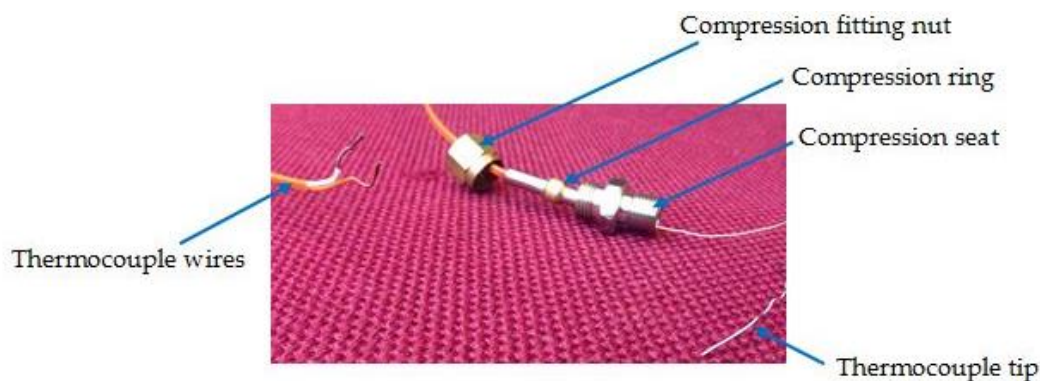


Figure 6-24, Assembly of thermocouple compression fitting

Type “K” thermocouples, are produced by “RS Pro” with a model number of “RS Pro 621-2158” with length of 1000 mm and can measure temperature in the range of -50 to 250°C. Two of these thermocouple cables are passed through the shell of the condenser via a feedthrough KF-flanged thermocouple connector of the “K” type, produced by “Kurt J. Lesker” company with the model number of “TFT2KY00008” as shown in Figure 6-25. The vacuum side terminals of the feedthrough thermocouple connector terminate in stainless steel nut and screw to allow for thermocouple cable connection. This type of feedthrough connection is specifically designed for vacuum applications as it sits on a KF-half nipple welded onto the shell of the condenser with an O-ring in between and are fixed together via a clamp (Figure 6-25).

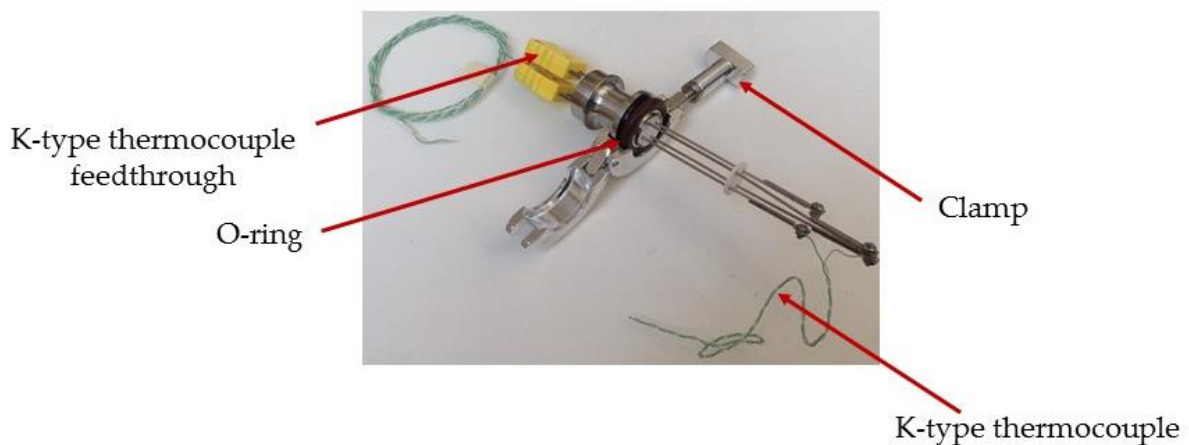


Figure 6-25, Assembly of thermocouple KF-flanged feedthrough

RTD thermocouples are produced by “RS Pro” with a model number of “RS Pro 123-5602” for measuring temperature in the range of -50 to 250°C. The sheath is 100 mm long, has a 6 mm OD and made from rigid 316 stainless-steel with a Teflon-insulated flexible head. This PT100 sensor is fixed into the water copper pipe via 1/8” BSPP compression fitting made by “OMEGA” with a part number of “SSLK-M30-18T”, as shown in Figure 6-26.

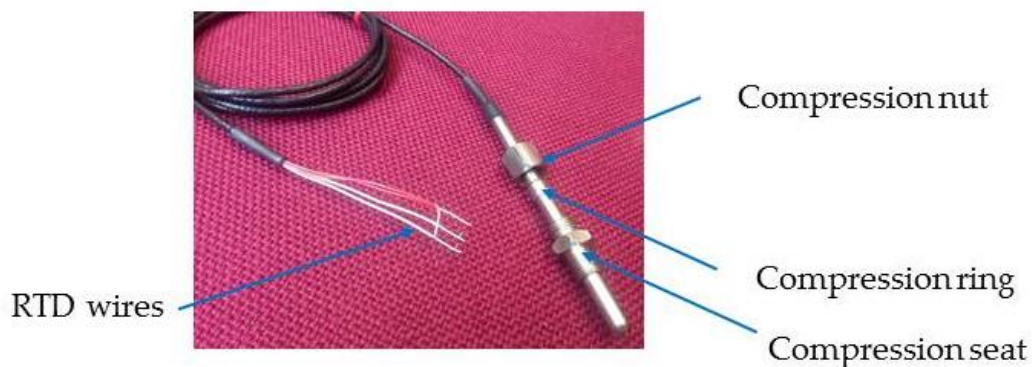


Figure 6-26, Assembly of RTD, PT100, thermocouple compression fitting

The thermocouples and pressure transducers are connected to the data logger via a 3.81 mm pitch straight PCB terminal block made by “RS Pro” with a part number of “RS Pro 790-0831”. The data logger used is produced by “dataTaker” company with model number of “DT85” (Figure 6-27), equipped with 16 analogue channels, each one could be connected with up to three inputs when shared terminals feature is used. The data logger is then connected to a PC to monitor and log all measuring devices.



Figure 6-27, Data logger used for logging temperature and pressure readings, “dataTaker DT85”

6.3.3 Flowrate measurements

Three manual flow meters measure flowrates of the adsorber bed cooling/heating water, the evaporator chilled water and the condenser cooling water. The flow meter of the adsorber bed water circuit is “A24S.S.Mk2” made by “Platon” (Figure 6-28), with the range of 4-40 L/min and accuracy of ± 1 L/min while that of the evaporator and condenser water circuits is “A12S.S.Mk2” made by “Platon”, with a range of 1-10 L/min and accuracy of ± 0.25 L/min. During system operation, various readings are taken and their average is used in further calculations.



Figure 6-28, Flow meter of adsorber bed water circuit

6.4 Test rig commissioning

The system was assembled as shown in Figure 6-1 with all pressure transducers and thermocouples connected to the data logger and ready for operation. Different leakage tests were performed for both pressurized (water pipes) and vacuumed parts (adsorber bed, evaporator and condenser) in the system. Water pumps were operated to deliver their maximum flowrates and water leakage from the fittings was inspected and stopped if found. For the vacuum side, different techniques were used to identify leakage points. Firstly, vacuum pumps were operated and connected to each component individually then a suitable vacuum leakage test was performed. For pipe fittings, a thick paste was applied around the line of contact between the pipe and the fitting then when a hole appeared on the paste because of air trying to pass through, this is a sign of leakage point as shown in Figure 6-29. Leakage for fittings on the side walls of the evaporator and condenser are identified using two techniques: (1) the shell is filled with water and vacuum is applied. The appearance of air bubbles in the water close to a fitting indicates the position of leakage. (2) Applying soapy water at the fittings while the shell is under vacuum. The appearance of soapy bubbles inside the evaporator /condenser indicates the position of leakage.

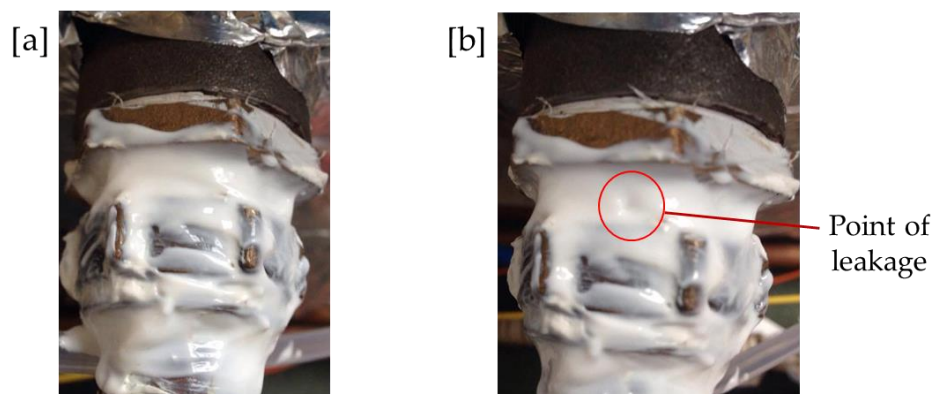


Figure 6-29, Vacuum inspection in pipe fittings; (a) no leakage, (b) leakage is detected

For leakage between the evaporator and condenser lids and their sealing gasket, the method of the soapy water was used. Finally, to identify leakage from Swagelok fittings used in the top lid of the adsorber beds, the soapy water method was also used. However, in addition to the soapy water, a thin diaphragm was also applied. When vacuuming is applied, the diaphragm was found to be pulled down in areas where leakage exist as shown in Figure 6-30.



Figure 6-30, Vacuum inspection using the diaphragm technique

After all these inspections and insuring vacuum sealing at all points, vacuum was applied to all components and the pressure was monitored showing that minimum pressure of 1 mbar can be maintained for more than 4 hours which is the time needed for system cyclic operation.

Electric heaters in the hot water tank and evaporator water reservoir were tested with their thermostats controllers. Finally, the solenoid valves were tested for the automatic operation, performed by the “Labview” software, that alternates between adsorption and desorption processes.

6.5 Testing procedure

The test is divided into three different stages: initialization and drying, cycling adsorption and desorption and finalizing. This section explains these three stages with steps listed for each stage.

6.5.1 Initialization

- a. At the beginning, the data logger is connected and its software, “dataTaker” is started to measure temperatures and pressures of the system components.
- b. Hot, cold and chilled water tanks are filled with water and the thermostats of the heaters are set to the required operating temperatures.
- c. If the chilled-water tank temperature is higher than the required evaporator operating temperature, the chiller is connected to the cooling coil of the chilled-water reservoir until two degrees below the required operating temperature is reached then chiller is disconnected.
- d. In the “Labview” software, the half-cycle time and the required number of cycles are entered then solenoid valves are operated to open the valves on the hot water circuit (valves 1 and 3 on Figure 6-1) to start adsorber bed drying, while the manual ball valves of the vacuum side are kept closed.
- e. The adsorber bed water-circuit pump is switched on and the two dry vacuum pumps are operated and connected to the adsorber bed until bed pressure reaches about 8 mbar while bed temperature is about 85°C.
- f. The chiller temperature is set at the condenser operating temperature and connected to the condenser cooling water circuit then vacuum pumps are connected to the condenser until pressure of 1 mbar is reached.

- g. The evaporator is filled initially with 1000 mL of seawater and the chilled-water pump is switched on then the dry vacuum pumps are connected to the evaporator until evaporator pressure reaches the corresponding saturation pressure of the evaporator working temperature.
- h. At this stage initialization is completed and the cycling stage is ready to be started.

6.5.2 Cycling

- a. Switching is performed to precool the adsorber bed over a specific period of time before the adsorption process starts. Therefore, the solenoid valves on the cold water circuit (valves 2 and 4 on Figure 6-1) are opened while valves 1 and 3 are closed so the adsorber bed is cooled down while manual valves are still closed.
- b. Adsorption starts as the evaporator is connected to the adsorber bed by opening the manual valve in between. Seawater evaporates and water vapor flows to the adsorber bed leaving brine in the evaporator. The process continues for the predefined duration of the half cycle time and at the end, the manual valve is closed.
- c. Another switching process is performed to preheat the adsorber bed before desorption process starts with both manual valves closed while the automatic solenoid valves 1 and 3 are opened and valves 2 and 4 are closed.
- d. Desorption starts as the condenser is connected to the adsorber bed by opening the manual valve. Water vapor is desorbed and flows to the condenser where it condenses and fresh water is produced. The process continues for the specified half-cycle time and at the end the manual valve is closed.
- e. At this stage one complete cycle is done, so steps “a” to “d” are repeated for the required number of cycles.

6.5.3 Finalizing

- a. After the required number of cycles is performed, the readings collected by the data taker are stored in the computer.
- b. Water pumps of the adsorber bed and evaporator water circuits are switched off then all solenoid valves are closed.
- c. After ensuring that all water vapor is condensed in the condenser, the chiller is switched off.
- d. Vacuum is released from the evaporator and condenser then brine and fresh water are collected and measured.
- e. Specific daily water production (SDWP) is calculated from the equation;

$$SDWP (m^3 \cdot tonne^{-1} \cdot day^{-1}) = \frac{\text{Collected amount of water (Litre)} \times 60 \times 24}{\text{Adsorber mass (kg)} \times \text{No. of cycles} \times \text{Total cycle time (min)}}$$

Where: *Total cycle time = 2 x (half cycle time + switching time)*

6.6 Repeatability test

To ensure that all system components are working consistently, three tests were performed at three different days at the same operating conditions listed in Table 6-3. Figure 6-31 shows the temperature profile for adsorber bed, evaporator and condenser while Figure 6-32 shows the time variation of the adsorber bed, evaporator and condenser pressures. The system water and cooling production amounts were calculated for the three tests and their values as well as the standard deviation are listed in Table 6-4 which shows maximum standard deviation of 1.91.

Table 6-3, Operating parameters of repeatability test

Parameter	Value
Desorption temperature	95°C
Adsorption temperature	15°C
Evaporator chilled water inlet temperature	10°C
Condenser cooling water inlet temperature	10°C
Adsorber bed water flow rate	7.25 Litre/min
Chilled water flow rate	4 Litre/min
Condenser cooling water flow rate	5 Litre/min
Half cycle time	12 minutes
Switching time	1 minute
Adsorbent material	CPO-27Ni

Table 6-4, Water and cooling production of repeatability test

Parameter	Test 1	Test 2	Test 3	Standard deviation
Water SDWP (m ³ .tonne ⁻¹ .day ⁻¹)	6.77	6.86	6.81	0.045
Cooling SCP (W.kg ⁻¹)	190.33	193.49	190.05	1.91

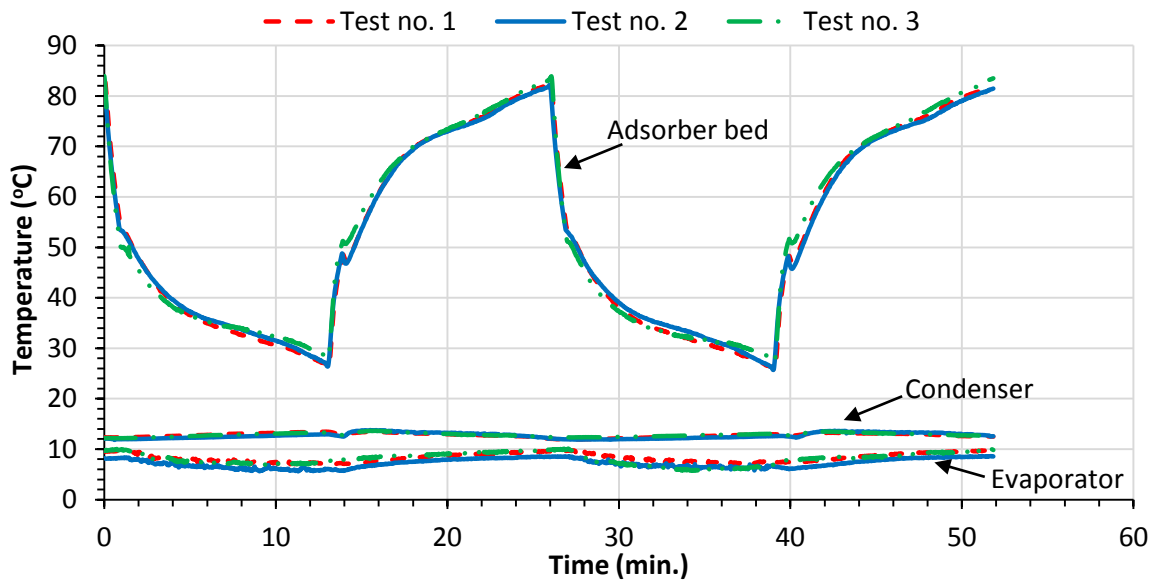


Figure 6-31, Adsorber bed, evaporator and condenser temperatures of repeatability test

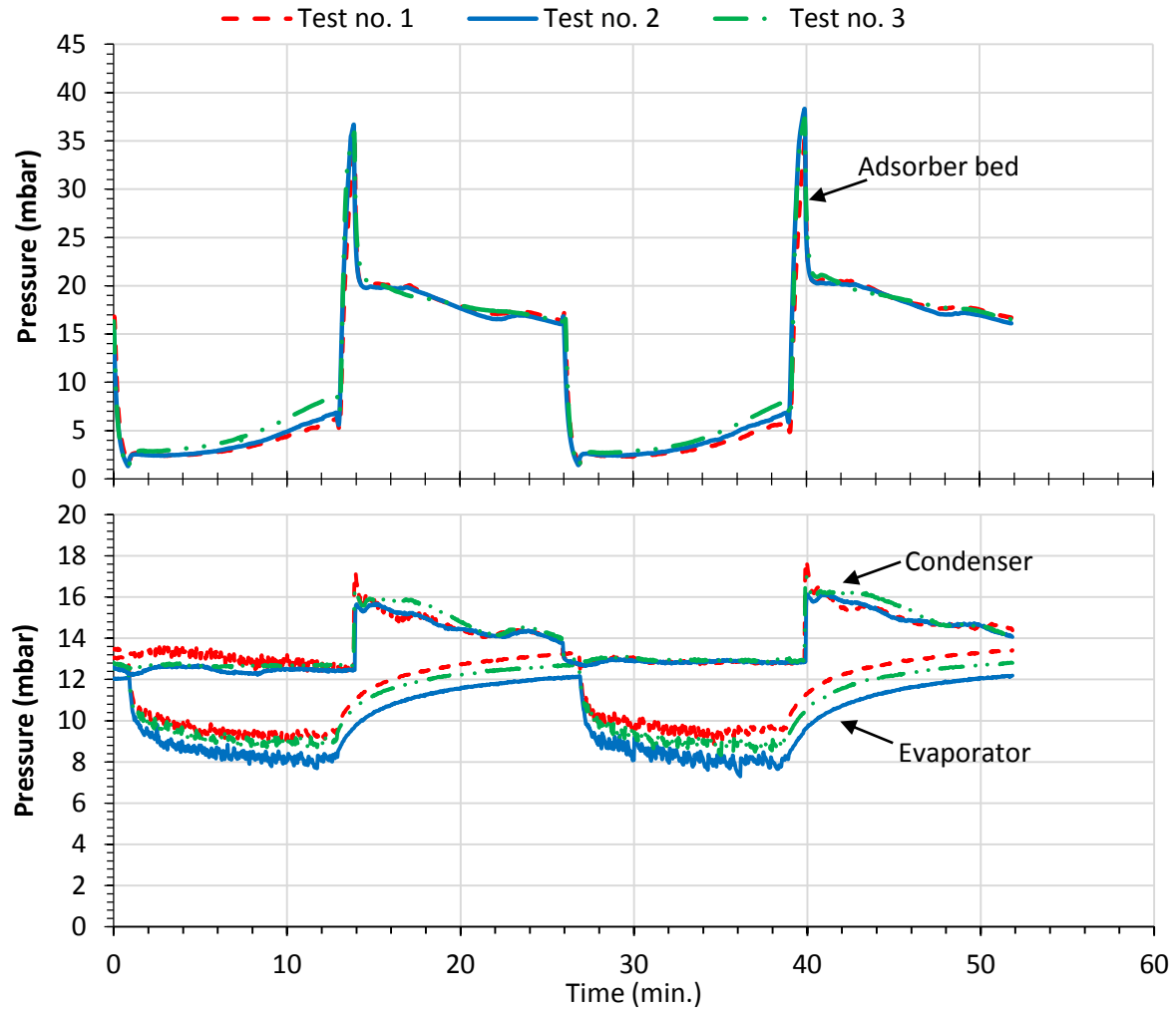


Figure 6-32, Adsorber bed, evaporator and condenser pressures of repeatability test

6.7 Validation of the Simulink model

Chapters 3 presented simulation model for adsorption desalination systems. In this section, validation for a 1-bed simulation model is performed via the obtained experimental results using CPO-27Ni as an adsorbent material. The operating conditions used in the test are the same as those of the repeatability test which are listed on Table 6-3. The validation is based on a comparison between temperature profiles of the adsorber bed, the evaporator and the condenser as well as specific daily water production and specific cooling power which are shown in Figure 6-33 and Figure 6-34, respectively [186]. Based on equation (3-41) and as

shown in Table 6-5 [186], the maximum instantaneous error between experimental and numerical results is within $\pm 8.3\%$ which reflects the validity of the developed simulation model.

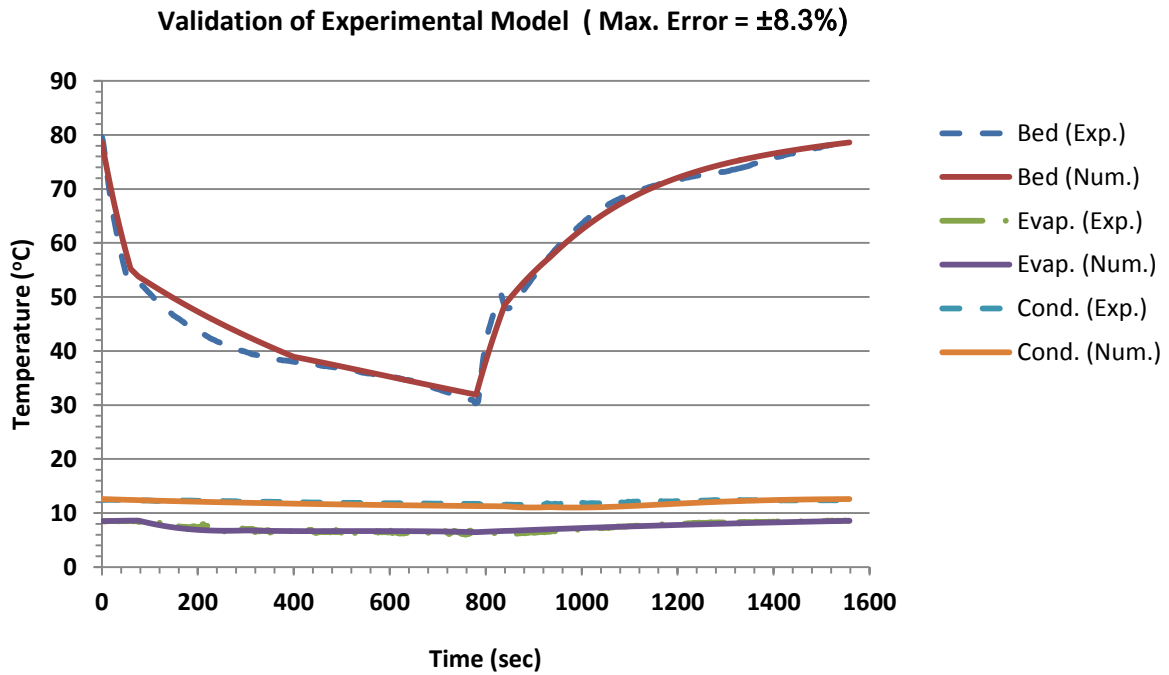


Figure 6-33, Validation of the single bed adsorption desalination Simulink model using CPO-27Ni, temperature profiles of adsorber bed, evaporator and condenser [186]

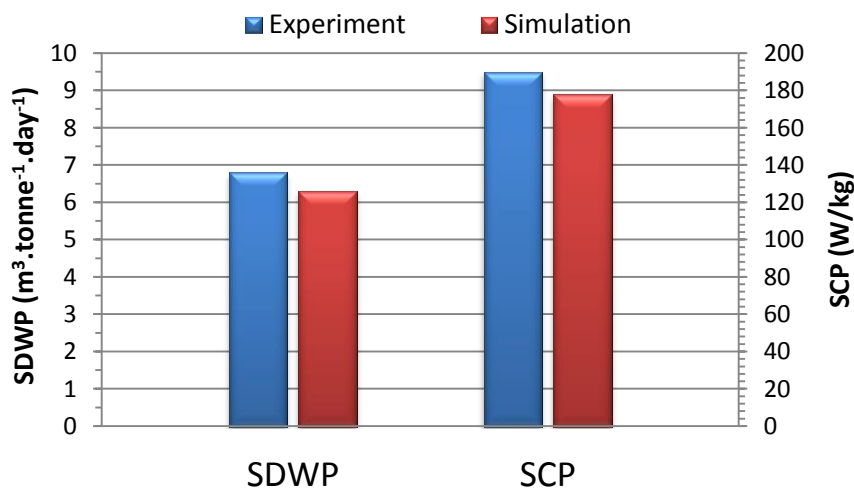


Figure 6-34, Comparison between experimental and simulation results of SDWP and SCP for CPO-27Ni [186]

Table 6-5, Error in the validation of the single bed adsorption desalination cycle using CPO-27Ni [186]

Parameter	Error
Adsorber bed	-8.3 to 7.6%
Condenser	-6.1 to 0.44%
Evaporator	-0.69 to 5.9%
Specific daily water production (SDWP)	7.3%
Specific cooling power (SCP)	6.3%

6.8 Experimental test results

As discussed in Chapter 4, the partial pressure ratio between adsorber bed and condenser affects the cycle performance. To investigate this effect, tests were carried out at partial pressure ratio in a range of 0.01 to 0.05, which corresponds to a condenser cooling water inlet temperatures of 5 to 30°C with a fixed adsorber bed desorption temperature of 95°C. Also switching and half cycle time's effect on system performance have been studied. All flowrates of cooling and heating water circuits are kept constant at those used in the repeatability test (see Table 6-3).

6.8.1 Effect of switching time

The time period when the adsorber bed is subjected to either cooling or heating while in the same time is isolated from both evaporator and the condenser is called the switching time [9, 186]. This delay is needed to allow for precooling or preheating of the adsorber bed which is necessary to achieve higher bed pressure than the condenser in the desorption process and to achieve lower bed pressure than the evaporator during the adsorption process. Five switching times have been investigated ranging from 1 to 5 minutes at half cycle time of 14

minutes and inlet water temperature of 10°C for both evaporator and condenser. As shown in Figure 6-35 [186], switching time is decreased by 1 minute every cycle starting from 5 minutes till it reached 1 minute after the fifth cycle. In the shown adsorber bed temperature profile, it is noticed that the switching time of 1 minute gives the smoothest temperature curve (highlighted by the two circles) which leads to the best utilization of cooling and heating energies supplied to the bed. Therefore, 1 minute switching time is the selected value for the next tests.

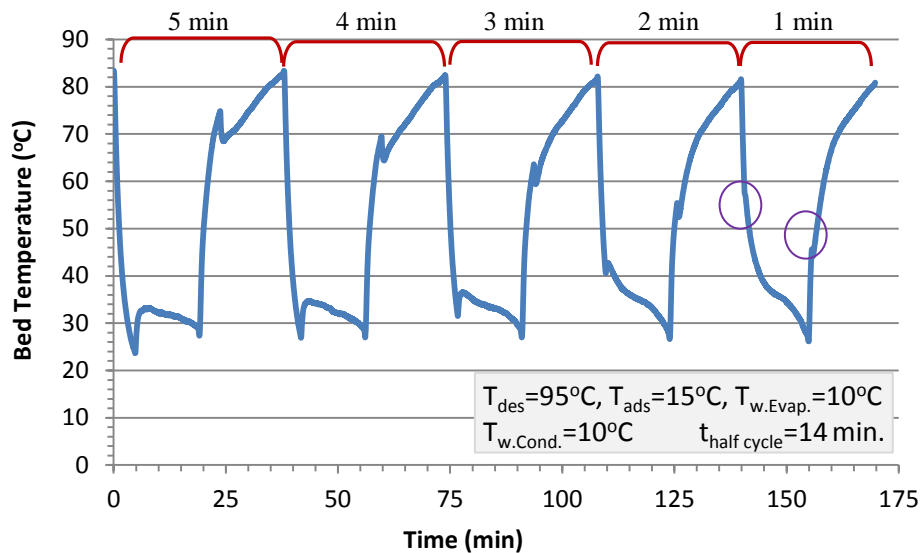


Figure 6-35, Temperature profile of adsorber bed through 5 consecutive cycles at various switching times [186]

6.8.2 Effect of half cycle time

As any adsorption cycle has two main processes; adsorption and desorption, the time period for each process is called half-cycle time when adsorber bed is connected either to the evaporator (adsorption process) or to the condenser (desorption process) [186]. The current test investigates the effect of half cycle times in the range of 8 to 18 minutes on SDWP and SCP as shown in Figure 6-36 and Figure 6-37 [186]. Although more water is collected at longer cycle times, as shown in Figure 6-36, the number of complete cycles per day decreases

which negatively affects the daily water production [186]. Therefore, the optimum half-cycle time is found to be 12 minutes which gives the highest SDWP of $6.8 \text{ m}^3 \cdot \text{tonne}^{-1} \cdot \text{day}^{-1}$ with 80 mL of fresh water collected per cycle. For the cooling production, as shown in Figure 6-37, it is obvious that SCP increases with shorter half cycle time which could be explained by the higher adsorption rate at the start of the adsorption process as the material pores are still not occupied by the water vapor. Therefore, lower average evaporator temperature could be observed at shorter cycle times [186]. In spite of the fact that 10 minutes is the best half cycle time for cooling production, 12 minutes is chosen to be the half cycle time for the next investigations as it resulted in the maximum amount of water which is the main focus of this research [186].

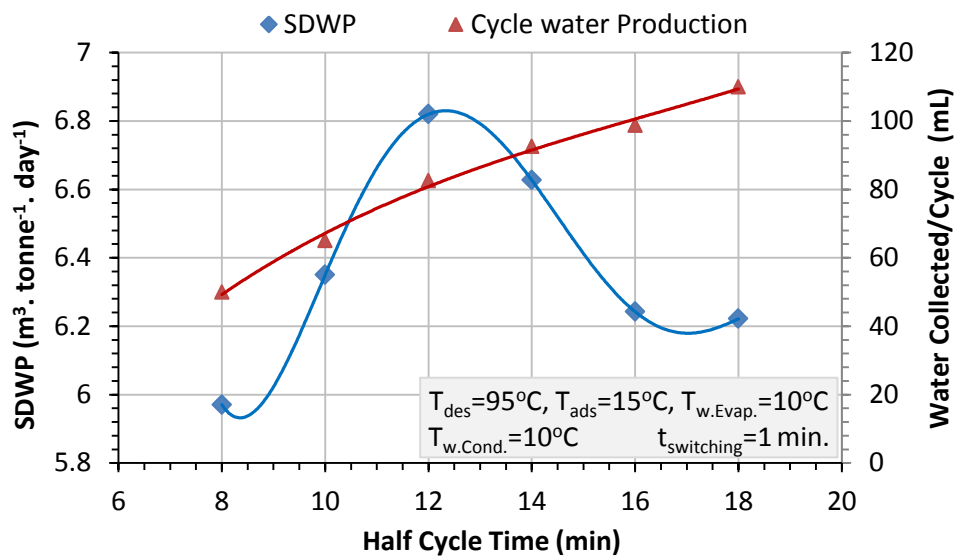


Figure 6-36, Specific daily water production and amount of water collected per cycle for various half cycle times [186]

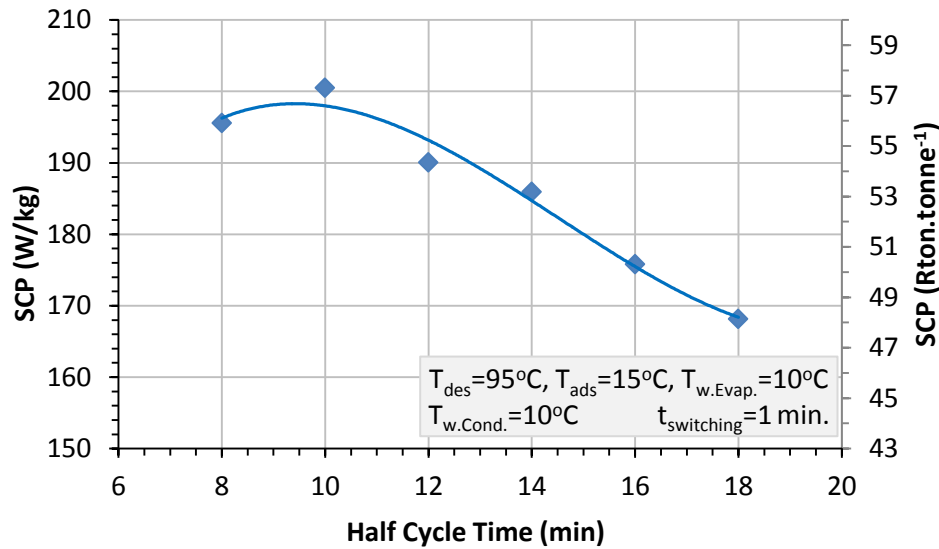


Figure 6-37, Specific cooling power⁴ for various half cycle times [186]

6.8.3 Effects of evaporator and condenser inlet water temperature

As adsorption desalination cycles are open loop systems where no refrigerant flows back from the condenser to evaporator [97], wide range of inlet water temperatures for evaporator (10-40°C) and condenser (5-30°C) are investigated with the condensing temperature is less than the evaporator temperature in some tests. As shown in Figure 6-38 and Figure 6-39 [186], increasing the condenser water inlet temperature has the same effect as decreasing the evaporator inlet water temperature resulting in less water production and cooling. The reason for that is the difference between the system's two partial pressure ratios, which depend on the condenser and evaporator operating temperatures. It is found that by decreasing the evaporator temperature from 40 to 10°C, water production decreases by 202% from 20.6 to 6.8 m³.tonne adsorbent⁻¹.day⁻¹ at condenser water inlet temperature of 10°C. Similarly, increasing the condenser water temperature from 5 to 30°C, decreases SDWP by 135% from 7.5 to 3.2 m³.tonne adsorbent⁻¹.day⁻¹ at evaporator water inlet temperature of 10°C.

⁴ SCP unit is either W.kg⁻¹ or Rton.tonne⁻¹ where "Rton" is the Ton of refrigeration defined as the amount of heat needed to melt 1000 kg of ice in 24 hours

The cooling effect produced by the cycle can be used for different applications depending on the evaporation temperature. For air conditioning applications where evaporation temperature of 10-20°C is required, the adsorption-desalination system can provide specific cooling capacity of 225 W.kg⁻¹. For process cooling where evaporation temperature of 40°C can be used, the adsorption desalination system can provide specific cooling power of 750 W.kg⁻¹.

As shown in Figure 6-40, the OCR has the same trend as SDWP and SCP where it increases by increasing the evaporator temperature and by decreasing the condenser temperature. It is noticed that OCR increases by 313% from 0.22 to 0.91 when evaporator inlet water temperature increases from 10 to 40°C at constant condenser temperature of 30°C. On the other hand it is found that this system can operate at a maximum OCR of 1.89 at the maximum evaporator inlet water temperature of 40°C and at the lowest condenser water inlet temperature of 5°C.

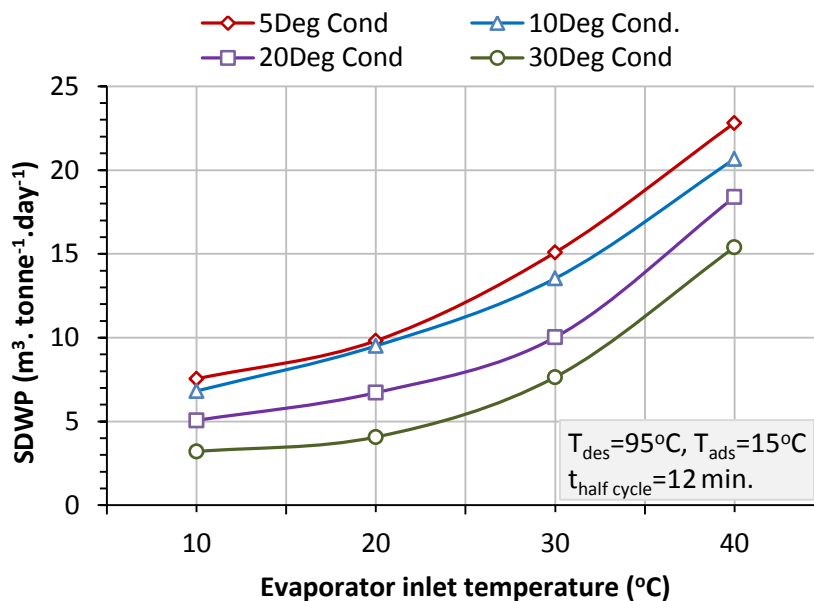


Figure 6-38, Specific daily water production at various evaporator and condenser water inlet temperatures [186]

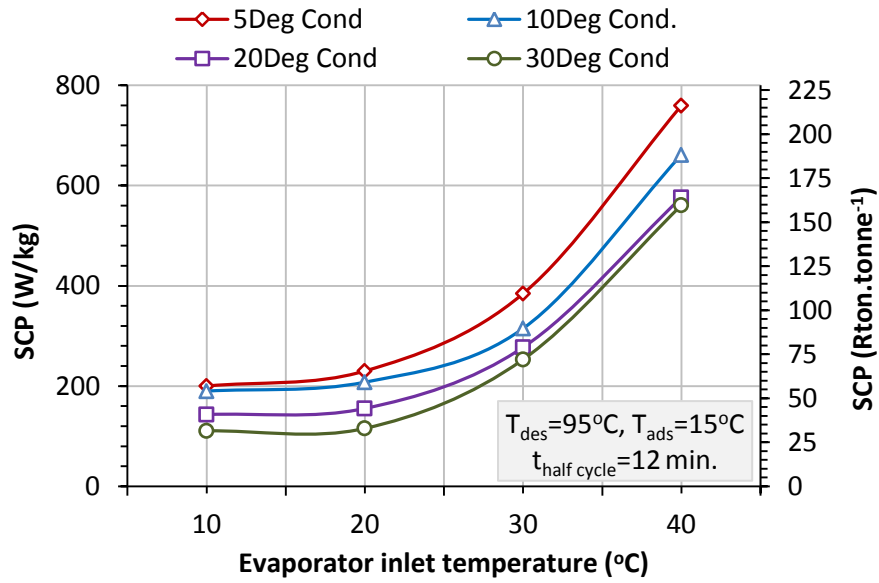


Figure 6-39, Specific cooling power for various evaporator and condenser water inlet temperatures [186]

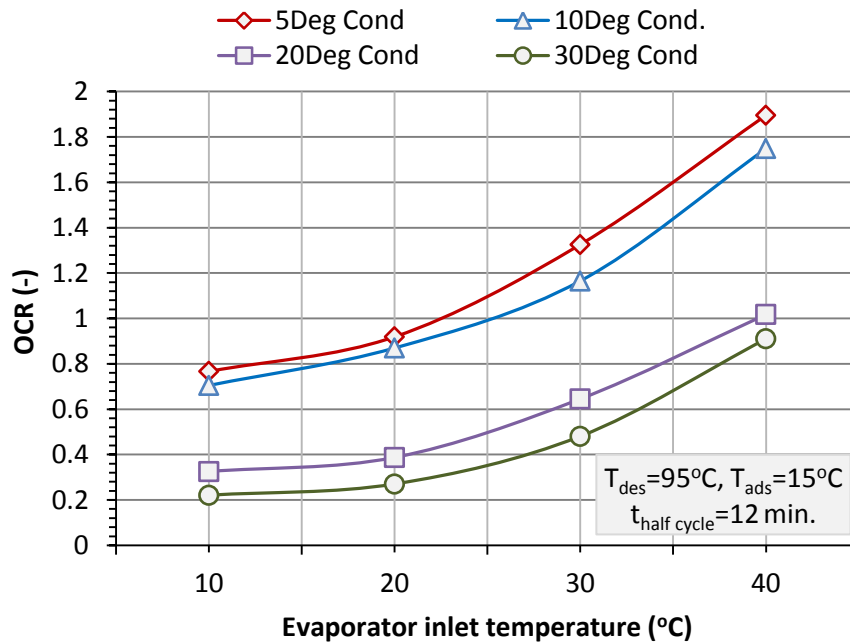


Figure 6-40, Overall conversion ratio of Single-bed system at various evaporator and condenser water inlet temperatures

Figure 6-41 [186], shows the temperature profile of the adsorber bed, evaporator and condenser at 10°C evaporator water inlet temperature with two condensing temperatures, 5°C and 30°C, which are denoted by (L) and (H) respectively. At lower condenser temperature, higher uptakes are achieved thus greater amount of heat is generated and absorbed during adsorption and desorption processes respectively [186]. Therefore, as shown in Figure 6-41 (a), temperature of point “1” cannot reach 22.8°C as point “2” similarly, point “3” cannot be heated up to 84.9°C like point “4”. For the evaporator temperature profile, shown in Figure 6-41(b), the hatched area shows the extra cooling achieved when lowering condenser temperature. Finally, Figure 6-41(c), presents how area “B” is bigger than area “A”, which indicates more water vapor condensation (i.e. production) in the case of low condensing temperature.

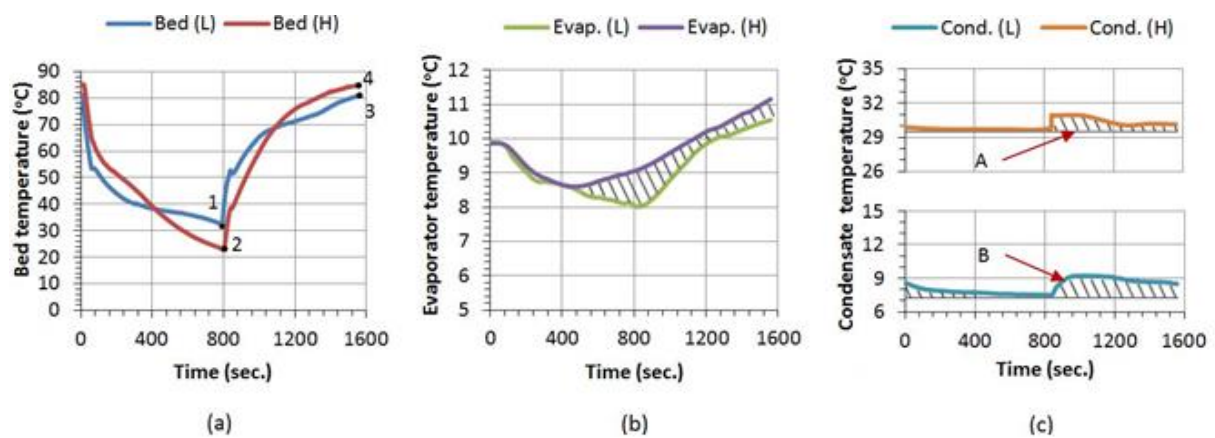


Figure 6-41, Temperature profiles of Adsorber bed (a), Evaporator (b) and Condenser (c) at condenser water inlet temperatures of 5°C (L) and 30°C (H) with an accuracy of $\pm 0.3^{\circ}\text{C}$

[186]

6.9 Summary

In this chapter, the single bed system has been described in detail with all its main components: adsorber bed, evaporator and condenser as well as the secondary systems such as chilled water reservoir, water chiller, cold water and hot water tanks in addition to all measuring and control devices. Vacuum leakage detecting techniques have been presented alongside with the test rig commissioning. Testing procedure has been explained with its three operating stages; initialization, cycling and finalizing. Repeatability tests were carried out and results showed that the system operates consistently. CPO-27Ni was the tested MOF adsorbent material at different operating conditions including evaporator and condenser inlet water temperatures. It was concluded that lower condensing temperatures improves cycle performance where maximum specific daily water production and specific cooling power of $22.8 \text{ m}^3.\text{tonne}^{-1}.\text{day}^{-1}$ and 759.6 W/kg were achieved. Moreover, the modelling technique developed in chapter 3 has been validated using the experimental results of CPO-27Ni with a deviation less than $\pm 8.3\%$ [186].

CHAPTER 7: EXPERIMENTAL INVESTIGATION OF DOUBLE BED ADSORPTION SYSTEM USING MOF MATERIALS

7.1 Introduction

This chapter presents the construction, commissioning and operation of a more advanced double-bed adsorption desalination system for continuous production of water and cooling. The performance of CPO-27Ni is first investigated then compared to that obtained using the single bed system. Also the performance of another MOF adsorbent called Aluminium Fumarate is studied at different heating and evaporator temperatures. In addition, effects of seawater salinity level and mass recovery times are also studied.

7.2 Test facility description

This adsorption desalination system consists of two adsorber beds, evaporator and condenser as presented schematically in Figure 7-1 and visually in Figure 7-2. Each adsorber bed is fitted with four parallel finned tube heat exchangers packed with a maximum capacity of 3 kg of adsorbent material per adsorber bed when the four heat exchangers are connected. Evaporator and condenser consist of stainless-steel dished chambers with an acrylic lid and copper coil inside to allow for the heat transfer between the adsorbate and the flowing water inside the coil tube. Five electrically actuated ball valves are used on the vacuumed water vapor lines to control water vapor flow from evaporator to adsorber bed, desorber bed to condenser and desorber bed to adsorber bed during mass recovery. Two water pumps are used to supply hot and cold water for the desorber and adsorber beds

respectively while eight electrically actuated ball valves are used to control the flow of the water streams to and from the adsorbing beds. Hot, cold and chilled water tanks are the same ones used in the single bed system as well as the chiller connected to the condenser. Eight ports brass manifold is used to connect the vacuum pump to adsorber beds, evaporator, condenser, freshwater / brine accumulator and finally a vacuum relief port with all ports equipped with a manual shut off ball valve. The next section will describe in more detail each component in the system as well as the measuring and controlling instruments used all over the system.

7.2.1 Adsorber bed

The adsorber bed is the prime mover of the adsorption system as it adsorbs the water vapor from the evaporator and desorbs it back to the condenser where fresh water is collected. It consists of a cylindrical steel shell topped with a lid and an O-ring in between to ensure vacuum sealing with four KF ports welded into the side wall to allow for water vapour, pressure transducer and thermocouple connections as in Figure 7-3. This system has two identical adsorber beds; each one is capable of having four finned tube heat exchangers to be connected in parallel as shown in Figure 7-4. Each heat exchanger has six tubes connected together via supply and return headers and its characteristics and dimensions are listed in Table 7-1. Supply and return headers are attached to the lower side of the top plate via a $\frac{3}{4}$ " brass Swagelok male connector while the upper side of the plate is connected to the water supply and return pipes via 22mm x $\frac{3}{4}$ " BSPP male iron coupler Boss compression fitting.

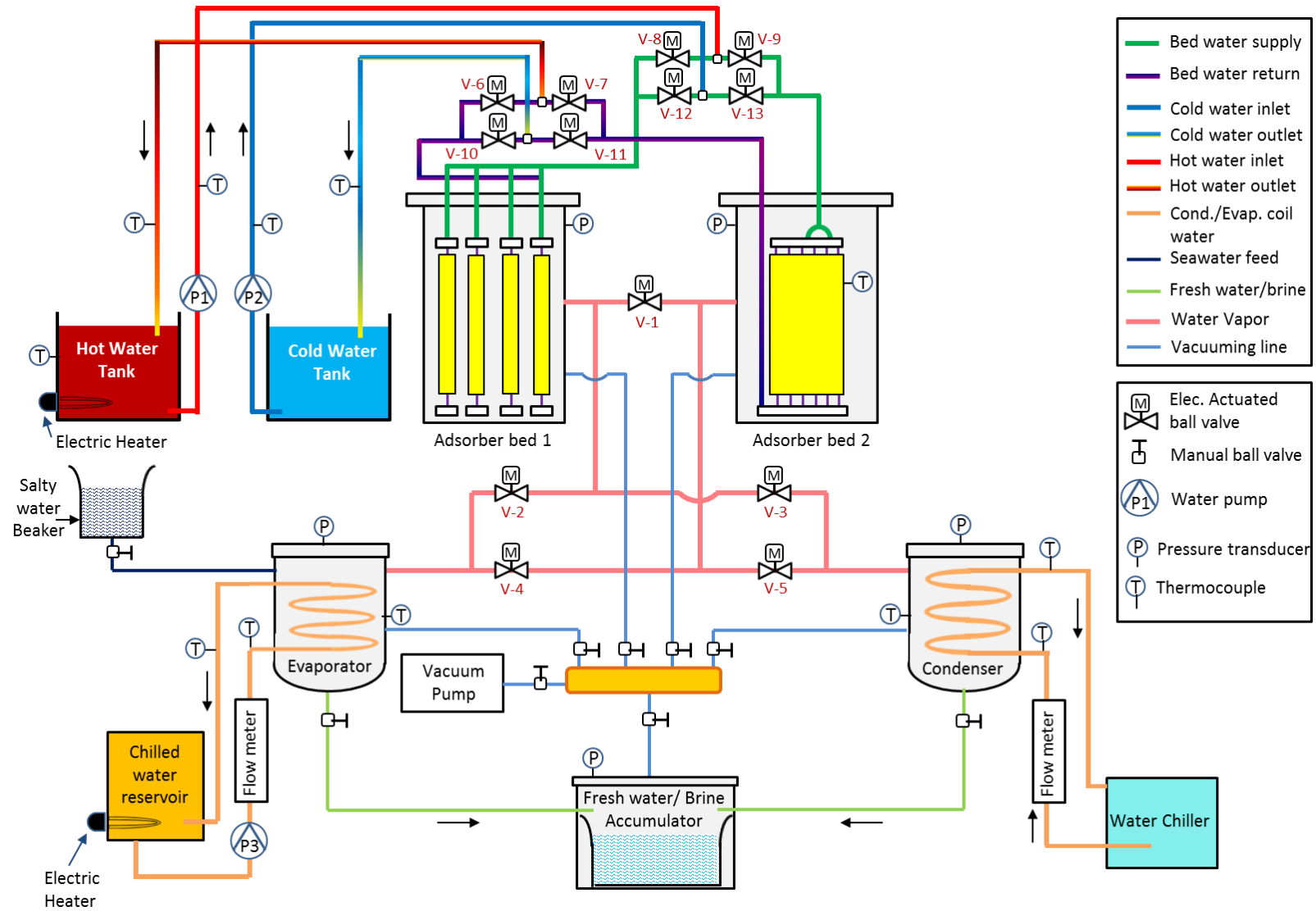


Figure 7-1, Schematic of the double-bed adsorption system



Figure 7-2, Testing facility of the double-bed adsorption system

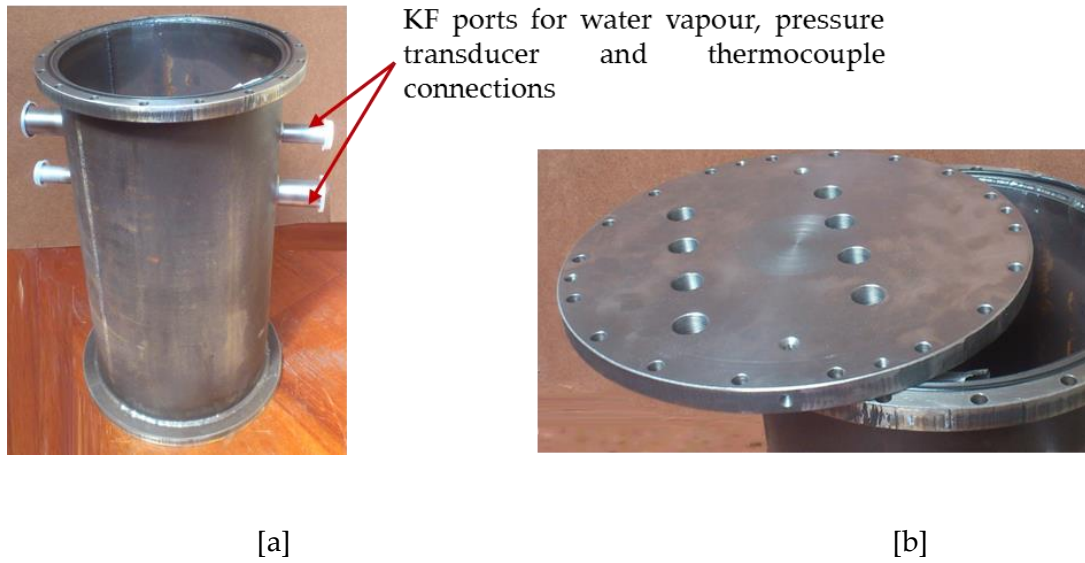


Figure 7-3, Adsorber bed; (a) Cylinder, (b) Top plate

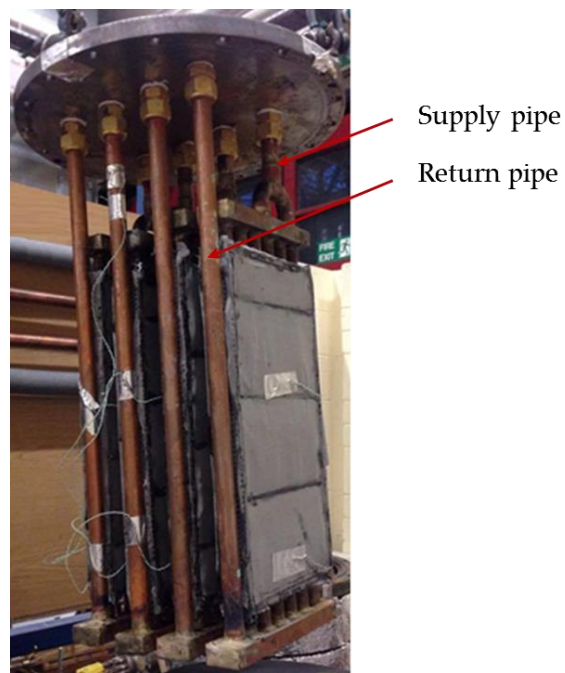


Figure 7-4, Finned tube heat exchangers of the adsorber bed

Table 7-1, Heat exchanger characteristics and dimensions (double-bed system)

Parameter	Value
Heat exchanger length	370 mm
Fin width	173 mm
Fin height	30 mm
Fin pitch	1.016 mm
Fin thickness	0.105 mm
Tube outer diameter	15.875 mm
Tube thickness	0.8 mm
Number of fins in one heat exchanger	364
Amount of Aluminium Fumarate packed in one heat exchanger	0.5 kg

7.2.2 Evaporator

As the evaporator is the component where seawater is fed into, the evaporator in this system consists of a copper coil and a custom made 26 litre corrosion resistant stainless-steel vacuum chamber manufactured by “Applied Vacuum Engineering” with an Acrylic lid that sits on a gasket for vacuum sealing. The vacuum chamber has a dished base to allow for brine collection in addition to the KF flanged vacuum connections and threaded sockets for the pressure transducer, thermocouples, chilled water coil, vacuum pump and water vapour ports as in Figure 7-5. The chilled water coil is made of 10 m long and 8mm OD copper tube in a helical form at two levels as shown in Figure 7-6. For seawater feed, an opened-top, graduated beaker is connected to the evaporator through 8 mm OD flexible tube to allow for seawater feeding during system operation and is controlled via manual ball valve as shown in Figure 7-7. Inside the evaporator, seawater flows inside a 6mm stainless steel tube that ends with a stainless steel nozzle to spray the water on the evaporator coil as shown in Figure 7-8. The spraying nozzle is a full cone nozzle manufactured by “Bete Limited” with a

part number of “MPL 0.42W” and is capable of working at low pressure of 0.7 bars, feeding 0.88 l/min of water and has a maximum spraying angle of 128°. Feeding of seawater relies on the pressure difference of pressure where the seawater in the graduated cylinder is at atmospheric pressure and the evaporator pressure is below atmospheric. Therefore, when seawater feeding is needed, the manual valve is opened and the seawater will be pressure forced to flow to the evaporator.

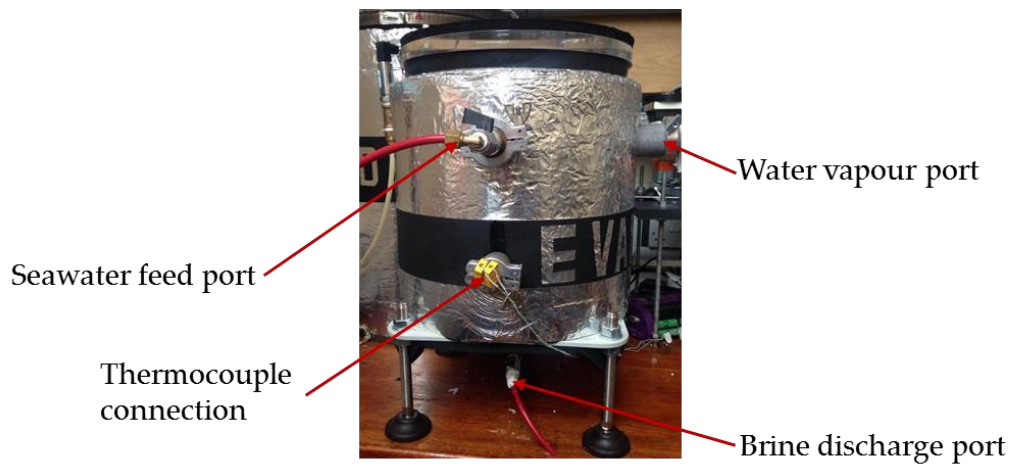


Figure 7-5, Pictorial view for the evaporator of the double bed system with different connecting ports



Top view



Side view

Figure 7-6, Pictorial view of the evaporator chilled water helical copper coil

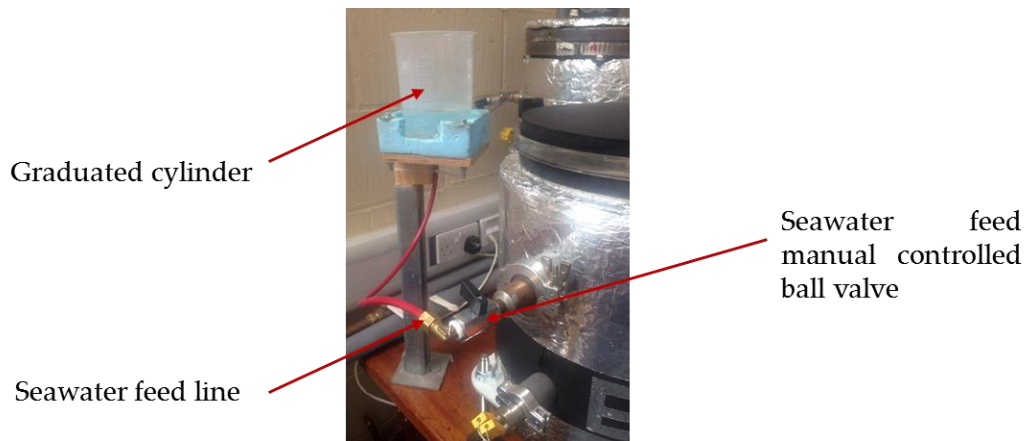


Figure 7-7, Seawater feed system

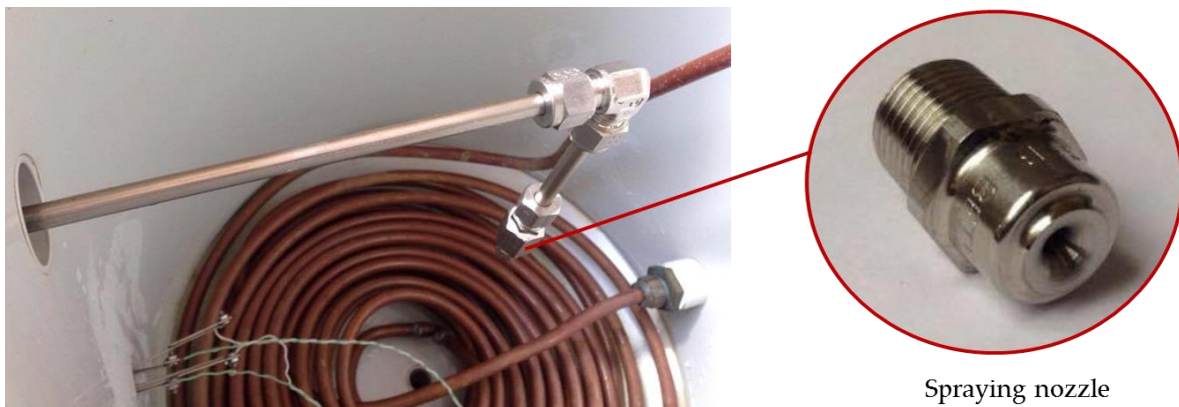


Figure 7-8, Seawater spraying nozzle in the evaporator

7.2.3 Condenser

The condenser shell in this system is identical to the evaporator as shown in Figure 7-9 and it is also made from stainless-steel to ensure cleanliness of the collected freshwater. The cooling coil is made of 10m long and 8mm OD copper coil formed in spiral cones as shown in Figure 7-10 to enhance condensation heat transfer through reducing of condensate liquid falling from upper tubes onto lower ones [189].

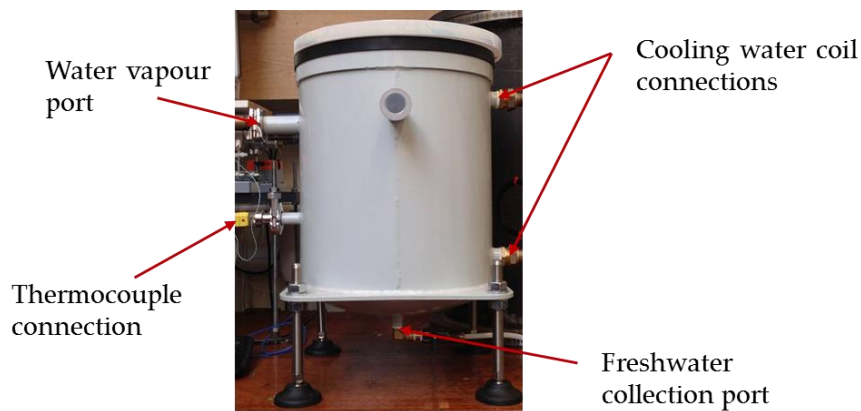


Figure 7-9, Pictorial view for the condenser of the double bed system with different connecting ports



Top view



Side view

Figure 7-10, Pictorial view of the condenser spiral conical copper coil

7.2.4 Freshwater/brine accumulator

One of the advantages of this system is its ability to operate continuously because of the presence of the freshwater/brine accumulator. This accumulator is designed to collect both high salinity brine and freshwater from evaporator and condenser respectively. Figure 7-11, shows the vacuum pump hose connected to the top lid of the accumulator and the delivery hoses of freshwater and brine are connected to the side wall ports. To start the collection process, vacuum pump is connected to the accumulator until its pressure becomes lower than the evaporator pressure (in case of brine collection) or lower than the condenser pressure (in case of freshwater collection) and then the corresponding ball valve connected to the evaporator or condenser dished base is opened. Due to the difference in pressure, water flows and accumulates in the designated internal bucket in the accumulator. After that, all valves are closed and vacuum pump is switched off then the accumulator pressure is allowed to reach the atmospheric pressure then lid is opened and the collected freshwater or brine is removed from the internal bucket.



Figure 7-11, Freshwater/brine accumulator

7.2.5 Water pumps

Two identical pumps are used in the system for cold and hot water circulation in adsorber and desorber beds respectively. As shown in Figure 7-12, the pump is a horizontal multi-stage close coupled and made of stainless steel. This pump is manufactured by “Calpeda” with the model number of “MXHM203E” which is capable of delivering wide range of water flow rates (0-70L/min) at head range of (0-33mH₂O) alongside a maximum operating temperature of 110°C.



Figure 7-12, Adsorber and desorber bed water pumps

7.2.6 Flow control valves

In this system three types of control valves exist, manual ball valves for system vacuuming circuit, electrically-actuated ball valve for bed heating/cooling water circuit and electrically-actuated manual ball valve for water vapor circuit.

For system initialisation eight manually-operated vacuum-proof ball valves are used to connect adsorber beds, evaporator, condenser and freshwater/brine discharge accumulator to the vacuum pump through a manifold as show in Figure 7-13. The valve is a ¼ turn vacuum valve manufactured by “easy composites”.



Figure 7-13, Manual ball valves connected to the manifold

Figure 7-14 shows the valve used in the control of the adsorber bed water circuit with the part number of “ABVM08S-2AR”. It is a 220VAC, two-way, normally closed actuated ball valve with a maximum closing/opening time of 5 seconds and can withstand a maximum temperature of 100°C for the flowing fluid. In this circuit, eight valves are used to regulate the flow of supply and return lines for both cold and hot water to the adsorber and desorber beds respectively.



Figure 7-14, Electrically-actuated ball valve for bed heating/cooling water circuit

To control the flow of water vapor between adsorber beds, evaporator and condenser, manual ball valves similar to those used in the 1-bed system shown in Figure 6-13, are used. As five valves are required to operate the double-bed system, these valves were fitted with electric actuators to operate them automatically as shown in Figure 7-15. The electric actuator, manufactured by “BELIMO” with a part number of “NMQ24A”, operates using 24V AC/DC with a maximum opening/closing time of 4 seconds and a maximum torque of 8 Nm.

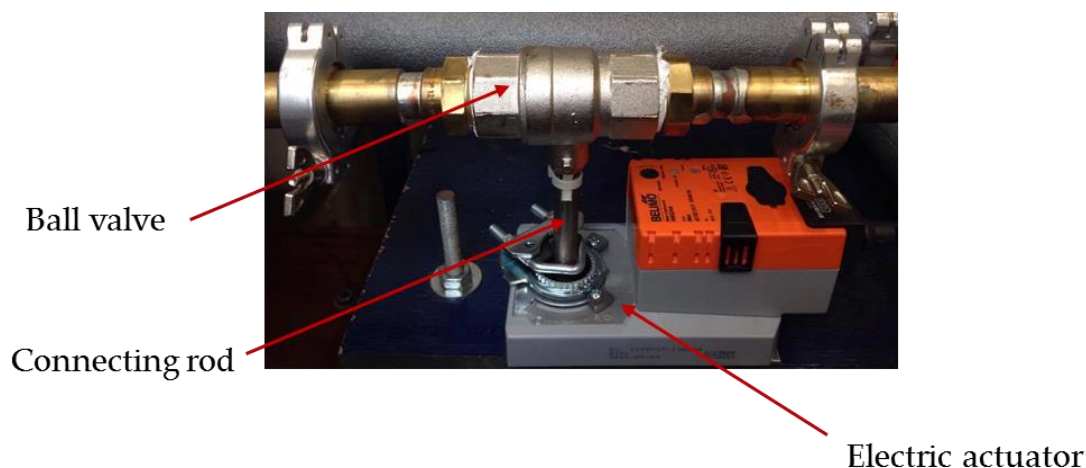


Figure 7-15, Electrically-actuated manual ball valve for water vapor circuit

These set of automated valves are controlled via “Labview” with the aid of a control board manufactured by “National Instruments” where two 4-channel relay modules, “NI-9482”, are connected to the computer through a 4-slot chassis, “cDAQ-9174” as shown in Figure 7-16. The programmed “Labview” software is designed to control the system automatically in seven sequential steps which are; “Drying”, “First half cycle Switching”, “Adsorption-Desorption”, “Mass recovery (1st half cycle)”, “Second half cycle Switching”, “

Desorption-Adsorption” and “Mass recovery (2nd half cycle)” as in Table 7-2. As shown in Figure 7-17, the inputs to this Labview code are half cycle, mass recovery and switching times in addition to number of operating cycles before system shutdown. More details on this code are presented in Appendix III.



Figure 7-16, National Instruments chassis and relay control board

Table 7-2, Automated valves On/Off schedule during system operation

Valve* Stage	V-1	V-2	V-3	V-4	V-5	V-6	V-7	V-8	V-9	V-10	V-11	V-12	V-13
Drying	X	X	X	X	X	O	O	O	O	X	X	X	X
1 st half cycle switching	X	X	X	X	X	X	O	X	O	O	X	O	X
Adsorption-Desorption	X	O	X	X	O	X	O	X	O	O	X	O	X
Mass Rec. (1 st cycle)	O	X	X	X	X	X	O	X	O	O	X	O	X
2 nd half cycle switching	X	X	X	X	X	O	X	O	X	X	O	X	O
Desorption-Adsorption	X	X	O	O	X	O	X	O	X	X	O	X	O
Mass Rec. (2 nd cycle)	O	X	X	X	X	O	X	O	X	X	O	X	O

*Valve numbers are show in the system schematic diagram, Figure 7-1.

O: denotes opened valve

X: denotes closed valve



Figure 7-17, User interface of the “Labview” software to control the actuated ball valves

7.2.7 Vacuum pump

Only one vacuum pump is used in this system for all vacuuming tasks as it is connected to any of the system components through the distribution manifold. It is an oil-lubricated rotary vane vacuum pump, Figure 7-18, manufactured by “DVP” with a model number of “LC.106” and has a capacity of 106 m³/h with a final pressure of 0.1 mbar.

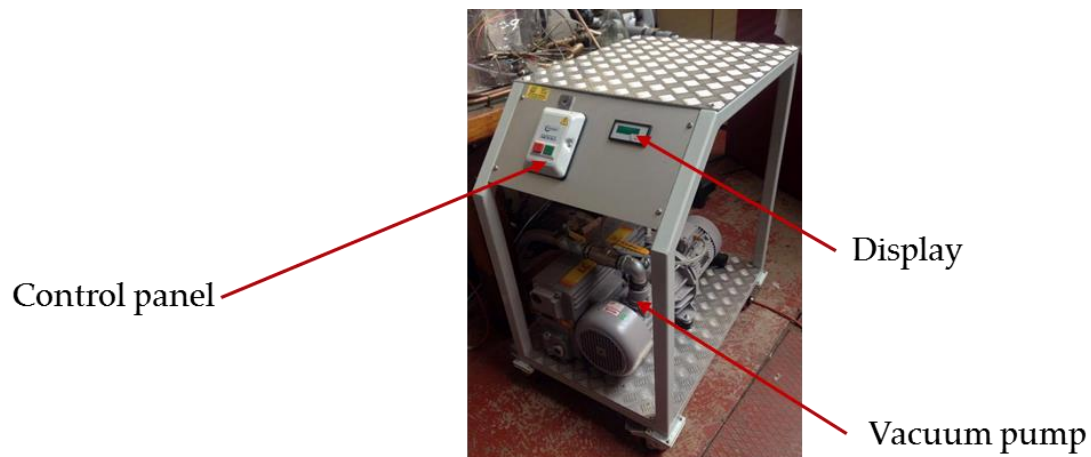


Figure 7-18, "DVP" Vacuum pump

7.3 Measuring devices

As discussed in chapter 6, measurements of pressure, temperature and flow rate are performed in the adsorption desalination system to evaluate its water production and cooling performance. In this two bed system, identical measuring devices were used for flow rate, pressure and temperature measurements.

As the condenser and evaporator of this system are made of stainless steel, seawater were used in the operation and hence salinity sensor was used to measure salinity of the feed seawater and the salinity of the produced fresh water. A hand held salinity sensor manufactured by "OMEGA" with the part number of "CDH-45", Figure 7-19, was used to measure the salinity with a capability to measure maximum salinity of 100,000 ppm at an accuracy of ± 1000 ppm.



Figure 7-19, Salinity sensor, “CDH-45”

7.4 Test rig commissioning

The system was assembled as shown schematically in Figure 7-1 and pictorially in Figure 7-2 with all pressure transducers and thermocouples fitted and connected to the data logging equipment as well as all electrically actuated valves were connected to their control board. Leakage tests were performed for each system component including adsorber beds, evaporator, condenser, vacuumed water vapor pipes and circulating water pipes as discussed earlier in chapter 6, section 6.4. Finally, all electrically actuated valves are tested for operation via “Labview” as well as hot water tank electric heater and the temperature controller chiller.

7.5 Testing procedure

In this double-bed adsorption system, there are three stages for system operation as firstly the system is initialised by drying the beds then cyclic operation starts which include six consequent processes and the last stage is system stopping, shutting down and collecting the data. Further details for each stage are given below.

7.5.1 Initialization

- a. At the beginning, the data logging instruments are connected to the PC and their software's started to measure temperatures and pressures of the system components.
- b. Hot and cold water tanks are filled with water and the thermostat of the heater is set to the needed operating desorption temperature and also, the seawater feed beaker is filled with 1000 ml of salty water.
- c. The "Labview" code of the double-bed adsorption system is started and the required data are inputted including half cycle, switching and mass recovery times in addition to required number of complete cycles.
- d. Hot circulating water pump is switched on then the run icon in "Labview", code is clicked to start the drying process where valves "V-6, V-7, V-8 and V-9" (see Figure 7-1) open to allow for hot water circulation onto both adsorber beds.
- e. Vacuum pump is switched on and connected to both adsorber beds by opening their corresponding manual ball valves connected to the manifold until beds pressure reach a value of about 8 mbar at a temperature of 85°C.
- f. When the required vacuum level is reached in the adsorber beds, manual ball valves are shut off and vacuum pump is then connected to both evaporator and condenser, again by opening their corresponding manual ball valves. At the same time, the water circulation of evaporator chilled water and condenser cooling water start after selecting the desired operating temperature.
- g. When vacuum level in the evaporator and condenser reach 1 mbar, all manual ball valves are shut off and vacuum pumps are then switched off. At this point, the whole system is at vacuum and each system component has the required operating

temperature. From experience it was noticed that as long as 1 mbar is maintained the results are repeatable and consistent.

- h. Now seawater feeding is ready to start so the manual ball valve is opened to allow for 500 ml of seawater to enter the evaporator.
- i. Cold circulating water pump is switched on so it is ready to deliver cold water to the adsorber bed but as the actuated valve is still closed, no cold water enters the adsorber bed.
- j. At this stage, system is ready to start operation in a cyclic manner through switching, adsorption/desorption and mass recovery phases.

7.5.2 Cycling

- a. To begin system operation, start icon in "Labview" code is clicked to start the 1st half cycle switching mode by opening valves "V-10 and V-12" and closing valves "V-6 and V-8". At this time, "bed-1" is cooled for adsorption phase preparation while "bed-2" is heated for desorption phase preparation.
- b. When switching time is completed, valves "V-2 and V-5" open automatically to allow for "Adsorption/Desorption" (bed-1 connected to evaporator and bed-2 connected to condenser) which continues until half cycle time elapses.
- c. After completion of the "Adsorption/Desorption" phase, valves "V-2 and V-5" close and valve "V-1" opens to start the mass recovery phase. At this stage, pressure equalization between the two adsorber beds is performed and any residual water vapor in the desorber bed moves to the lower pressure adsorber bed.
- d. The first half cycle is now finished and the second half cycle is ready to start with the 2nd half cycle switching phase. Therefore, valves "V-1, V-2, V-3, V-4, V-5, V-7, V-9, V-

10, V-12" are closed and valves "V-6, V-8, V-11, V-13" are opened. By doing that, "bed-1" is now heated for desorption phase preparation and "bed-2" is cooled for adsorption phase preparation.

- e. After the switching time completion, valves "V-3 and V-4" open for the "Desorption/Adsorption" process to start, where (bed-1 is connected to condenser and bed-2 is connected to evaporator) until the half cycle time is elapsed.
- f. Finally, mass recovery of the 2nd half cycle is performed by closing valves "V-3 and V-4" and opening "V-1".
- g. Now a one complete cycle is reached and any number of cycles could be carried out as desired where seawater can be fed during operation when necessary as in "Initialization, stage h". Also, fresh water and brine collection could be performed during operation as explained under section 7.2.4. Therefore, as long as the number of desired completed cycles is not reached, system will continue operation otherwise stop icon in "Labview" is clicked.

7.5.3 Finalizing

- a. When system stops, all actuated valves close automatically and then all pumps has to be switched off.
- b. All measured data, collected by the data taker is uploaded and stored into the PC.
- c. Chiller is switched off and all manual water valves are closed.
- d. The procedure explained at section 7.2.4 is performed to collect any remaining brine or freshwater at evaporator or condenser respectively.
- e. The total amount of fresh water collected is measured then the specific daily water production is calculated using the following equation;

$$\text{SDWP (m}^3 \cdot \text{tonne}^{-1} \cdot \text{day}^{-1}) = \frac{\text{Collected amount of water (Litre)} \times 60 \times 24}{\text{Adsorber mass (kg)} \times \text{No. of cycles} \times \text{Total cycle time (min)}} \quad (7-1)$$

Where:

$$\text{Total cycle time} = 2 \times (\text{half cycle time} + \text{switching time} + \text{mass recovery time}) \quad (7-2)$$

7.6 Double bed system compared to single bed system

To assess firstly the consistency of both the single-bed and double-bed adsorption systems' results and secondly the effect of the advanced double bed system design on the performance of CPO-27Ni, the double-bed system has been packed with CPO-27Ni and operated at similar operating conditions like the single bed system and the results were compared. Table 7-3 lists the operating conditions of the tests while SDWP and SCP are shown in Figure 7-20 and Figure 7-21 respectively.

Table 7-3, Operating conditions of the CPO-27Ni test on double bed system

Parameter	Value
Desorption temperature	95°C
Adsorption temperature	19°C
Evaporator chilled water inlet temperature	10-30°C
Condenser cooling water inlet temperature	10-30°C
Adsorber bed water flow rate	11 Litre/min
Chilled water flow rate	3 Litre/min
Condenser cooling water flow rate	5 Litre/min
Half cycle time	12 minutes
Switching time	1 minute
Adsorbent material	CPO-27Ni

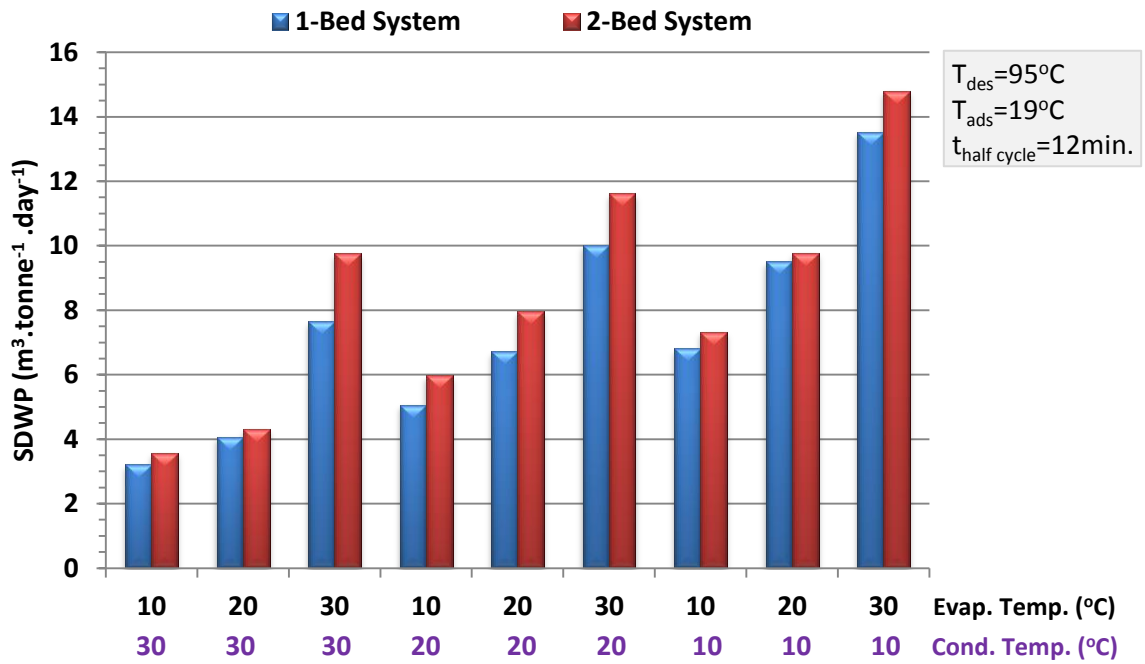


Figure 7-20, Comparison of specific daily water production for Single and Double bed adsorption systems using (CPO-27Ni)

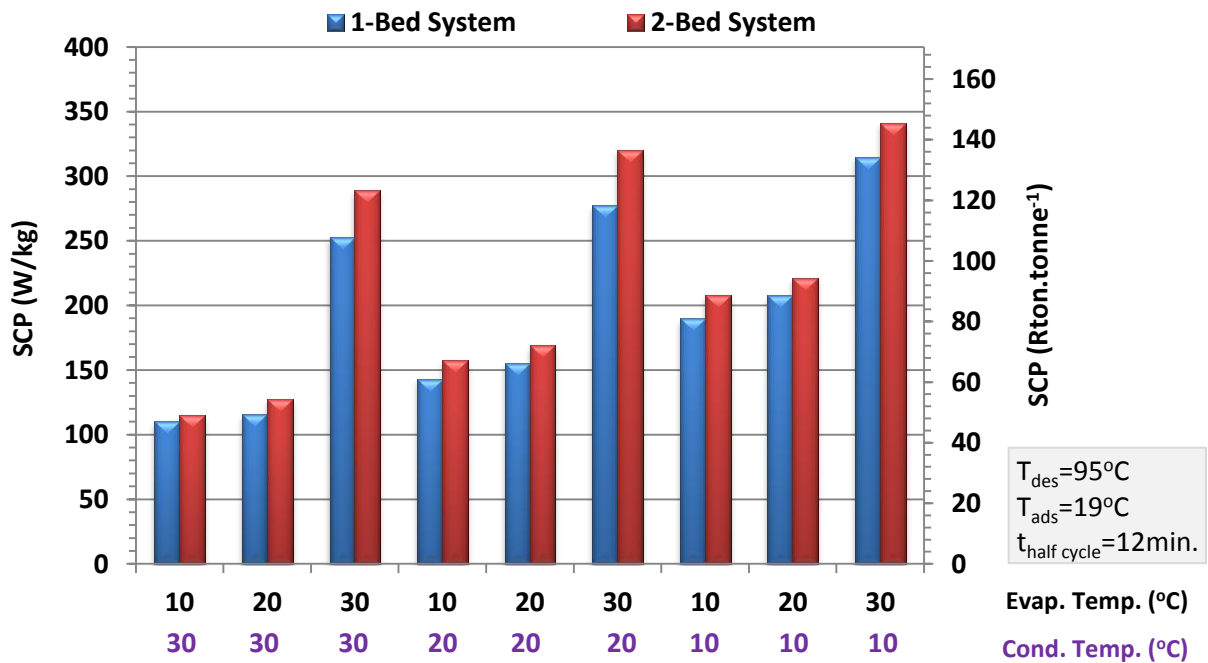


Figure 7-21, Comparison of specific cooling power⁵ for Single and Double bed adsorption systems using (CPO-27Ni)

⁵ SCP unit is either W.kg⁻¹ or Rton.tonne⁻¹ where “Rton” is the Ton of refrigeration defined as the amount of heat needed to melt 1000 kg of ice in 24 hours.

The results show that the double bed system performance is consistently higher than that of the single bed system where the water production is increased by 3-27% and specific cooling power is increased by 4-15%. This improvement in performance could be attributed to the increased heat transfer coefficient in evaporator due to the use of spraying nozzle in the evaporator in addition to the enhanced adsorber bed water feeding system design which ensure same water feed temperature to each heat exchanger module because of the parallel water feed configuration.

7.7 Experimental test results

The double bed adsorption system has been tested to investigate the effects of half cycle time, mass recovery time, desorption temperature, evaporator temperature and seawater salinity on cycle water and cooling production. Aluminium Fumarate is the adsorbent material used in this system, where a total of 2 kg were packed in the two adsorber beds. The operating conditions tested in this parametric study are listed in Table 7-4.

Table 7-4, Operating conditions of the double bed system parametric study

Parameter	Value
Adsorption temperature	19°C
Condenser cooling water inlet temperature	30°C
Adsorber bed water flow rate	11 Litre/min
Chilled water flow rate	3 Litre/min
Condenser cooling water flow rate	5 Litre/min
Switching time	1 minute
Adsorbent material	Al-Fumarate

7.7.1 Effect of half cycle time

The first parameter under investigation is the half cycle time where it was changed in the range of 4 to 12 minutes while desorption and evaporator inlet water temperatures were fixed at 95°C and 30°C respectively. As shown in Figure 7-22, at longer half cycle times, the amount of collected fresh water from the condenser increases however, SDWP starts at minimum value of 16.2 m³.tonne⁻¹.day⁻¹ at half cycle time equal to 4 min and reaches its peak at 8 min at a value of 16.7 m³.tonne⁻¹.day⁻¹ with 430 ml of water are collected per cycle. As cycle time increases, SDWP decreases and reaches its minimum value of 15.4 m³.tonne⁻¹.day⁻¹ at 12 min while the water collected per cycle equal to 571.4 ml. As for the cooling, it is shown in Figure 7-23 that the amount of cooling produced reaches its maximum at half cycle times of 6 and 8 min where it equals to 496 W/kg while longer cycle times reduces the amount of cooling produced which is the same case as in the single bed system that was discussed in section 6.8.2. Therefore, half cycle time of 8 min is selected for all further investigations.

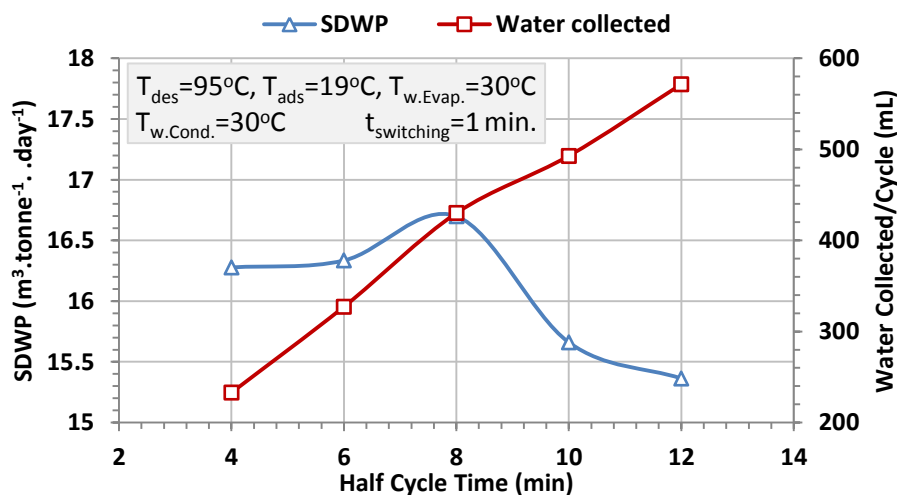


Figure 7-22, Specific daily water production and amount of produced fresh water per cycle at various half cycle times using (Al-Fumarate)

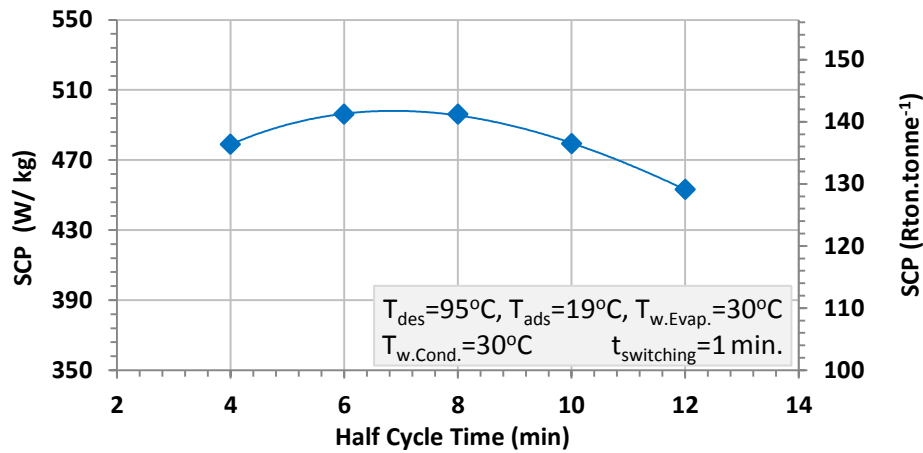


Figure 7-23, Specific cooling power at different half cycle times using (Al-Fumarate)

7.7.2 Effect of mass recovery time

As discussed in section 6.8.1, the switching time is needed for the adjustment of adsorber and desorber beds pressures before being connected to the evaporator and condenser respectively where pressure is varied as a result of swapping heating and cooling streams. Another common technique that helps in adjusting adsorber/desorber bed pressures is the mass recovery where a valve connecting adsorber and desorber beds is opened after adsorption/desorption phase to equalize the pressure of the two beds then the switching technique is utilized [190]. In this mass recovery phase or pressure equalization technique, when the desorber bed is connected to the adsorber bed, the remaining water vapor flows from the higher pressure bed (desorber bed) to the lower pressure bed (adsorber bed) until an intermediate pressure is reached which helps increasing the specific daily water production.

As shown in Figure 7-24 applying mass recovery technique, improves the amount of water produced per cycle by 4.6% when it increases from 0 to 5 seconds. However, longer mass

recovery time results in no significant increase in the amount of water produced as only 2.2% increase in collected water is found when mass recovery time increases from 5 to 45 seconds. On the other hand, as number of complete cycles per day decreases with the increase in total cycle time, it is found that optimum mass recovery time is 5 seconds where maximum SDWP of $17.3 \text{ m}^3 \cdot \text{tonne}^{-1} \cdot \text{day}^{-1}$ is achieved. The effect of mass recovery time on cooling is shown in Figure 7-25 where it is found that short mass recovery times less than 15 seconds has less effect on cooling production as it changes by 1.2%. Longer recovery time more than 15 seconds while increasing total cycle time, degrades cycle cooling production dramatically by an amount up to 24% at mass recovery time of 45 seconds where SCP drops to 397 W/kg adsorbent. From SDWP and SCP results, it is found that 5 seconds is the mass recovery time that will be selected for all oncoming investigations.

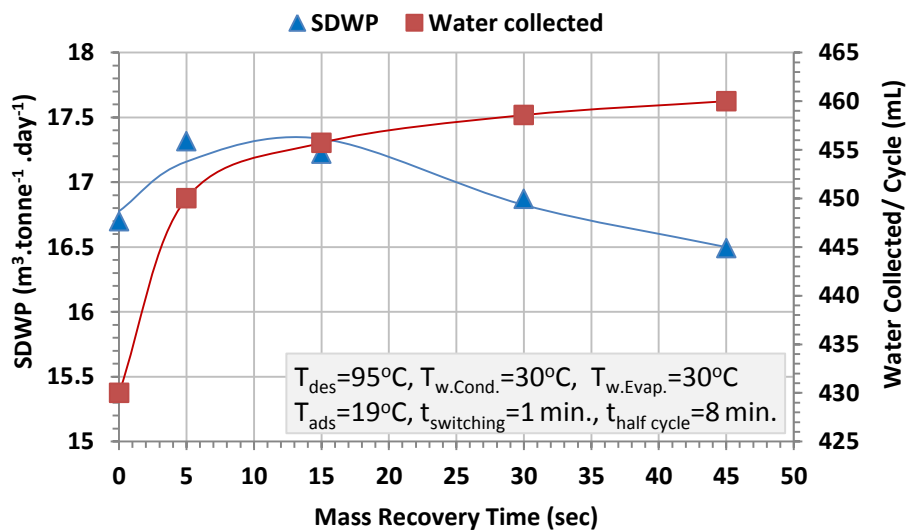


Figure 7-24, Specific daily water production and amount of produced fresh water per cycle at various mass recovery times using (Al-Fumarate)

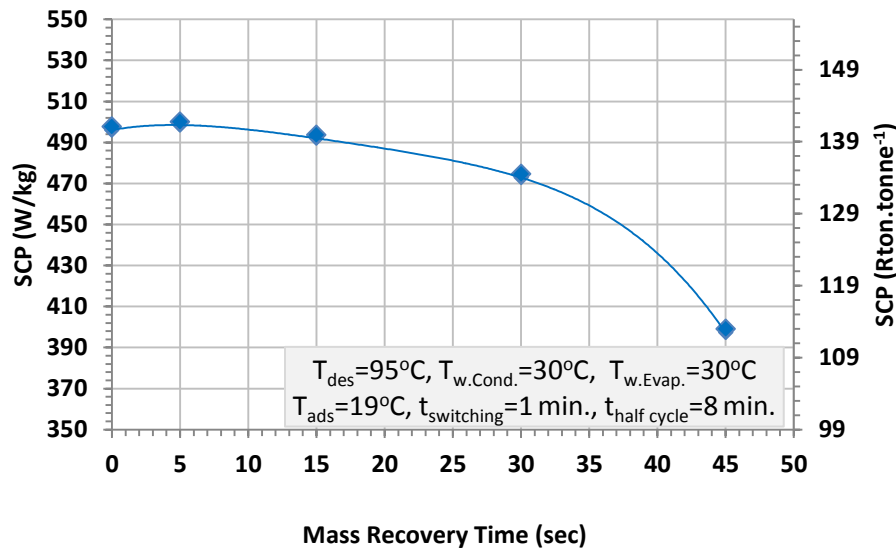


Figure 7-25, Specific cooling power at different mass recovery times using (Al-Fumarate)

7.7.3 Effects of desorption and evaporator water inlet temperature

As was concluded from section 4.2.1.3, Al-Fumarate performance highly depends on the evaporator water inlet temperature while desorption temperature has a little effect, it was important to study these parameters experimentally. In this section, desorption temperature is investigated in the range of 65 to 95°C at different evaporator water inlet temperatures ranging from 10 to 40°C and at fixed half cycle and mass recovery times of 8 mins. and 5 seconds respectively while all other parameters are the same as in Table 7-4.

As shown in Figure 7-26 and Figure 7-27, evaporator water inlet temperature significantly affects cycle outputs where SDWP increased by 366% from 5.4 to 25.2 m³.tonne⁻¹.day⁻¹ and SCP increased by 464% from 140 to 790 W/kg when evaporator inlet water temperature increased from 10 to 40°C. On the other hand, desorption temperature has a minimal effect on cycle outputs specially at low evaporator temperatures less than 20°C where water and cooling production rise by 17% and 13% respectively when desorption temperature

increases from 65 to 95°C. This behaviour is attributed to the S-shape of Aluminium Fumarate isotherm where the uptake value is almost constant at all pressure ratios <0.2 , therefore changing desorption temperature (i.e. the lower pressure ratio) does not affect the system uptake and hence the system performance. It is found that 95°C desorption temperature and 40°C evaporator water inlet temperature achieve maximum SDWP and SCP of $25.3 \text{ m}^3 \cdot \text{tonne}^{-1} \cdot \text{day}^{-1}$ and 789.4 W/kg , respectively.

Figure 7-28 shows the OCR of the system where it is found that it increases with the decrease of desorption temperature and with the increase of the evaporator water inlet temperature as discussed in section 4.2.1.3. A maximum value of 0.99 for the OCR is found to be at the lowest desorption temperature of 65°C and at inlet evaporator water temperature of 40°C. According to these results, a compromise between having maximum cycle production and working at maximum OCR is needed when choosing the desorption temperature of the Aluminium Fumarate system.

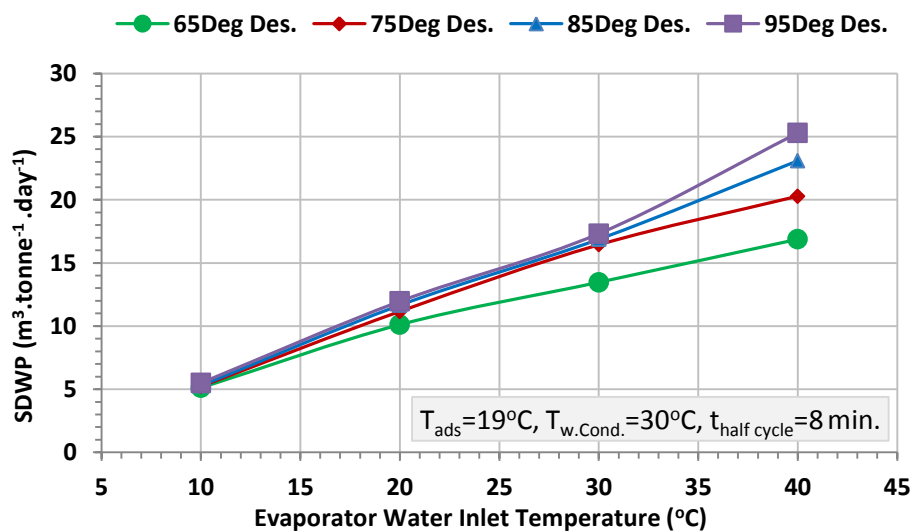


Figure 7-26, Specific daily water production at various desorption and evaporator water inlet temperatures using (Al-Fumarate)

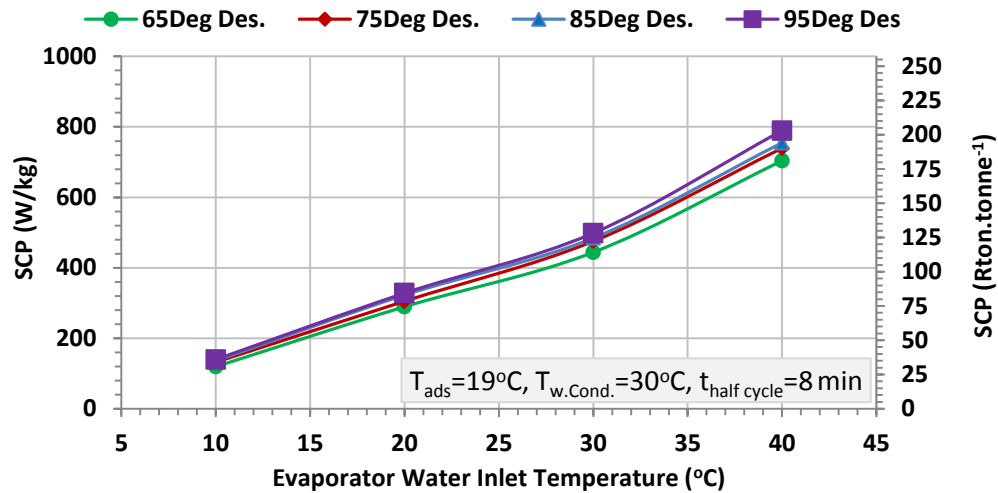


Figure 7-27, Specific cooling power at various desorption and evaporator water inlet temperatures using (Al-Fumarate)

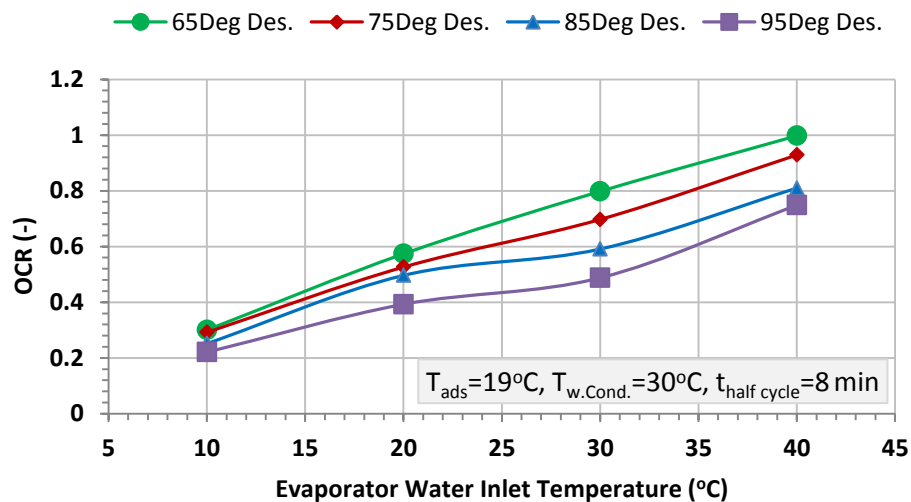


Figure 7-28, Overall conversion ratio of double-bed system at various desorption and evaporator water inlet temperatures using (Al-Fumarate)

7.7.4 Effect of inlet seawater salinity

In all of the previous testing runs, the feed water to the evaporator was tap water (at 0 ppm salinity) as the main purpose of these investigations were to prove the concept of adsorption system cyclic operation and to find the best operating conditions. At this point, effect of seawater salinity on adsorption cycle performance is assessed where three different seawater

salinity concentrations are investigated at constant desorption and evaporator water inlet temperatures of 95 and 30°C, respectively.

The seawater of the first test is real seawater that was collected from the Bristol Channel at “Penarth, town in Wales, UK” while the other two tests were performed on prepared lab samples where sea salt was mixed with distilled water at different concentrations. The sea salt used in these experiments has been brought from an aquarium shop in one batch to ensure consistency between experiments and its characteristics are given on Table 7-5. As shown in Figure 7-29, seawater were fed in the evaporator at concentrations of 24000, 44000 and 64000 ppm while the measured salinity of the potable water collected from the condenser were found to be 0 ppm in all cases which indicates that adsorption technology is capable of producing high quality potable water of less than 500 ppm as required by the World Health Organization (WHO) standards [6]. On the other hand, it was found that the concentration of the salty brine left in the evaporator is increasing with the increase of fed seawater salinity where a salinity of 74000 and 110000 ppm were recorded for the first two tests, respectively while the concentration in the third test was out of the salinity meter range.

For the cycle outputs, it is found that feed water salinity affects cycle water and cooling productions as shown in Figure 7-30. It is shown that SDWP and SCP decrease by 21.8% and 10.9%, respectively when fed water salinity increases from 24000 to 64000 ppm as the boiling point of the salty water increases with the increase of seawater salinity [191]. In other words, evaporation from a fresh water surface is higher than that from a saline water surface due to the increased cohesive forces between the dissolved salts and the water. Therefore, based on Raoult’s law, the saturation vapor pressure above a saline surface decreases with water

salinity and hence in reduced evaporation [192]. The lowest SDWP and SCP were found to be $13.8 \text{ m}^3 \cdot \text{tonne}^{-1} \cdot \text{day}^{-1}$ and 401.2 W/kg at the highest fed seawater salinity level of 64000 ppm.

Table 7-5, Sea salt chemical characterization

Component	Percentage
Chloride (Cl)	38.95%
Sodium (Na)	12.54%
Magnesium (Mg)	4.22%
Calcium (Ca)	1.95%
Sulphur (S)	0.79%
Potassium (K)	0.38%
Bromine (Br)	0.2%

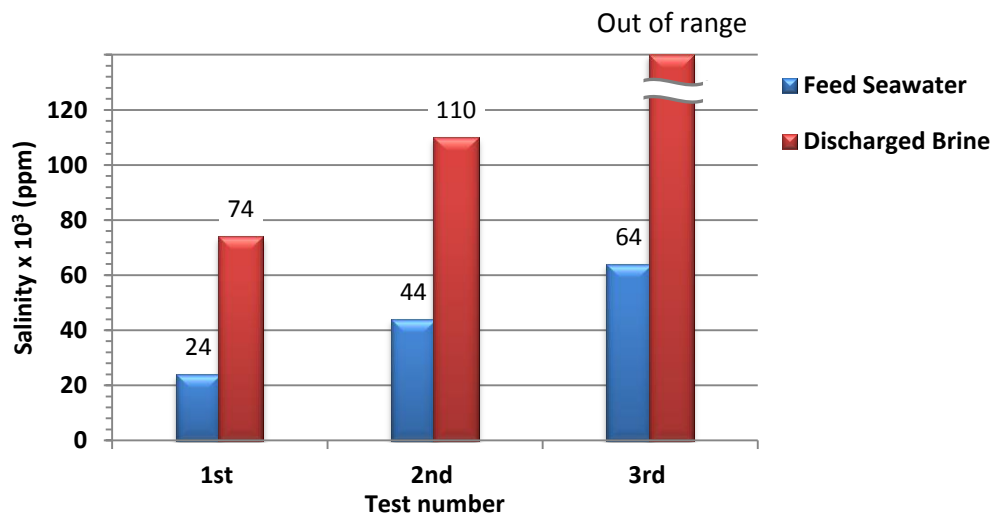


Figure 7-29, Salinity of feed seawater and discharged brine at different test runs using (Al-Fumarate)

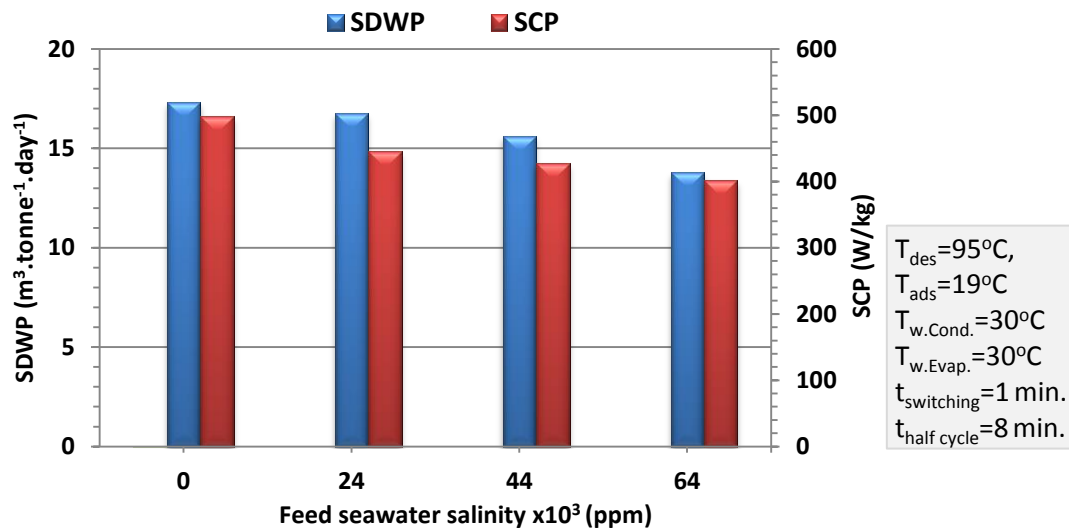


Figure 7-30, Specific daily water production and specific cooling power at different fed seawater salinity using (Al-Fumarate)

7.8 Validation of double-bed Simulink model using Aluminium Fumarate

The measured experimental results gained from the operation of the double bed adsorption system are used to validate the developed double-bed adsorption desalination Simulink model. The operating conditions of the validation test are listed in Table 7-6 while Aluminium Fumarate is the used adsorbent material. The validation is based on a comparison between temperature profiles of both adsorber beds, evaporator and the condenser as well as specific daily water production and specific cooling power which are shown in Figure 7-31 and Figure 7-32 respectively. Based on equation (3-41) and as shown in Table 7-7, the maximum instantaneous error between experimental and numerical results is within $\pm 9.8\%$ which reflects the accuracy of the Simulink model.

Table 7-6, Operating conditions of the validation test using Aluminium Fumarate

Parameter	Average deviation
Heating water temperature	95°C
Cooling water temperature	19°C
Condenser cooling water inlet temperature	30°C
Evaporator chilled water inlet temperature	30°C
Adsorber bed circulating water flowrate	11 Litre.min ⁻¹
Condenser cooling water flowrate	5 Litre.min ⁻¹
Evaporator chilled water flowrate	3 Litre.min ⁻¹
Half cycle time	8 minutes
Switching time	1 minute
Mass recovery time	5 seconds

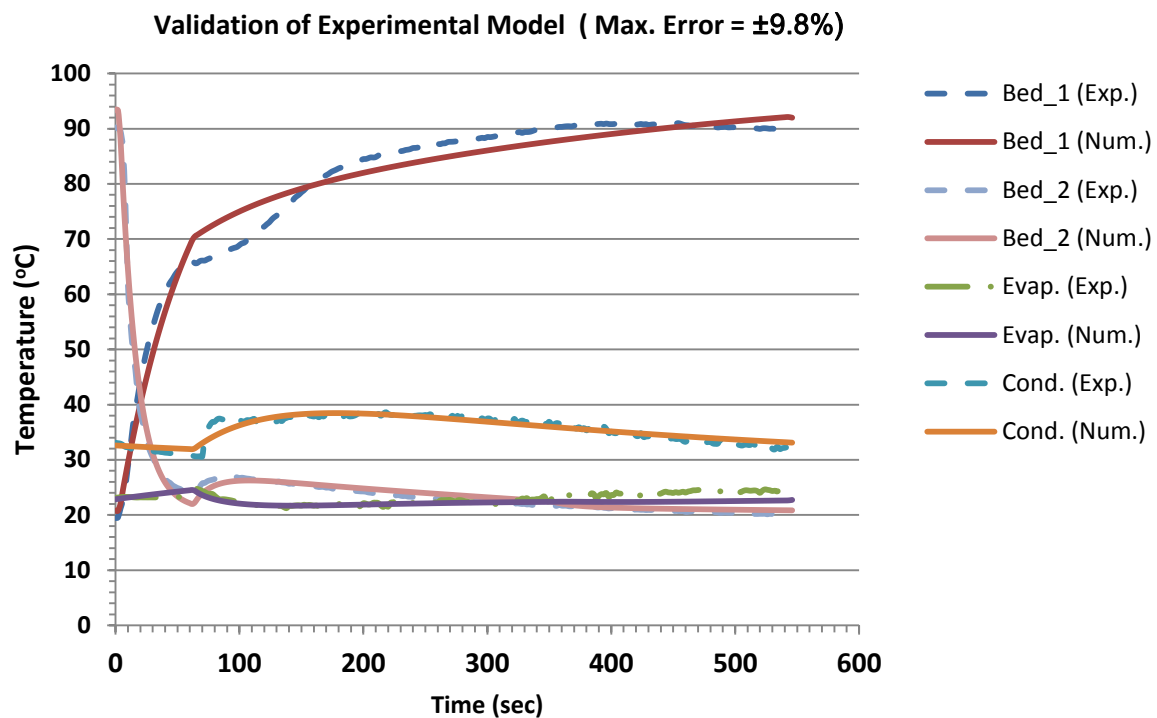


Figure 7-31, Validation of the double bed adsorption desalination Simulink model using Aluminium Fumarate, temperature profiles of adsorber beds, evaporator and condenser

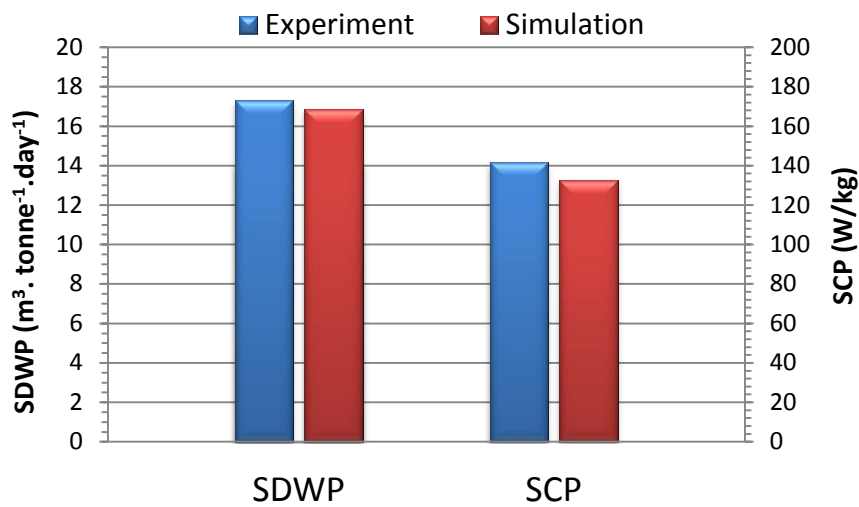


Figure 7-32, Comparison between experimental and simulation results of SDWP and SCP for Aluminium Fumarate

Table 7-7, Error in the validation of the double bed adsorption desalination Simulink model using Aluminium Fumarate

Parameter	Error
1 st Adsorber bed	-9.8 to 9.1%
2 nd Adsorber bed	-9.1 to 4.4%
Condenser	-7.4 to 7.9%
Evaporator	-8.4 to 4.5%
Specific daily water production (SDWP)	2.5%
Specific cooling power (SCP)	6.4%

7.9 Summary

In this chapter, the developed double bed adsorption system has been introduced in terms of the two adsorber beds, evaporator, condenser and the potable water/ brine accumulator. In addition, feeding of the seawater in the evaporator has been performed using a full cone spray nozzle which resulted in better heat transfer coefficient. Moreover, the Labview control code of the system automated valves has been shown for the different operating modes and the testing procedure has been explained through a three steps of initialization, cycling and finalization. The system was tested initially with CPO-27Ni packed in the adsorber bed and the system performance was compared to the single bed system and improvements of 27% and 15% were found on the specific daily water production (SDWP) and specific cooling power (SCP), respectively. Furthermore, another MOF material called Aluminium Fumarate was tested in the system at different operating conditions and it was found that it can work at low desorption temperatures as low as 65°C while at 95°C maximum SDWP of 25.3 m³.tonne⁻¹.day⁻¹ and SCP of 789.4 W/kg were obtained. In addition, effect of seawater salinity level on system performance was investigated and it was found that the adsorption desalination system was able to desalinate seawater with a salinity of 64000ppm while the potable collected water has a salinity of 0 ppm. Finally, the developed Simulink model has been validated against the measured experimental results of testing Aluminium Fumarate and it was found that maximum deviation is less than ±9.8%.

CHAPTER 8: CONCLUSIONS AND FUTURE WORK

8.1 Introduction

The human race is facing a challenging problem of drinking water shortages due to continuous population growth and limited fresh water resources. As salty water counts for 97.5% of the available water in the world, water desalination is becoming increasingly important where it can offer means of producing potable water from salty water found in seas and oceans. Various desalination technologies have been introduced many decades ago but issues like high energy consumption and production costs have limited their widespread. Heat powered adsorption desalination technology has attracted significant research work in the last few years due to their potential to reduce energy requirements and the associated CO₂ emissions. Therefore this thesis experimentally and numerically assesses the performance of adsorption desalination systems using new advanced microporous adsorbent materials. Initially adsorption desalination technology was compared to another 13 different desalination technologies. Then four different adsorbent materials that have not been investigated before for desalination applications were compared numerically to the only adsorbent used in such systems (*Silica-gel*). Moreover, a novel adsorption cycle for the purposes of desalination and cooling was introduced and numerically investigated. Finally, two adsorption experimental systems were developed and two different high-performance metal organic framework (MOF) adsorbent materials were tested experimentally using these systems at different operating conditions.

8.2 Conclusions

This PhD work aimed to understand the different commercially available desalination technologies while focusing deeply on adsorption desalination systems as a new method of desalination that has attracted interest in recent years. The study investigated ways of enhancing the performance of adsorption desalination using different adsorbent materials and to assess their performance at different operating conditions in terms of water production and cooling.

The following subsections outline the main conclusions:

8.2.1 Comparison between desalination technologies

Adsorption desalination technology was compared to other 13 desalination technologies categorized in three classifications namely; “Thermal”, “Membrane” and “Chemical” in terms of feed seawater salinity, produced potable water salinity, type and amount of energy required, carbon dioxide emissions and potable water production cost.

Findings:

- Adsorption desalination technology has the ability to produce potable water with salinity as low as 10 ppm from feed seawater with a salinity as high as 67000 ppm while “Reverse Osmosis (RO)” technology cannot desalinate seawater with a salinity higher than 45000 ppm.
- Adsorption desalination technology utilizes waste heat alongside 1.38 kWh/m³ of electrical energy for operation, while other technologies like RO consumes 8.2 kWh/m³ of electrical energy and “Multi-stage Flash (MSF) desalination technology consumes a total of 24.6 kWh/m³ of combined thermal and electrical energies.

Therefore adsorption desalination technology was found to be one of the lowest carbon dioxide emitting systems where it results in CO₂ emissions of 0.64 kg/m³ and accordingly, adsorption technology costs only 0.2 US\$/m³ compared to RO and MSF which cost 0.75 US\$/m³ and 0.96 US\$/m³ respectively based on the running cost.

- From literature, it was found that “Silica-gel” is the only adsorbent material used in all of the available published literature on adsorption desalination cycles including; double-beds, four beds master and slave, double-beds with heat recovery circuit between evaporator and condenser and double-beds with integrated evaporator/condenser device . Also it was found that the maximum experimentally obtained specific daily water production (SDWP) using “Silica-gel” is 13.5 m³per tonne of adsorbent per day.

8.2.2 Simulink model development

A numerical model using Simulink has been built in order to predict the performance of a two-bed adsorption desalination system at different operating conditions using one of the following five different adsorbents; “Silica-gel”, “AQSOA-Z02 (Zeolite material)”, “Aluminium Fumarate (MOF material)”, “CPO-27Ni (MOF material)” and “MIL-101Cr (MOF material)”.

Findings:

- The developed double-bed Simulink model has been validated against published Silica-gel experimental results with an instantaneous error less than ±9.7% based on experimental and numerical temperatures measured in degree Celsius.
- The selection of adsorbent material could be based on the available heat source temperature as follows:

- When desalination is the only required output and the available heat source temperature is higher than 90°C, CPO-27Ni, MIL-101Cr and AQSOA-Z02 are the best adsorbents where the maximum specific daily water production (SDWP) achieved is 24.1, 24 and 21.1m³.tonne⁻¹.day⁻¹ respectively.
- If only heat source at temperature less than 90°C is available and desalination is the only needed output, MIL-101Cr, Al-Fumarate and AQSOA-Z02 are the recommended adsorbents where maximum SDWP achieved is 23, 11.7 and 6.7m³.tonne⁻¹.day⁻¹ respectively.
- In cases where cooling is needed in addition to desalination and high temperature heat source is available (above 90°C), CPO-27Ni, AQSOA-Z02 and Al-Fumarate are to be selected as maximum SDWP obtained is 19.6, 19.4 and 10.7m³.tonne⁻¹.day⁻¹ respectively while the produced specific cooling power (SCP) is 146, 163 and 81 Rton.tonne⁻¹ respectively.
- For cooling and desalination as the two required outcomes while only low temperature heat source is accessible, MIL-101Cr, Al-Fumarate and AQSOA-Z02 are the suggested adsorbents where SDWP reach 11.8, 10.2 and 6.4m³.tonne⁻¹.day⁻¹, respectively while SCP is 52.6, 73.2 and 54.6 Rton.tonne⁻¹, respectively.

8.2.3 Integrated adsorption desalination cycle

A new integrated adsorption desalination cycle has been introduced and modelled which enhances adsorption desalination system's performance and produces cooling as another by-product. System performance is improved via decreasing the condenser temperature by the utilization of the cooling generated from the existing evaporators. AQSOA-Z02 was used

in this investigation to illustrate the capability of the new cycle through working at three operating scenarios according to desalinated water and cooling needs and the new system performance were compared to that of the conventional 2-bed system.

Findings:

- At evaporator chilled water inlet temperature of 10°C, the new system resulted in an increase of water production by 35% in addition to an enhancement of the produced cooling effect by 35% in scenario '1'. In the case of scenario '2', SDWP increased by 250% but with a reduction in the cooling output by 26%. For operating scenario '3', when all the generated cooling is utilized within the system, the maximum achieved SDWP was 314% greater than that of the conventional 2-bed cycle.
- Economic analysis of the new system performance showed that an average water production cost of 0.15 US\$.m⁻³ is achieved which is less than the lowest reported value of 0.18 US\$.m⁻³.

8.2.4 Experimental investigation of single-bed adsorption desalination system

An existing single-bed adsorption cooling prototype has been modified to work as a desalination/cooling system where different components were added and an advanced MOF material called "CPO-27Ni" has been tested for the first time for desalination purposes at different operating conditions and cooling was produced as a secondary product.

Findings:

- This MOF material is very sensitive to the condenser cooling water temperature where decreasing it from 30°C to 5°C increases SDWP by 49% from 15.3 to 22.8 m³.tonne⁻¹.day⁻¹ and increases SCP by 35.4% from 159.4 to 215.9 Rton.tonne⁻¹.

- The developed Simulink model has been validated using CPO-27Ni experimental results with a deviation less than $\pm 8.3\%$.

8.2.5 Experimental investigation of double-bed adsorption desalination system

A complete fully automated double-bed adsorption system has been constructed and tested using “CPO-27Ni” initially for comparison purposes with the single bed system then was packed with another MOF material called “Aluminium Fumarate” and tested at different operating conditions and feed seawater salinity levels.

Findings:

- Comparing double and single bed systems performance with CPO-27Ni used as the adsorbent, an improvement in SDWP by 27% and in SCP by 15% was achieved in the double bed system due to the use of evaporator spraying nozzle which increased the evaporator heat transfer coefficient.
- From the experimental investigations conducted using the double-bed system on Aluminium Fumarate, it was found that:
 - A mass recovery period helps in adjusting adsorber and desorber beds' pressures before the switching phase is reached. Only 5 seconds are adequate as a mass recovery time where the remaining water vapor flows from the higher pressure bed (desorber bed) to the lower pressure bed (adsorber bed) until an intermediate pressure is reached which helps in increasing the specific daily water production by 3.6%.
 - Al-Fumarate can work at low desorption temperatures as low as 65°C while at 95°C maximum SDWP of 25.3 m³.tonne⁻¹.day⁻¹ and SCP of 789.4 W/kg were obtained.

- This adsorption desalination system was able to desalinate seawater with a salinity of 64000ppm while the potable collected water has a salinity of 0 ppm.
- Higher seawater salinity reduces SDWP and SCP by 21.8% and 10.9% respectively when feed water salinity increases from 24000 to 64000 ppm as the boiling point of the salty water increases with the increase of seawater salinity.
- The obtained results from testing Aluminum Fumarate have been used to validate the developed Simulink model with a deviation less than $\pm 9.8\%$.

Finally this work has shown that metal organic framework materials have the potential to double the amount of produced fresh water and cooling compared to commercial materials like "Silica gel" leading to significant reduction in the system size and cost.

8.3 Future work

Further improvements on the performance of the adsorption desalination system could be achieved through the following points.

- A study is needed to investigate various adsorber bed designs and the method of integrating the adsorber materials to help in increasing the heat transfer between the adsorbent material granules and the adsorber bed heating/cooling fluid.
- Investigating various evaporator configurations to enhance the evaporation heat transfer coefficient including developing a method for circulating the seawater inside

the evaporator to achieve continuous spraying of seawater which aids in improving the evaporator performance.

- A continuous measure of evaporator seawater salinity level is needed so that a study can be conducted to determine the optimum time for discharging the concentrated brine to achieve the highest rate of evaporation which will improve the system water production.
- Investigating various configurations of condenser to achieve higher heat transfer coefficients in addition to assessing the effect of collected potable water level on the condenser performance as discharging the collected water regularly, helps in lowering the condenser pressure which in turn improves system performance.
- Building and testing of the integrated adsorption desalination and cooling system that has been modelled in chapter 5 as it can work at different operating modes and can produce higher amounts of desalinated water and cooling compared to conventional systems.

REFERENCES

- [1] T. Distefano, S. Kelly. Are we in deep water? Water scarcity and its limits to economic growth. *Ecological Economics*. 2017;142:130-47.
- [2] J. E. Miller. Review of Water Resources and desalination technologies. Sandia National Laboratories 2003.
- [3] T. L. Anderson, B. Scarborough, L. R. Watson. Water Crises, Water Rights, and Water Markets* A2 - Shogren, Jason F. *Encyclopedia of Energy, Natural Resource, and Environmental Economics*. Waltham: Elsevier; 2013. p. 248-54.
- [4] H. T. El-Dessouky, H. M. Ettouney. *Fundamentals of salt water desalination: ELSEVIER*; 2002.
- [5] K. C. Ng, K. Thu, B. B. Saha, A. Chakraborty. Study on a waste heat-driven adsorption cooling cum desalination cycle. *International Journal of Refrigeration*. 2012;35:685-93.
- [6] X. Wang, K. C. Ng. Experimental investigation of an adsorption desalination plant using low-temperature waste heat. *Applied Thermal Engineering*. 2005;25:2780-9.
- [7] P. G. Youssef, S. M. Mahmoud, R. K. Al-Dadah. Performance analysis of four bed adsorption water desalination/refrigeration system, comparison of AQSOA-Z02 to silica-gel. *Desalination*. 2015;375:100-7.
- [8] E. Elsayed, R. Al-Dadah, S. Mahmoud, P. A. Anderson, A. Elsayed, P. G. Youssef. CPO-27(Ni), aluminium fumarate and MIL-101(Cr) MOF materials for adsorption water desalination. *Desalination*. 2017;406:25-36.
- [9] K. C. Ng, K. Thu, Y. Kim, A. Chakraborty, G. Amy. Adsorption desalination: An emerging low-cost thermal desalination method. *Desalination*. 2013;308:161-79.
- [10] A. Asushi, C. Anutosh, G. Lizhen, K. Takao, K. S. C. O. K. Univ, N. K. Choon, S. B. Baran, W. X. Ling. Apparatus and method for desalination. Google Patents; 2006.
- [11] P. G. Youssef, S. M. Mahmoud, R. K. Al-Dadah. Numerical simulation of combined adsorption desalination and cooling cycles with integrated evaporator/condenser. *Desalination*. 2016;392:14-24.
- [12] B. Shi. Development of an MOF based adsorption air conditioning system for automotive application: University of Birmingham; 2015.
- [13] H. Furukawa, F. Gándara, Y.-B. Zhang, J. Jiang, W. L. Queen, M. R. Hudson, O. M. Yaghi. Water Adsorption in Porous Metal–Organic Frameworks and Related Materials. *Journal of the American Chemical Society*. 2014;136:4369-81.
- [14] H. W. B. Teo, A. Chakraborty, Y. Kitagawa, S. Kayal. Experimental study of isotherms and kinetics for adsorption of water on Aluminium Fumarate. *International Journal of Heat and Mass Transfer*. 2017;114:621-7.

- [15] J. Liu, Y. Wang, A. I. Benin, P. Jakubczak, R. R. Willis, M. D. LeVan. CO₂/H₂O Adsorption Equilibrium and Rates on Metal–Organic Frameworks: HKUST-1 and Ni/DOBDC. *Langmuir*. 2010;26:14301-7.
- [16] F. Jeremias, A. Khutia, S. K. Henninger, C. Janiak. MIL-100(Al, Fe) as water adsorbents for heat transformation purposes-a promising application. *Journal of Materials Chemistry*. 2012;22:10148-51.
- [17] S. K. Henninger, F. Jeremias, H. Kummer, C. Janiak. MOFs for Use in Adsorption Heat Pump Processes. *European Journal of Inorganic Chemistry*. 2012;2012:2625-34.
- [18] P. G. Youssef, S. M. Mahmoud, R. K. Al-Dadah. Seawater Desalination Technologies. *International Journal of Innovation Sciences and Research*. 2015;4:402-22.
- [19] P. G. Youssef, R. K. Al-Dadah, S. M. Mahmoud. Comparative Analysis of Desalination Technologies. *Energy Procedia*. 2014;61:2604-7.
- [20] E. Glueckauf. Seawater desalination in perspective. *Nature*. 1966;211:1227-30.
- [21] J. Frederick. Desalination: Can it be greenhouse gas free and cost competitive? : Yale School of Forestry and Environmental Studies; 2010.
- [22] K. Thu, H. Yanagi, B. B. Saha, K. C. Ng. Performance analysis of a low-temperature waste heat-driven adsorption desalination prototype. *International Journal of Heat and Mass Transfer*. 2013;65:662-9.
- [23] T. Younos, K. E. Tulou. Overview of desalination techniques. *Journal of contemporary water research and education*. 2005;132:3-10.
- [24] U. S. B. o. Reclamation, S. N. Laboratories. Desalination and water purification technology roadmap report. 2003.
- [25] A. N. A. Mabrouk. Technoeconomic analysis of once through long tube MSF process for high capacity desalination plants. *Desalination*. 2013;317:84-94.
- [26] M. Shatat, M. Worall, S. Riffat. Opportunities for solar water desalination worldwide: Review. *Sustainable Cities and Society*. 2013;9:67-80.
- [27] L. F. Greenlee, D. F. Lawler, B. D. Freeman, B. Marrot, P. Moulin. Reverse osmosis desalination: water sources, technology, and today's challenges. *Water Res*. 2009;43:2317-48.
- [28] A. D. Khawaji, I. K. Kutubkhanah, J.-M. Wie. Advances in seawater desalination technologies. *Desalination*. 2008;221:47-69.
- [29] N. Misdan, W. J. Lau, A. F. Ismail. Seawater Reverse Osmosis (SWRO) desalination by thin-film composite membrane—Current development, challenges and future prospects. *Desalination*. 2012;287:228-37.
- [30] B. A. Bolto, K. H. Eppinger, M. B. Jackson, R. V. Siudak. An ion-exchange process with thermal regeneration XVI oxygen-resistant polyamine resins. *Desalination*. 1982;42:273-90.
- [31] L. LAZARE. The Puraq Seawater Desalination Process. *Desalination*. 1982;42:11-6.
- [32] K.-n. Park, S. Y. Hong, J. W. Lee, K. C. Kang, Y. C. Lee, M.-G. Ha, J. D. Lee. A new apparatus for seawater desalination by gas hydrate process and removal

- characteristics of dissolved minerals (Na^+ , Mg^{2+} , Ca^{2+} , K^+ , B^{3+}). *Desalination*. 2011;274:91-6.
- [33] K. Thu, A. Chakraborty, Y.-D. Kim, A. Myat, B. B. Saha, K. C. Ng. Numerical simulation and performance investigation of an advanced adsorption desalination cycle. *Desalination*. 2013;308:209-18.
- [34] H. Cooley, P. H. Gleick, G. Wolff. *Desalination, with a grain of salt- a California Perspective*. 2006.
- [35] H. Baig, M. A. Antar, S. M. Zubair. Performance evaluation of a once-through multi-stage flash distillation system: Impact of brine heater fouling. *Energy Conversion and Management*. 2011;52:1414-25.
- [36] M. Abduljawad, U. Ezzeghni. Optimization of Tajoura MSF desalination plant. *Desalination*. 2010;254:23-8.
- [37] P. Druetta, P. Aguirre, S. Mussati. Optimization of Multi-Effect Evaporation desalination plants. *Desalination*. 2013;311:1-15.
- [38] H. T. El-Dessouky, H. M. Ettouney, F. Mandani. Performance of parallel feed multiple effect evaporation system for seawater desalination. *Applied Thermal Engineering*. 2000;20:1679-706.
- [39] M. Al-Shammeri, M. Safar. Multi-effect distillation plants- state of the art. *Desalination*. 1999;126:45-59.
- [40] H. El-Dessouky, I. Alatiqi, S. Bingulac, H. Ettouney. Steady-State Analysis of the Multiple Effect Evaporation Desalination Process. *Chemical Engineering and Technology*. 1998;21:437-51.
- [41] M. Al-Sahali, H. Ettouney. Developments in thermal desalination processes: Design, energy, and costing aspects. *Desalination*. 2007;214:227-40.
- [42] J. Shen, Z. Xing, X. Wang, Z. He. Analysis of a single-effect mechanical vapor compression desalination system using water injected twin screw compressors. *Desalination*. 2014;333:146-53.
- [43] R. Bahar, M. N. A. Hawlader, L. S. Woei. Performance evaluation of a mechanical vapor compression desalination system. *Desalination*. 2004;166:123-7.
- [44] H. S. Aybar. Analysis of a mechanical vapor compression desalination system. *Desalination*. 2002;142:181-6.
- [45] A. Karameldin, A. Lotfy, S. Melchemar. The Red Sea area wind-driven mechanical vapor compression desalination system. *Desalination*. 2002;153:47-53.
- [46] K. M. El-Khatib, A. S. Abd El-Hamid, A. H. Eissa, M. A. Khedr. Transient model, simulation and control of a single-effect mechanical vapour compression (SEMVC) desalination system. *Desalination*. 2004;166:157-65.
- [47] J. M. Veza. Mechanical vapour compression desalination plants- A case study. *Desalination*. 1995;101:1-10.
- [48] J. A. Miller, J. H. Lienhard V. Impact of extraction on a humidification-dehumidification desalination system. *Desalination*. 2013;313:87-96.

- [49] A. E. Kabeel, M. H. Hamed, Z. M. Omara, S. W. Sharshir. Water Desalination Using a Humidification-Dehumidification Technique—A Detailed Review. *Natural Resources*. 2013;04:286-305.
- [50] K. Bourouni, M. T. Chaibi, L. Tadriss. Water desalination by humidification and dehumidification of air: state of the art. *Desalination*. 2001;137:167-76.
- [51] L. Garcia-Rodriguez, A. I. Palmero-Marrero, C. Gomez-Camacho. Comparison of Solar thermal technologies for applications in seawater desalination. *Desalination*. 2002;142:135-42.
- [52] L. Garcia-Rodriguez, C. Gomez-Camacho. Perspectives of solar-assisted seawater distillation. *Desalination*. 2001;136:213-8.
- [53] J. Lindblom. Solar Thermal Technologies for Seawater Desalination state of the art. *Renewable Energy systems*, Luleå University of Technology 2010.
- [54] L. Garcia-Rodriguez. Seawater desalination driven by renewable energies: a review. *Desalination*. 2002;143:103-13.
- [55] H. E. S. Fath. Solar distillation: a promising alternative for water provision with free energy, simple technology and a clean environment. *Desalination*. 1998;116:45-56.
- [56] G. MINK, M. M. ABOABBOUD, E. KARMAZSIN. Air blown solar still with heat recycling. *Solar Energy*. 1998;62:309-17.
- [57] G. N. TIWARI, K. MUKHERJEE, K. ASHOK, Y. P. YADAV. Comparison of various designs of solar stills. *Desalination*. 1986;60:191-202.
- [58] O. M. Haddad, M. A. Al-Nimr, A. Maqableh. Enhanced solar still performance using a radiative cooling system. *Renewable Energy*. 2000;21:459-65.
- [59] M. S. SODHA, A. KUMAR, G. N. TIWARI, R. C. TYAGI. Simple multiple wick solar still: analysis and performance. *Solar Energy*. 1981;26:127-31.
- [60] P. A. Davies, C. Paton. The Seawater Greenhouse in the United Arab Emirates: thermal modelling and evaluation of design options. *Desalination*. 2005;173:103-11.
- [61] F. Grater, M. Durrbeck, J. Rheinlander. Multi-effect still for hybrid solar/fossil desalination of sea-and brackish water. *Desalination*. 2001;138:111-9.
- [62] T. Mtombeni, J. P. Maree, C. M. Zvinowanda, J. K. O. Asante, F. S. Oosthuizen, W. J. Louw. Evaluation of the performance of a new freeze desalination technology. *International Journal of Environmental Science and Technology*. 2013;10:545-50.
- [63] A. Rich, Y. Mandri, D. Mangin, A. Rivoire, S. Abderafi, C. Bebon, N. Semlali, J.-P. Klein, T. Bounahmidi, A. Bouhaouss, S. Veessler. Sea water desalination by dynamic layer melt crystallization: Parametric study of the freezing and sweating steps. *Journal of Crystal Growth*. 2012;342:110-6.
- [64] M. S. Rahman, M. Ahmed, X. D. Chen. Freezing-Melting Process and Desalination: I. Review of the State-of-the-Art. *Separation & Purification Reviews*. 2006;35:59-96.
- [65] A. Antonelli. Desalinated water production at LNG-terminals. *Desalination*. 1983;45:383-90.

- [66] W. Lin, M. Huang, A. Gu. A seawater freeze desalination prototype system utilizing LNG cold energy. *International Journal of Hydrogen Energy*. 2017;42:18691-8.
- [67] C. Xie, L. Zhang, Y. Liu, Q. Lv, G. Ruan, S. S. Hosseini. A direct contact type ice generator for seawater freezing desalination using LNG cold energy. *Desalination*. 2017.
- [68] Z. Lu, L. Xu. Freezing Desalination process. *Thermal desalination processes: Encyclopedia of Desalination and Water Resources (DESWARE)*; 2010.
- [69] J. P. Guyer. *Introduction to Membrane Techniques for Water Desalination*. Continuing Education and Development, Inc; 2013.
- [70] M. E. Williams. *A Brief Review of Reverse Osmosis Membrane Technology*. EET Corporation and Williams Engineering Services Company 2003.
- [71] C. Fritzmann, J. Löwenberg, T. Wintgens, T. Melin. State-of-the-art of reverse osmosis desalination. *Desalination*. 2007;216:1-76.
- [72] A. D. Khawaji, I. K. Kutubkhanah, J.-M. Wie. A 13.3 MGD seawater RO desalination plant for Yanbu Industrial City. *Desalination*. 2007;203:176-88.
- [73] G. Danasamy. *Sustainability of Seawater Desalination Technology- Assessing Forward Osmosis as a Potential Alternative Technology*: Imperial College London; 2009.
- [74] B. S. Chanukya, S. Patil, N. K. Rastogi. Influence of concentration polarization on flux behavior in forward osmosis during desalination using ammonium bicarbonate. *Desalination*. 2013;312:39-44.
- [75] J. R. McCutcheon, R. L. McGinnis, M. Elimelech. A novel ammonia-carbon dioxide forward (direct) osmosis desalination process. *Desalination*. 2005;174:1-11.
- [76] S. Phuntsho, S. Hong, M. Elimelech, H. K. Shon. Osmotic equilibrium in the forward osmosis process: Modelling, experiments and implications for process performance. *Journal of Membrane Science*. 2014;453:240-52.
- [77] A. M. Hassan, M. A. K. Al-Sofi, A. S. Al-Amoudi, A. T. M. Jamaluddin, A. M. Farooque, A. Rowaili, A. G. I. Dalvi, N. M. Kither, G. M. Mustafa, I. A. R. Al-Tisan. A new approach to membrane and thermal seawater desalination process using nanofiltration membranes (Part1). *Desalination*. 1998;118:35-51.
- [78] A. AlTae, A. O. Sharif. Alternative design to dual stage NF seawater desalination using high rejection brackish water membranes. *Desalination*. 2011;273:391-7.
- [79] D. X. Vuong. Two stage nanofiltration seawater desalination system. US2006.
- [80] H. M. N. AlMadani. Water desalination by solar powered electro dialysis process. *Renewable Energy*. 2003;28:1915-24.
- [81] C. Charcosset. A review of membrane processes and renewable energies for desalination. *Desalination*. 2009;245:214-31.
- [82] F. Valero, A. Barceló, R. Arbós. *Electrodialysis Technology Theory and Application*. In: M Schorr, editor. *Desalination, Trends and Technologies: In Tech*; 2011.

- [83] M. Greiter, S. Novalin, M. Wendland, K.-D. Kulbe, J. Fischer. Desalination of whey by electrodialysis and ion exchange resins-analysis of both processes with regard to sustainability by calculating their cumulative energy demand.pdf>. *Journal of Membrane Science*. 2002;210:91-102.
- [84] Y. EGOZY, E. KORNGOLD, N. C. DALTROPHE, M. REBHUN. Waste water recycling by Ion Exchange- II partial desalination. *Desalination*. 1980;33:333-46.
- [85] C. E. HARLAND. *Water Treatment. Ion Exchange: Theory and Practice*. second ed: Royal Society of Chemistry; 1994.
- [86] C. F. C. Michaud. Ion Exchange Reactions a review. *Water Conditioning & Purification Magazine*2011.
- [87] J. Javanmardi, M. Moshfeghian. Energy consumption and economic evaluation of water desalination by hydrate phenomenon. *Applied Thermal Engineering*. 2003;23:845-57.
- [88] M. D. Max, R. E. Pellenbarg. *Desalination through gas hydrate*. 2000.
- [89] A. M. Aliev, R. Y. Yusifov, A. R. Kuliev, Y. G. Yusifov. Method of gas hydrate formation for evaluation of water desalination. *Russian Journal of Applied Chemistry*. 2008;81:588-91.
- [90] M. Milosevic, K. J. J. Staal, B. Schuur, A. B. de Haan. Extractive concentration of aqueous salt solutions in aqueous two phase systems. *Desalination*. 2013;324:99-110.
- [91] E. M. Polykarpou, V. Dua. Sustainable Water Desalination Using Waste Heat: Optimization of a Liquid-Liquid Extraction Process. 22nd European Symposium on Computer Aided Process Engineering. London2012.
- [92] G. Férey, C. Mellot-Draznieks, C. Serre, F. Millange, J. Dutour, S. Surblé, I. Margiolaki. A Chromium Terephthalate-Based Solid with Unusually Large Pore Volumes and Surface Area. *Science*. 2005;309:2040.
- [93] J. W. Wu, M. J. Biggs, E. J. Hu. Thermodynamic analysis of an adsorption-based desalination cycle. *Chemical Engineering Research and Design*. 2010;88:1541-7.
- [94] P. G. Youssef, R. K. Al-Dadah, S. M. Mahmoud, H. J. Dakkama, A. Elsayed. Effect of Evaporator and Condenser Temperatures on the Performance of Adsorption Desalination Cooling Cycle. *Energy Procedia*. 2015;75:1464-9.
- [95] K. Thu, B. B. Saha, A. Chakraborty, W. G. Chun, K. C. Ng. Study on an advanced adsorption desalination cycle with evaporator–condenser heat recovery circuit. *International Journal of Heat and Mass Transfer*. 2011;54:43-51.
- [96] K. Thu, K. C. Ng, B. B. Saha, A. Chakraborty, S. Koyama. Operational strategy of adsorption desalination systems. *International Journal of Heat and Mass Transfer*. 2009;52:1811-6.
- [97] J. W. Wu, M. J. Biggs, P. Pendleton, A. Badalyan, E. J. Hu. Experimental implementation and validation of thermodynamic cycles of adsorption-based desalination. *Applied Energy*. 2012;98:190-7.

- [98] K. Thu, A. Chakraborty, B. B. Saha, W. G. Chun, K. C. Ng. Life-cycle cost analysis of adsorption cycles for desalination. *Desalination and Water Treatment*. 2012;20:1-10.
- [99] K. Thu. Adsorption desalination Theory and experiment: National University of Singapore; 2010.
- [100] D. D. Ratnayaka, M. J. Brandt, M. K. Johnson. Specialized and advanced water treatment processes. *Water Supply*. sixth ed: ELSEVIER; 2009.
- [101] S. A. Kalogirou. Solar Desalination Systems. *Solar Energy Engineering: Elsevier*; 2014. p. 431-79.
- [102] R. K. McGovern, G. P. Thiel, G. Prakash Narayan, S. M. Zubair, J. H. Lienhard. Performance limits of zero and single extraction humidification-dehumidification desalination systems. *Applied Energy*. 2013;102:1081-90.
- [103] A. M. EL-NASHAR. Abu Dhabi Solar Distillation Plant. *Desalination*. 1985;52:217-34.
- [104] M. Mahdavi, A. H. Mahvi, S. Nasser, M. Yunesian. Application of Freezing to the Desalination of Saline Water. *Arabian Journal for Science and Engineering*. 2011;36:1171-7.
- [105] A. Altaee, A. Mabrouk, K. Bourouni. A novel Forward osmosis membrane pretreatment of seawater for thermal desalination processes. *Desalination*. 2013;326:19-29.
- [106] H. MÜLLER-HOLST. Solar thermal desalination using the multiple effect humidification (MEH)-method. In: L Rizzuti, HM Ettouney, A Cipollina, editors. *Solar desalination for the 21st century*: Springer; 2007.
- [107] R. A. McCormack, R. K. Andersen. Clathrate desalination plant preliminary research study. US Bureau of Reclamation Water Treatment Technology Program 1995.
- [108] W. J. HAHN. Measurements and control in freeze-desalination plants. *Desalination*. 1986;59:321-41.
- [109] Tinos, NTUA, C. S.A. Report on the evaluation of desalination systems driven by renewable energy sources: focus on solar energy systems used in different desalination applications. *Sol-Brine*; 2012.
- [110] J. H. Lienhard. Purification of Water in Phaeton and Paulette. 2500 *Desalination and Water Purification* 2009.
- [111] A. Mehta, A. Vyas, N. Bodar, D. Lathiya. Design of Solar Distillation System. *International Journal of Advanced Science and Technology*. 2011;29:67-74.
- [112] T. Thorsen, H. Fløgstad. Nanofiltration in drinking water treatment. *TECHNEAU* 2006.
- [113] S. D. Chi, B. J. Cha, J. H. Lee, D. R. Kim, S. J. Lim. Forward Osmosis Membrane for seawater desalination and method for preparing the same. 2012.
- [114] B. Djebdjian, H. Gad, I. Khaled, M. A. Rayan. Reverse Osmosis Desalination Plant in Nuweiba City (Case Study). Eleventh International Water Technology Conference, IWTC11. Sharm El-Sheikh, Egypt 2007.

- [115] M. Marcovecchio, P. Aguirre, N. Scenna, S. Mussati. Global Optimal Design of Mechanical Vapor Compression (MVC) Desalination Process. 2010;28:1261-6.
- [116] H. M. Qiblawey, F. Banat. Solar thermal desalination technologies. *Desalination*. 2008;220:633-44.
- [117] MODERNWATER. Forward Osmosis Applied to Desalination and Evaporative Cooling Make-up Water. 3rd Osmosis Summit2012.
- [118] G. P. Narayan, M. H. Sharqawy, E. K. Summers, J. H. Lienhard, S. M. Zubair, M. A. Antar. The potential of solar-driven humidification–dehumidification desalination for small-scale decentralized water production. *Renewable and Sustainable Energy Reviews*. 2010;14:1187-201.
- [119] A. Al-Karaghoul, L. L. Kazmerski. Energy consumption and water production cost of conventional and renewable-energy-powered desalination processes. *Renewable and Sustainable Energy Reviews*. 2013;24:343-56.
- [120] A. CHAKRABORTY, K. THU, B. B. SAHA, K. C. NG. Adsorption - Desalination Cycle. In: N Lior, editor. *Advances in water desalination*: WILEY; 2013.
- [121] R. C. Cheng, T. J. Tseng, K. L. Wattier. Two-Pass Nanofiltration Seawater Desalination Prototype Testing and Evaluation. U.S. Department of the Interior, Bureau of Reclamation; 2013.
- [122] G. P. Narayan, R. K. McGovern, G. P. Thiel, J. A. Miller, J. H. L. V. Status of humidification dehumidification desalination technology. World Congress/Perth Convention and Exhibition Centre (PCEC). Perth, Western Australia2011.
- [123] K. E. Thomas. Overview of Village Scale, Renewable Energy Powered Desalination. National Renewable Energy Laboratory; 1997.
- [124] A. S. Moon, M. Lee. Energy Consumption in Forward Osmosis Desalination Compared to Other Desalination Techniques. *World Academy of Science, Engineering and Technology*. 2012;65:537-9.
- [125] M. R. LUBIS. Desalination Using Vapor-Compression Distillation: Texas A&M University; 2009.
- [126] K. Thanapalan, V. Dua. Using Low-Grade Heat for Solvent Extraction based Efficient Water Desalination. 21st European Symposium on Computer Aided Process Engineering – ESCAPE 212011. p. 1703-7.
- [127] T. Mezher, H. Fath, Z. Abbas, A. Khaled. Techno-economic assessment and environmental impacts of desalination technologies. *Desalination*. 2011;266:263-73.
- [128] F. Banat. Economic and Technical assessment of desalination technologies. Geneva: Jordan University of Science and Technology; 2012.
- [129] R. Balch, L. Li, S. Muraleedharan, J. Harvard. Cost-Effective Treatment of Produced Water Using Co-Produced Energy Sources for Small Producers. RPSEA: New Mexico Institute of Mining and Technology, New Mexico Petroleum Recovery Research Center; 2012.

- [130] A. Eslamimanesh, M. S. Hatamipour. Economical study of a small-scale direct contact humidification–dehumidification desalination plant. *Desalination*. 2010;250:203-7.
- [131] J. E. Boysen, J. A. Harju. Evaluation of the Natural Freeze-Thaw Process for the Desalinization of Groundwater from the north Dakota Aquifer to Provide Water for Grand Forks, North Dakota. *Water Treatment Technology Program: U.S. DEPARTMENT OF THE INTERIOR, Bureau of Reclamation*; 1999.
- [132] J. E. Miller. Review of Water Resources and Desalination Technologies. SAND 2003-0800: Sandia National Laboratories; 2003.
- [133] T.-w. Kim, S. Park, K. Yeh. Cost-effective design of a draw solution recovery process for forward osmosis desalination. *Desalination*. 2013;327:46-51.
- [134] Y. P. G., S. M. Mahmoud, R. K. Al-Dadah, E. Elsayed, O. El-Samni. Numerical Investigation of Aluminum Fumarate MOF adsorbent material for adsorption desalination/cooling application. *The 9th Int. conference on applied energy, ICAE 2017. Cardiff, UK2017*.
- [135] K. C. Ng, K. Thu, A. Chakraborty, B. B. Saha, W. G. Chun. Solar-assisted dual-effect adsorption cycle for the production of cooling effect and potable water. *International Journal of Low-Carbon Technologies*. 2009;4:61-7.
- [136] S. Mitra, K. Srinivasan, P. Kumar, S. S. Murthy, P. Dutta. Solar Driven Adsorption Desalination System. *Energy Procedia*. 2014;49:2261-9.
- [137] A. Dąbrowski. Adsorption — from theory to practice. *Advances in Colloid and Interface Science*. 2001;93:135-224.
- [138] S. K. Yeboah, J. Darkwa. A critical review of thermal enhancement of packed beds for water vapour adsorption. *Renewable and Sustainable Energy Reviews*. 2016;58:1500-20.
- [139] A. Rezk. Theoretical and experimental investigation of silica gel / water adsorption refrigeration systems [PhD Dissertation]: University of Birmingham; 2012.
- [140] K. C. Ng, H. T. Chua, C. Y. Chung, C. H. Loke, T. Kashiwagi, A. Akisawa, B. B. Saha. Experimental investigation of the silica gel-water adsorption isotherm characteristics. *Applied Thermal Engineering*. 2001;21:1631-42.
- [141] H. T. Chua, K. C. Ng, A. Chakraborty, N. M. Oo, M. A. Othman. Adsorption Characteristics of Silica Gel + Water Systems. *Journal of Chemical Engineering Data*. 2002;47:1177-81.
- [142] K. Thu, A. Chakraborty, B. B. Saha, K. C. Ng. Thermo-physical properties of silica gel for adsorption desalination cycle. *Applied Thermal Engineering*. 2013;50:1596-602.
- [143] Y. Hamamoto, K. C. A. Alam, B. B. Saha, S. Koyama, A. Akisawa, T. Kashiwagi. Study on adsorption refrigeration cycle utilizing activated carbon fibers. Part 1. Adsorption characteristics. *International Journal of Refrigeration*. 2006;29:305-14.

- [144] İ. Solmuş, C. Yamalı, B. Kaftanoğlu, D. Baker, A. Çağlar. Adsorption properties of a natural zeolite–water pair for use in adsorption cooling cycles. *Applied Energy*. 2010;87:2062-7.
- [145] A. Gorbach, M. Stegmaier, G. Eigenberger. Measurement and Modeling of Water Vapor Adsorption on Zeolite 4A—Equilibria and Kinetics. *Adsorption*. 2004;10:29-46.
- [146] S. Kayal, S. Baichuan, B. B. Saha. Adsorption characteristics of AQSOA zeolites and water for adsorption chillers. *International Journal of Heat and Mass Transfer*. 2016;92:1120-7.
- [147] H. Wei Benjamin Teo, A. Chakraborty, W. Fan. Improved adsorption characteristics data for AQSOA types zeolites and water systems under static and dynamic conditions. *Microporous and Mesoporous Materials*. 2017;242:109-17.
- [148] Y. K. Ryu, S. J. Lee, J. W. Kim, C.-H. Leef. Adsorption equilibrium and kinetics of H₂O on zeolite 13x. *Korean Journal of Chemical Engineering*. 2001;18:525-30.
- [149] S. Mitra, P. Kumar, K. Srinivasan, P. Dutta. Performance evaluation of a two-stage silica gel + water adsorption based cooling-cum-desalination system. *International Journal of Refrigeration*. 2015.
- [150] A. Akahira, K. C. Amanul Alam, Y. Hamamoto, A. Akisawa, T. Kashiwagi. Mass recovery four-bed adsorption refrigeration cycle with energy cascading. *Applied Thermal Engineering*. 2005;25:1764-78.
- [151] K. C. A. Alam, A. Akahira, Y. Hamamoto, A. Akisawa, T. Kashiwagi. A four-bed mass recovery adsorption refrigeration cycle driven by low temperature waste/renewable heat source. *Renewable Energy*. 2004;29:1461-75.
- [152] D. Tang, D. Li, Y. Peng. Optimization to the tube–fin contact status of the tube expansion process. *Journal of Materials Processing Technology*. 2011;211:573-7.
- [153] Y. I. Aristov. Challenging offers of material science for adsorption heat transformation: A review. *Applied Thermal Engineering*. 2013;50:1610-8.
- [154] A. Rezk, R. Al-Dadah, S. Mahmoud, A. Elsayed. Characterisation of metal organic frameworks for adsorption cooling. *International Journal of Heat and Mass Transfer*. 2012;55:7366-74.
- [155] M. Verde, L. Cortés, J. M. Corberán, A. Sapienza, S. Vasta, G. Restuccia. Modelling of an adsorption system driven by engine waste heat for truck cabin A/C. Performance estimation for a standard driving cycle. *Applied Thermal Engineering*. 2010;30:1511-22.
- [156] MITSUBISHI PLASTICS, Zeolite, AQSOA. https://www.mpi.co.jp/english/products/industrial_materials/im010.html
- [157] J. A. Coelho, A. M. Ribeiro, A. F. P. Ferreira, S. M. P. Lucena, A. E. Rodrigues, D. C. S. d. Azevedo. Stability of an Al-Fumarate MOF and Its Potential for

- CO₂Capture from Wet Stream. *Industrial & Engineering Chemistry Research*. 2016;55:2134-43.
- [158] M. Rubio-Martinez, T. D. Hadley, M. P. Batten, K. Constanti-Carey, T. Barton, D. Marley, A. Monch, K. S. Lim, M. R. Hill. Scalability of Continuous Flow Production of Metal-Organic Frameworks. *ChemSusChem*. 2016;9:938-41.
- [159] E. Elsayed, R. Al-Dadah, S. Mahmoud, A. Elsayed, P. A. Anderson. Aluminium fumarate and CPO-27(Ni) MOFs: Characterization and Thermodynamic Analysis for Adsorption Heat Pump Applications. *Applied Thermal Engineering*. 2016;99:802-12.
- [160] E. Elsayed, R. Al-Dadah, S. Mahmoud, P. A. Anderson, A. Elsayed, P. G. Youssef. CPO-27(Ni), aluminium fumarate and MIL-101(Cr) MOF materials for adsorption water desalination. *Desalination*. 2016.
- [161] E. Haque, S. H. Jhung. Synthesis of isostructural metal–organic frameworks, CPO-27s, with ultrasound, microwave, and conventional heating: Effect of synthesis methods and metal ions. *Chemical Engineering Journal*. 2011;173:866-72.
- [162] E. Elsayed, H. Wang, P. A. Anderson, R. Al-Dadah, S. Mahmoud, H. Navarro, Y. Ding, J. Bowen. Development of MIL-101(Cr)/GrO composites for adsorption heat pump applications. *Microporous and Mesoporous Materials*. 2017;244:180-91.
- [163] W. Y. Hong, S. P. Perera, A. D. Burrows. Manufacturing of metal-organic framework monoliths and their application in CO₂ adsorption. *Microporous and Mesoporous Materials*. 2015;214:149-55.
- [164] C. A. Akisawa Asushi, Gao Lizhen, Kashiwagi Takao, Koyama Shigeru C O Kyushu Univ, Ng Kim Choon, Saha Bidyut Baran, Wang Xiao Ling. Apparatus and method for desalination. 2006.
- [165] F. Rouquerol, J. Rouquerol, K. Sing. *Adsorption by Powders and Porous Solids*. San Diego: Academic Press; 1999.
- [166] M. Suzuki. *Adsorption engineering*. Amsterdam: Kodansha ; Elsevier; 1990.
- [167] B. B. Saha, I. I. El-Sharkawy, M. W. Shahzad, K. Thu, L. Ang, K. C. Ng. Fundamental and application aspects of adsorption cooling and desalination. *Applied Thermal Engineering*. 2016;97:68-76.
- [168] H. T. Chua, K. C. Ng, A. Malek, T. Kashiwagi, A. Akisawa, B. B. Saha. Modeling the performance of two-bed, silica gel-water adsorption chillers. *International Journal of Refrigeration*. 1999;22:194-204.
- [169] B. Sun, A. Chakraborty. Thermodynamic formalism of water uptakes on solid porous adsorbents for adsorption cooling applications. *Applied Physics Letters*. 2014;104:201901.
- [170] J. Yan, Y. Yu, C. Ma, J. Xiao, Q. Xia, Y. Li, Z. Li. Adsorption isotherms and kinetics of water vapor on novel adsorbents MIL-101(Cr)@GO with super-high capacity. *Applied Thermal Engineering*. 2015;84:118-25.
- [171] D. D. Do. *Adsorption Analysis: Equilibria and Kinetics*. University of Queensland, Australia: Imperial College Press; 1998.

- [172] B. Shi, R. Al-Dadah, S. Mahmoud, A. Elsayed, E. Elsayed. CPO-27(Ni) metal-organic framework based adsorption system for automotive air conditioning. *Applied Thermal Engineering*. 2016;106:325-33.
- [173] S. K. Henninger, M. Schicktanz, P. P. C. Hügenell, H. Sievers, H. M. Henning. Evaluation of methanol adsorption on activated carbons for thermally driven chillers part I: Thermophysical characterisation. *International Journal of Refrigeration*. 2012;35:543-53.
- [174] Y. I. Aristov. Adsorptive transformation of heat: Principles of construction of adsorbents database. *Applied Thermal Engineering*. 2012;42:18-24.
- [175] S. Sircar, J. R. Hufton. Why Does the Linear Driving Force Model for Adsorption Kinetics Work? *Adsorption*. 2000;6:137-47.
- [176] E. Glueckauf. Theory of chromatography. Part 10-Formula for diffusion into spheres and their application to chromatography. *Trans Faraday Soc*. 1955;51:1540-51.
- [177] L. K. Wang, J. P. Chen, Y.-T. Hung, N. K. Shamma. *Membrane and Desalination Technologies*: Springer Science & Business Media; 2010.
- [178] V. H. Morcos. Performance of shell-and-dimpled-tube heat exchangers for waste heat recovery. *Heat Recovery Systems and CHP*. 1988;8:299-308.
- [179] J. H. Lienhard. *A Heat Transfer Text Book* Forth ed: Phlogiston Press Cambridge, Massachusetts, USA; 2016.
- [180] B. S. Petukhov. *Heat transfer and friction in turbulent pipe flow with variable physical properties*. New York: Academic Press, Inc.; 1970.
- [181] N. K. Choon, A. Chakraborty, S. M. Aye, W. Xiaolin. New pool boiling data for water with copper-foam metal at sub-atmospheric pressures: Experiments and correlation. *Applied Thermal Engineering*. 2006;26:1286-90.
- [182] F. P. Incropera. *Fundamentals of heat and mass transfer* / Frank P. Incropera, David P. DeWitt. fifth ed: New York ; Chichester : Wiley, 2002; 2002.
- [183] Mathworks help files.<https://uk.mathworks.com/help/simulink/ug/types-of-solvers.html>
- [184] P. G. Youssef, S. M. Mahmoud, R. K. Al-Dadah. Effect of Evaporator Temperature on the Performance of Water Desalination / Refrigeration Adsorption System Using AQSOA-ZO2. *International Journal of Environment, Chemical, Ecological, Geological Engineering*. 2015;9:679-83.
- [185] Electricity Rates Around the World.2015,<http://www.worldatlas.com/articles/electricity-rates-around-the-world.html>
- [186] P. G. Youssef, H. Dakkama, S. M. Mahmoud, R. K. Al-Dadah. Experimental investigation of adsorption water desalination/cooling system using CPO-27Ni MOF. *Desalination*. 2017;404:192-9.
- [187] H. J. Dakkama, P. G. Youssef, R. K. Al-Dadah, S. Mahmoud. Adsorption ice making and water desalination system using metal organic frameworks/water pair. *Energy Conversion and Management*. 2017;142:53-61.
- [188] Beta-Tech CU Series features.2012,<http://beta-techcontrols.co.uk>

- [189] R. W. Bonner. Correlation for dropwise condensation heat transfer: Water, organic fluids, and inclination. *International Journal of Heat and Mass Transfer*. 2013;61:245-53.
- [190] X. Wang, K. C. Ng, A. Chakarborty, B. B. Saha. How Heat and Mass Recovery Strategies Impact the Performance of Adsorption Desalination Plant: Theory and Experiments. *Heat Transfer Engineering*. 2007;28:147-53.
- [191] C. A. Hampel. Densities and Boiling Points of Sea Water Concentrates. *Industrial & Engineering Chemistry*. 1950;42:383-6.
- [192] A. Salhotra, E. Adams, D. Harleman. Effect of Salinity and Ionic Composition on Evaporation: Analysis of Dead Sea Evaporation Pans. *Water Resources Research*.21:1336-44.
- [193] A. M. Elsayed. Heat transfer in helically coiled small diameter tubes for miniature cooling systems. 2011.
- [194] K. Cheatle. *Fundamentals of test measurement instrumentation: Research Triangle Park, NC : ISA--Instrumentation, Systems, and Automation Society;* 2006.

Appendix I : Simulink Model

- Simulink model of conventional double bed system

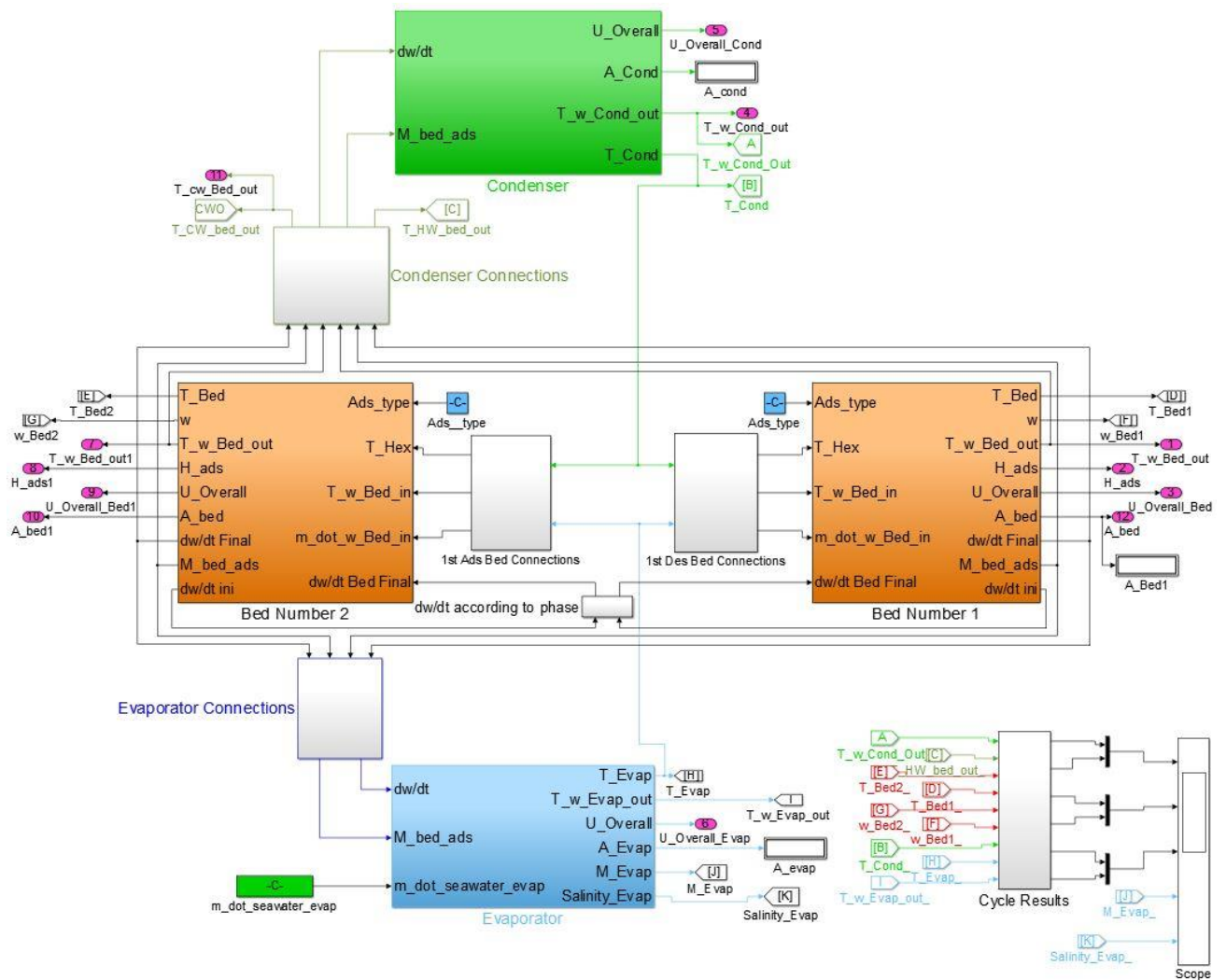


Figure A.I- 1, Main block diagram of the double bed system

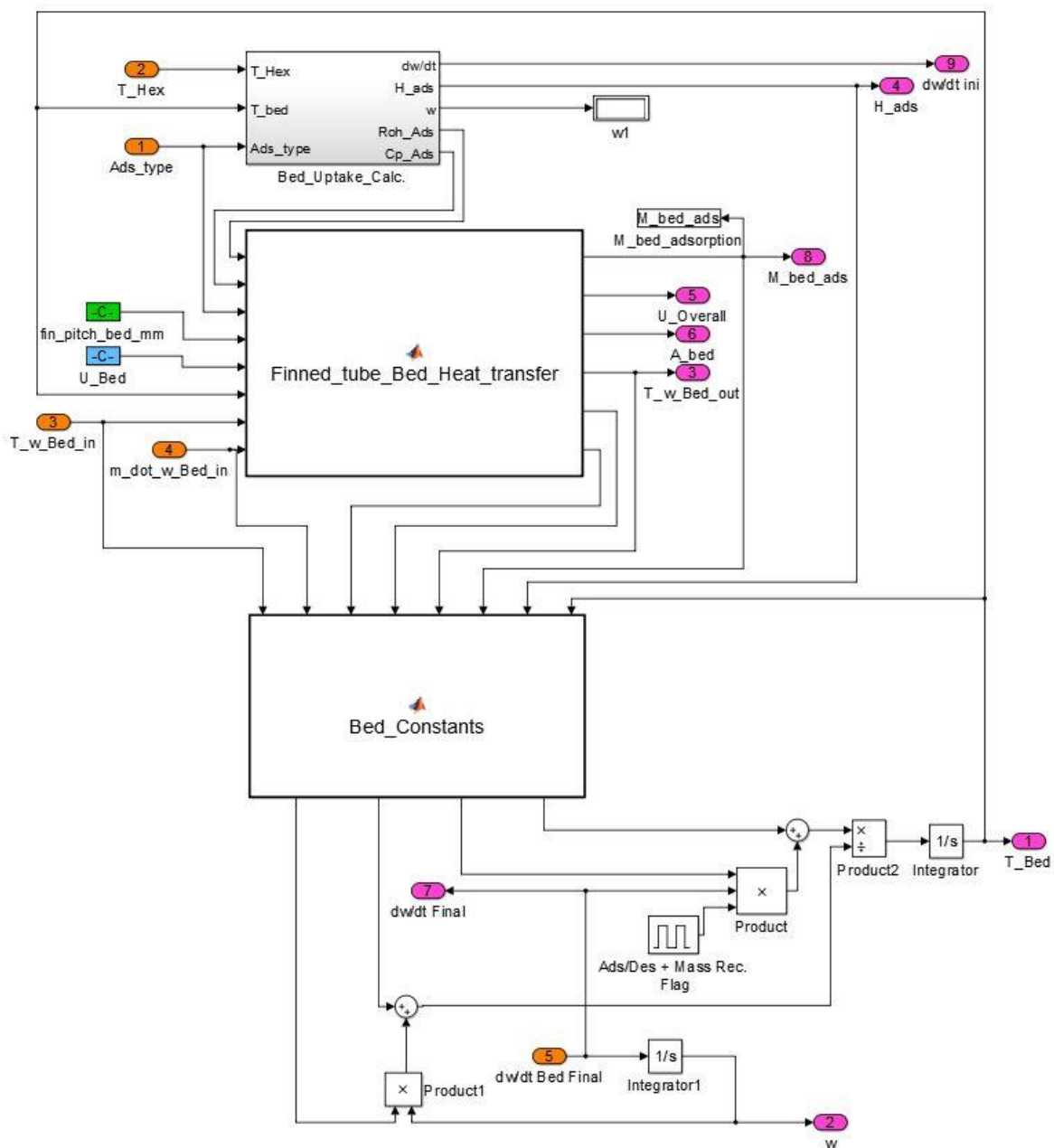


Figure A.I- 2, Simulink sub blocks of the Adsorption bed block (Double bed Cycle)

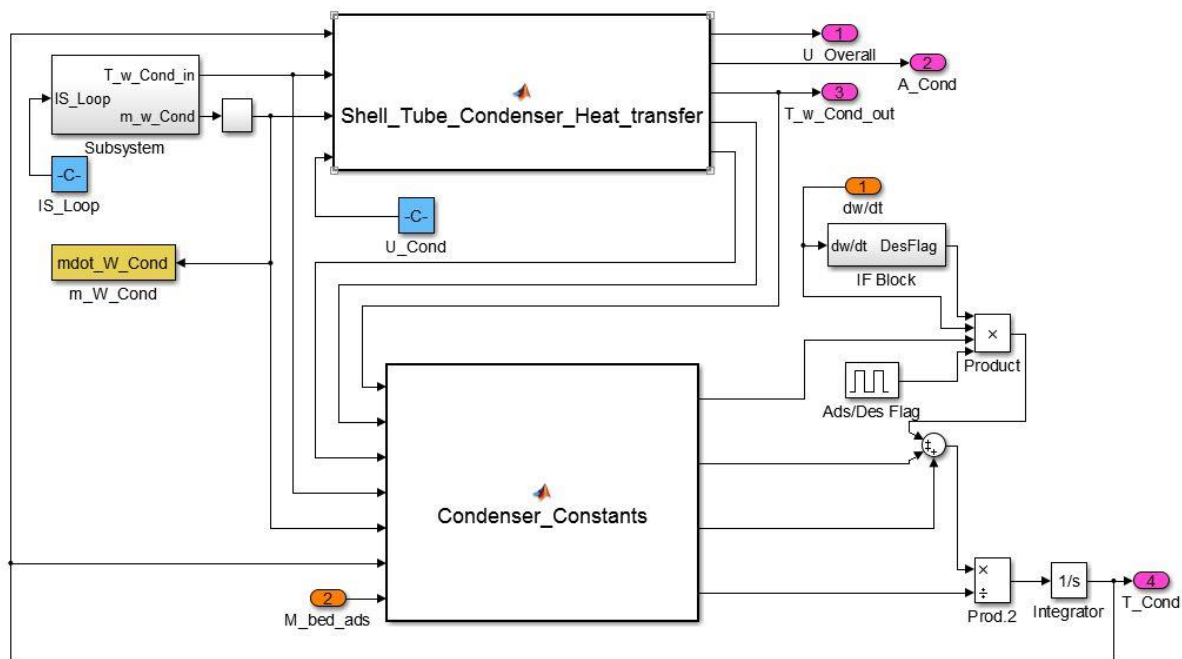


Figure A.I- 4, Simulink sub blocks of the Condenser block (Double bed Cycle)

- Simulink model of the new integrated adsorption cycle

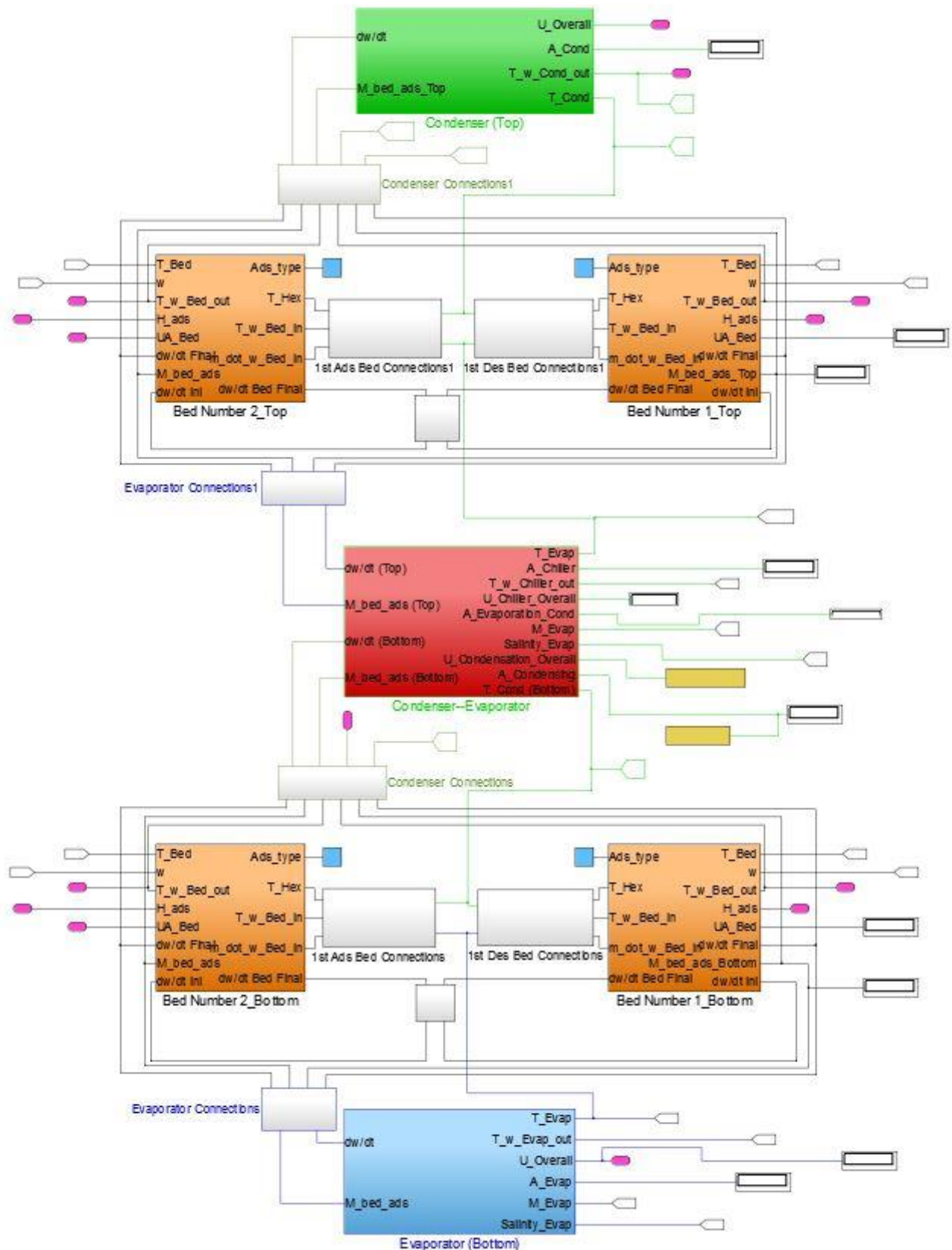


Figure A.I- 5, Main block diagram of the integrated adsorption desalination/cooling cycle

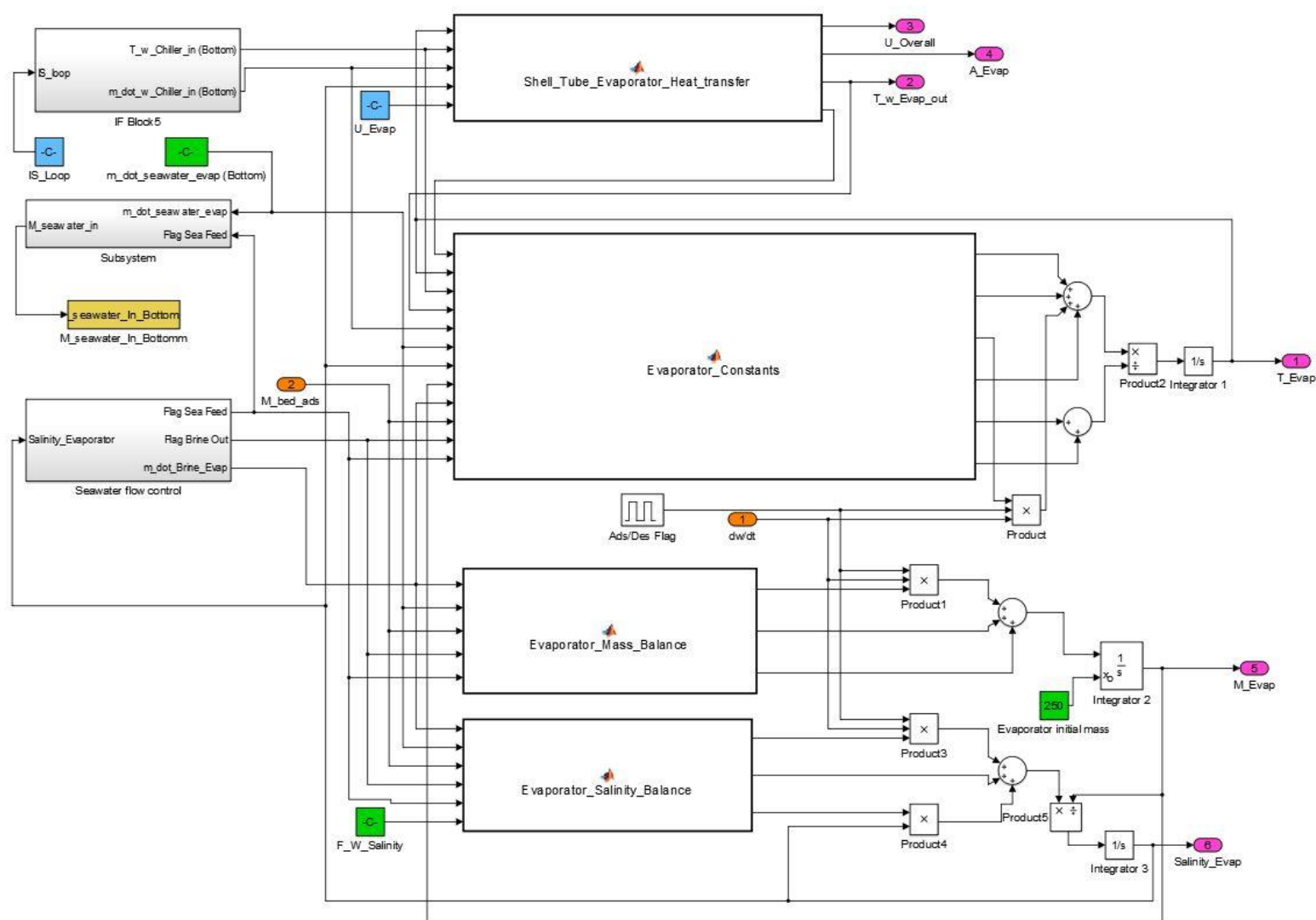


Figure A.I- 7, Simulink sub blocks of the Lower Evaporator block (Integrated Cycle)

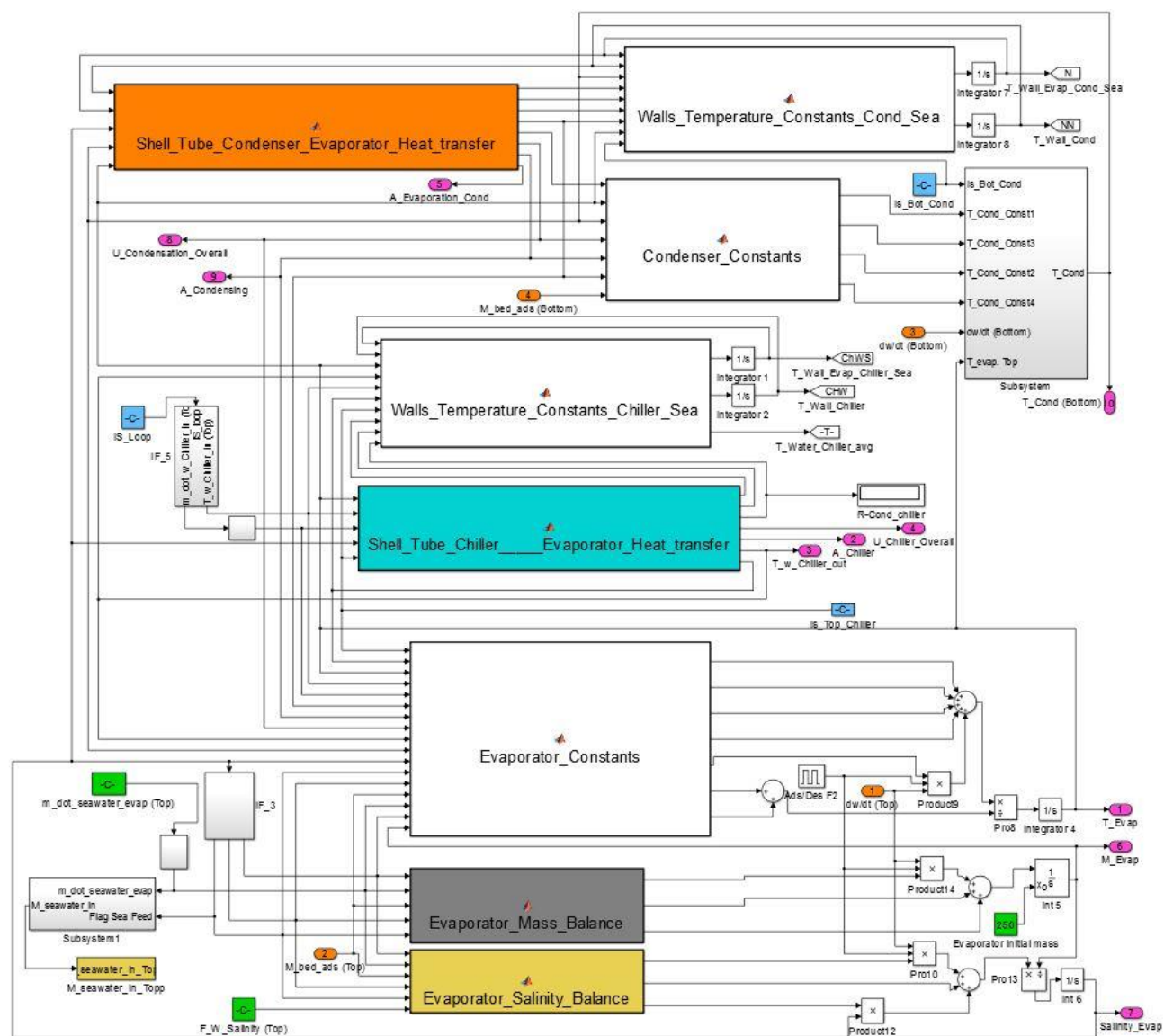


Figure A.I- 8, Simulink sub blocks of the Combined Evaporator-Condenser block (Integrated Cycle)

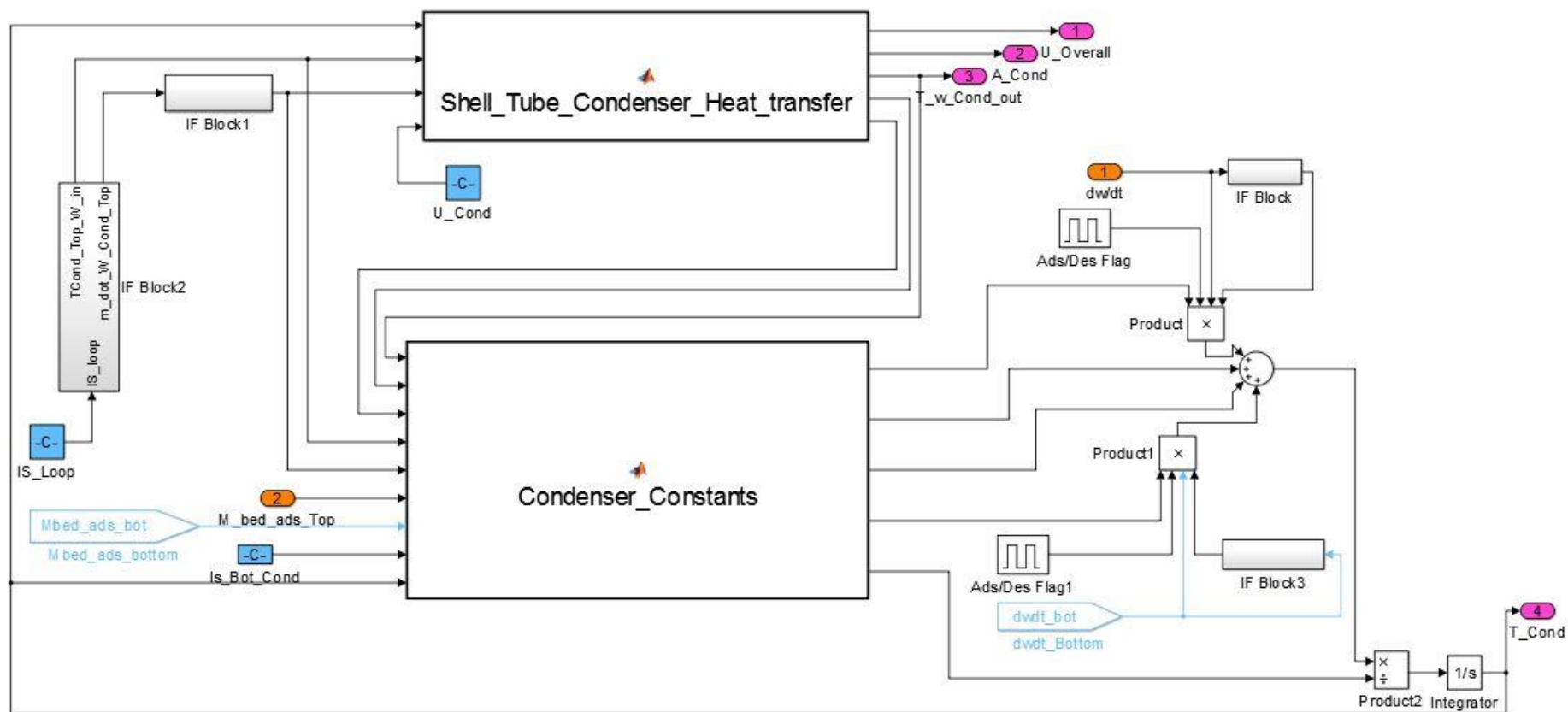


Figure A.I- 9, Simulink sub blocks of the Upper Condenser block (Integrated Cycle)

Appendix II : Uncertainty Calculations

Different factors affect the accuracy of measuring instruments which are categorized as random (Precision) and systematic (Bias) errors. Systematic errors ($U_{\text{systematic}}$) are constant at all readings; therefore they can be estimated from the calibration process. In case of random errors (U_{random}), their value is not the same at all times therefore their values has to be estimated by the uncertainty analysis. As the random (repeatability) errors are statistical in nature, they can be calculated using the mean standard deviation with 95% confidence level while the overall uncertainty can be calculated using equations (A.II-1 to A.II-3) [193, 194]

$$U_{\text{overall}} = \pm \sqrt{U_{\text{systematic}}^2 + U_{\text{random}}^2} \quad (\text{A.II-1})$$

$$U_{\text{random}} = t_{n-1, 95\%} \cdot S_{\bar{x}} \quad (\text{A.II-2})$$

$$S_{\bar{x}} = \frac{1}{\sqrt{n}} \sqrt{\frac{1}{(n-1)} \sum_{i=1}^n (X_i - \bar{X})^2} \quad (\text{A.II-3})$$

Where, $t_{n-1, 95\%}$ is the student distribution factor for a degree of freedom equals to (n-1), n is the number of data points in the sample, $S_{\bar{x}}$ is the standard deviation of the mean, X_i is the standard reading (alcohol thermometer or standard pressure gauge), \bar{X} is the curve fit value and $(X_i - \bar{X})$ is the deviation [193, 194]

As presented in section 6.3, pressure transducers and thermocouples were used to measure pressure and temperature in both testing facilities. As shown in Figure A.II- 1, thermocouples are calibrated against standard alcohol thermometer where water bath temperature is varied at several steps and the thermocouples readings are recorded as well

as readings of the standard alcohol thermometer. Pressure transducers are calibrated using a standard vacuum gauge as shown in Figure A.II- 2, and the pressure readings are recorded using the data logger.

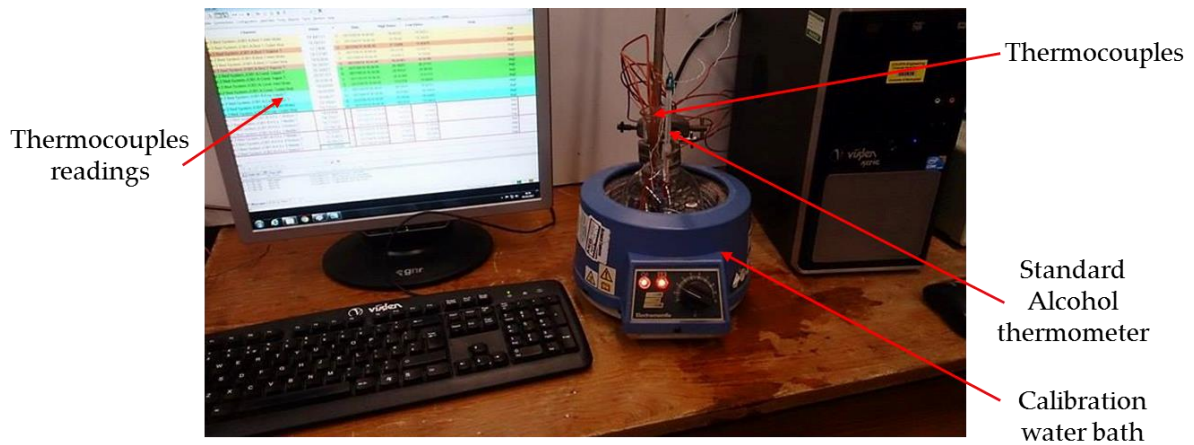


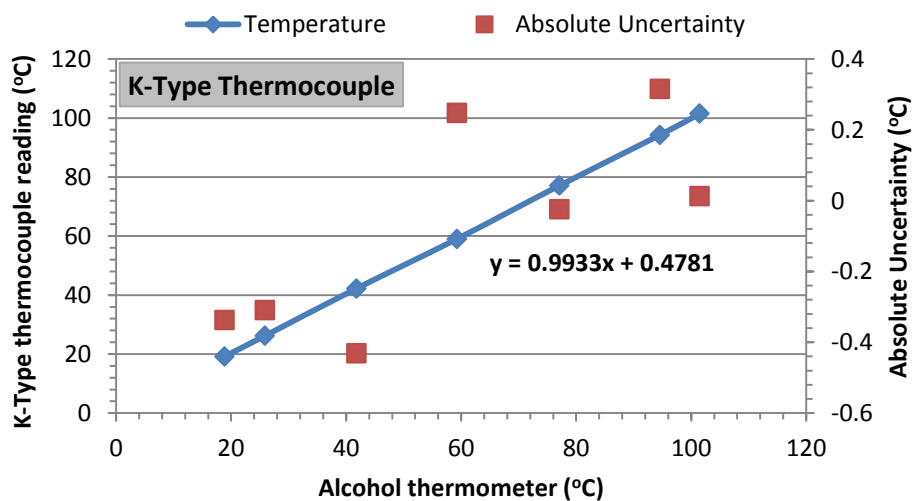
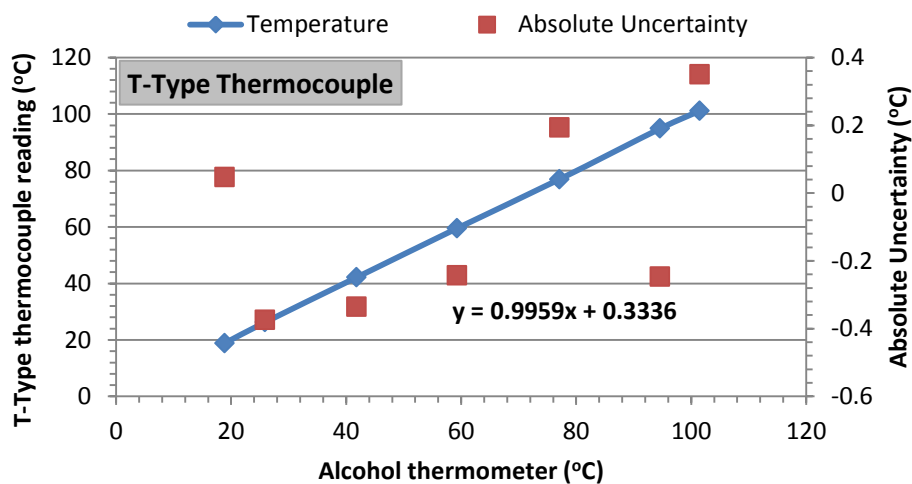
Figure A.II- 1, Thermocouples calibration kit



Figure A.II- 2, Pressure transducer calibration kit

- *Single bed measuring devices uncertainty calculations*

In this system, there are seven thermocouples of type “T” located in the adsorber bed and the evaporator in addition to two thermocouples of type “K” located in the condenser while three pressure transducers are used to measure pressures of adsorber bed, evaporator and condenser. The absolute uncertainty defined as the difference between standard and measured readings, is calculated for temperature and pressure measuring devices at each measured point and sample calibration charts are shown in Figure A.II- 3 and Figure A.II- 4 for temperature and pressure measurements respectively. The overall uncertainties for all thermocouples and pressure transducers are listed in Table A.II- 1 and Table A.II- 2.



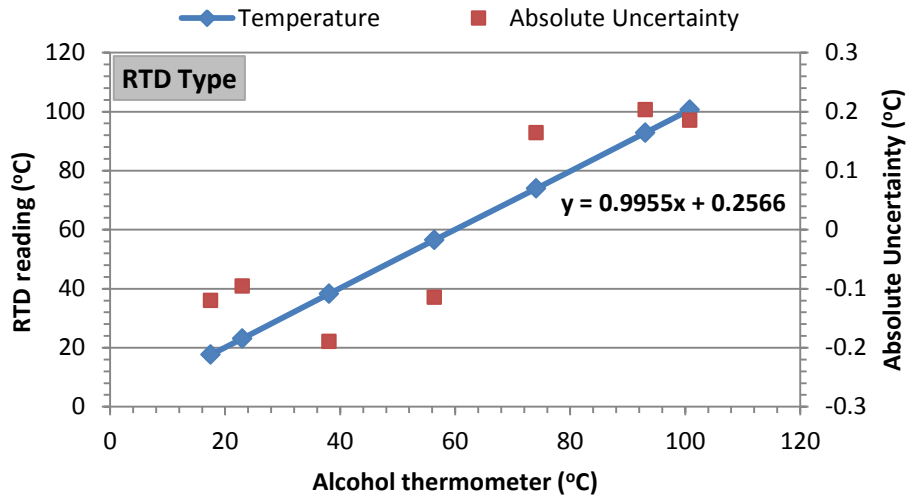


Figure A.II- 3, Calibration chart for different types of thermocouples, Single-bed system

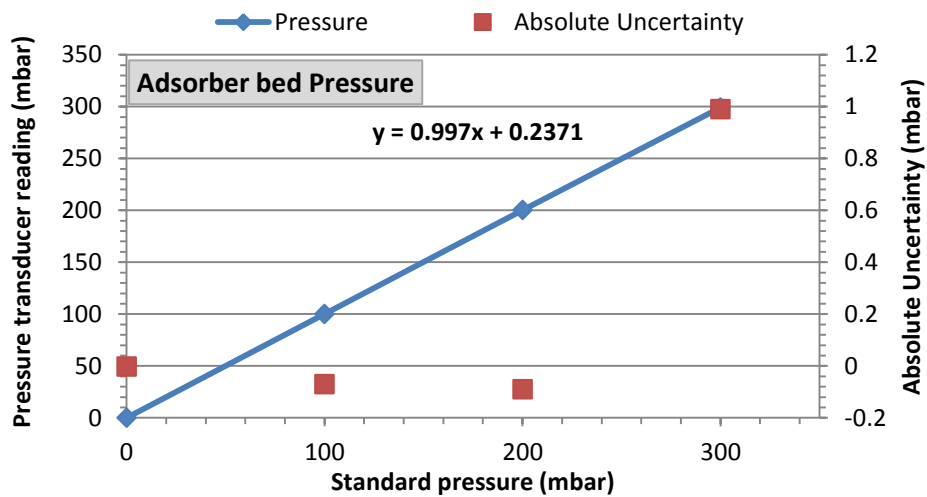


Figure A.II- 4, Calibration chart for adsorber bed pressure transducer, Single-bed system

Table A.II- 1, Uncertainties of all thermocouples of the single bed adsorption system

T/C Type	Number	Location	Curve fit formula	Absolute Uncertainty	Random Uncertainty	Overall Uncertainty
Type-T	T-1	Adsorber bed: 1 st H.Ex. Centre	$1.0011 \cdot T_{ref} + 0.0840$	$\pm 0.457 \text{ }^\circ\text{C}$	$\pm 0.381 \text{ }^\circ\text{C}$	$\pm 0.386 \text{ }^\circ\text{C}$
	T-2	Adsorber bed: 1 st H.Ex. Bottom	$0.9971 \cdot T_{ref} + 0.2773$	$\pm 0.414 \text{ }^\circ\text{C}$	$\pm 0.322 \text{ }^\circ\text{C}$	$\pm 0.327 \text{ }^\circ\text{C}$
	T-3	Adsorber bed: 2 nd H.Ex. Centre	$0.9958 \cdot T_{ref} + 0.3335$	$\pm 0.374 \text{ }^\circ\text{C}$	$\pm 0.380 \text{ }^\circ\text{C}$	$\pm 0.384 \text{ }^\circ\text{C}$
	T-4	Adsorber bed: 2 nd H.Ex. Bottom	$0.9999 \cdot T_{ref} + 0.1814$	$\pm 0.398 \text{ }^\circ\text{C}$	$\pm 0.408 \text{ }^\circ\text{C}$	$\pm 0.413 \text{ }^\circ\text{C}$
	T-5	Adsorber bed: Vapour	$1.0000 \cdot T_{ref} + 0.0704$	$\pm 0.437 \text{ }^\circ\text{C}$	$\pm 0.408 \text{ }^\circ\text{C}$	$\pm 0.413 \text{ }^\circ\text{C}$
	T-6	Evaporator: Seawater	$0.9998 \cdot T_{ref} + 0.2169$	$\pm 0.458 \text{ }^\circ\text{C}$	$\pm 0.482 \text{ }^\circ\text{C}$	$\pm 0.486 \text{ }^\circ\text{C}$
	T-7	Evaporator: Vapour	$0.9990 \cdot T_{ref} + 0.2909$	$\pm 0.374 \text{ }^\circ\text{C}$	$\pm 0.483 \text{ }^\circ\text{C}$	$\pm 0.487 \text{ }^\circ\text{C}$
Type-K	T-8	Condenser: Potable water	$1.0000 \cdot T_{ref} + 0.1050$	$\pm 0.482 \text{ }^\circ\text{C}$	$\pm 0.378 \text{ }^\circ\text{C}$	$\pm 0.382 \text{ }^\circ\text{C}$
	T-9	Condenser: Vapour	$0.9932 \cdot T_{ref} + 0.4781$	$\pm 0.431 \text{ }^\circ\text{C}$	$\pm 0.467 \text{ }^\circ\text{C}$	$\pm 0.471 \text{ }^\circ\text{C}$
RTD	T-10	Adsorber bed: Inlet water (cooling/heating)	$0.9976 \cdot T_{ref} + 0.0524$	$\pm 0.289 \text{ }^\circ\text{C}$	$\pm 0.272 \text{ }^\circ\text{C}$	$\pm 0.279 \text{ }^\circ\text{C}$
	T-11	Adsorber bed: Outlet water (cooling/heating)	$0.9954 \cdot T_{ref} + 0.2566$	$\pm 0.203 \text{ }^\circ\text{C}$	$\pm 0.287 \text{ }^\circ\text{C}$	$\pm 0.293 \text{ }^\circ\text{C}$
	T-12	Evaporator: Inlet chilled water	$0.9986 \cdot T_{ref} + 0.0108$	$\pm 0.226 \text{ }^\circ\text{C}$	$\pm 0.229 \text{ }^\circ\text{C}$	$\pm 0.237 \text{ }^\circ\text{C}$
	T-13	Evaporator: Outlet chilled water	$0.9960 \cdot T_{ref} + 0.2101$	$\pm 0.229 \text{ }^\circ\text{C}$	$\pm 0.257 \text{ }^\circ\text{C}$	$\pm 0.264 \text{ }^\circ\text{C}$
	T-14	Condenser: Inlet cooling water	$0.9968 \cdot T_{ref} + 0.2539$	$\pm 0.279 \text{ }^\circ\text{C}$	$\pm 0.257 \text{ }^\circ\text{C}$	$\pm 0.264 \text{ }^\circ\text{C}$
	T-15	Condenser: Outlet cooling water	$0.9960 \cdot T_{ref} + 0.3015$	$\pm 0.241 \text{ }^\circ\text{C}$	$\pm 0.291 \text{ }^\circ\text{C}$	$\pm 0.297 \text{ }^\circ\text{C}$

Table A.II- 2, Uncertainties of pressure transducers' measurements of the single-bed adsorption testing facility

Number	Location	Curve fit formula	Absolute Uncertainty	Random Uncertainty	Overall Uncertainty
P-1	Adsorber bed	$0.9970 \cdot P_{\text{ref}} + 0.2371$	± 0.99 mbar	± 1.539 mbar	± 1.771 mbar
P-2	Evaporator	$1.0021 \cdot P_{\text{ref}} - 0.0320$	± 1.1 mbar	± 1.601 mbar	± 1.825 mbar
P-3	Condenser	$0.9972 \cdot P_{\text{ref}} + 0.6200$	± 0.9 mbar	± 1.781 mbar	± 1.984 mbar

- *Double bed measuring devices uncertainty calculations*

In this system there are ten thermocouples of type-K and eight of the RTD type while four pressure transducers were used in the system. Thermocouples and pressure transducers were calibrated as in Figure A.II- 1 and Figure A.II- 2 respectively. A sample of the thermocouples and pressure transducers calibration charts are shown in Figure A.II- 5 and Figure A.II- 6 respectively and their overall uncertainties are presented in Table A.II- 3 and Table A.II- 4 respectively.

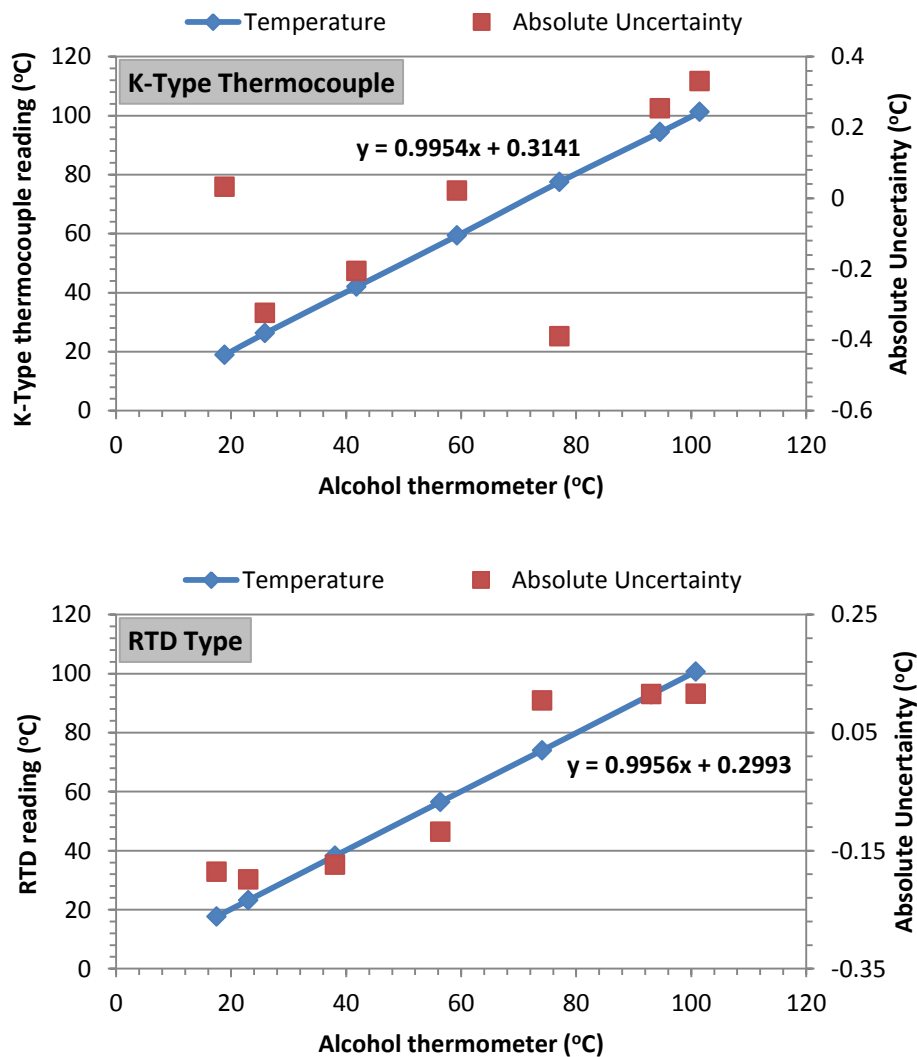


Figure A.II- 5, Calibration chart for different types of thermocouples, Double-bed system

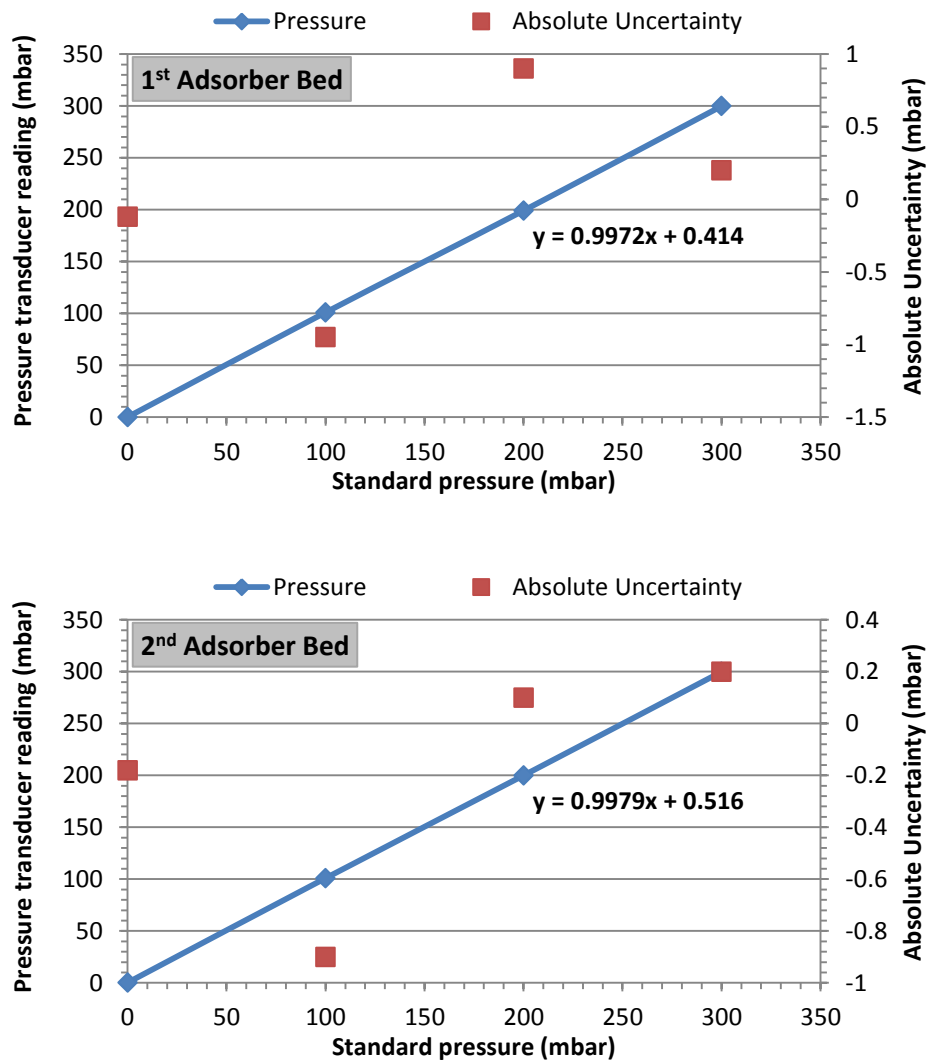


Figure A.II- 6, Calibration chart for adsorber beds' pressure transducers, Double-bed system

Table A.II- 3, Uncertainties of all thermocouples of the double bed adsorption system

T/C Type	Number	Location	Curve fit formula	Absolute Uncertainty	Random Uncertainty	Overall Uncertainty
Type- K	T-1	1 st Adsorber bed: H.Ex. Centre	$0.9992^* T_{ref} + 0.0756$	$\pm 0.346^{\circ}\text{C}$	$\pm 0.256^{\circ}\text{C}$	$\pm 0.263^{\circ}\text{C}$
	T-2	1 st Adsorber bed: H.Ex. Bottom	$0.9984^* T_{ref} + 0.3155$	$\pm 0.441^{\circ}\text{C}$	$\pm 0.486^{\circ}\text{C}$	$\pm 0.490^{\circ}\text{C}$
	T-3	1 st Adsorber bed: Vapour	$0.9954^* T_{ref} + 0.3141$	$\pm 0.390^{\circ}\text{C}$	$\pm 0.358^{\circ}\text{C}$	$\pm 0.363^{\circ}\text{C}$
	T-4	2 nd Adsorber bed: H.Ex. Centre	$0.9996^* T_{ref} + 0.1244$	$\pm 0.408^{\circ}\text{C}$	$\pm 0.320^{\circ}\text{C}$	$\pm 0.325^{\circ}\text{C}$
	T-5	2 nd Adsorber bed: H.Ex. Bottom	$1.0013^* T_{ref} + 0.0462$	$\pm 0.390^{\circ}\text{C}$	$\pm 0.325^{\circ}\text{C}$	$\pm 0.331^{\circ}\text{C}$
	T-6	2 nd Adsorber bed: Vapour	$0.9991^* T_{ref} + 0.2860$	$\pm 0.450^{\circ}\text{C}$	$\pm 0.496^{\circ}\text{C}$	$\pm 0.500^{\circ}\text{C}$
	T-7	Evaporator: Seawater	$0.9961^* T_{ref} + 0.2182$	$\pm 0.316^{\circ}\text{C}$	$\pm 0.274^{\circ}\text{C}$	$\pm 0.280^{\circ}\text{C}$
	T-8	Evaporator: Vapour	$1.0004^* T_{ref} - 0.0022$	$\pm 0.310^{\circ}\text{C}$	$\pm 0.223^{\circ}\text{C}$	$\pm 0.231^{\circ}\text{C}$
	T-9	Condenser: Potable water	$0.9986^* T_{ref} + 0.2881$	$\pm 0.401^{\circ}\text{C}$	$\pm 0.446^{\circ}\text{C}$	$\pm 0.450^{\circ}\text{C}$
	T-10	Condenser: Vapour	$0.9974^* T_{ref} + 0.1942$	$\pm 0.324^{\circ}\text{C}$	$\pm 0.270^{\circ}\text{C}$	$\pm 0.277^{\circ}\text{C}$
RTD	T-11	1 st Adsorber bed: Inlet water (cooling/heating)	$0.9994^* T_{ref} - 0.0497$	$\pm 0.313^{\circ}\text{C}$	$\pm 0.270^{\circ}\text{C}$	$\pm 0.276^{\circ}\text{C}$
	T-12	1 st Adsorber bed: Outlet water (cooling/heating)	$0.9982^* T_{ref} + 0.0060$	$\pm 0.309^{\circ}\text{C}$	$\pm 0.260^{\circ}\text{C}$	$\pm 0.267^{\circ}\text{C}$
	T-13	2 nd Adsorber bed: Inlet water (cooling/heating)	$0.9956^* T_{ref} + 0.2993$	$\pm 0.198^{\circ}\text{C}$	$\pm 0.286^{\circ}\text{C}$	$\pm 0.293^{\circ}\text{C}$
	T-14	2 nd Adsorber bed: Outlet water (cooling/heating)	$0.9966^* T_{ref} + 0.2512$	$\pm 0.285^{\circ}\text{C}$	$\pm 0.267^{\circ}\text{C}$	$\pm 0.273^{\circ}\text{C}$
	T-15	Evaporator: Inlet chilled water	$0.9971^* T_{ref} + 0.1747$	$\pm 0.237^{\circ}\text{C}$	$\pm 0.289^{\circ}\text{C}$	$\pm 0.207^{\circ}\text{C}$
	T-16	Evaporator: Outlet chilled water	$1.0005^* T_{ref} + 0.0365$	$\pm 0.189^{\circ}\text{C}$	$\pm 0.198^{\circ}\text{C}$	$\pm 0.179^{\circ}\text{C}$
	T-17	Condenser: Inlet cooling water	$0.9963^* T_{ref} + 0.2902$	$\pm 0.279^{\circ}\text{C}$	$\pm 0.169^{\circ}\text{C}$	$\pm 0.295^{\circ}\text{C}$
	T-18	Condenser: Outlet cooling water	$0.9958^* T_{ref} + 0.2485$	$\pm 0.307^{\circ}\text{C}$	$\pm 0.285^{\circ}\text{C}$	$\pm 0.292^{\circ}\text{C}$

Table A.II- 4, Uncertainties of pressure transducers' measurements of the double-bed adsorption testing facility

Number	Location	Curve fit formula	Absolute Uncertainty	Random Uncertainty	Overall Uncertainty
P-1	1 st Adsorber bed	$0.9971 \cdot P_{\text{ref}} + 0.4140$	± 0.95 mbar	± 1.575 mbar	± 1.801 mbar
P-2	2 nd Adsorber bed	$0.9978 \cdot P_{\text{ref}} + 0.5160$	± 0.90 mbar	± 1.308 mbar	± 1.574 mbar
P-3	Evaporator	$0.9997 \cdot P_{\text{ref}} + 0.1440$	± 0.5 mbar	± 0.611 mbar	± 1.067 mbar
P-4	Condenser	$0.9992 \cdot P_{\text{ref}} + 0.0784$	± 0.85 mbar	± 0.916 mbar	± 1.267 mbar

- *Uncertainty of calculated SDWP and SCP*

When an experimental result (y) is a function of (i) independent variables (x_1, x_2, \dots, x_i), the uncertainty in the result y is given by [193]:

$$U_y = \pm \sqrt{\left[\frac{\partial y}{\partial x_1} U_{x_1}\right]^2 + \left[\frac{\partial y}{\partial x_2} U_{x_2}\right]^2 + \dots + \left[\frac{\partial y}{\partial x_i} U_{x_i}\right]^2} \quad (\text{A.II-4})$$

The specific daily water production is given by

$$\text{SDWP (m}^3 \cdot \text{tonne}^{-1} \cdot \text{day}^{-1}) = \frac{\text{Collected amount of water (Litre)} \times 60 \times 24}{\text{Adsorber mass (kg)} \times \text{No. of cycles} \times \text{Total cycle time (min)}} \quad (\text{A.II-5})$$

Therefore the following equation can be used to estimate the uncertainty in its calculation:

$$\frac{U_{\text{SDWP}}}{\text{SDWP}} = \sqrt{\left[\frac{U_{\text{collected water amount}}}{\text{collected water amount}}\right]^2 + \left[\frac{U_{\text{Adsorber mass}}}{\text{Adsorber mass}}\right]^2} \quad (\text{A.II-6})$$

Where

$U_{\text{collected water amount}}$ is the uncertainty in the reading of the collected water amount. The amount of collected water was measured using graduated cylinder with an uncertainty of 0.01 litres.

$U_{\text{Adsorber mass}}$ is the uncertainty in the reading of the adsorbent mass. The amount of packed adsorbent mass was measured using a digital balance with an uncertainty of 0.001 kg.

By substituting in equation A.II-6 with the above values, it is found that the uncertainty in calculating the SDWP is in the range of 0.43% at high water production rates to 2.1% at the lowest water production rate.

The specific cooling power is given by

$$\text{SCP (W.kg}^{-1}\text{)} = \frac{\dot{m}_{Evap.} (\text{kg.s}^{-1}). C_p (\text{J.kg}^{-1}\text{K}^{-1}). (T_{Evap.i} - T_{Evap.o})(K)}{\text{Adsorber mass (kg)}} \quad (\text{A.II-7})$$

The uncertainty equation for calculating the specific cooling power (SCP) is given by

$$\frac{U_{\text{SCP}}}{\text{SCP}} = \sqrt{\left[\frac{U_{\dot{m}_{Evap.}}}{\dot{m}_{Evap.}}\right]^2 + \left[\frac{U_{C_p}}{C_p}\right]^2 + \left[\frac{U_{T_{Evap.in}}}{T_{Evap.i} - T_{Evap.o}}\right]^2 + \left[\frac{U_{T_{Evap.out}}}{T_{Evap.i} - T_{Evap.o}}\right]^2 + \left[\frac{U_{\text{Adsorber mass}}}{\text{Adsorber mass}}\right]^2} \quad (\text{A.II-8})$$

Where

$U_{\dot{m}_{Evap.}}$ is the uncertainty in the reading of the evaporator water flow rate. The evaporator water flow rate was measured using flow meter with an uncertainty of 0.25 L.min⁻¹.

U_{C_p} is the uncertainty in water specific heat. Since the specific heat was obtained from tabulated property data, the uncertainty in its value is negligible.

$U_{T_{Evap.in}}$ is the uncertainty in evaporator inlet water temperature. From Table A.II- 3, the uncertainty of this temperature measurement is 0.207°C.

$U_{T_{Evap.out}}$ is the uncertainty in evaporator outlet water temperature. From Table A.II- 3, the uncertainty of this temperature measurement is 0.179°C.

By substituting in equation A.II-8 with the above values, it is found that the uncertainty in calculating the SCP is in the range of 8.9% at high chilled water temperature difference to 17.4% at the lowest chilled water temperature difference. However, these values represent the pessimistic option of treating the temperature measurements as independent variables, thus the uncertainty in each temperature measurement was taken regardless of the effect of the uncertainty of the other temperature measurements. Knowing that all the thermocouples

were made from the same material and in the same way, it will be expected that they will respond similarly to each other. Therefore, the error in one thermocouple will be similar to the error in others, consequently the error in measuring the temperature difference should decrease and the results of the SCP uncertainty would decrease significantly.

Appendix III: Labview Control Code

Figure A.III- 1 shows the front panel of the Labview code where adsorption/desorption, mass recovery, switching times are entered to the program. In addition, a preparation time is entered before real cycle is started and finally number of cycles needed before system stops.

Monitoring panel is located on the right where different indicators exist to show which bed is connected to evaporator or condenser, whether it is heated or cooled and finally which phase is running (i.e. Adsorption/desorption, mass recovery or switching). Figure A.III- 2 shows the main block diagram of the labview code where “True” of “False” conditions are given to the Data Acquisition (DAQ) port which in turn controls the electrically actuated valves through a relay board.

In this code, there is a case structure that contains 8 different cases for different operating scenarios during system running. These cases are listed below while their corresponding figures are shown further below.

1. “Drying”, (Two adsorber beds are heated), Figure A.III- 3.
2. “Preparation” (1st Bed Heating – 2nd Bed Cooling), Figure A.III- 4.
3. “Switching 1” (1st Bed Cooling - 2nd Bed Heating), Figure A.III- 5.
4. “Ads-Des” (1st Bed Adsorption - 2nd Bed Desorption), Figure A.III- 6.
5. “Mass rec. 1” (Mass recovery after 1st half cycle), Figure A.III- 7.
6. “Switching 2” (1st Bed Heating - 2nd Bed Cooling), Figure A.III- 8.
7. “Des- Ads” (1st Bed Desorption - 2nd Bed Adsorption), Figure A.III- 9.
8. “Mass rec. 2” (Mass recovery after 2nd half cycle), Figure A.III- 10.

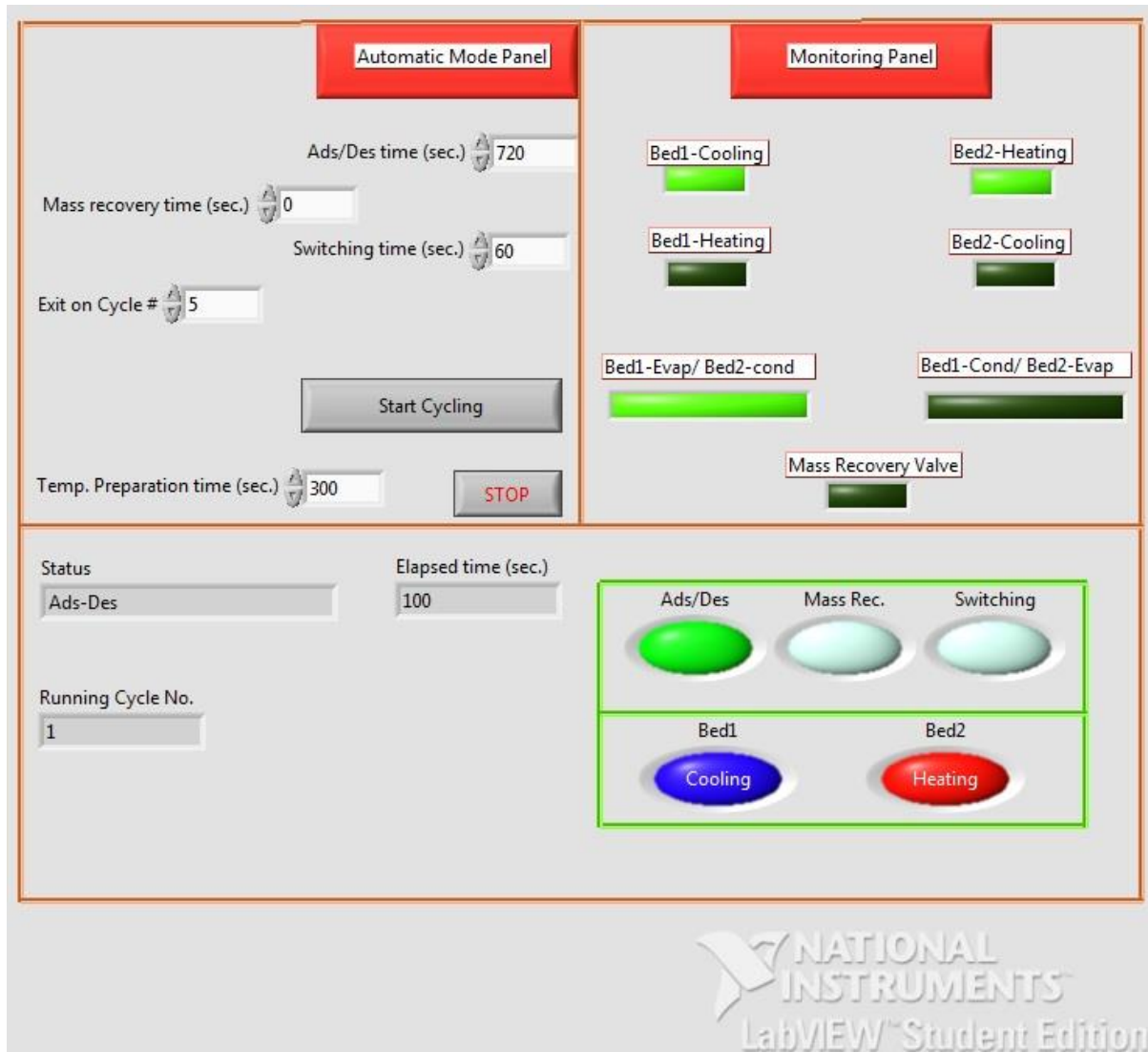


Figure A.III- 1, Front panel of the Labview code

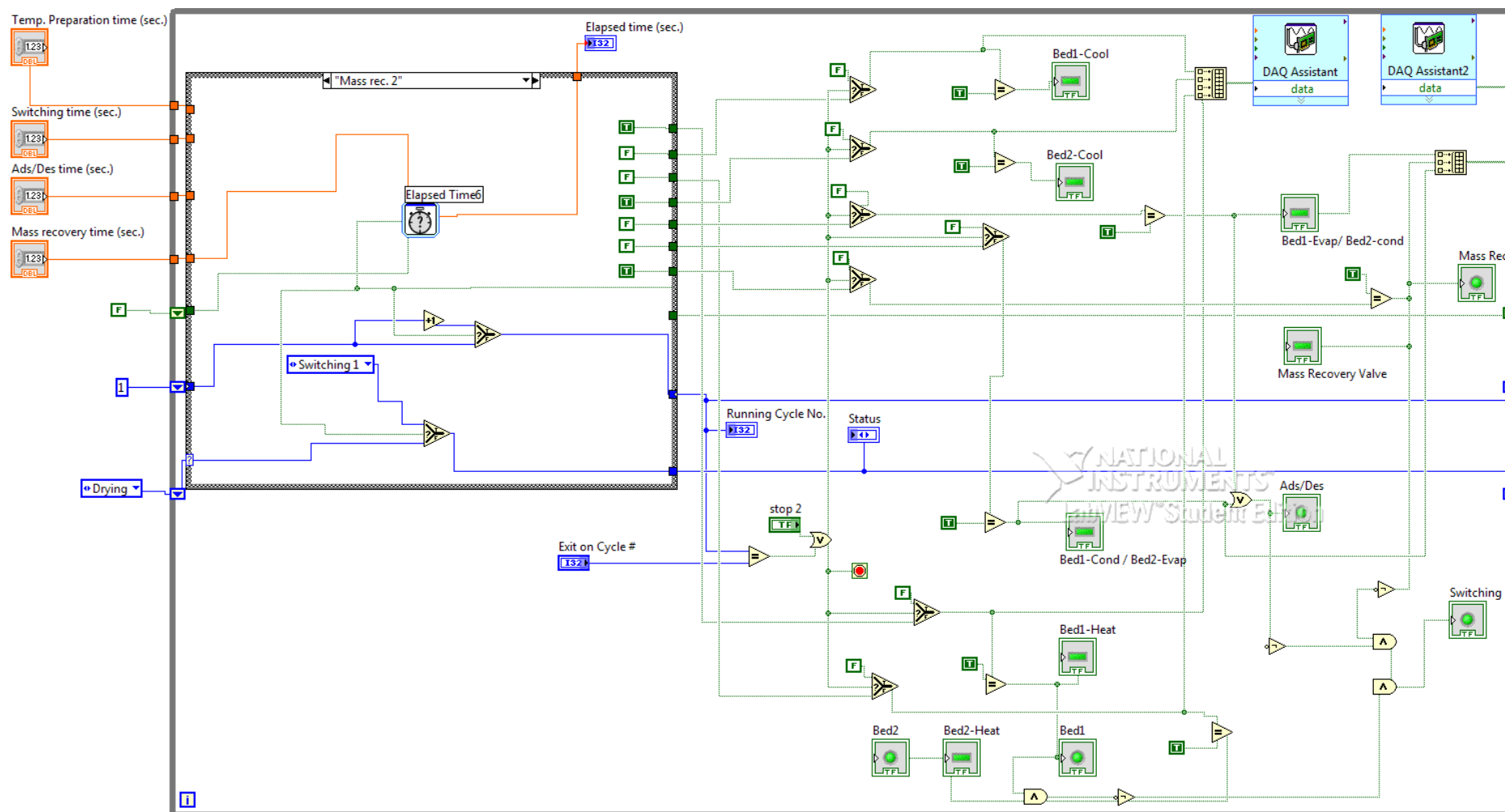


Figure A.III- 2, Main block diagram of the Labview control code

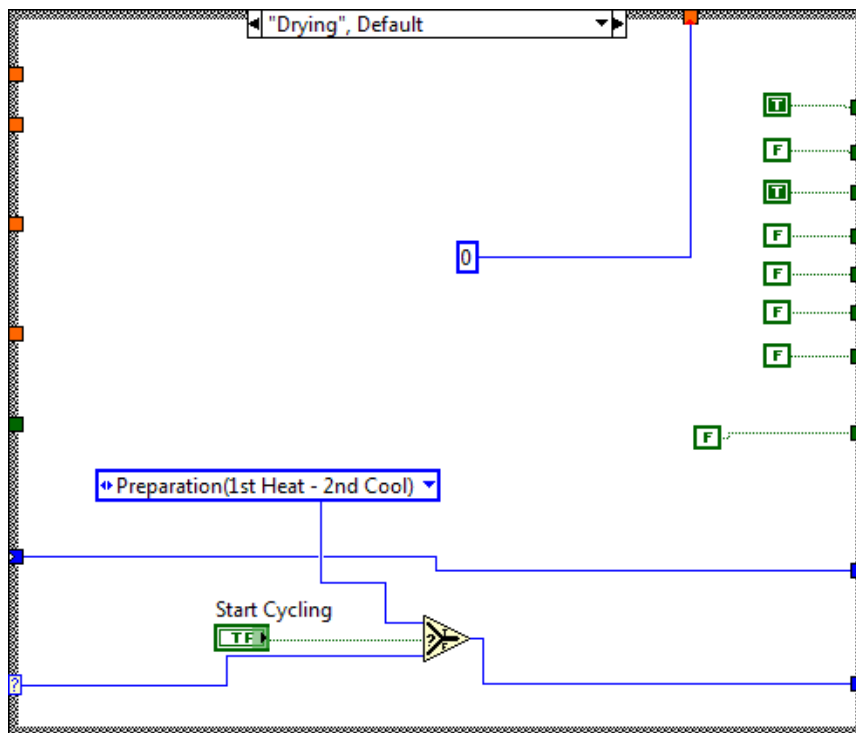


Figure A.III- 3, Case no. 1, "Drying"

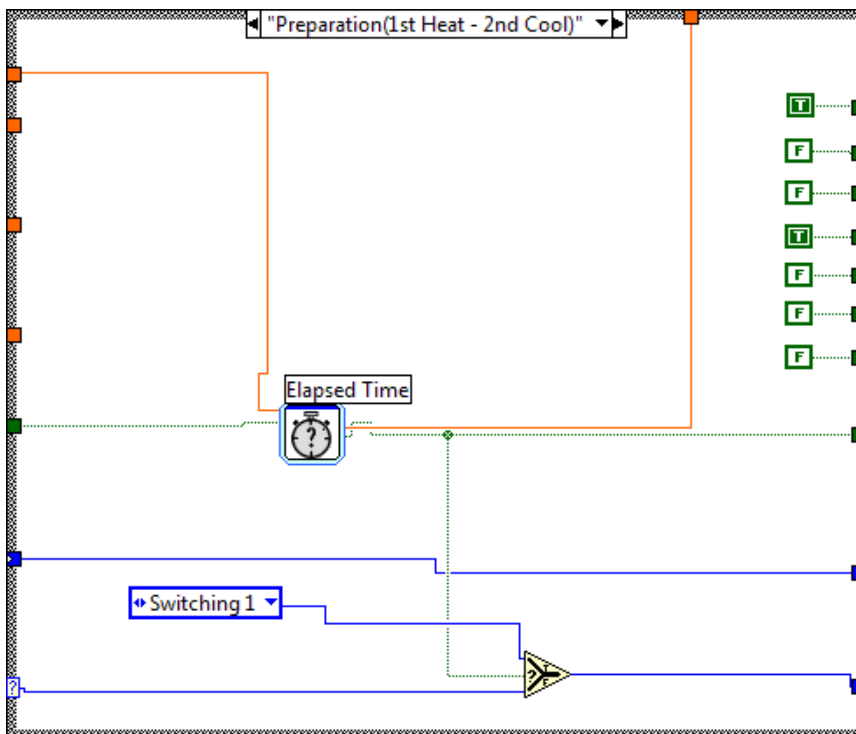


Figure A.III- 4, Case no. 2, "Adsorber bed temperature preparation before cycle starting"

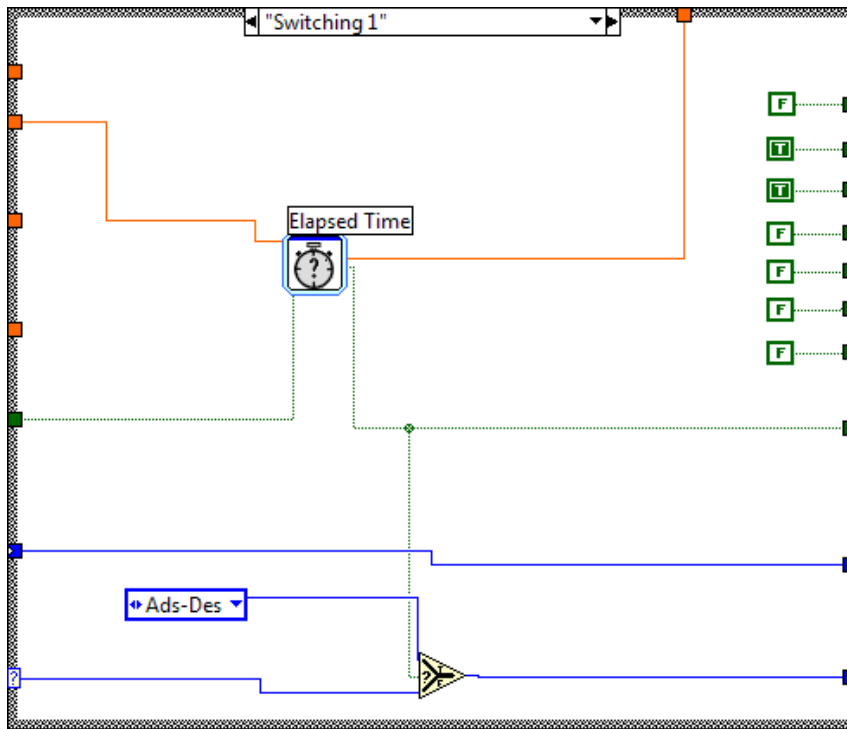


Figure A.III- 5, Case no. 3, "Switching 1"

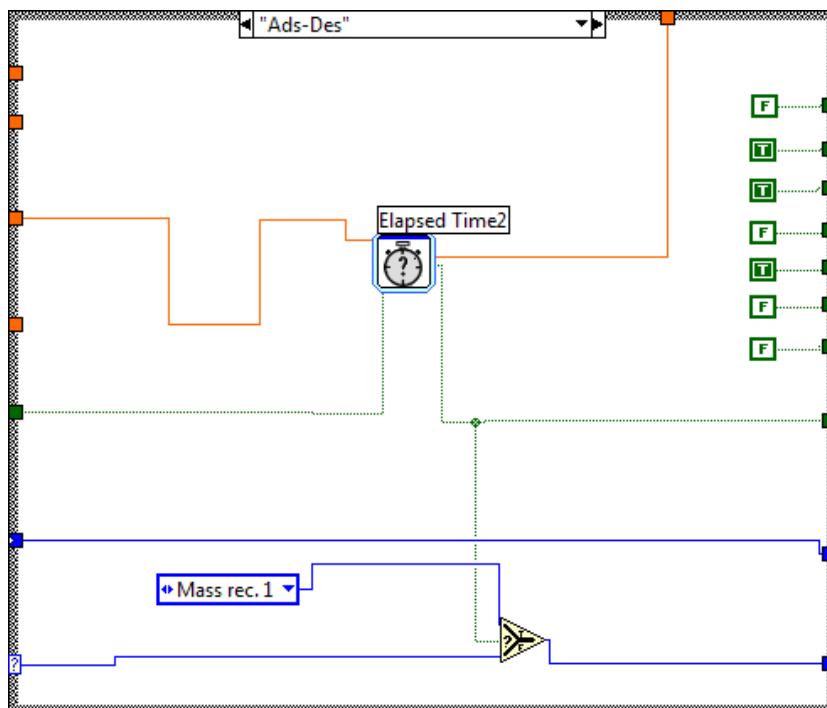


Figure A.III- 6, Case no. 4, "Adsorption-Desorption"

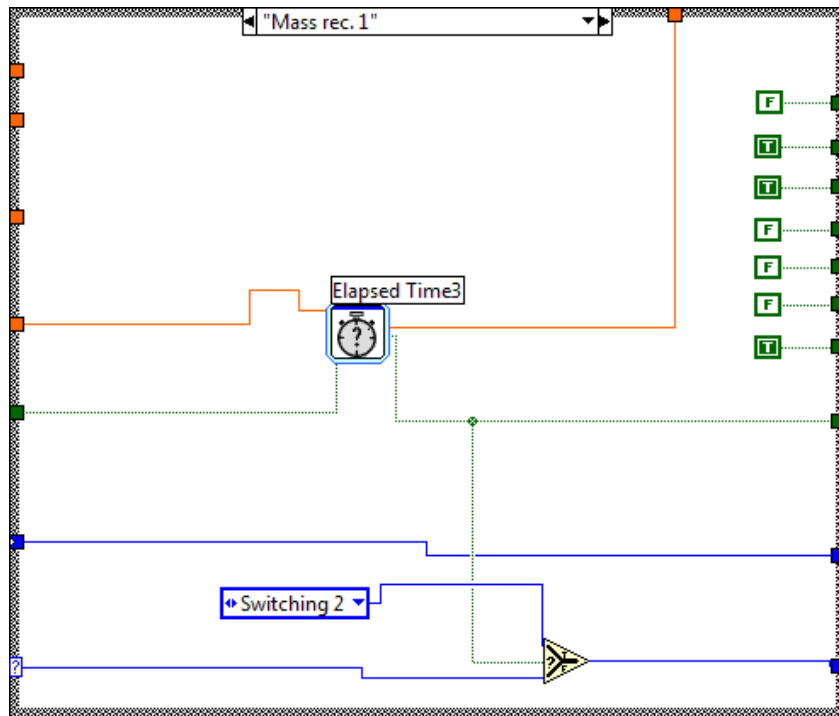


Figure A.III- 7, Case no. 5, "Mass recovery 1"

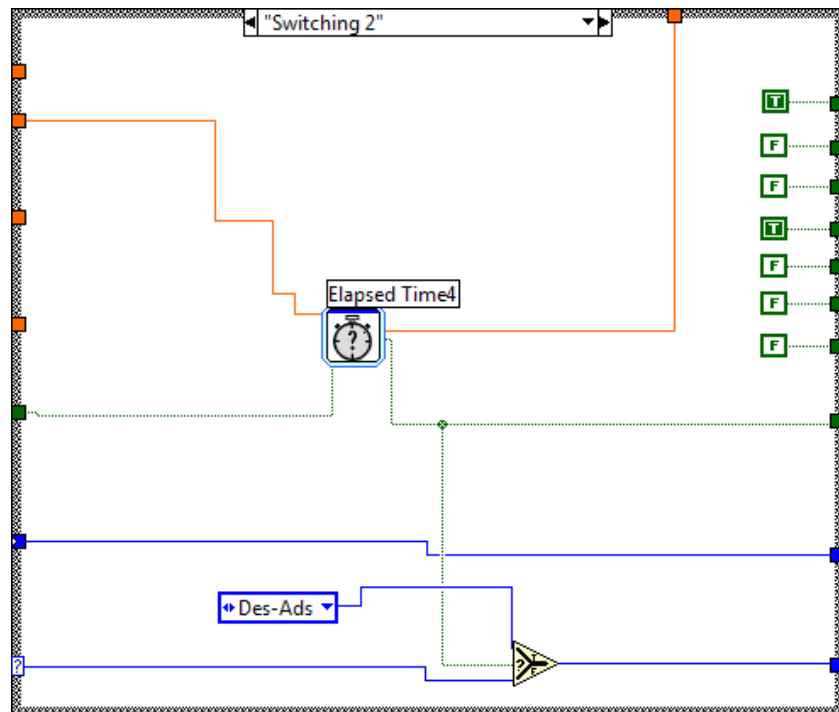


Figure A.III- 8, Case no. 6, "Switching 2"

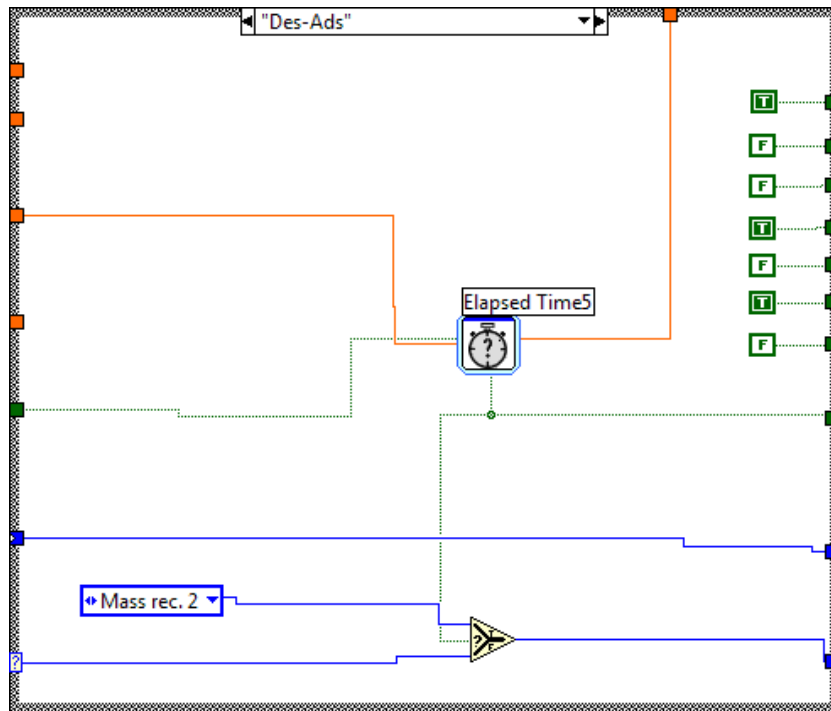


Figure A.III- 9, Case no. 7, "Desorption-Adsorption"

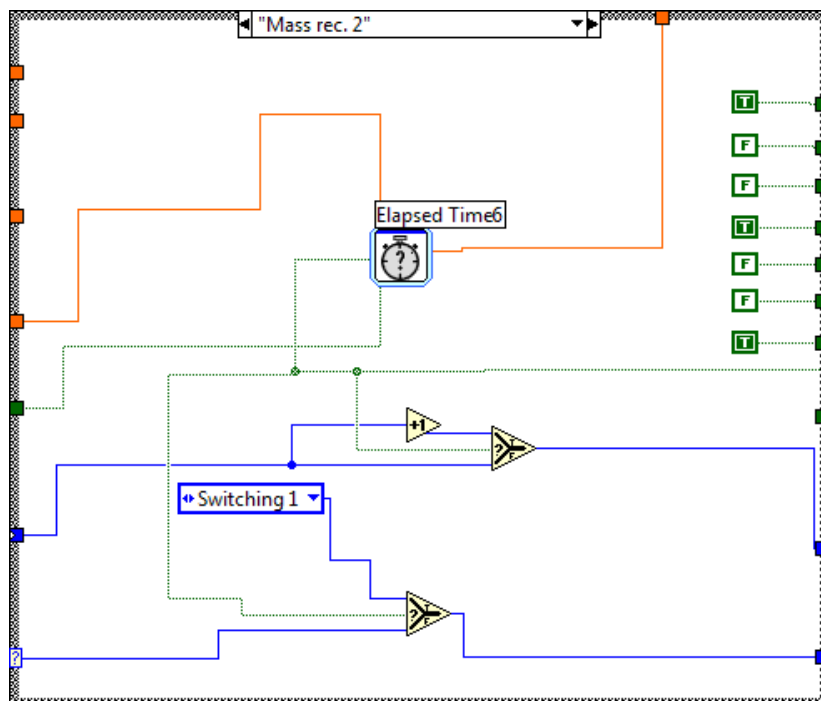


Figure A.III- 10, Case no. 8, "Mass recovery 2"